Julius-Maximilians-Universität Würzburg

Dissertation

Ultra-Wideband Wireless Network for Enhanced Intra-Spacecraft Communication

Autor:
Martin Drobczyk

Gutachter:
Prof. Dr.-Ing. Sergio Montenegro
Prof. Dr.-Ing. Ulf Kulau

Zur Erlangung des

naturwissenschaftlichen Doktorgrades

in der

Fakultät für Mathematik und Informatik

Institut für Informatik

April 22, 2024

"The future cannot be predicted, but futures can be invented."

Dennis Gabor, 1963

Abstract

Wireless communication networks already comprise an integral part of both the private and industrial sectors and are successfully replacing existing wired networks. They enable the development of novel applications and offer greater flexibility and efficiency. Although some efforts are already underway in the aerospace sector to deploy wireless communication networks on board spacecraft, none of these projects have yet succeeded in replacing the hard-wired state-of-the-art architecture for intra-spacecraft communication. The advantages are evident as the reduction of the wiring harness saves time, mass, and costs, and makes the whole integration process more flexible. It also allows for easier scaling when interconnecting different systems.

This dissertation deals with the design and implementation of a wireless network architecture to enhance intra-spacecraft communications by breaking with the state-of-the-art standards that have existed in the space industry for decades. The potential and benefits of this novel wireless network architecture are evaluated, an innovative design using ultra-wideband technology is presented. It is combined with a Medium Access Control (MAC) layer tailored for low-latency and deterministic networks supporting even mission-critical applications. As demonstrated by the Wireless Compose experiment on the International Space Station (ISS), this technology is not limited to communications but also enables novel positioning applications.

To adress the technological challenges, extensive studies have been carried out on electromagnetic compatibility, space radiation, and data robustness. The architecture was evaluated from various perspectives and successfully demonstrated in space.

Overall, this research highlights how a wireless network can improve and potentially replace existing state-of-the-art communication systems on board spacecraft in future missions. And it will help to adapt and ultimately accelerate the implementation of wireless networks in space systems.

Acknowledgements

I would like to express my deep gratitude to all those who have enabled me to carry out my research over the past years and to complete this thesis. First and foremost, I would like to thank my supervisor, Prof. Sergio Montenegro. His enthusiasm for wireless networks, which fascinated me from the first time we met at the DLR Institute of Space Systems, laid the foundation for this thesis. His constant encouragement and support have been invaluable. Special thanks go to Prof. Ulf Kulau, my co-examiner, whose fascination with wireless networks has been a source of inspiration throughout this journey. His commitment to officially supervising this thesis is deeply appreciated and has been immensely valuable.

My appreciation extends to my Head of Department Dr. Frank Dannemann, who has never ceased to motivate and encourage me and has contributed greatly to my motivation to complete this dissertation. I am also grateful to former Head of Department Prof. Görschwin Fey, whose helpful insights have significantly improved the quality of this work and made the results more valuable. I would also like to thank all my colleagues and students, both those who worked directly with me on this topic and those who I supervised. Their different perspectives and critical thoughts have enriched my understanding and approach.

Special thanks go to Andre Lübken, with whom I have led the wireless networking topic for years and who has played a major role in the software implementation. I'm grateful to Marcus Lehmann for his expert guidance on EMC and to Jan Budroweit for the opportunity to test my components for radiation exposure.

My sincere appreciation goes to the entire Wireless Compose team whose efforts made the experiment possible. Without them, especially Christian Strowik, this experiment would not have been possible. I am also grateful to the DLR Agency and ESA for their funding, the opportunity to send my experiment into space, and for providing the images used in this thesis.

A special thanks goes to astronaut Alexander Gerst, who performed the experiment on the ISS and played a crucial role in the success of this experiment and the demonstration of the wireless network.

Last but not least, I would like to thank my family, who have accompanied me on this journey for many years. Their encouragement, especially from my wife Inga and my lovely children Kira and Liana, who had to spend countless hours without me, enabled me to dedicate time outside of work to complete this thesis.

Contents

List of Figures

List of Tables

Abbreviations

ACK Acknowledge

ACL Asynchronous Connectionless

ACS Attitude Control System

Al Aluminum

AM Anchor Mote

AOCS Attitude and Orbit Control System

AP Anchor Point

API Application Programming Interface

AoA Angle of Arrival

AOCS Attitude and Orbit Control System

ARM Advanced RISC Machines

AIT Assembly, Integration, Test

BAN Body Area Network

BPM Burst Position Modulation

BPSK Bi-Phase Shift Keying

BSS Basic Service Set

BS Base Station

CAN Controller Area Network

CAP Contention Access Period

CC Convolutional Code

CCSDS Consultative Committee for Space Data Systems

CD Collision Detection

CDH Command and Data Handling

CFP Contention-Free Period

CFRP Carbon-Fiber-Reinforced Plastics

CFS Chirp Spread Spectrum

CoAP Constrained Application Protocol

COMMS Communication System

COTS Commercial off the Shelf

CRC Cyclic Redundancy Check

CSMA Carrier Sense Multiple Access

CSMA-CA Carrier Sense Multiple Access/Collision Avoidance

CSMA-CD Carrier Sense Multiple Access/Collision Detection

CTB Cargo Transfer Bag

CSS Chirp Spread Spectrum

CPU Central Processing Unit

DAG Direct Acyclic Graph

DCF Distributed Coordination Function

DLL Data Link Layer

DLR Deutsches Zentrum für Luft- und Raumfahrt e.V.

DS-TWR Double-Sided Two-Way Ranging

DSSS Direct Sequence Spread Spectrum

DUT Device Under Test

DW Decawave

ECC Error Correction Codes

ECLSS Environmental Control and Life Support System

ECSS European Cooperation for Space Standardization

EGSE Electrical Ground Support Equipment

EIRP Effective Isotropic Radiated Powe

EKF Extended Kalman Filter

EMC Electromagnetic Compatibility

EPS Electrical Power System

ESA European Space Agency

ESS Extended Service Set

ESCC European Space Components Coordination

Eu:CROPIS Euglena – Combined Regenerative Organic Food Production in Space

FCC Federal Communications Commission

FCS Frame Checksum

FDTD Finite-Difference-Time-Domain

FFD Full Functional Device

FHSS Frequency Hopping Spread Spectrum

FCS Frame Checksum

FreeRTOS Free Real-Time Operating System

GACK Group Acknowledgement

GPIO General Purpose Inputs/Outputs

GNC Guidance, Navigation and Control

GNSS Global Navigation Satellite System

GPS Global Position System

GTS Guaranteed Time Slots

HART Highway Addressable Remote Transducer

HCI Host Controller Interface

HTTP Hypertext Transfer Protocol

IBSS Independent Basic Service Set

IC Integrated Circuit

IEEE Institute of Electrical and Electronic Engineers

IFS Interframe Space

IMU Inertial Measurement Unit

IoT Internet of Things

IR-UWB Impulse Radio Ultra-Wideband

ISA International Society of Automation

ISI Intersymbol Interference

ISO International Organisation for Standardisation

ISM Industrial, Scientific and Medical

ISS International Space Station

JAXA Japanese Space Agenc

JSC Johnson Space Center

ITU International Telecommunication Union

KPI Key Performance Indicator

L2CAP Link Control and Adaptation Protocol

LAN Local Area Network

LEO Low Earth Orbit

LET Linear Energy Transfer

LLC Logical Link Control

LLS Linear Least Squares

LIFS Long Interframe Space

LLDN Low Latency Deterministic Networks

LMP Link Manager Protocol

LoS Line-of-Sight

LQI Link Quality Indication

M2M Machine-to-Machine

MAC Medium Access Control

MAN Metropolitan Area Network

MCDA Multi-Criterion Decision Analysis

MCS Modulation and Coding Schemes

MEMS Micro-Electro-Mechanical System

MFR MAC Footer

MIC Message Integrity Code

MHR MAC Header

MIL-STD United States Military Standard

MIMO Multiple Input Multiple Output

MOS Metal-Oxide Semiconductor

MSI Multi-Spectral Imager

NLoS Non Line of Sight

NASA National Aeronautics and Space Administration

OBC On-Board Computer

OFDM Orthogonal Frequency Division Multiplexing

OS Operating System

OSI Open System Interconnection

OTP One-time Programmable Memory

PAN Personal Area Network

PCB Printed Circuit Board

PCDU Power Control and Distribution Unit

PDR Packet Delivery Ratio

PHY Physical Layer

PHR Physical Header

PI Principial Investigator

PLCP hysical Layer Convergence Procedure

PLEN Preamble Length Parameter

PMD Physical Medium Dependent

PPDU Physical Protocol Data Unit

PRF Pulse Repetition Frequency

PSDU PHY Service Data Unit

PSK Phase Shift Keying

QAM Quadrature Amplitude Modulation

QoS Quality of Service

QPSK Quadrature Phase Shift Keying

RAMIS Radiation Measurement in Space

Rad-Hard Radiation-hardened

RE Radiated Emissions

RF Radio Frequency

RFCOMM Radio Frequency Communication

RFD Reduced Functional Device

RFID Radio Frequency Identification

RFIC Radio Frequency Integrated Circuit

ROBEX Robotische Exploration unter Extrembedingungen

RMSE Root Mean Square Error

RSS Received Signal Strength

RSSI Received Signal Strength Indicator

RPL Routing Protocol for Low-Power Lossy Networks

RS Reed-Solomon Code

RS Radiated Susceptibility

RTC Real-Time Clock

RTU Remote Terminal Unit

S/S Subsystem

SCO Synchronous Connection-oriented

SD Secure Digital

SEE Single Event Effect

SEL Single Event Latchup

SEU Single Event Upset

SFD Start of Frame Delimiter

SHR Synchronisation Header

SIFS Short Interframe Space

SIG Bluetooth Special Interest Group

Skith Skip the Harness

SMA SubMiniature Version A Connector

SNR Signal-to-Noise Ratio

SPENVIS Space Environment Information System

SPI Serial Peripheral Interface

SS-TWR Single-Sided Two-Way Ranging

SSCS ervice Specific Convergence Sublayer

SSCV Flight Control and Management System

SSPE Power Distribution System

SSSA Safety System

SSTM Telemetry System

ST STMicroelectronics

TCP Transmission Control Protocol

TCS Thermal Control System

TDD Time Division Duplexing

TDMA Time Division Multiplexing

TDoA Time Difference of Arrival

TID Total Ionizing Dose

TM Tag Mote

ToA Time of Arrival

ToF Time of Flight

TS Timeslot

TSCH Time Slotted Channel Hopping

TSMP Time Synchronised Mesh Protocol

UART Universal Asynchronous Receiver-Transmitter

UDP User Datagram Protocol

USB Universal Serial Bus

UTC Universal Time Coordinated

UWB Ultra-Wideband

VEB Vehicle Equipment Bay

VoIP Voice over Internet Protocol

WAIC Wireless Avionics Intra-Communication

WAN Wide Area Network

WLAN Wireless Local Area Network

WLS Weighted Least Squares

Wi-Fi Wireless Fidelity

Wireless Compose Wireless Communication and Positioning Experiment

WICO2 Wireless Communication and Positioning Experiment 2

WPAN Wireless Personal Area Network

WSN Wireless Sensor Network

Chapter 1

Introduction

1.1 Motivation

Spacecraft avionics systems consist of various electronic components and subsystems that interact and exchange data to ensure the safe operation of the spacecraft. The communications architecture used is a critical guarantor of spacecraft reliability and performance, ensuring that a spacecraft can be monitored and controlled from the development phase through to its operation in space, thereby guaranteeing in-orbit functionality (1).

To do this, a variety of telemetry data must be read out that originates from both the bus-side and the payload electronics. This data exchange necessitates a complex network of cable harnesses, creating a backbone for the continuous data flow. To maintain seamless interoperability among components and sensors, the state-of-the-art avionics sector relies on established wired standards, offering specific interfaces and protocols. Depending on the communication topology, robust point-to-point connections or data buses such as SpaceWire and United States Military Standard (MIL-STD)-1553 may be used (2, Section 3). Since these wired standards have been tested and used for many years, the concept of wired connections will continue to be widely used.

Modern radio-based technologies have yet to gain significant traction and have not been able to complement or even replace the state-of-the-art architecture for data communication on board spacecraft. However, they offer many advantages over cabled data links at different levels and have the potential to replace them completely, thereby opening up new perspectives and opportunities (3, Section 2.1). Although efforts are already underway to integrate wireless networks into state-of-the-art architectures, they are far from being widely adopted (4). Their ability to withstand the harsh space conditions and the requisite robustness remains a subject of ongoing research (5).

This gap in technology adoption underscores the need for extensive research to evaluate the feasibility, capabilities, and limitations of wireless networks in the context of aerospace. It was this very gap that triggered my own research journey, which began in 2008 at the Institute of Space Systems of the German Aerospace Center (DLR). It was here that I started researching and conceptualising wireless networks, exchanging ideas with Prof. Dr. Sergio Montenegro, the former head of the Avionics Systems Department. This collaboration laid the foundation for my dissertation and further research in this area. As the primary objective of this dissertation I explore the enhancement of the state-of-the-art intra-spacecraft communication architectures to encompass wireless networks. This research aims to identify viable candidates for wireless networking on board a spacecraft and to initiate an establishment process, potentially revolutionising future avionics architectures. This includes designing and implementing a wireless network on board a space system, and demonstrating its feasibility in orbit.

1.2 Problem definition

Wired data links are an integral part of any spacecraft avionics architecture. Interfaces and standards have continued to evolve, and the use of modern, high-speed data buses enables more efficient data transmission. This allows the bundling of data lines and the reduction of mass, which was already a firm goal of the major space agencies 20 years ago to reduce complexity, mass, and hence mission costs (6). Although the ongoing development towards data buses such as SpaceWire represents an important milestone in the reduction of cables, the issue of cable reduction continues to be an important area of research for space agencies, as it has the potential to further reduce the overall cost of a mission and two European Space Agency (ESA) presentations (7; 8) on “Harness Reduction” from 2017 show the topicality of the subject. The solutions they present try to achieve the reduction by changing the state-of-the-art infrastructure of cables and connectors and, in this context, using wireless networks could represent another important step towards this goal.

However, introducing new technologies into aerospace sector is challenging due to the highly conservative culture in aerospace development, whereby new space systems are usually developed similarly to their predecessors, using the same technologies, to minimise programmatic risk. Hence, innovation only takes place in small incremental steps, and technologies that have proven themselves in flight will continue to be used in the development of future spacecraft. This perspective is particularly prevalent among project engineers who are under pressure to complete projects on time and within budget, while always minimising risk (cf. 9, p. 2).

Because the disadvantages of cable connections are well understood and their risks are well calculated, they are still preferred to novel methods. Some of the key risks of cable connections are outlined below:

- **Complexity** – Complex cable harnesses are produced that negatively affect the mass balance and thus increase the overall cost of the project. In addition, the mass has a significant effect on the dynamic behaviour of the structure, which can have undesirable effects, particularly in lightweight construction. This aspect is examined in detail in (10). In addition, the design, integration, and testing of these harnesses is often a time-consuming process that must be repeated several times if design changes are made.
- **Handling** – As the number of interfaces increases, so does the complexity of the data handling system, and this is compounded by the fact that many of these interfaces are different (6). Component mating is also risky because of the potential for damage to components from mismatched pins in the connector definition or the effects of electromagnetic discharge.
- **Inflexibility** – The rapid disassembly of components that have already been integrated is only possible to a limited extent, as the cable harnesses also have to be disassembled (11).

Other challenges in this context include interference and signal loops that can lead to signal degradation and even component damage, similarly to their wireless counterparts (12). However, the ability to predict and shield these effects is a major advantage of wired connections. Another advantage is that many of the transducers being used are available as Radiation-Hardened (Rad-Hard) variants, making them robust to the harsh conditions in space. In recent years, the approaches to risk assessment and component selection have been reconsidered to significantly reduce the cost of space missions (13). In particular, the privatisation and commercialisation in the aerospace sector, which has also given rise to the NewSpace movement, has contributed to the growing acceptance of commercial components from the automotive sector and their increasing use in conventional space projects.

1.3 Benefits of wireless communication

In this context, and based on the brief overview provided, the question arises whether the problems described here can be solved by wireless data communication. The assumption that this is theoretically possible was highlighted in some of the studies published on the subject many years ago and the first notable considerations in the literature on

wireless intra-spacecraft communications are found in (14). However, concepts and studies become more concrete from 2007 onwards (15; 5), marking the beginning of my own research in this area. And from 2010 and onwards, more research has been conducted, e.g. (16; 17). This is also due to the fact that wireless networks were also increasingly becoming accepted in terrestrial applications (17).

This is because an increasing number of industries are taking advantage of the benefits of wireless networks to link complex systems together and exchange important data. As it reflects the achievements of mobility like no other technology, wireless communication is an integral part of consumer electronics and has enabled many new applications such as the use of wearables or Smart Home devices. While Bluetooth and Wireless Fidelity (Wi-Fi) are now well-established standards, new standards are also developed such as ZigBee, which is becoming increasingly common, especially in the field of smart monitoring (18, Chapter 13) in Smart Home applications. Wireless sensor networks have also been used in industry for years, although in the industrial sector, there are often higher requirements for reliability and determinism, which has led to the emergence of industry standards that specifically address these requirements. These include, in particular, applications for the monitoring of automation processes in the context of the Industry 4.0 revolution (19, Section IV).

A shift towards increased reliance on wireless networks has taken place in the automotive industry. In this context, terms such as the Internet of Things (IoT) or Machine-to-Machine (M2M) communications have arisen, which have also benefited from the wireless developments (20). The aviation sector – which is closest to the aerospace industry in terms of development processes and quality management – has also approached the wireless world and passengers are increasingly using wireless technologies. Soon, sensors for critical monitoring of aircraft characteristics will be read out over wireless networks. To this end, the Wireless Avionics Intra-Communication (WAIC) organisation was established, which has been working for several years to standardise the use of wireless technology in aviation and, in 2016, was allocated a dedicated frequency for these applications by the International Telecommunication Union (ITU) (21).

On this basis, it is reasonable to assume that wireless systems will be used in aerospace in the future, as they have many advantages over wired communication that were already been successfully demonstrated in other industries, whereby a quote from the 2012 National Aeronautics and Space Administration (NASA) progress report on technology roadmaps of promising future technologies supports this view:

> Wireless spacecraft technology was added to the observatories subarea of the original NASA roadmap because the use of wireless systems in spacecraft

> avionics and instrumentation can usher in a new, game-changing methodology in the way spacecraft and space missions will be designed and implemented. Wireless avionics can provide reliable subsystem-to-subsystem communications that facilitate a new fault-tolerant, inherently cross-strapped, extensible, and reliable architectural approach. (cf. 22, p. 339)

The following advantages have already been described and analysed in the literature:

- **Elimination of complex cable harnesses** – Providing wireless connectivity would be a realistic alternative for space applications to efficiently and safely replace long and complex wiring harnesses. For example, the German Aerospace Center CompactSat Euglena - Combined Regenerative Organic Food Production in Space (Eu:CROPIS) mission (< 250 kg) has shown that the use of cables is a complex engineering task in which the design, routing, manufacturing, and laying of cables can take up to several years (23). In addition, wireless links are useful for the connection of components that require contactless interfaces such as rotating or moving components including robotic arms or solar panels/sail deployment mechanisms.
- **Reducing mass and volume** – Satellites weighing between 500 kg and 1000 kg typically generate up to 20 km of cables (24). By eliminating these cables and the associated parts such as cable ties and connectors, up to 10% of the total mass of even smaller satellites can be saved. At the same time, only approximately 30% of these cables are typically reserved for power supply and the vast majority is used for data connections (6). Therefore, the overall mass would also be significantly reduced by eliminating cables for data communication only. It would also simplify and reduce the volume of components and sensors by eliminating dedicated cable paths and the additional space required for connecting cables due to bending radii and connector dimensions. This, in turn, has a positive effect on the overall volume.
- **Simplification of Assembly, Integration, Test (AIT) processes** – The wireless approach makes it possible to streamline AIT activities since using wireless networks to interface with components and sensors simplifies the integration process. It also significantly reduces the extent of the electrical interface testing that is required as even in the event of a failure or subsequent modifications, the wireless approach makes it easier to modify spacecraft after integration is finished. Wireless interfaces can also be used as a connection to the Electrical Ground Support Equipment (EGSE), thereby simplifying checkout procedures and this use-case was investigated in this master thesis (25). Alternatively, they can be used as a data acquisition system for the sensor technology that is needed to monitor the satellite during environmental campaigns. In particular, thermal-vacuum campaigns use

up to several hundred sensors, which often remain as dead mass and overcoming this disadvantage by using wireless networking was successfully demonstrated in (26).

- **Minimising risks and induced failures** – The reduction in the number of cable harnesses leads to fewer connectors and thus a reduction in the sources of error, without compromising the efficiency or performance of the system. Connecting different components with cables requires specific and time-consuming considerations such as design (including shielding, connector and pin definition, brackets and cable ties), conducted Electromagnetic Compatibility (EMC) testing, and thermal analysis, taking project-specific requirements and guidelines into account. Most of this work is eliminated when using wireless connections. Moreover, errors that can occur, for example, in the definition of the pin assignment or the connection of several devices in the AIT process (27) are also eliminated.

- **Developing new networking and redundancy concepts** – Wireless communication makes it possible to build low-complexity, low-power wireless networks that provide deterministic and reliable communication while accommodating different network topologies. This opens up new possibilities for intra- and inter-satellite communication and networking, e.g. in satellite clusters. These concepts, together with redefining and improving the current concept of failure and redundancy of cable connections, are also of interest for future robotic or manned space missions in which different small units, such as rovers, communicate with larger units, such as the base.

- **Expanding functionality** – In addition to providing a communication link, wireless communication also offers the ability to measure range and position. The simultaneous communication and positioning opens up new possibilities for robotic and manned missions in which the movement of objects and crew members is an important aspect. For example, DLR participated in the Robotische Exploration unter Extrembedingungen (ROBEX) exploration study that investigates robotic exploration under extreme conditions (28) and also studies the use of wireless networks. Demonstrating the effectiveness of wireless networks for positioning is also the aim of the Wireless Communication and Positioning experiment (Wireless Compose) (29) presented in Chapter 6.

In summary, since wireless communication offers significant advantages, it is desirable that future space missions should be equipped to take advantage of these benefits. At one extreme of this vision is the wireless satellite, which requires no wiring at all, as presented in (30) with the InnoCube satellite that utilizes the Skip the Harness (Skith) infrastructure that originates from the University of Würzburg (31). This would open

up a wide range of new possibilities, including the fact that large deployable structures would no longer necessarily need to be mechanically connected to each other. The Gossamer/Gossolar project (32), also a project in collaboration with University of Würzburg, has demonstrated the beneficial use of wireless technologies in the deployment of SolarSails. In addition, manned spaceflight in particular could benefit from the use of wireless communication because astronauts need a great deal of room to be transported into space and thus inflatable modules would be a suitable solution for this purpose. It is evident that using wireless networks would be a great advantage here, as shown by (33). Furthermore, satellite clusters could also be more easily realised in the future, since wireless networks could cover greater distances depending on the range supported (34). However, the wireless satellite vision also includes another component, namely power, which is also wired in today's architectures and distributed power and wireless power transfer are interesting approaches to solving this problem in the future (35). Although progress in these areas could indirectly accelerate the deployment of wireless data networks, these exciting research aspects are not part of this thesis due to scope limitations.

1.4 Challenges to overcome

To approach the vision of a wireless satellite from a communications perspective, several technological challenges must be overcome to provide a robust architecture for wireless intra-spacecraft communication. Particularly in space, the harsh environment places severe demands on the operation of wireless on board systems, whether due to the electromagnetic or radiation environment (36) and the resilience towards them play a decisive role in the choice of the technology. The challenges for deployment are broadly the same for both manned and unmanned space missions and need to be addressed on an ongoing basis:

- **Electromagnetic compatibility** – An important requirement for the use of wireless technologies on board space systems is the electromagnetic compatibility with other Radio Frequency (RF)-sensitive systems. As the communication takes place inside a spacecraft, the radiated power is significantly lower than that typically required for radio communication with ground stations. However, the distances can be only a few centimetres to a few metres, which means that the radiation can interfere with other RF-sensitive systems inside the spacecraft. In addition, the electromagnetic immunity to other radiated signals, is an important evaluation criterion.

- **Technological maturity** – Another challenge is technological maturity. Despite the overwhelming success of wireless networks in terrestrial applications, the components and modules used are not yet mature for use in space and need to be characterised or tested accordingly under space conditions. This applies to radiation and its effects over the Total Ionising Dose (TID), which can lead to the total destruction of the component, and Single Event Effects (SEE) which can induce bit flips and latch-ups, causing temporary or irreversible damage to the electronics or can degrade the communication.

- **Data robustness** - Robustness encompasses several factors, including the robustness of the electronics to the harsh space environment described above. However, the aspect important to consider for robust communication is data robustness, as wireless communications within a spacecraft or other space system can adversely affect signal characteristics due to signal scattering and multipath propagation (22, p. 71).

- **Defining new architectures and standards** - is also important for a technology to gain wide acceptance and to define guidelines, rules, and conditions under which engineers can work on new projects. On the one hand, this involves the sensible integration of the technology into existing state-of-the-art architectures to provide an incentive to use it without having to completely change what is familiar. On the other hand, there is a need for standardisation to ensure interoperability and compatibility.

Much remains to be done before wireless systems can truly replace state-of-the-art wired architectures and be integrated into the existing communication infrastructure. Thus, the investigation outlined in the next Chapters aims to remove these bottlenecks and take an important step towards this goal.

1.5 Objectives and structure

Due to aforementioned benefits, wireless networks have significant potential for future space missions, although technological challenges still need to be overcome. With this background, the main objective of this thesis is to design and implement a wireless network that can enhance state-of-the-art wired intra-spacecraft communications. It also includes the verification and the demonstration in a space environment. In a broader context, this work aims to accelerate the adaptation of wireless networks on board spacecraft and to establish them in space systems.

To achieve the main objective, the work is focused on the examination of the first two communication layers, the physical layer and the Medium Access Control (MAC) layer.

For a comprehensive understanding of these layers within the context of the Open System Interconnection (OSI) model, please refer to Subsection 2.2. The physical layer is an essential part, as it provides techniques to minimise the effects of interference, which are essential for a robust communication system. The MAC layer is particularly important as it controls access to the data being transmitted, which is essential when more than two parties are communicating. It also provides techniques to ensure reliable communication, thereby increasing the overall robustness of the system. It also paves the way for the deterministic networks required in time-critical systems such as a spacecraft's attitude control system.

The structure of the work unfolds as follows:

Chapter 2 serves as an introduction to the fundamentals of common wireless communication standards. It provides a comprehensive overview of the basic concepts and technologies of wireless communication networks that are relevant to understanding and analysing candidates for the proposed achievement. The focus is on Wireless Local Area Networks (WLANs) from the Institute of Electrical and Electronic Engineers (IEEE) 802.11 family and Wireless Personal Area Networks (WPANs), such as Bluetooth and Zigbee. Industrial protocols such as WirelessHART and ISA100.11a, as well as newer MAC schemes such as Time-Slotted-Channel Hopping (TSCH) or Low Latency and Deterministic Networks (LLDN) from the recently published IEEE 802.15.4e MAC amendment, are also considered for their improved robustness behaviour.

Chapter 3 explores the possible applications of wireless intra-spacecraft communications and discusses the technological challenges involved. A requirements analysis is carried out for the evaluation of the possible applications of wireless networks for space-related application fields. The focus is on the investigation of the suitability of different wireless communication standards for use in space systems that takes requirements such as latency, robustness, and determinism into account. The Multi-Criterion Decision Analysis (MCDA) is used to perform an assessment. Since the outcome of the assessment shows that Impulse Radio - Ultra-Wideband (IR-UWB) on physical layer and the LLDN scheme in MAC layer perform best in the different applications, the focus in the next Chapter is based on them.

In **Chapter 4**, a system concept is presented that will serve as the basis for a new wireless network architecture. The selected stack, based on IR-UWB and the LLDN scheme, is presented and analysed and its integration into various avionics architectures is discussed. Subsequently, the technical implementation and performance evaluation is presented.

The technological challenges of adapting wireless networks in space systems are discussed in **Chapter 5**, with particular emphasis on verifying the data robustness of the implemented wireless network, including the electromagnetic and radiation environment, in

view of the in-orbit demonstration by the Wireless Compose experiment on board the International Space Station.

Chapter 6 presents the results of the first-ever demonstration of a IR-UWB-based wireless network in space that was part of the Wireless Compose experiment. Although IR-UWB has already been investigated for space applications in other studies, such as in (37; 38; 39), these studies only concentrated on investigating the properties in the physical layer and a final demonstration in a space environment was not yet successful, what has now been achieved with the operation of this experiment in orbit. The ambitious Wireless Comspose experiment is described in detail and the results are presented and reviewed.

Finally, **Chapter 7** summarises and discusses the main theses and results and provides an outlook on further research and steps needed to establish the technologies. The issue of standardisation is also emphasised as a crucial step in this process.

1.6 Innovation and relevance

In order to meet the ever-increasing demands and challenges of the aerospace sector, the development and establishment of new technologies is crucial. This dissertation provides a forward-looking perspective that is both innovative and highly relevant by focusing on the design, implementation, and in-orbit demonstration of an innovative wireless network architecture, leveraging IR-UWB and LLDN for communication and positioning.

It represents a significant **innovation** in several respects:

- **Holistic approach** – Rather than focusing exclusively on technical aspects, my work provides a holistic approach, ranging from analysis, design and implementation to adaptation and establishment of the proposed wireless communication architecture in future space missions. Previous assessments have mainly been limited to technical considerations and have neglected the whole process required for successful adaption.
- **First-time use of IR-UWB in space** – For a historic first-time, the IR-UWB network was not only theoretically analysed, but also practically demonstrated in-orbit in a space system, including its application for communication and positioning.
- **Innovative combination in MAC and physical layer** – The combination of IR-UWB with specific aspects of the MAC layer is an innovation. Previously,

the individual protocols and standards were not natively interoperable and no adaption of LLDN to IR-UWB exists. In particular, the use of the 802.15.4e low latency and deterministic MAC scheme, originally intended for 2.4 GHz narrowband physical layer, combined with the strengths of the UWB physical layer for space applications, distinguishes this work from previous approaches.

- **Initiation of the standardisation process** – My work has not only provided scientific and technical knowledge, but has also taken an important step towards the standardisation of the proposed wireless architecture in the aerospace context. The potential to become a true aerospace standard within the scope of the Consultative Committee for Space Data Systems (CCSDS) underlines the importance and impact of my work.

Moreover, the **relevance** of my dissertation is particularly evident in the on-going impact on the aerospace sector:

- **Application within German Aerospace Center** – The results of my dissertation have found wide practical application within the DLR. Many projects already benefit from the wireless network architecture developed here. In particular, this protocol architecture has become a real baseline for applications in DLR satellites, space station experiments and lunar habitat prototypes that make use of the robust wireless intra-spacecraft communication. Moreover, it is a reflection of the applicability of the research that it has become core part of the DLR integrated core avionics framework.
- **Promoting international collaboration** – The research and results presented here have opened doors to international collaborations utilizing IR-UWB in space missions, such as with the Japanese Space Agency (JAXA). Such partnerships are essential to standardise and establish new technologies in a global context.
- **Support from major organisation** – The work has not only attracted the attention of different space agencies, but also the support of major organisations for standarization such as the CCSDS. This demonstrates the high potential and relevance of the architecture and approach presented.
- **Reflection and decision support for wireless networks** – The results of this work contribute significantly to the reflection and understanding of the strengths and drawbacks of wireless networks in specific space applications. This knowledge will enable system engineers to take informed decisions on the deployment and integration of these technologies in future space systems. Rather than simply developing new wireless systems this work provides a framework for assessing when and how these technologies can be used most effectively.

1.7 Personal contributions already published

Some of the results presented in this dissertation I have published in various publications. In all of the following work, I was significantly involved in the conception and implementation of the research design.

- **Protocol architecture concept and evaluation** – The concept presented in this thesis is based on my publication (40), in which I introduce the protocol architecture and perform an analytical study of the latency performance. The implementation of this protocol architecture was done as part of the master thesis (41), in which I had a major role in the conception and design, and which I supervised. I have also published and discussed the results of this work in (42).
- **Challenges verification** – My publication (43) and the corresponding master thesis (44) deal with the analysis and characterisation of the presented system concept under harsh electromagnetic conditions. In the thesis I provided the primary concept and supervised the work. Furthermore, I prepared the measurements and assisted in their execution and evaluation. The results of the radiation test campaign, which I prepared and carried out, have been published in (45).
- **Demonstration** – In addition, I led a notable project, the Wireless Compose experiment on the International Space Station (ISS), which demonstrated the IR-UWB-based network that was developed and operated within the scope of my dissertation. I have published the concept in the cited paper (46). As the principal investigator, my personal contribution covered the entire process: from the initial concept design to the implementation, execution and analysis of the experiment results.

Chapter 2

Fundamentals

The continuing evolution of wireless communication technologies provides an exciting foundation for applying to innovative environments such as space. Although wireless networks are omnipresent today, their application in the harsh space environment requires a deep understanding of the fundamental concepts and technologies.

This second Chapter sets the basis for the later discussion and analysis of an appropriate architecture for wireless intra-spacecraft communication networks. First, it introduces the basics of common wireless communication standards. Special emphasis is placed on short-range wireless networks: the IEEE 802.11 WLAN family and WPAN standards such as Bluetooth and ZigBee. The first two communication layers, the physical layer and the MAC layer, are central to this research. The physical layer provides techniques to minimise the effects of interference - a critical aspect for a robust communication system in the space context. The MAC layer ensures not only reliable access to the transmitted data, but also the necessary robustness of the system. Industrial protocols such as WirelessHART and ISA100.11a, as well as newer MAC schemes such as Time-Slotted-Channel Hopping or Low Latency and Deterministic Networks from the recently published IEEE 802.15.4e MAC amendment, are also investigated to understand their improved robustness characteristics. The physical layer of IR-UWB, as defined in the 802.15.4a standard amendment, is another focus to be examined, as its increased robustness is particularly relevant.

Moreover, the fundamental concepts of positioning are presented. Various algorithms for position estimation, as well as the Kalman filter fundamentals are introduced.

This Chapter is intended to form a solid basis for the discussion and analysis that follows. The aim is to provide the necessary knowledge to understand and evaluate the applicability of the different wireless communication technologies.

2.1 Introduction to wireless networks

Wireless networks have undergone rapid development in recent years, and today they represent an interesting alternative – or at least a complement – to wired networks. These technologies are now affordable, of high quality, and can be used in a wide range of applications. Fundamentally, a network exists when two computers are connected to each other and exchange data and, in the case of wireless networks, there must be at least one transmitter and one receiver that use the same modulation technique and operate on the same frequency. In most cases, however, it is common for more than two participants to take part in a network.

The predecessor of wireless networks was developed in the late 1960s and was called **Alohanet**. It was introduced by Professor Norman Abramson, who developed the system at the University of Hawaii. Located on the island of Oahu, the Alohanet connected seven campuses on four Hawaiian islands. The main objective of the system was to evaluate the performance of wireless networks and to study the advantages of wireless networks compared to wired connections. The main concept today is a "Random Access Channel" architecture, also known as the Aloha channel, which is widely used in wireless communications. It is the basis for work on the Carrier Sense Multiple Access (CSMA) mechanism developed at the University of California in Los Angeles. CSMA is now a standard and is used for collision avoidance in many wireless network standards (47).

After the realisation of the Aloha networks, it took more than 20 years for the first commercial wireless solutions to appear on the market, and even then, due to their limited range and low data rate, they were not a viable alternative to wired networking such as Ethernet.

In 1990, the IEEE 802 committee, which deals with various IEEE networking standards, formed a new working group, IEEE 802.11, to address the topic of wireless networking. The main objective was to develop a MAC protocol and a physical layer specification with the aim of operating the wireless network in the Industrial, Scientific and Medical (ISM) frequency bands. However, wireless networks were also becoming increasingly interesting for other applications. In particular, since the year 2000 further standards have been introduced for the communication between devices and peripheral equipment, as well as for sensor networks. Since then, these standards have been in a state of constant evolution, while others have been added.

When using standards, a distinction is usually made according to the application area, with the distance between devices playing an important role. As a result, different network topologies have emerged over the years, depending on the distance (cf. 48, p. 16):

- **Body Area Network (BAN)** - This term refers to wired or wireless networks that are integrated into the human body to measure various medical parameters such as heart rate or blood pressure. They can also be integrated into clothing or worn as a wearable device.

- **Personal Area Network (PAN)** - PAN refers to networks that connect different end devices that are typically a few metres apart. This could include notebooks, mobile phones, printers, computer mice, or keyboards. PAN can also be used to communicate within a larger network, such as that required for sensor networks. The term **Wireless Personal Area Network** specifically refers to wireless networks including, for example, the Bluetooth and Zigbee standards.

- **Local Area Network (LAN)** - These are networks that usually connect computers or other terminals in specific areas such as buildings, floors, offices, or houses and could comprise as few as two computers in a household or as many as 1000 computers in a company. A LAN is typically used for fast connections with high data rates and the Ethernet is a widely used standard for this. If these networks are operated by radio, they are called a **Wireless Local Area Network**. WLANs are part of the IEEE 802.11 family of standards and are capable of data rates up to several Gbps.

- **Metropolitan Area Network (MAN)** - This is where several LAN networks are connected in a geographical area which can comprise a number of offices but can also include a whole city. In most cases, these connections are made by the network operators using fibre optic cables.

- **Wide Area Network (WAN)** - The term WAN is used to describe networks that extend over large areas and which can cover entire countries or continental areas. They link regional and inter-regional MANs and can be expanded to form a Global Area Network (GAN).

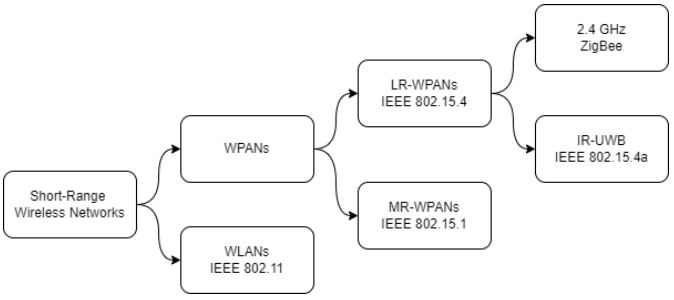

FIGURE 2.1: IEEE wireless networking standards (49, p. 29)

Due to the relatively short distance between the components, so-called short-range wireless networks are considered for communication on board spacecraft. These can be divided into two types, namely WLAN and WPAN networks and the most important standards are shown in Figure 2.1, including:

- IEEE 802.11, also known as WLAN or Wi-Fi,
- IEEE 802.15.1, which is the basis of Bluetooth communication, and
- IEEE 802.15.4, which is especially used for sensor networks, including
  - ZigBee (2.4 GHz narrowband)
  - IEEE 802.15.4a (IR-UWB)

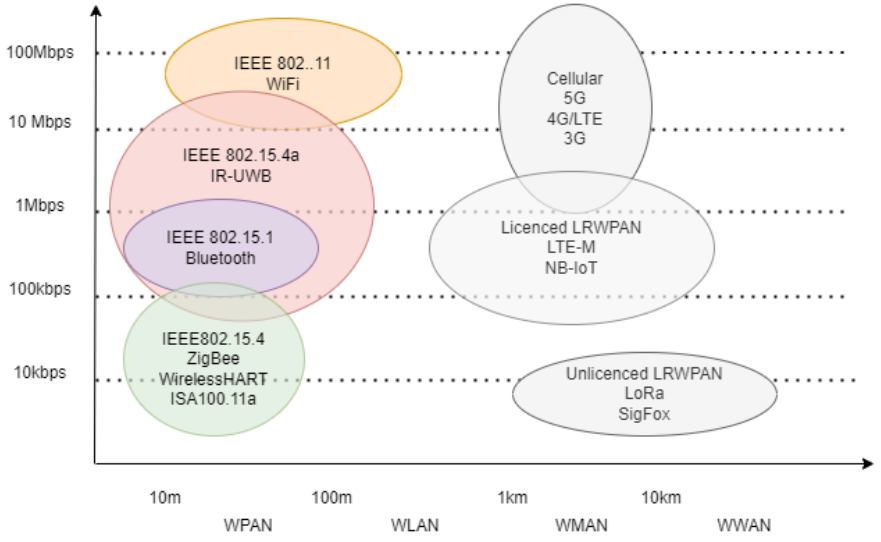

FIGURE 2.2: The IEEE wireless networking standard

Figure 2.2 shows that the main difference between the standards is in the data rate that is provided and in the distance covered. However, as the data rate increases, so does the complexity and power consumption. It is also worth noting that there is an overlap between IR-UWB and other short range standards. This means that IR-UWB is able to cover a wider range of applications that previously required either one standard or the other. This versatility allows IR-UWB also to be used in areas where multiple standards were previously required.

2.2 The OSI layered model

The OSI model is an open-layer model for communication between information systems that contains standardised procedures and rules for the exchange of data. The

model has been under development by the International Organisation for Standardisation (ISO) since the end of the 1970s and is thus also known as the ISO/OSI model. The OSI model consists of seven hierarchically structured layers, each of which provides services and operates independently of the others. This abstraction makes it easier for engineers to work within a layer, for example when developing hardware. It also contains the requirements for connecting two nodes in a telecommunications network, making it possible to develop systems that are compatible enough to communicate with one another. To ensure compatibility and interoperability between their telecommunications technologies, manufacturers use the OSI model as a reference and interface. The network comprises a "stack" of layers, each with its own functions and services, according to the layered network concept. While the framework describes what the layers are supposed to do and how these layers interact with each other (and with the layers above and below them), it does not specify which protocols the layers are supposed to use (50).

The **physical layer (PHY)** defines the media, signal and binary transmission, as well as electrical and physical interface specifications (transmission medium, voltage level, data rate, maximum transmission distances, transmission mode). This layer is responsible for the adaptation of the transmitter signal to the channel (modulation and conversion) and the transmission of the signal as a bit stream.

The second layer, known as the **data link layer (DLL)**, is responsible for organising the bits into logical frames. It also ensures the reliable transmission of the data by means of error detection and correction. This layer is composed of two sub-layers, namely the MAC and Logical Link Control (LLC).

- The **MAC layer** is the lowest sub-layer and is responsible for framing/de-framing, collision resolution, and media access control for broadcast media and networks. It ensures reliable point-to-point and point-to-multipoint communications. Because it regulates the sharing of the transmission channel, the MAC layer is critical to the operation of a network and, in doing so, it has two main objectives. The first objective is the establishment of the network infrastructure and the second is the fair and efficient sharing of the transmission channel.
- The **LLC layer** acts as an interface between the network layer and the MAC layer and its main tasks are multiplexing (thereby allowing different network protocols to coexist), segmentation, and flow control. The IEEE has standardised the LLC sub-layer as the IEEE 802.2 standard, which is the same for all of the 802 family of standards.

The main functions of the **network layer** are the logical addressing and the routing between two hosts. It manages the connectivity between the nodes and ensures that the

packets are sent from the source host on one network to the desired destination host on a different network. Routers operate at this level to enable packets to get routed.

The **transport layer** of the OSI model is responsible for the "Quality of Service" (QoS) which includes error checking, security through encryption/decryption, and error recovery. Another important function of this layer is flow control, which is a method for ensuring the proper flow and information rate, whereby one node on the link indicates to the other node on the link when to slow down the transmission rate.

The fifth layer of the OSI model is the **session layer**, which is responsible for establishing, managing, and terminating sessions between two telecommunications nodes. In this context, the term session refers to the ongoing communication between two hosts.

The next layer is the **presentation layer**, which is responsible for the functions (encrypting/decrypting, reformatting, compressing/decompressing, etc.) that enable the end-user application to understand the message.

The **application layer** is the last layer of the OSI model. It is the closest to the user and provides the application interface (e.g. email or file transfer).

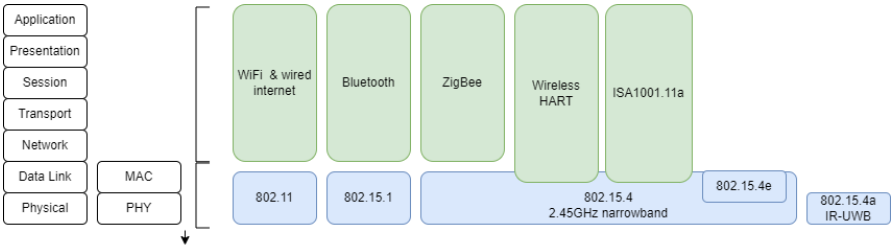

FIGURE 2.3: The IEEE 802 family in the OSI model

The main IEEE standards for wireless networks in the context of WLAN and WPAN and their relationship to the OSI model are shown in Figure 2.3.

The IEEE 802 family is therefore an important foundation for various wireless communication technologies. It always specifies the two lower layers of the OSI model, as these define wireless access to each other and ensure that multiple nodes can form a network. However, they are not used to the same extent by all communication standards. For example, Wi-Fi, Bluetooth and ZigBee use the physical and MAC layers of the 802 standards. In contrast, wirelessHART and ISA100.11a are only compatible with the physical layer of the 802.15.4 standard. Instead, both use their own MAC layer implementations to improve the reliability of their communications.

The IEEE itself has also introduced innovative extensions to the MAC layer that will be introduced later in the Subsection 2.5.5.2. Examples include schemes such as LLDN or TSCH, which were developed specifically for the 2.4 GHz narrowband physical layer and are covered in the 802.15.4e extension. There is also an extension to the 802.15.4 layer

that uses IR-UWB and is specified in the 802.15.4a amendment. However, no dedicated MAC layer has been defined for IR-UWB, as this standard is primarily designed for positioning purposes.

The standards presented here will now be examined in more detail in the following Sections. The focus will be on a brief introduction to the specification, the network topology and the lower protocol layers.

2.3 IEEE 802.11: Wi-Fi

Wi-Fi represents a wireless communication standard initially specified by the IEEE under the primary identifier 802.11 in 1997. Since then, it has undergone constant enhancements and refinements.

Although the fundamental idea was to wirelessly connect clients to networks, thus ensuring straightforward and rapid access, it took seven years before the first version of the 802.11 standard was ratified. Initially, due to the low data rates of just 2 Mbps and limited support of devices utilising this technology, Wi-Fi did not gain widespread popularity and it was originally employed when data transmission via cable connections was either not possible or only feasible with significant effort (51, Chapter 1). A marked increase in Wi-Fi-compatible devices was only noted with the rising popularity of laptops and the desire for constant, location-independent internet connection via radio contributed to the success of the technology by facilitating flexibility and mobility (52, p. 438f). Today's 802.11 devices achieve transmission rates of several Gbps and support a variety of multimedia applications, including Voice over Internet Protocol (VoIP) and video streaming.

To support and ensure the establishment of WLAN technology, the Wi-Fi Alliance was founded in 1999. This non-profit organisation consists of leading manufacturers of Wi-Fi technology, electronics, and consumer goods, and verifies device compatibility according to the Wi-Fi standard for certification (53, p. 428). Currently, the organisation comprises over 300 members, including Microsoft, Sony, Texas Instruments, Intel, Dell, Philips, and Nokia.

Over the past 20 years, numerous 802.11 standards have been released, some of which found less favour while others still dominate today's Wi-Fi devices, including:

- 802.11g: This standard, introduced in 2003, implemented the most recently standardised physical layer and is still widely preferred for networks in the ISM band.

- 802.11n: An extension of the a and g standards with a higher data rate and Multiple Input Multiple Output (MIMO) technology, as well as operation in the 2.4 GHz and 5 GHz bands.
- 802.11ac: An extension of 802.11n with data rates up to several Gbps, introduced in 2013.
- 802.11ax: Already in use, with the first devices being available on the market since 2019. It further improves the ac standard, achieving even greater throughput and higher data rates.

The 802.11 Wi-Fi specification distinguishes between three essential **network topologies** (52, p. 16ff):

- The simplest topology is an ad-hoc network, referred to as an **Independent Basic Service Set** (IBSS), with which even two wireless devices can establish a Wi-Fi connection. This configuration requires no additional active elements as each device forms a radio cell, and as long as the devices are within a cell or the cells overlap, communication between various devices is possible. However, this type of topology is relatively uncommon for 802.11 WLANs and is rarely utilised. Such ad-hoc networks are more frequently used with infrared and Bluetooth wireless standards.
- If the range of a radio cell is too small, it can be extended by an Access Point (AP). When one device needs to communicate with another, it sends the data to the AP, which then forwards the data to the destination. Moreover, the AP can act as a bridge or switch and establish a connection to another WLAN or any LAN network. This type of topology is known as an **Infrastructure Basic Service Set (BSS)**.
- However, even the Infrastructure BSS has limited coverage, which can be expanded by connecting several BSSs to an **Extended Service Set (ESS)** (see Figure 3). Within an ESS, the BSS can be changed automatically without additional management in a process referred to as roaming. Linking several access points of the BSSs can be facilitated by a backbone network, which could be a LAN, for instance. All access points within an ESS share the same Service Set ID, which serves as the network "name" for users.

The 802.11 standards do not contain information on the location of individual BSSs which may be spatially separated or partially or entirely overlap, making it possible to wirelessly network larger spatial areas.

The operation of the 802.11 standard is primarily specified at the physical and MAC layers. The **physical layer** is divided into two sub-layers: the Physical Layer Convergence Procedure (PLCP) layer and the Physical Medium Dependent (PMD) layer. The PLCP serves as the interface between radio transmission and the MAC layer, adding its own header with a preamble to aid in synchronising the transmission. The PMD's main task is to transmit the bits coming from the PLCP via radio, which involves framing, scrambling, and modulating the signal (53, pp. 422).

Initially, bits were transmitted using a Frequency Hopping Spread Spectrum (FHSS) and the Direct Sequence Spread Spectrum (DSSS) method. Moreover, a physical infrared layer was defined but remained largely unknown. Subsequent revisions of 802.11 added additional methods that have established themselves to this day, particularly the Orthogonal Frequency Division Multiplexing (OFDM) approach that is mainly used in 802.11a, 802.11g, and the newer standards.

OFDM is a multicarrier technique and diverges significantly from FHSS and DSSS as, instead of modulating a single carrier, several thousand carriers are modulated simultaneously. Each individual carrier is modulated with Quadrature Amplitude Modulation (QAM), which combines Phase Shift Keying (PSK) and Amplitude Shift Keying (ASK). A possible constellation of a 16-QAM signal compared to a Bi-Phase Shift Keying (BPSK) signal is shown in Figure 2.4 and demonstrates the efficiency of QAM, which allows the transmission of 4 bits per symbol due to varying phase and amplitude states (cf. 54, p. 382f).

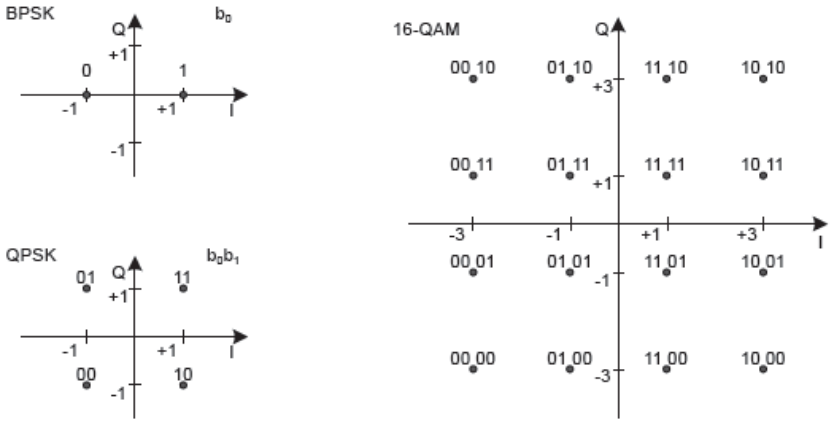

FIGURE 2.4: BPSK, QPSK, and a 64-QAM constellation diagram (54, p. 383)

The data is transmitted in parallel, allowing high data rates and high throughput. To be able to distinguish the individual signals when demodulating at the receiver, the carriers must be orthogonal in the frequency space since this makes them less likely to influence each other. Figure 2.5 shows an example of this in which the subcarrier allocation for the 802.11a OFDM signal is portrayed with a total of 52 subcarriers, including 48

subcarriers for data and four subcarriers for pilot data. The data subcarriers are all modulated using the same scheme, with the control rate defined in the PLCP header. The pilot subcarriers are used to increase the robustness of the coherent acquisition to frequency shifts and phase noise. To avoid the generation of spectral lines, they are modulated with a pseudo-binary BPSK sequence.

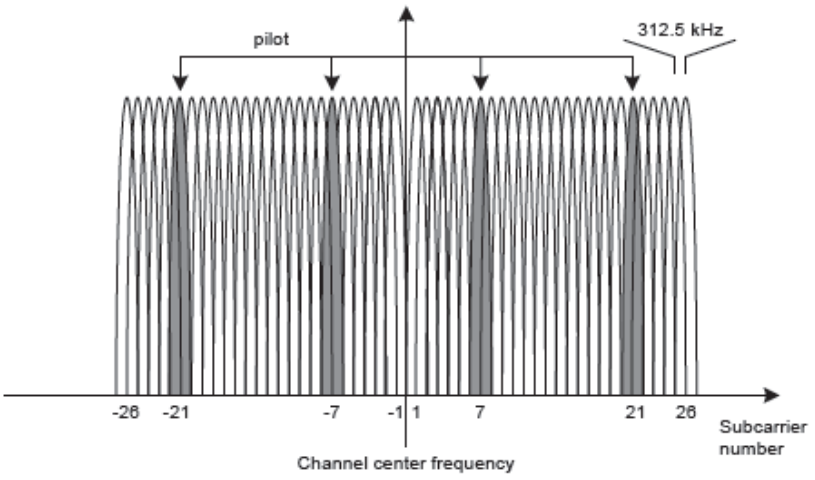

FIGURE 2.5: IEEE 802.11a OFDM subcarrier (54, p. 379)

The **MAC layer** describes a set of rules that define how to access the media and send data, whereby the access method is specified in detail and is also called a Distributed Coordination Function (DCF). The MAC protocol employs Carrier Sense Multiple Access-Collision Avoidance (CSMA-CA) for the DCF. In contrast to the wired versions of Ethernet (which use CSMA - Collision Detection (CD)), Wi-Fi does not use collision detection because collisions cannot be distinguished from interfering signals in a wireless network and thus collision avoidance is used instead. As an option, the prioritisation of the packets can also be specified in the MAC layer and these are handled by the Point Coordination Function. The LLC sublayer, on the other hand, is used more uniformly and describes how to access the various techniques used in the MAC layer (54).

2.4 IEEE 802.15.1: Bluetooth

Bluetooth is a standard for a universal wireless interface and is frequently used to connect portable devices such as mobile phones, wearables, headphones, or laptops.

Until the 1990s, infrared was used for such connections. However, infrared has the disadvantage that it requires direct Line-of-Sight (LoS) (55) and thus, in 1994, Ericsson started a feasibility study to develop a radio-based replacement that could overcome the difficulties encountered when using infrared. The result of the study was a successful

exploration of a radio-based technology, and a few years later, based on this architecture, the Bluetooth Special Interest Group (SIG) was founded together with well-known manufacturers such as Ericsson, Nokia, IBM, Toshiba, and Intel. To date, the SIG boasts a membership of 34000 companies, and several standards with ongoing improvements have been designed (56, p. 10f).

The first final specification, version SIG 1.0a, was published in July 1999, and version 1.0 B followed in December 1999. Two years later, in February 2001, version 1.1 was released, which comprised the first serious description for consumer products, as the previous versions had some inaccuracies, errors, and security issues. From this specification, the IEEE derived the 802.15.1 standard for a WPAN and since then, it has been involved in the further development of the Bluetooth standard. However, the IEEE project only addressed the lower two layers, namely the data link and the MAC layers.

In version 1.2, published in 2003, Adaptive Frequency Hopping was added which made the technology less sensitive to noise, while new packets for synchronous transmission were also introduced. Since then, although the Bluetooth standard has continuously evolved, it was no longer ratified by the IEEE but was mainly advanced by the SIG (49, p. 256). In 2004, standard 2.0 followed, adding new features and an increased data rate of up to 2.1 Mbps and in 2009, Bluetooth 3.0 primarily introduced a high-speed service with transfer speeds of up to 24 Mbps, based on a hybrid connection with Wi-Fi. Some other improvements, such as enhanced power control, complemented the specification. However, later versions of Bluetooth no longer use this high-speed service. Bluetooth 4.0 was released in 2010 and its main feature is the low-power protocol, which facilitates a very energy-efficient use of Bluetooth and enabled its application in cost-reduced single-chip systems, thereby allowing the use of Bluetooth in highly integrated and compact devices. The latest standard is Bluetooth 5.0, with an improved range and an optimised data rate of 2 Mbps.

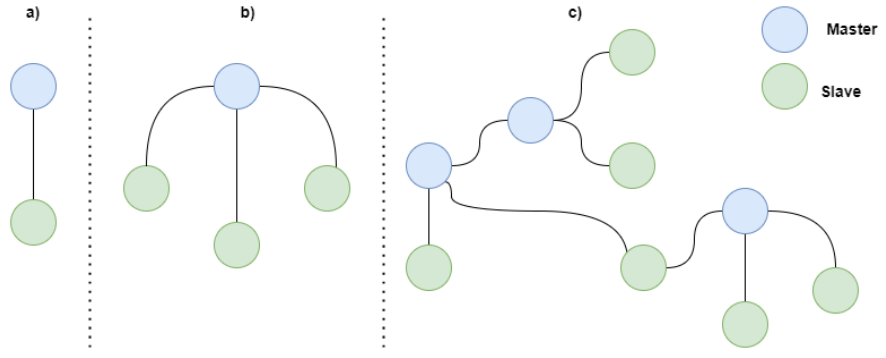

FIGURE 2.6: Piconet/Scatternet (57, p. 65)

Bluetooth is based on so-called wireless **Ad-hoc Piconets** which are local networks that require no infrastructure. Each device can communicate with up to seven devices within a Piconet at the same time and a given device can be a member of multiple Piconets,

thereby making the protocol very flexible and extendable. Such a Piconet consists of a master and up to eight slave nodes. Figure 2.6 shows a) a Piconet with one slave and b) with multiple slaves.

In addition to the seven active slave nodes, other nodes may be present, one of which is called a parked device. Although these nodes cannot actively communicate and have no connection, they are known in the Piconet and can be reactivated within milliseconds. Another group of nodes comprises devices in standby mode that do not participate in the Piconet and have no address. As FHSS is used, the devices within a Piconet must be synchronised with each other. Therefore, the first step in setting up a Piconet is for the future master device to send its globally unique 48-bit device address and the value of its internal clock, which determines the hop sequence. However, as all devices in a Piconet follow the same hop sequence, they occupy the same 1 MHz channel and thus the throughput decreases as more devices are added to a Piconet.

As a workaround, **Scatternets** were introduced and Figure 2.6 c shows a Bluetooth Scatternet consisting of three Piconets. In this example, a slave device is a member of both Piconets although each Piconet has its own hop sequence, which is defined by the master device. If a device wants to participate in more than one Piconet, it has to synchronise with the Piconet it wants to use at a certain time. After synchronisation, it is a slave in the new Piconet but not a member of the Piconet it previously participated in.

Bluetooth devices are divided into several performance classes, as shown in Table 2.1 and manufacturers are free to choose which class to apply to their devices. However, there is sometimes a relationship between profiles and power classes, as profiles are often used for a specific application (type) and peripherals such as mice, keyboards, or mobile phones with small batteries are often classified as Class 2 while printers, modems and laptops are often classified as Class 1 with a power of 100 mW (53, p. 471f).

Table 2.1: Bluetooth performance classes

Class	**Maximum permitted power**		**Range**
	(mW)	(dBm)	up to (m)
Class 1	100	20	100
Class 1.5 (low power)	10	10	30
Class 2	2.4	4	10
Class 3	1	0	1

The basic sublayers of the Bluetooth standard are the radio layer and baseband in the physical layer, and the Link Manager Protocol (LMP) and Link Control and Adaptation Protocol (L2CAP) in the MAC layer. These are also governed by the IEEE 802.15.1

standard. The higher layers are application-specific and are defined and managed by the SIG and summarised as Application Related Profiles (see 58, p. 233ff):

- **Radio Layer** – This layer is responsible for the radio transmission, frequencies used, modulations, and output power. It operates in the 2.4 GHz ISM band and consists of 79 channels, each occupying 1 MHz. There is a guard band at the lower end with a bandwidth of 2 MHz and a 3.5 MHz band at the upper end which avoids out-of-band interference with other radio services. The frequency hopping spread spectrum combined with Time Division Duplexing (TDD) is used for transmission. A channel is divided into 625 μs slots and each slot uses a different hop frequency which results in a hop rate of 1600 hops per second. Since the slots are allocated according to the TDD scheme, the transmitter and receiver are allowed to transmit alternately.

- **Baseband** – This layer describes the connection establishment, together with the framing and timing mechanisms. Bluetooth supports two main types of connection: Synchronous Connection-oriented (SCO) and Asynchronous Connectionless (ACL) logical transport, whereby SCO connections are mainly used for traditional voice transmission such as those required for telephony services. Two consecutive slots are booked at fixed intervals and thus a fixed bandwidth is reserved, allowing a maximum of three SCO connections per device. ACL links are used for typical data applications and provide packet-switched point-to-multipoint connections and broadcast services in which only one connection is possible between master and slave.

- **Link Manager** – The link management protocol extends the baseband layer but does not completely cover the baseband layer, and thus some upper layers can still access it. LMP packets are transmitted over ACL links and identified by a special entry in the packet header. The link manager provides several functions like the authentication & encryption, synchronisation or power control.

The remaining layers consist of several different protocols that are often summarised as the middleware layer. Above the L2CAP layer is the Radio Frequency Communication (RFCOMM) layer, which emulates serial interfaces to replace cables. The Host Controller Interface (HCI) provides access to the baseband and primarily acts as an interface between hardware and software. Above this are the protocols for the application-specific profiles, such as telephony management.

2.5 IEEE 802.15.4: Low-Rate WPAN

2.5.1 Specification

The IEEE 802.15.4 standard was published in 2003 and is aimed at networks that do not necessarily need to be connected to the internet but prefer a cost-effective solution with as little complexity and communication overhead as possible. This includes wireless devices used in the home, such as fridges, door openers, and heating systems, which can benefit from exchanging information with each other. However, even in the industrial sector or for monitoring environmental parameters, networks do not necessarily need to be connected to the Internet and other factors are important instead, such as the longevity of the sensors, which requires an energy-efficient and Internet-independent network (see 59, p. 351). Wireless Sensor Networks (WSNs) which were specifically targeted by this standard, are a good example of this.

The 802.15.4 standard describes the requirements for the physical and MAC layers. It was decided not to define the LLC layer but rather to allow protocols to define it at the discretion of the application and directly communicate with the MAC layer, for example. The standard has been extended and revised several times with the most important revisions being made in 2011 and 2015, when alternative communication techniques and procedures were added to the physical and MAC layers, respectively, to ensure support for more applications, especially in the industrial sector:

- 802.14.4-2011: including the integration of IR-UWB for higher data rate communication and distance measurement (see Subsection 2.5.5.1).
- 802.15.4-2015: including the addition of several MAC schemes for deterministic networks, which is especially used in the industrial sector (see Subsection 2.5.5.2).

2.5.2 Network topology

For communication between network devices, the IEEE 802.15.4 standard allows the deployment of star and peer-to-peer topologies (see 60, p. 49):

- In the **star topology**, there is a central unit called the PAN coordinator through which communication is handled. The PAN coordinator is also responsible for managing all the major network functions. This topology is particularly suitable for time-critical applications as network congestion can occur if all sending and receiving are done through the coordinator.

- In the **peer-to-peer topology** there is still a PAN coordinator. However, each network device can communicate with any other device within its range which allows the topology to form more complex network formations, such as ad-hoc and self-configuring networks. The routing mechanisms required for multi-hopping are part of the network layer and thus outside the scope of IEEE 802.15.4.

An example of what such a network formation might look like can be illustrated using the Zigbee protocol which was published by the ZigBee Alliance in 2003 and has since been used in many WSN applications. It consists of several layers that are stacked on top of the MAC layer, allowing for additional network formations, security features, and interoperable application profiles. The addition of a network layer thus extends the properties of the 802.15.4 standard, as there are no restrictions on network formation. Overall, the Zigbee protocol defines two types of devices. A Full Functional Device (FFD) can take on any role and function within the network while a Reduced Functional Device (RFD) has a reduced scope and can, for example, only communicate with FFD devices. Both types of devices can take on different roles within the network, including (see 60, p. 48):

- **ZigBee coordinator**: This is an FFD responsible for forwarding, coordinating, initiating, capturing, and storing tasks (network information, security keys). This device forms the origin of the network and a bridge to other networks. Generally, a ZigBee coordinator is assigned to every network.
- **ZigBee router**: This is also an FFD that acts as an intermediate router for the transmission of data from one device to another.
- **ZigBee end device**: This is a low-power device that can only communicate with the parent node, which could either be a coordinator or a router. On the other hand, it cannot forward data from other devices. This technique allows for extending the battery life since the node can be in sleep mode for a considerable time. A ZigBee end device is usually an RFD and generally has a small memory size and limited processing capabilities and functions. Therefore, it is typically the least expensive device in the network.

The **star topology** is no different from the previously described star topology of the 802.15.4 network. It consists of a coordinator, which is responsible for the network, and several end devices that communicate directly with the coordinator.

A **mesh network** allows for full peer-to-peer communication, where packets go through multiple hops to reach destinations. It usually consists of a coordinator, several routers, and end devices. The network coordinators are responsible for network initiation and maintenance while routers can be used to extend network coverage.

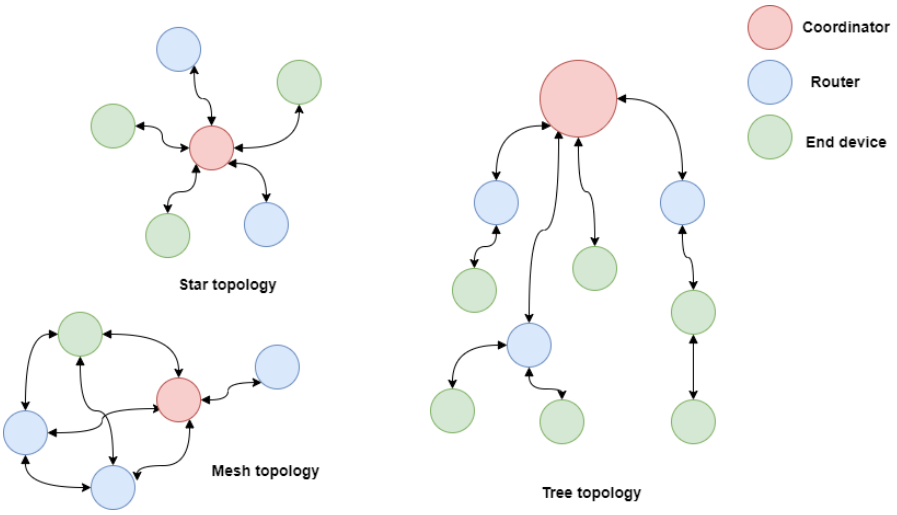

FIGURE 2.7: Zigbee topologies

The **tree topology** is the combination of the star and mesh networks and has the characteristics of both topologies, whereby the coordinator is connected to multiple routers and end devices (subordinate coordinators) and is responsible for network initiation and maintenance, as shown in Figure 2.8. The router is used to extend the network and control the flow of data using hierarchical routing strategies within the network.

2.5.3 Protocol stack

The standard version spreads the signal in the physical layer using DSSS, which is then modulated using Offset Quadrature Phase Shift Keying (QPSK). The data rate is 250 kbps in the unlicensed 2.4 GHz ISM band, 40 kbps at 915 MHz, and 20 kbps at 868 MHz whereby a higher-order modulation scheme is responsible for the higher rate and the lower frequencies are typically used when longer ranges are required. However, throughput is lower and latency is higher and a total of 16 channels are available between 2.4 and 2.4835 GHz. The channels can be selected dynamically by using a scan function in the MAC layer, which scans a list of supported channels when searching for a beacon. The physical layer is responsible for energy detection, link quality indication, and channel switching. The network uses these functions to establish its initial operating channel and to change it if a prolonged failure is detected (see (61)).

The standard also specifies that data is transmitted at 1 mW and, as a result, ranges of 10–20 m are typically achieved although, depending on the application requirements, the actual transmission power may be lower. While mesh network topologies can be an attractive alternative for applications requiring greater range, much higher latencies can be expected due to multi-hopping.

In total, the physical layer provides two services, the PHY data service and the PHY management service, which are responsible for managing the link. To simplify communication with the MAC layer, both services use the same frame structure, the so-called physical protocol data unit (PPDU) as shown in Figure 2.8.

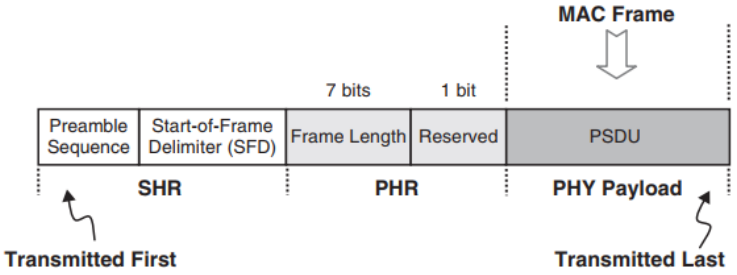

FIGURE 2.8: PPDU format (49, p. 44)

Each PPDU contains a synchronisation header that consists of the preamble and the start of frame delimiter. The 32-bit preamble is designed to capture symbol and chip timing and can also be used for coarse frequency settings in some cases. The PPDU also contains a PHY header and a physical service data unit (PSDU). Within the PHY header, 7 bits are used to indicate the length of the payload in bytes, which results in a supported packet size between 0 and 127 bytes. When reading sensor data, as in many Smart Home applications, packet sizes are in the order of 30–60 bytes. However, if more information is exchanged or more bytes are used for addressing due to multi-hopping, the packet size will increase.

The **MAC layer** has several functions and is responsible for device registration and deregistration, beacon management, frame delivery and validation, access control, and time slot (TS) management. It also supports encryption although the exchange of keys is delegated to higher layers (49, Chapter 3.3).

In the 802 family, the LLC sublayer is typically used above the MAC layer and, together with the MAC layer, it forms the data link layer. The LLC layer is responsible for multiplexing the protocols transported over the MAC layer, as well as flow control and detection, and retransmission of lost packets. However, the IEEE 802.15.4 standard has left open the possibility of communicating with the LLC layer via the Service Specific Convergence Sublayer (SSCS). Another commonly used option is to access the MAC layer directly through the higher layers, as shown in Figure 2.9.

Many proprietary networks, as well as the ZigBee standard, use this path to interact with the MAC layer which opens up new possibilities for network design. The MAC layer provides two different services to exchange data and configuration with higher layers, namely the MAC Data Service and the MAC Management Service. The MAC Data Service provides a mechanism for passing data to and from the next higher layer while the

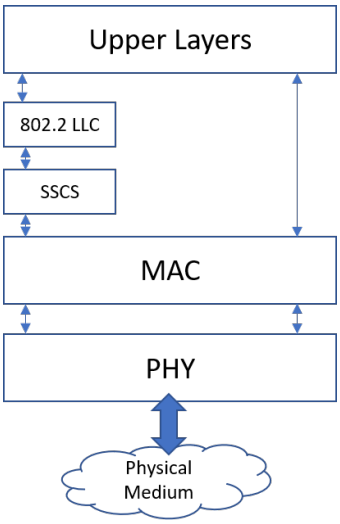

FIGURE 2.9: 802.15.4 stack (61, p. 9)

MAC Management Service offers mechanisms to control the settings for communication, radio, and network functions from the next higher layer.

The MAC layer uses the CSMA-CA method for access control and, depending on the network configuration in beacon or non-beacon mode, there is a distinction between slotted and unslotted CSMA-CA.

In simple unslotted mode, there is no beacon synchronisation and participants use the CSMA-CA access procedure to send their messages. Each participant checks whether the channel is busy before sending and, if it is, they wait for a random period of time before trying to send again. After several attempts, a transmission error is signalled. The disadvantage is that both the transmitter and receiver must be active at all times and cannot take advantage of a low-power mode.

The more complex slotted mode synchronises transmission by assigning a superframe. This is especially important for applications that require low latency and some bandwidth. The superframe consists of an active and an optional inactive period, during which the network nodes and the PAN coordinator are in low-power mode and do not occupy the channel. The interval size of the beacons can vary between 15 ms and 245 seconds. Regardless of the interval size, the time in the active period is divided into 16 equal time slots during which the participants can communicate with the PAN coordinator. The active period is further divided into the Contention Access Period (CAP) and the Contention-Free Period (CFP), as shown in Figure 2.10.

In the CAP, channel access is controlled by a slotted CSMA-CA scheme in which the back-off time is synchronised with the time slots and the channel is thus open to all users at the same time. The first station to occupy the channel continues to transmit until its transmission is finished. If another participant notices that the channel is

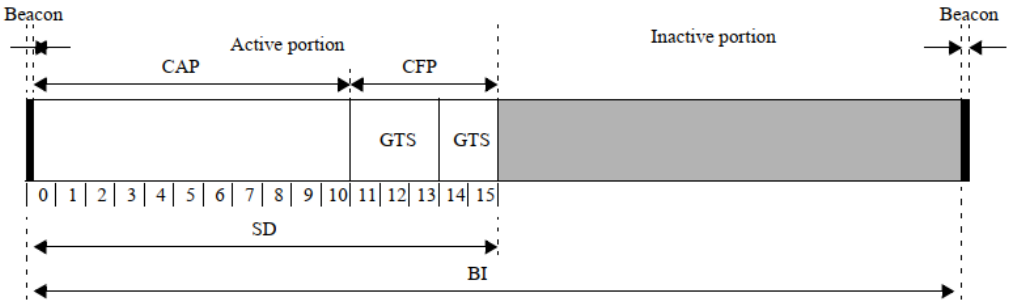

FIGURE 2.10: An example of the superframe structure (62, p. 58)

occupied, it waits a random back-off time and tries again. While this procedure is most commonly used in large networks, there is no guarantee that participants will be able to use the channel when they need it. In CFP, TSs can be assigned exclusively to certain participants in the network in so-called Guaranteed Time Slots (GTS). The PAN coordinator can assign up to seven GTS, and a GTS can occupy more than one TS, which means that participants do not have to use CSMA-CA to gain access to the channel. This option is especially beneficial for low latency applications where potentially long wait periods for the channel to become free cannot be tolerated. The use of CSMA-CA is not permitted during this time.

Other layers are not defined in the 802.15.4 standard and are part of the application. The most popular protocol, Zigbee, is also based on this standard. However, the CSMA-CA method used here also has some weaknesses. In particular, it is not suitable for deterministic and time-critical applications because access to the channel is not exclusively granted by the CSMA-CA mechanism and, instead, participants compete for free slots to transmit data. As a result, as the number of nodes increases, the packet delivery rate decreases, so that not all packets can be delivered in time, as shown in (63) and Figure 2.11.

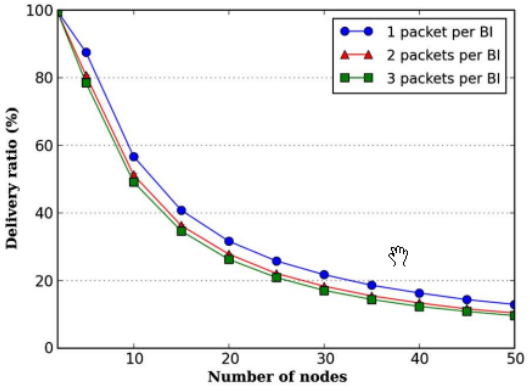

FIGURE 2.11: Impact of the packet generation rate on the delivery ratio (63, p. 59)

CSMA-CA also has other disadvantages. For example, collisions can occur when two nodes are so far apart that they can communicate with the PAN coordinator and receive

its beacons, but cannot receive each other. This can lead to both participants transmitting at the same time, assuming that the channel is not occupied. Finally, using the original IEEE 802.1.5.4 standard, a minimum theoretical refresh time of a sensor is not less than 15.36 ms, which is not acceptable in industrial real-time systems (64, Chapter 2).

Industrial protocols attempt to address these and other weaknesses by placing more stringent requirements on communication in terms of determinism, latency, reliability, and interference. In particular, the WirelessHART and ISA100.11a protocols are worth mentioning. They use the physical layer of the 802.15.4 standard but feature some modifications in the MAC layer to eliminate the weaknesses mentioned above and to incorporate other functions to make the protocol more robust and reliable.

2.5.4 Industrial standards

2.5.4.1 WirelessHART

WirelessHART is the wireless version of the Highway Addressable Remote Transducer (HART) protocol, which is widely used in automation and industrial applications. The protocol was specified in 2007 as part of HART 7 and is compatible with current HART devices, tools, and systems. It is based on the 802.15.4 physical layer and, like ZigBee, operates in the unlicensed ISM band at 2.4 GHz. The specification also allows the use of IEEE 802.15.4-2006 compliant 2.4 GHz DSSS transceivers and supports star and mesh topologies, or a combination of both, to improve network scalability. It also offers high reliability and immunity to interference, making it ideal for time-critical industrial applications. Its other features include the self-organisation and self-healing capabilities of the network while integrity and security are achieved by synchronising time and using encryption (60, p. 53).

In contrast to the IEEE 802.15.4 Data Link Layer, WirelessHART uses a modified version of the MAC layer. By using the Time Synchronised Mesh Protocol (TSMP), mechanisms are introduced into the MAC layer to make communication deterministic and reliable. This is achieved by using a Time Division Multiplexing (TDMA) technique in combination with a frequency hopping method. TDMA is a commonly used access method to ensure collision-free and deterministic communication whereby all data traffic takes place within a fixed TS with a duration of 10 ms. Communication between one or more source and destination devices can therefore be scheduled to take place in a specific TS and the time slot can be allocated to a single source device or support communication between multiple devices (19, Chapter 31.4.2). Within the TS, at least one message and the Acknowledge (ACK) are always sent to signal that the message has been received at the destination device. However, no ACK is sent for a broadcast message.

Multiple timeslots form a TDMA superframe as shown in Figure 2.12 and all devices must support multiple superframes, starting with superframe zero. At least one superframe is always active, while additional superframes can be activated or deactivated. The superframe length is also fixed, forming a network cycle with a fixed repetition rate so that superframes can continuously be repeated.

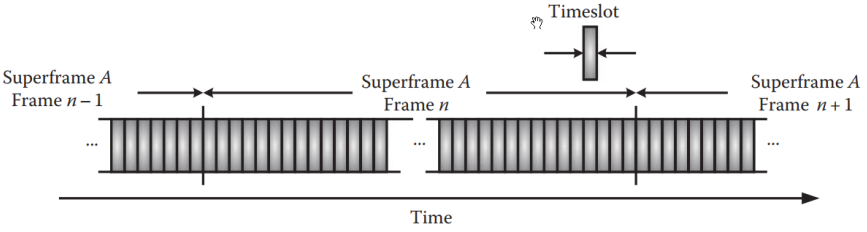

FIGURE 2.12: Structure of TDMA timeslots, superframes, and frames (19, pp. 33-6)

To increase reliability, channel hopping is combined with TDMA (65, p. 9711). Channel hopping provides frequency diversity, which helps to avoid interference and reduce multipath fading effects. TDMA enables efficient, low-power and reliable channel-hopping communications, also known as Time-slotted Channel Hopping. An example of this method is shown in Figure 2.13.

All devices must support multiple connections, whereby the number of possible connections is usually equal to the number of channels used by a network multiplied by the number of slots in the superframe. For example, using 15 channels and 9000 slots per superframe results in 135000 possible connections. An example of this method is shown in Figure 2.13 with 15 channels and 15 time slots. Channel hopping provides channel diversity so that each slot can simultaneously be used by different devices on multiple channels. This can be achieved by creating links on the same timeslot but with different channel offsets. Each device must have a list of the channels it uses, and all devices on a network must have identical channel lists. To increase robustness against interference, individual channels can also be excluded using channel blacklisting (19, pp. 31-9). This is particularly useful when other networks or other wireless connections are in use.

2.5.4.2 ISA 100.11a

The ISA100.11a open standard was introduced in September 2009 by the ISA100 Standardisation Committee, part of the non-profit International Society of Automation (ISA). Its purpose is to support the use of wireless networks in industrial monitoring and control of automation processes by providing reliable and deterministic communication. ISA100.11a upholds star and mesh topologies and operates in the unlicensed 2.4 GHz ISM frequency band. It supports the physical layer of the IEEE 802.15.4 standard, such as WirelessHART and uses a channel-hopping method to facilitate the coexistence with

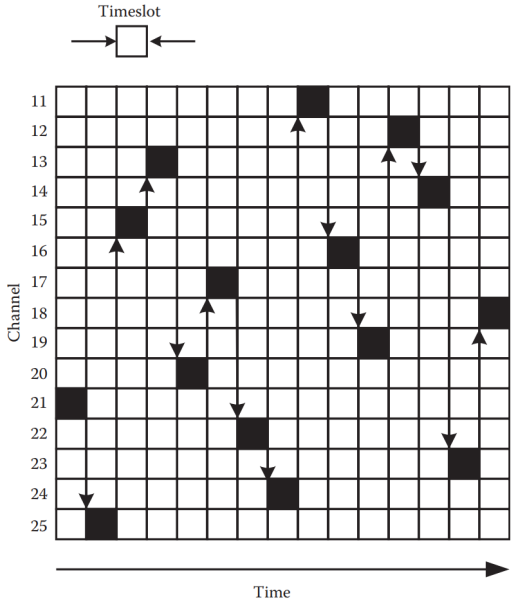

FIGURE 2.13: WirelessHART and ISA100.11a (slotted) frequency hopping (19, pp. 33-6)

other networks and increase reliability, by focusing on low power consumption, scalability, robustness, and interoperability with other industrial standards (19, Chapter 32).

The ISA100.11a DLL is very similar to the WirelessHART DLL, with some variations in structure and extensions in functionality. It is divided into a MAC sublayer, a MAC extension layer, and a top DLL. The MAC sublayer is a subset of the IEEE 802.15.4 MAC layer and ensures compatibility with the services and functions of the IEEE standard for sending and receiving messages. However, the MAC extension layer provides additional functionality not supported by IEEE 802.15.4, primarily by adding additional time-division multiplexing and frequency-hopping techniques. The upper DLL handles link and mesh aspects above the MAC layer and is responsible for routing. This is a significant difference from WirelessHART and ZigBee, where routing is done at the higher layer of the network layer (66).

For communication security in the DLL layer, ISA uses a 4–16 byte long Message Integrity Code (MIC) to ensure data confidentiality. Unlike WirelessHART, the length of the time slots is freely configurable and the superframe structure is adjustable. By adjusting the time slots, stations can send a message that can be received and acknowledged by multiple devices in the same slot. Furthermore, ISA100.11a supports channel blacklisting, for example when additional networks are in operation and certain channels are occupied. As mentioned earlier, ISA also uses the TSCH method, although this has been enhanced by the addition of an adaptive hopping method (19, Chapter 32-11). By

measuring the sensitivity to interference and switching to less disturbed channels, reliability is improved by avoiding occupied channels and reducing the utilisation of a single channel. This improves the coexistence of ISA100.11a with other networks in the same spectrum but introduces some overhead by requiring additional data to be exchanged concerning the channel state and selection.

The TS configuration can follow two different patterns: Slotted Channel Hopping and Slow Channel Hopping, whereby both methods can naturally also be combined. With Slow Channel Hopping, time slots can be grouped together to be transmitted on a single frequency channel which is especially useful when large amounts of data are being transmitted, such as during a firmware upgrade upload or calibration checks. Unlike regular channel hopping, Slotted Channel Hopping uses CSMA-CA to control access to the time slots on each channel. This has the advantage that stations that are ready to transmit can send their messages more quickly. However, all devices must constantly check the occupancy of the channel, which is why the procedure also requires a higher power consumption.

In addition, as is the case with WirelessHART, the term frame is used to separate instances of a particular superframe over time, as shown in Figure 2.12.

The protocol can support multiple superframes of variable length. To monitor communication within a network, the system manager assigns a source and a destination device to a time slot, similar to WirelessHART. Within a single time slot, the source device sends a data packet to the target device. After successfully receiving a data packet, the target device sends an ACK packet back to the source device. If the sender does not receive an ACK, the packet is retransmitted during the next available time slot. ISA also provides the ability to send broadcast messages by designating multiple devices in the same time slot as target devices.

To further increase efficiency, routing based on graphs is also performed in the upper DLL. This simplifies and speeds up the routing of data and also results in power savings. However, WirelessHART and ISA100.11a can be expected to have very high latency, sometimes more than one second, due to their ability to perform multi-hops (67).

2.5.5 Extensions

2.5.5.1 Ultra-wideband

Ultra-Wideband (UWB) technology was introduced by the Office of the Secretary of Defense/Defense Advanced Research Project Agency (OSD/DARPA) in the 1980s. It is a promising technology that gained popularity after the Federal Communications Commission (FCC) in the USA allowed unlicensed use of UWB devices subject to emission

limits in February 2002. Power was limited to -41.3 dBm/MHz between 3.1 GHz and 10.6 GHz (68, p. 48). Europe, Japan, and several other countries followed suit a few years later but to this day there are differences in the frequency range in which UWB can be used, as shown in Figure 2.14.

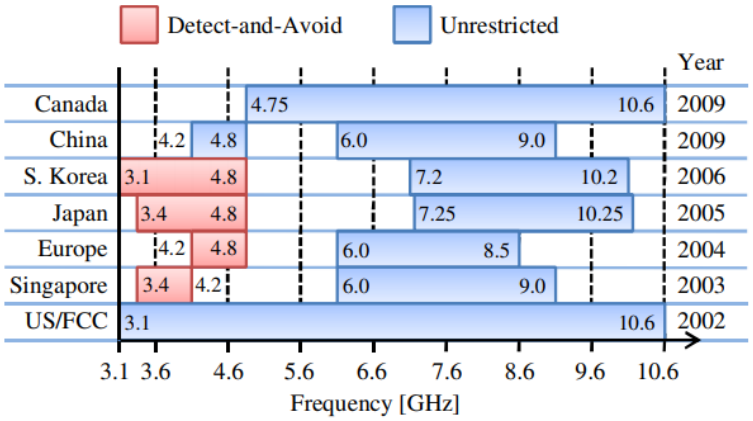

FIGURE 2.14: UWB Spectrum for different regions (69, Figure 1)

The IEEE has also been trying to promote this technology since 2001 and, as mentioned earlier, the IEEE 802.15.3 standard that enabled UWB-based communication at very high data rates in the WPAN range was published in 2004. However, this standard failed to gain traction due to competing interests and was abandoned. Only a few years later, the IEEE made another attempt to exploit the promising technology. This time, however, the focus was on wireless sensor networks with lower data rates and the ability to perform distance measurements. This proposal was specified in an extension to the 802.15.4 standard for the physical layer, labelled "a", and was incorporated into the regular standard IEEE 802.15.4-2011 in 2011 (70, p. 874).

IEEE 802.15.4a is the first international standard to specify a wireless physical layer to enable accurate distance measurement. As a modification of the popular IEEE 802.15.4-2006 standard, the IEEE 802.15.4a extension adds new functions to the physical layer to achieve higher data rates, extended range, and improved interference resistance and mobility, thereby enabling new applications based on the distance information of devices in the low-rate WPAN. The final version of IEEE 802.15.4a in March 2007 specifies two additional physical layers (68, Table 1):

- An IR-UWB physical layer operating in the unlicensed UWB spectrum
- A Chirp Spread Spectrum (CSS) physical layer operating in the unlicensed 2.4 GHz spectrum

The IR-UWB PHY layer defined in IEEE 802.15.4a is used to achieve higher throughput, lower latency, or lower duty cycles. It is very efficient, can perform precision ranging, and is very robust even at low transmit power levels (68).

A UWB signal is known for its very large bandwidth compared to conventional narrowband systems since it occupies a much wider frequency band as shown in Figure 2.15. This characteristic allows UWB technology to offer significant advantages, including high data rates, high multi-path resistance, high penetration capacity, and precise positioning capabilities.

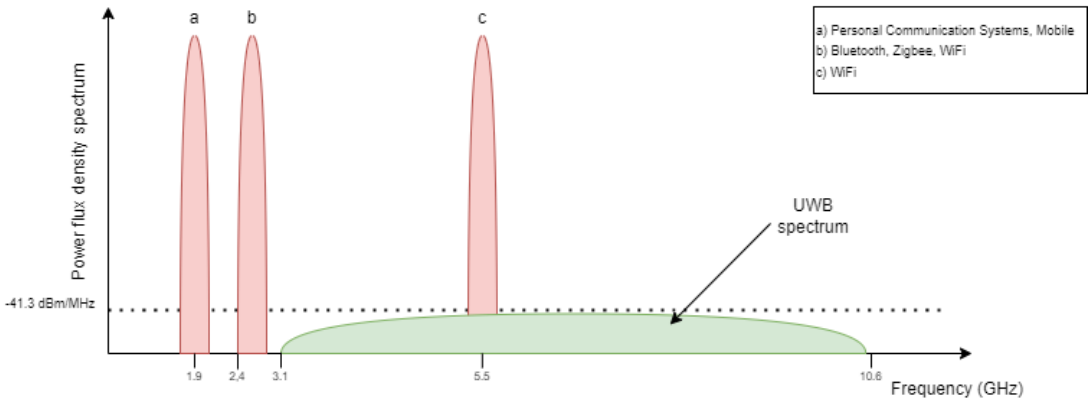

FIGURE 2.15: Frequency occupation for different systems (71, Figure 2.6)

It must have an absolute bandwidth of at least 500 MHz or a normalised bandwidth greater than 20%. The absolute bandwidth is calculated as the difference between the upper frequency (f_H) of the "-10 dB emission point" and the lower frequency (f_L), starting from the "-10 dB emission point", as shown in Equation (2.1) (cf. (71, p. 20f):

$$B = f_H - f_L \tag{2.1}$$

Therefore, the normalised bandwidth (B_{frac}) is formulated as follows

$$B_{frac} = B/f_c \tag{2.2}$$

where (f_c) is the centre frequency with

$$f_c = (f_H + f_L)/2 \tag{2.3}$$

From Equations (2.2) and (2.3), the normalised bandwidth (B_{frac}) can be expressed as

$$B_{frac} = 2(f_H - f_L)/(f_H + f_L) \tag{2.4}$$

The Shannon capacity formula illustrates the advantages of UWB signals for high-speed data transmission. It states that the data rate of a channel – for a given Signal-to-Noise Ratio (SNR) – increases with increasing bandwidth B (see (71, p. 24)):

$$C = B \log_2(1 + \text{SNR}) \ \text{(bits/second)} \tag{2.5}$$

The implication is that the more bandwidth available, the greater the amount of information that can be transmitted from a transmitter to a receiver, as shown in Figure 2.16.

With very wide bandwidths, such as those provided by UWB, the signal strength can even be reduced. This has two significant benefits: firstly, it extends the battery life of devices as less energy is required for transmission, and secondly, it minimises the interference that could affect other systems operating in the same frequency range.

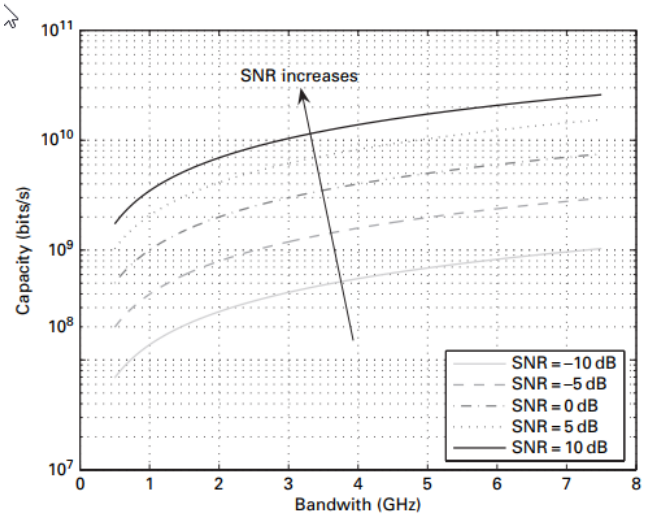

FIGURE 2.16: Capacity vs bandwidth for different UWB systems (71, Figure 2.5)

The UWB signal at the physical layer is based on an impulse radio approach, whereby information is carried by a defined sequence of short data pulses, rather than being modulated onto a carrier frequency. This allows a UWB system to operate in the baseband, i.e. UWB pulses can be transmitted without a sinusoidal carrier frequency (carrier-free). In this case, the system does not require any IF processing, which enables low-cost implementations. Typically, the data pulses are in the order of a nanosecond per information symbol, with information carried by the positions or polarities. Each pulse is contained within an interval called a frame, and the positions of the pulses within the frame are determined according to a Time-hopping Code by assigning a specific time-shift pattern. Figure 2.17 shows examples of IR-UWB signals with a rectangular pulse and a Gaussian pulse in the time domain. The spectrum of the rectangular pulse (a sinc curve) has sidelobes which are significant compared to a Gaussian pulse because it behaves like a Gaussian pulse in the frequency domain. Since the pulses carry their energy at low frequencies, their spectrum is often shifted upwards by mixing with a sine wave, resulting in the pulse shapes shown in Figure 2.17. In practice, the resulting output pulses have a shape somewhere in between (see (69, p. 3285)).

This mixer makes enables the implementation of different operating ranges and channels which, in the 802.15.4a standard, are subdivided into

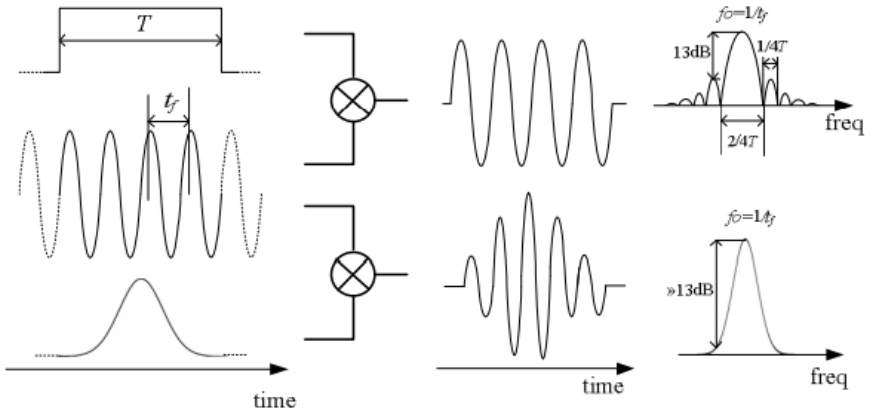

FIGURE 2.17: Modulated rectangular and Gaussian pulses (69, Figure 2)

1. The **Sub-Gigahertz band**, consisting of a single channel (channel 0) occupying the spectrum from 249.6 to 749.6 MHz
2. The **Low-Band**, comprising four channels 1:4 and occupying the spectrum from 3.1 to 4.8 GHz
3. The **High-Band**, consisting of 11 channels 5:15 and occupying the frequency range from 5.8 to 10.6 GHz.

The standard also includes the necessary hooks to facilitate dynamic channel selection within the operating frequency. For example, the physical layer has several functions such as receiver Energy Detection, Link Quality Indication (LQI), and channel switching functions that allow channel evaluation and frequency agility according to (68, p. 48).

A combination of Burst Position Modulation (BPM) and BPSK is used to transmit information which supports both coherent and non-coherent receivers. Combined BPM-BPSK is used as the modulation technique, with each symbol consisting of an active burst of UWB pulses and the supported data rates are 0.11 Mbps, 0.85 Mbps, 6.81 Mbps, and 27.24 Mbps, which are significantly higher than protocols based on the 2.4 GHz ISM band.

2.5.5.2 MAC layer improvements

In order to meet the growing demands of embedded industrial applications for low-power wireless networks and robust communications, in autumn 2012 the IEEE Standards Association decided to extend the IEEE 802.15.4 standard with an “e” designation, which essentially extends the MAC layer and thus enables new application areas, particularly in the industrial sector.

The IEEE 802.15.4e standard provides new MAC behaviour modes, three of which support real-time communication. Each mode defines its own superframe structure, which is not compatible with the original 802.15.4 MAC mode. It borrows many ideas from existing standards for industrial applications (mainly from WirelessHART and ISA 100.11.a), including various schemes such as allocated time slots via time division multiplexing, multi-channel communication, and frequency hopping to make the communication more deterministic and robust. General functional improvements have also been incorporated into the new standard, making it well-prepared for the future challenges of wireless sensor networks. According to (72, p. 7f), the most important functional improvements are enhanced beacons allowing a greater flexibility and multipurpose frames that can address a range of MAC operations (cf. (73)).

The new MAC schemes are an extension to original standard and offer a variety of new applications. The two most important ones according to (73; 74) are briefly described here:

Time Slotted Channel Hopping is already used in the WirelessHART and ISA100.11a MAC layer. It supports multi-hop and multi-channel access with a TDMA access scheme. This allows multiple parallel communications on the network to occur simultaneously by separating transmissions by channel, not just time. In addition, channel hopping can prevent interference with other networks, ensuring a reliable communications. In addition to TDMA, CSMA-CA can also be used to avoid repeated retransmissions. This access method targets several application areas such as industrial automation and process control.

The **Low Latency Deterministic Networks** method is tailored to applications that require low and deterministic latency combined with high reliability. This is achieved by transmitting data in a well-defined cycle within a star topology. Here, multiple nodes periodically send data to a central sink (i.e. the PAN coordinator). Each network operates on a single channel and transmission ACKs are optional and are only used if they do not affect the latency characteristics. Within the LLDN, time is divided into superframes that follow each other seamlessly. A node accesses the wireless medium during a portion of the superframe using a TDMA scheme. However, time slots for shared groups can be configured to allow multiple accesses for a group of nodes (via a CSMA algorithm). Exclusive channel access combined with DSSS coding ensures highly secure communications. Therefore, the number of time slots in a superframe determines how many nodes can access the medium. If many nodes need to send their data, the IEEE 802.15.4e standard recommends that the PAN coordinator shall be equipped with multiple transceivers to enable simultaneous communication on different channels. For this reason, also scalability improvements to LLDN, such as Multichannel LLDN (MC-LLDN) (75) exist, that enable multi-channel network configurations.

The TSCH scheme has been used as a reliable part of the MAC layer in WirelessHART and ISA100.11a even before it was introduced in the 802.15.4e extension. However, it requires that the hardware is designed to allow fast frequency hopping. This can be achieved with the 802.15.4 physical layer in the 2.4 GHz narrowband, where 2 MHz channels are available to allow continuous hopping across the entire 75 MHz bandwidth.

However, the choice of IR-UWB as the PHY layer imposes a number of constraints on the TSCH method, as the hardware must be able to support fast channel hopping. Unlike 2.4 GHz physical layer, UWB channels are very wide, and only 500 MHz or wider channels are available in the entire UWB spectrum from 3.1 to 10.6 GHz. Fast switching of these channels during operation is not supported in state-of-the-art IR-UWB transceivers and would introduce unnecessary latency and complexity. As the immunity to interference is already provided by IR-UWB itself, the TSCH method is not strictly necessary to increase overall resilience against interference. This makes LLDN particularly suitable for operating with IR-UWB, as no channel switching is required during normal operation. For this reason, LLDN is considered as the preferred scheme for the MAC layer in combination with IR-UWB in the further analysis in Chapter 3. Although the IR-UWB standard did not originally define a MAC layer, and although LLDN was originally designed for 2.4 GHz narrowband only, this consideration is an innovation, as is its implementation and verification.

2.6 Positioning

Since Global Position Systems (GPS) became available for civilian use in the 1990s, location has become an essential part of everyday life. Almost every car and smartphone now has a GPS-enabled receiver that can determine its position within a few metres. However, since the signals are often too weak to be received indoors, positioning technologies that can specifically be used indoors to fill the gap left by outdoor positioning systems are becoming increasingly popular. An additional advantage is that the accuracy can be further improved depending on the measurement method and technology used. IR-UWB is a good example of a system that is well-suited to indoor positioning and capable of high-accuracy measurements. Typical accuracies achieved with Wi-Fi, for example, are several metres (76, Figure 1), whereas UWB systems can achieve accuracies of 10 cm (77; 78). IR-UWB has, thus, laid the groundwork at the physical layer for accurate distance measurements, even in complex indoor environments. For this reason, the focus of this Section will be on IR-UWB, where the ranging techniques are first introduced. Then there will be an introduction to the concept of trilateration and its mathematical derivation. Finally, the principle of the Kalman filter will be explained, which is of particular importance for motion tracking.

2.6.1 Ranging

A key driver of accuracy is the distance measurement method (see (79, p. 1270ff)). The **Time of Flight (ToF)** measurement from the transmitter to the receiver, as used in a IR-UWB based systems, is proportional to the distance and is simple to implement and yet accurate.

IR-UWB uses a marker, the ranging marker (RMarker), which indicates the position of the first chip after the start of the frame delimiter and acts as a timestamp. It is used to accurately determine the distance between two points in a network. A variety of ranging techniques are used in this process and the following three methods differ in their approach and accuracy according to (80, p. 211 ff).

In **One-way Ranging**, a message is sent from one device (device A) to another (device B) and the time taken to send it is measured. This simple technique requires minimal information exchange. However, it requires perfect synchronisation of the clocks of the sending and receiving devices. Due to the difficulties associated with maintaining perfect synchronisation in a wireless network, this method is rarely used in the real world.

In **Single-Sided Two-Way Ranging** (SS-TWR), device A sends a message to device B, which in turn sends a response back to it, as shown in Figure 2.18. Both devices measure the send and receive times of the message frames and from this, the times T_{round} and T_{reply} can be estimated. The following equation can then be used to calculate the estimated propagation delay T_{prop}:

$$T_{prop} = \frac{T_{round} - T_{reply}}{2} \tag{2.6}$$

The distance between the devices is estimated by multiplying T_{prop} by the speed of light. An advantage of SS-TWR is that only one message exchange is required, thereby saving time and energy. In addition, there is no need for perfectly synchronised clocks as the time measurement is at a single point (device A).

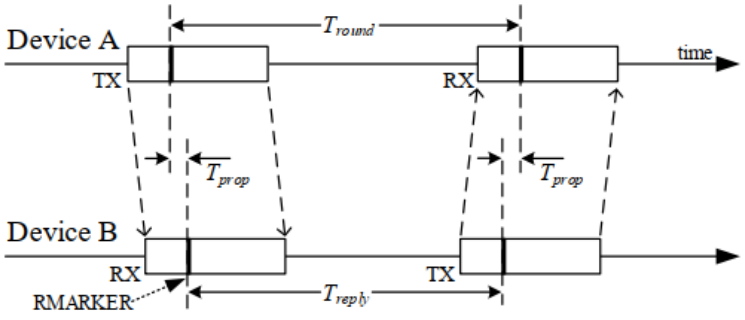

FIGURE 2.18: Single-Sided Two-way Ranging (81, Figure 36)

A disadvantage of this approach is that the T_{round} and T_{reply} times are measured by the device with its local clock, which may have some time offset error. This error can have a significant effect on the estimation of the ToF, especially if the response time T_{reply} becomes longer. SS-TWR is therefore suitable for specific applications in which accurate clocks are used and the communication range is relatively short.

Double-Sided Two-Way Ranging (DS-TWR) can be divided into two variants: four or three messages. With four messages, device A initiates the first round-trip measurement to which device B responds:

$$T_{prop} = \frac{T_{round1} - T_{reply1}}{2} \tag{2.7}$$

Device B then initiates the second round trip measurement, to which device A responds, thus completing the DS-TWR exchange:

$$T_{prop} = \frac{T_{round2} - T_{reply2}}{2} \tag{2.8}$$

The four DS-TWR messages can be reduced to three by using the first round trip response as the initiator for the second round trip, as shown in Figure 2.19.

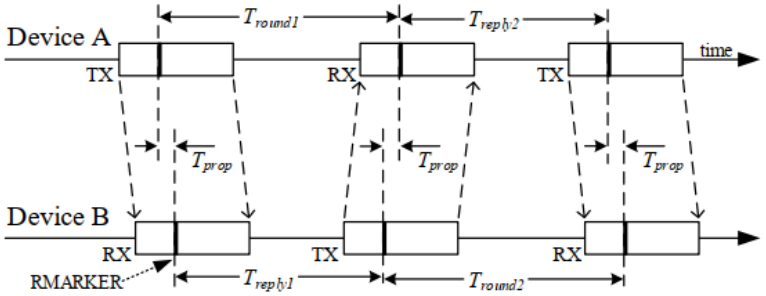

FIGURE 2.19: Double-Sided Two-way Ranging with three messages (81, Figure 38)

In either case, the estimated travelling time T_{prop} can be calculated by multiplying both and rearranging the resulting term to the following expression

$$T_{prop} = \frac{T_{round1} \cdot T_{round2} - T_{reply1} \cdot T_{reply2}}{T_{round1} + T_{round2} + T_{reply1} + T_{reply2}}. \tag{2.9}$$

This DS-TWR method has the advantage over SS-TWR in reducing the influence of clock errors and improving the accuracy of the distance measurement. Therefore, in situations in which clock errors and long response delays (T_{reply}) can be a problem, this method is advantageous. The disadvantages are that it is more complex and requires more time and energy than SS-TWR because more messages need to be exchanged.

Both schemes are referred to as **asymmetric** since they do not require the response times of each device to be the same. This feature does not rely on perfectly synchronised response times, thereby allowing greater flexibility in different application scenarios.

A special case of DS-TWR called **symmetric** DS-TWR requires that T_{reply1} and T_{reply2} are equal or as close to equal as possible. In this case, the estimated ToF $_{Tprop}$ is calculated as follows:

$$T_{prop} = \frac{T_{round1} - T_{reply2} + T_{round2} - T_{reply1}}{4}. \tag{2.10}$$

This method is more computationally efficient because it does not require multiplication.

Finally, the choice between SS-TWR and DS-TWR depends on the specific requirements and constraints of the system under consideration and the factors to be considered are the accuracy requirements, the time and power available, and the environment in which the system will be used. Since all methods have advantages and disadvantages, they should be evaluated and selected according to the specific requirements.

2.6.2 Position estimation methods

Ranging initially only provides a distance measurement, with no indication of direction. In a 2D space, this could be used to draw a distance circle within which the tag is located. However, to perform 2D localization, multiple circles, and thus multiple measurements from different tags, are required to determine the positions. In a 2D space, this is possible if there are at least three reference points or anchors for which ToF measurements have been taken. Using trilateration and the intersection of the distance circles, the position of the mobile device or tag can be determined. In the **Time of Arrival (ToA)** method, the equation for calculating the distance circles and determining the position of the tag is expressed as follows:

$$d_i = \sqrt{(x_i - x)^2 + (y_i - y)^2} = c \times T_{prop,i} \tag{2.11}$$

where c is the speed of light, $T_{prop,i}$ the ToF, (x_i, y_i) the coordinate of the anchor node i, and (x, y) the coordinate of the tag node.

Another method of calculating position is the **Time Difference of Arrival (TDoA)** method which, unlike ToA, calculates the difference in arrival time at different anchors to determine position. By calculating the difference, the errors introduced by the absolute ToA method can be avoided, potentially giving a more accurate result. However, to use this method, the time in the system must also be synchronised in order to calculate the

difference. Since time synchronisation in wireless networks is difficult to implement, this method is not often used. Unlike ToA, TDoA uses hyperbolas to represent the possible position of the tag and the intersection of all hyperbolas can be calculated using the following equation:

$$d_{i,j} = \sqrt{(x_i - x)^2 + (y_i - y)^2} - \sqrt{(x_j - x)^2 + (y_j - y)^2} = c(T_{prop,i} - T_{prop,j}) \quad (2.12)$$

where (x_i, y_i) and (x_j, y_j) are the coordinates of anchor i and j, (x, y) the coordinates of the tag, and $T_{prop,i}$ and $T_{prop,j}$ the ToF of the message.

The **Angle of Arrival (AoA)** is another method for determining position which measures the angles of two anchors to the tag to determine the tag's position. The advantage of this method is that far fewer anchors are required, namely only two, and time synchronisation is not necessary. Directional antennas or antenna arrays are usually used for measurement. However, the measurement becomes less accurate as the distance increases and AoA is difficult to use indoors due to multipath effects. The angle equation is expressed as follows:

$$\tan\theta_i = \frac{x - x_i}{y - y_i}, i = 1, 2 \quad (2.13)$$

The **Received Signal Strength (RSS)** method, which uses the received signal strength to calculate the distance, should also be mentioned in this context. This method is only accurate if the propagation model for the signal is well-known. Ideally, an line-of-sight environment exists. However, when making measurements, especially indoors, there will always be obstacles in the environment that create multipath effects and affect the propagation of the signal. An accurate estimate is thus only possible if propagation models of the environment exist or if reference measurements of signal propagation were performed beforehand.

2.6.3 Trilateration

For ToF measurements and the resulting ToA, trilateration algorithm is utilised for position estimation, in which at least three Anchor Motes are involved. In the following, an approach for the solution of the trilateration problem in accordance with (82) is presented. To describe the positioning problem in three dimensions, the basic equation (2.11) is as follows

$$(x - x_i)^2 + (y - y_i)^2 + (z - z_i)^2 = d_i^2 \quad (2.14)$$

In this equation, d_i is the ith distance between the Tag and an Anchor Mote with a total of n equations and $r = [xy]^T$ describes the coordinates to be determined. The coordinates r_i describe the Anchor Mote coordinates in Cartesian coordinates and there are n distance measurements for n Anchor Motes.

To linearise Equation 2.14, a reference node must be selected and all other equations are derived from the reference Anchor Mote equation. For this derivation, the first Anchor Mote is selected as the reference anchor, although other linearisation techniques are also possible. Linearisation occurs when all other equations are subtracted from the reference equation.

$$\begin{aligned}&[(x-x_1)^2+(y-y_1)^2+(z-z_1)^2]-\\&[(x-x_2)^2+(y-y_2)^2+(z-z_2)^2]\\&=d_1^2-d_2^2\end{aligned} \tag{2.15}$$

First, square the expressions in brackets:

$$\begin{aligned}&[x^2-2xx_1+x_1^2+y^2-2yy_1+y_1^2+z^2-2zz_1+z_1^2]-\\&[x^2-2xx_2+x_2^2+y^2-2yy_2+y_2^2+z^2-2zz_2+z_2^2]\\&=d_1^2-d_2^2\end{aligned} \tag{2.16}$$

and then resolve the remaining parentheses:

$$\begin{aligned}&x^2-2xx_1+x_1^2+y^2-2yy_1+y_1^2+z^2-2zz_1+z_1^2-\\&x^2+2xx_2-x_2^2-y^2+2yy_2-y_2^2-z^2+2zz_2-z_2^2\\&=d_1^2-d_2^2\end{aligned} \tag{2.17}$$

Now, the squared unknown r coordinates disappear:

$$\begin{aligned}&-2xx_1-2yy_1-2zz_2+2xx_2+2yy_2+2zz_1\\&+x_1^2+y_1^2+z_1^2-x_2^2-y_2^2-z_2^2=d_1^2-d_2^2\end{aligned} \tag{2.18}$$

The final steps are to rearrange the equation, whereby everything that is known, such as the Anchor Mote coordinates r_i, is grouped together with the dimensions d_i on the right-hand side of the equation while the unknown Tag Mote coordinates r are grouped on the left-hand side of the equation.

$$\begin{aligned} &2x(x_2 - x_1) - 2y(y_2 - y_1) + 2z(z_2 - z_1) \\ &= d_1^2 - d_2^2 - x_1^2 - y_1^2 - z_1^2 + x_2^2 + y_2^2 + z_2^2 \end{aligned} \tag{2.19}$$

To simplify the notation, a new symbol is introduced: $k_i = x_i^2 + y_i^2 + z_i^2$ which makes the notation more compact.

$$2x(x_2 - x_1) - 2y(y_2 - y_1) - 2z(z_2 - z_1) = d_1^2 - d_2^2 - k_1 + k_2 \tag{2.20}$$

Writing this derivation more generally, denoting the reference Anchor Mote by l, and deriving the i-th equation, one obtains:

$$2x(x_i - x_l) - 2y(y_i - y_l) - 2z(z_i - z_l) = d_l^2 - d_i^2 - k_l + k_i \tag{2.21}$$

A linear system of equations is obtained for four Anchor Motes, and this system of equations is written in matrix notation:

$$\begin{bmatrix} 2(x_2 - x_1) & 2(y_2 - y_1) & 2(z_2 - z_1) \\ 2(x_3 - x_1) & 2(y_3 - y_1) & 2(z_3 - z_1) \\ 2(x_4 - x_1) & 2(y_4 - y_1) & 2(z_4 - z_1) \end{bmatrix} \begin{bmatrix} x \\ y \\ z \end{bmatrix} = \begin{bmatrix} d_1^2 - d_2^2 - k_1 + k_2 \\ d_1^2 - d_3^2 - k_1 + k_3 \\ d_1^2 - d_4^2 - k_1 + k_4 \end{bmatrix} \tag{2.22}$$

This problem is subsequently solved using linear algebra:

$$r = A^{-1}b \tag{2.23}$$

2.6.4 Least Squares

In trilateration with ToA utilising more than four anchors, an over-determined system arises. In such cases, the Linear Least Squares (LLS) method is often employed to minimise measurement noise and other disturbances and to find a common intersection of circles around the given Anochor Motes. The LLS has, thus, established as a quasi-standard reference for localisation (83, p. 47). The equation to be solved for trilateration

is then as follows:

$$r = \arg\min_{x,y,z} \sum_{i=1}^{N} \Big[(x - x_i)^2 + (y - y_i)^2 + (z - z_i)^2 - d_i \Big]^2 \tag{2.24}$$

To determine the solution for (x, y, z) the sum of the squares of the residuals is minimised:

$$r = \arg\min_{r} \Big[(Ar - b)^T (Ar - b) \Big] = (A^T A)^{-1} A^T b \tag{2.25}$$

where $[\cdot]^T$ represents the transposition of the matrix.

Weighted Least Squares In the LLS method, all measured distances are treated equally. However, different anchors can have varying measurement errors. This leads to the Weighted Least Squares (WLS) method, where different weights are assigned to the measurements to mitigate these errors. By introducing weights into LLS, the equations are modified as follows:

$$r = \arg\min_{r} \Big[(Ar - b)^T W (Ar - b) \Big] = (A^T W A)^{-1} A^T W b \tag{2.26}$$

where W is the weighting matrix. Theoretically, W for trilateration is set as follows:

$$W = \operatorname{diag} \left[\frac{1}{\sigma^2(d_1)}, \ldots, \frac{1}{\sigma^2(d_i)} \right] \tag{2.27}$$

where $\sigma^2(.)$ indicates the variance.

2.6.5 Kalman Filter

For static positioning, the least squares method is usually sufficient to achieve good results. The often used Kalman filter does not necessarily give better results in such scenarios and also increases the complexity. However, when the objective is tracking, i.e. when there is time-dynamic behaviour and movements need to be tracked, the Kalman filter becomes useful.

The Kalman filter is a recursive algorithm that estimates the current state of a system from noisy measurement data. It provides an optimal estimate for linear systems with Gaussian noise. The filter combines a state prediction with actual measurements to produce an updated estimate of the state. By combining prediction and measurement, the Kalman filter attempts to estimate the true state of the system as accurately as possible. The uncertainties of both the system model and the measurements are taken

into account in this process. The following derivation follows the approach outlined in (84, Chapter 5.3.1):

The Kalman filter has two steps: prediction and correction. At each time step, the filter makes a state prediction and then corrects this prediction with the current measurements. The Kalman gain K, often referred to as Kalman amplification, determines the ratio between the prediction and the measurement correction.

The Kalman filter model assumes that the current state at time k is derived from the state at time $k-1$. Note that $\hat{x}$ and $\tilde{x}$ notation represents the a priori and a posteriori state estimate, respectively. Therefore, the process equation is as follows

$$\hat{\mathbf{x}}_{k-1} = \mathbf{A}\hat{\mathbf{x}}_{k-1} + \mathbf{B}\mathbf{u}_{k-1} + \mathbf{w}_{k-1} \tag{2.28}$$

whereas A the transition matrix. $\mathbf{w}_k$ is the zero white Gaussian process noise with covariance Q and the control matrix B relates the previous external input vector u_k. The control input u can be either known or unknown.

The observation vector $\mathbf{z}_k$ is given by:

$$\mathbf{z}_k = \mathbf{H}\hat{\mathbf{x}}_{k-1} + \mathbf{v}_k \tag{2.29}$$

where H is the state transition matrix and $\mathbf{v}_k$ the measurement noise, which is also assumed to be zero white Gaussian noise with covariance R.

Q and R are expressed as:

$$\mathbf{Q} = E\{\mathbf{w}\mathbf{w}^T\} \tag{2.30}$$

$$\mathbf{R} = E\{\mathbf{v}\mathbf{v}^T\} \tag{2.31}$$

In the prediction phase of the Kalman filter, the most recent state estimate is extrapolated to the current time. This prediction is realised by two central equations, the state prediction and the prediction of the state estimate covariance $\mathbf{P_k}$:

$$\mathbf{P}_{k-1} = \mathbf{A}\mathbf{P}_{k-1}\mathbf{A}^T + \mathbf{Q} \tag{2.32}$$

In the correction step, the measurement updates the correct value. The posteriory estimate is then computed as:

$$\hat{x}_k = \hat{x}_{k-1} + K_k(z_k - H\hat{x}_{k-1}) \tag{2.33}$$

where, the Kalman gain is computed as:

$$K_k = P_{k-1}H^T(HP_{k-1}H^T + R)^{-1} \tag{2.34}$$

and the updated state estimate covariance is computed as:

$$P_k = (I - K_kH)P_{k-1} \tag{2.35}$$

Extended Kalman Filter for trilateration: The Extended Kalman Filter (EKF) is particularly valuable in situations where the system being modelled is non-linear. In real-world motion measurement scenarios, where many factors are simultaneously influencing the measurements, such non-linear behaviour is common. The EKF is specifically designed for such non-linear systems and provides a stable state estimate even with complex system behaviour. This is achieved by approximating the non-linear system through linearisation around the current estimation point.

A good example of a nonlinear problem is trilateration. The inherent nonlinearity of this problem predestines the EKF as a good tool to solve it. By linearising near the current estimation point, the EKF is able to efficiently overcome the challenges of trilateration.

In the Extended Kalman Filter applied for tracking, the initial unfiltered position is derived from the LLS equations. This initial position is used to set the EKFs starting state. The EKF employs nonlinear functions that govern the systems behaviour, expressed as follows for the system state x_k and the observations z_k, $f(.)$ and $h(.)$ are the nonlinear process and measurement functions.

$$x_k = f(x_{k-1}, u_{k-1}, w_{k-1}) \tag{2.36}$$

$$z_k = h(x_k, v_k) \tag{2.37}$$

Here, the state vector x_k denotes the estimated position of the Tag Mote, while the output vector z_k represents the measured distances to the Anchor Motes. The function h serves as a crucial link between x_k and z_k, and the function f correlates the system state at time k with that at $k-1$. It includes the trilateration equations from equation (2.22) and computes the approximated system output z_k, which is then used to refine the current estimation x_k.

$$z_k \approx z_{k-1} + C_k \cdot (x_k - x_{k-1}) + V_k \cdot v_k \tag{2.38}$$

In addition, the detailed distance equation is given by:

$$\begin{bmatrix} r_1 \\ r_2 \\ \vdots \\ r_n \end{bmatrix} = \begin{bmatrix} \sqrt{(x_x - x_1)^2 + (x_y - y_1)^2 + (x_z - z_1)^2} \\ \sqrt{(x_x - x_2)^2 + (x_y - y_2)^2 + (x_z - z_2)^2} \\ \vdots \\ \sqrt{(x_x - x_n)^2 + (x_y - y_n)^2 + (x_z - z_n)^2} \end{bmatrix} \tag{2.39}$$

As equation (2.39) is not linear, it must be linearized and the EKF algorithm can be adopted. At each time step, the Jacobian matrix C_k is obtained by taking the first-order Taylor expansion as:

$$C_k \triangleq \begin{bmatrix} \frac{\partial r_1}{\partial x_x} & \frac{\partial r_1}{\partial x_y} & \frac{\partial r_1}{\partial x_z} & 0 & 0 & 0 & 0 & 0 & 0 \\ \frac{\partial r_2}{\partial x_x} & \frac{\partial r_2}{\partial x_y} & \frac{\partial r_2}{\partial x_z} & 0 & 0 & 0 & 0 & 0 & 0 \\ \vdots & \vdots & \vdots & \vdots & \vdots & \vdots & \vdots & \vdots & \vdots \\ \frac{\partial r_n}{\partial x_x} & \frac{\partial r_n}{\partial x_y} & \frac{\partial r_n}{\partial x_z} & 0 & 0 & 0 & 0 & 0 & 0 \end{bmatrix} \tag{2.40}$$

where

$$\begin{cases} \dfrac{\partial r_i}{\partial x_x} = \dfrac{x_x - x_i}{\sqrt{(x_x - x_i)^2 + (x_y - y_i)^2 + (x_z - z_i)^2}} \\ \dfrac{\partial r_i}{\partial x_y} = \dfrac{x_y - y_i}{\sqrt{(x_x - x_i)^2 + (x_y - y_i)^2 + (x_z - z_i)^2}} \\ \dfrac{\partial r_i}{\partial x_z} = \dfrac{x_z - z_i}{\sqrt{(x_x - x_i)^2 + (x_y - y_i)^2 + (x_z - z_i)^2}} \end{cases} \tag{2.41}$$

Since the EKF linearises the non-linear state or observation equations, it inevitably introduces linearisation errors, which can lead to degradation and divergence if the linearisation assumption is not true (85, p. 3138).

The filter dynamically tracks changing Tag Mote positions using the measured distances to Anchor Motes as input parameters. Each position is subject to an initial state prediction, which is then corrected on the basis of known error covariances and the measured values.

The EKF prediction equations are summarized to:

$$\hat{x}_{k-1} = f(\hat{x}_{k-1}, u_{k-1}, 0) \tag{2.42}$$

$$P_{k-1} = A_k P_{k-1} A_k^T + Q_k \tag{2.43}$$

And the EKF correction equations are:

$$K_k = P_{k-1} H_k^T (H_k P_{k-1} H_k^T + V_k R_k V_k^T)^{-1} \tag{2.44}$$

$$\hat{x}_k = \hat{x}_{k-1} + K_k (z_k - h(\hat{x}_{k-1}, 0)) \tag{2.45}$$

$$P_k = (I - K_k H_k) P_{k-1} \tag{2.46}$$

The ability to integrate data from different sensors for more accurate predictions is another advantage of the EKF. To determine the position of an object more accurately, data such as acceleration, velocity and distance can be processed together. In various research projects, the EKF has been used to fuse data from gyroscopes and accelerometers with UWB data to improve the accuracy. Table 2.2 is an extract of the research projects with the accuracies achieved by EKF sensor fusion with UWB and IMU data:

Table 2.2: Accuracy of EKF with IR-UWB and sensor fusion in prior works

Accuracy	Research work	Year
0.20 m	(86)	2015
0.18 m	(87)	2017
0.39 m	(88)	2018
0.17 m	(77)	2018
0.21 m	(89)	2022

Obviously, the accuracies achieved vary because of several factors. These include sensor accuracy, environmental conditions (LoS/NLoS) as well as modelling and parameterising the EKF and data fusion. All of these factors play a crucial role in determining the performance and reliability of the positioning system. Careful selection and tuning of EKF parameters and efficient data fusion are also essential to achieve improved positioning accuracy. However, when considering the research results presented in Table 2.2, an avarage accuracy of approx. 0.23 m can be expected.

2.6.6 Challanges in positioning with IR-UWB

When comparing the positioning characteristics of the standards presented here, it is clear that IR-UWB has very good characteristics, as it can measure very accurately and can also cover more distant objects up to 150 m away, and only optical and ultrasonic systems can make even more precise measurements (see (76, Figure 1)). An important reason for this is that Bluetooth and Wi-Fi use the RSS method, whereas IR-UWB can use the ToF method by transmitting pulses, thereby allowing precise measurements even without detailed information about the environment.

Despite these advantages, the accuracy of IR-UWB measurements can be negatively affected by several factors. For example, multipath effects are also a problem with UWB (71, Chapter 5.2.1) as the incoming pulses can be reflected so that several reflected pulses arrive at the receiver at different times. Depending on the reflection, delays of up to several hundred nanometres can occur. One difficulty is determining which pulse to evaluate, as the reflected pulses are often stronger than the first arriving pulse, as

shown in Figure 2.20. This can happen if there is no LoS and an obstacle between the transmitter and receiver which attenuates the signal, as later arriving reflections sent around the object will then be received more strongly. Another problem arises with moving objects when the antenna is no longer perfectly aligned. In such cases, reflected signals from other directions may be received more strongly than those from the direct path to the transmitter. In such scenarios, the algorithm must evaluate the very first peak rather than the highest, which is more complex.

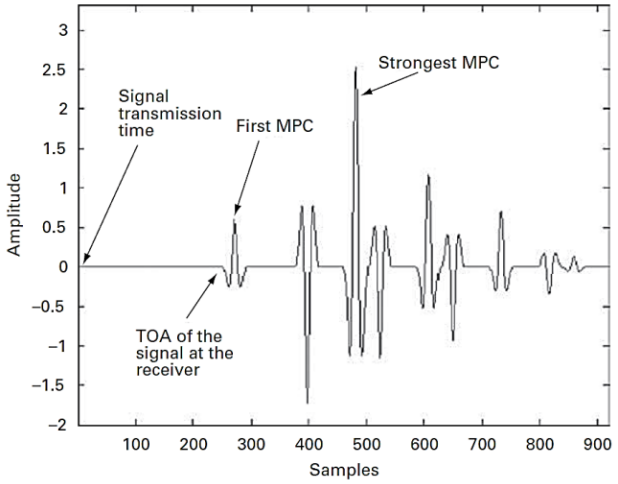

FIGURE 2.20: ToA estimation in a multipath channel (71, Figure 5.2)

Clock inaccuracies can also be a challenge. Particularly when using cheap hardware, clocks often have jitter or drift, which can be a problem, especially in broadband systems and thus it is important to know the specifications and the limits of the system used.

2.7 Summary

This Chapter introduced the basic concepts and technologies of wireless communication networks relevant to understanding and analysing the proposed architecture for wireless intra-spacecraft communication networks. First, an introduction to wireless networks was provided, followed by a detailed explanation of the OSI layer model which serves as the basic reference model for communication protocols.

On this basis, the main wireless communication standards that could potentially be relevant to the design of the architecture of interest were examined. These include the IEEE 802.11 standard, which is characterised by high data rates, the IEEE 802.15.1 standard, with its low power consumption and moderate data rates, and the IEEE 802.15.4 standard, which is optimised for resource-constrained devices and supports various industry standards such as WirelessHART and ISA 100.11a.

The enhancements and extensions to the IEEE 802.15.4 standard, such as IR-UWB and the MAC layer improvements, were also described and the examination of these technologies provided a comprehensive overview of the various possibilities for wireless communication networks for spacecraft.

The following Table 2.3 summarises the main parameters of the different standards presented in relation to the first two layers, without evaluating their capabilities in terms of space-specific applications.

Table 2.3: Comparison of different wireless standards focussing on the physical and MAC layer

Parameter	**Wi-Fi**	**Bluetooth**	**ZigBee**	**Industrial 802.15.4-based**	**IR-UWB (& LLDN MAC)**
Specification	IEEE 802.11	IEEE 802.15.1	IEEE 802.15.4	WirelessHART ISA100.11a IEEE 802.15.4e	IEEE 802.15.4a IEEE 802.15.4e
Frecuency band	2.4 GHz; 5 GHz	2.4 GHz	868/915 MHz, 2.4 GHz	2.4 GHz	3.1 - 10.6 GHz
RF channels	14 (2.4 GHz)	79	1/10; 16	15	16
Data rate	>200 Mbps	2 Mbps	250 kbps	250 kbps	27 Mbps
Nominal range	>100 m	10 m	10 - 50 m	10 - 100 m	10 - 100 m
Power consumption	> 500 mW	30 mW	10 mW	5 mW	180 mW
Tx power	10 - 20 dBm	0 - 10 dBm	0 - 10 dBm	0 - 10 dBm	-41 dBm/MHz
Channel bandwith	20 - 40 MHz	1 MHz	0.3/0.6 MHz; 2 MHz	2 MHz	500 MHz
Modulation	BPSK, QPSK, QAM	GFSK	BPSK; O-QPSK	O-QPSK	BPSK-PPM
Spreading scheme	DSSS, OFDM	FHSS	DSSS	DSSS	pulses
Robustness	MIMO used, moderate reliability depending on traffic load	poor robustness	no hopping, poor robustness	frequency hopping used, highly reliable	multipath fading immune, reliable MAC scheme
Collision avoidance / Determinism	CSMA-CA	TDMA	CSMA-CA	TDMA & CSMA-CA	TDMA
Latency	< 1ms	50 ms	100 ms	> 100 ms	< 10ms
Network topology	star	star	star, tree, mesh	mesh	star
Max number of nodes	>32	8	65000	65000	1024
Ranging accuracy	1 - 3 m	1 - 3 m	1 - 3 m	1 - 3 m	0.1 - 0.5 m

The fundamentals of positioning were also explained. In particular, IR-UWB offers significant accuracy advantages over other wireless standards because the time of flight can be determined by transmitting the pulse. This enables accurate positioning using ToA and trilateration. For static positioning, the least squares method is sufficient. In the case of time-dynamic and non-linear systems like tracking, the Extended Kalman Filter is used.

In Chapter 3, the standards and technologies discussed are evaluated in terms of their suitability for use in space systems, whereby various requirements such as robustness, latency, power consumption, and determinism will be considered. The results of this evaluation will serve as a basis for the selection of appropriate technologies and communication protocols in the following Chapters, where the identified architecture for on board wireless networks will be implemented and verified.

Chapter 3

Analysis

This third Chapter initially explores the potential of different space applications for wireless intra-spacecraft networks, providing detailed examples, with a focus on short-range communication networks as utilized in satellites, launcher or within space station. Subsequently, the Multi-Criteria Decision Analysis method is employed to evaluate the suitability of selected wireless protocols for the different applications. Specific criteria, which are interpreted as requirements for the respective applications, are defined. A qualitative assessment of these applications is carried out based on the aforementioned criteria. Following this, the protocols are evaluated against the same set of criteria. The culmination of this process is a matrix, demonstrating the most suitable protocol for each application. The outcome of the matrix are then analyzed and a suitable, universally applicable protocol architecture is identified for the progressive steps of this dissertation.

The analysis forms the foundation for the following Chapter, wherein an architecture proposal based on the technologies and standards discussed here, is implemented and verified.

3.1 Potential applications in space systems

In order to improve the communication and control capabilities of a spacecraft, wireless networks have become increasingly interesting in recent years. These networks offer several potential benefits, including increased flexibility and the ability to reduce harness complexity and mass. However, there are also numerous technological challenges associated with the implementation of wireless intra-spacecraft communication including the required robustness to operate in the harsh space environment and the limited power and bandwidth resources available on board a spacecraft.

Significantly, wireless networks are not limited to being utilised on board spacecraft and their future potential extends to other space systems.

A comprehensive overview of the possible future role of wireless communication networks on board different space systems is given below, highlighting their potential for transformation and enhancement of the current architecture in several applications.

Overall, two core aerospace domains have been identified that will benefit from the advantages of wireless networks which are spacecraft and launcher as well as space station and habitats (see (3, Chapter 2.2), (3, Chapter 2.3), and (90, Chapter 2)).

3.1.1 Avionics architecture

In order to identify the possible applications of wireless intra-vehicular networks in these domains, an understanding of the avionics architecture is required. The avionics architecture does not differ in any fundamental way between the various space systems, whether they are satellites, launch vehicles or modules of a space station. Although each system has its specific characteristics, they are generally the same set of subsystems necessary for the provision of the core functionality for operations. The difference lies in the specific design and functionality of these systems, depending on the mission requirements and their use cases.

Therefore, the architecture of the Eu:CROPIS satellite serves as an example. Although Eu:CROPIS is classified as a small satellite, it demonstrates that the architectural design does not necessarily depend on the size of the spacecraft. In both traditional spacecraft and small satellite, avionics can be centralised or distributed, simplex or fault-tolerant, modular or monolithic. The Eu:CROPIS satellite is an example of a centralised avionics architecture. In contrast, a bus architecture, such that used on the Sentinel 2A satellite, connects the main components via one common data bus like the MIL-STD 1553.

3.1.1.1 Example: Eu:CROPIS satellite

Overview The DLR carried out a small satellite mission called Eu:CROPIS in 2018/19 to demonstrate how a closed life-support system can be operated over the long term. Inside the satellite, tomato plants were grown in a pressurised carbon-fibre composite tank, while two coupled systems supply the plants with nitrogen from artificial urine and detoxify the entire system. During its mission, the 250 kg satellite simulated two different gravitational forces while orbiting at an altitude of 600 km. In addition to the biological experiment, the spacecraft carried three secondary payloads: Radiation Measurement in Space (RAMIS), which measures radiation levels inside and outside

the satellite; a NASA photosynthesis measurement on algae; and a prototype onboard processing unit SCORE, which collected flight data and controlled a camera (91).

FIGURE 3.1: Eu:CROPIS satellite (Source: DLR e.V.)

The various subsystems will be examined as an example in this subsection to showcase a typical satellite avionics architecture. The focus lies on the different subsystem functions and their utilisation of sensors for internal onboard monitoring, as well as the possibilities of where to replace wired sensors with wireless counterparts. It also includes the details of the different subsystems and sensors used on the satellite, including the communication strategies using interfaces such as RS422 and SpaceWire. Understanding the role that wireless communication can play in replacing wired sensors with wireless sensors provides an indication of how this technology can enable the satellite to perform its intended functions and tasks more efficiently.

Avionics Architecture The avionics architecture of the satellite is composed of several subsystems (S/S) that work together to ensure its operation and control. These have different functions, which are described below (91, Chapter 1.3).

In a centralised avionics architecture such as that of Eu:CROPIS, the **Command and Data Handling (CDH)** subsystem consists of an Onboard Computer (OBC) as a single, centralised unit that is responsible for the management and control of all the sub-systems of the satellite. Although this approach is simple and easy to implement, it offers less flexibility and scalability than other architectures. For the on board communication, Eu:CROPIS relies on a point-to-point communication. This approach allows each subsystem to communicate directly with the OBC by connecting the OBC and other subsystems via dedicated point-to-point communication channels and although it

can be more complex to implement and manage, it provides greater flexibility and higher data rates. The main communication protocols that are used are SpaceWire or RS422.

The **Attitude and Orbit Control System (AOCS)** is a subsystem that is responsible for the attitude and orbit control of the satellite which ensures that the satellite remains in the desired position and orientation and that its movements are controlled with precision. In contrast, a Guidance, Navigation and Control (GNC) system is commonly used for the on-board segment, when the satellite position is controlled in closed loop, for instance in case of rendezvous and formation flying. The AOCS system of the spin-stabilised Eu:CROPIS satellite uses three magnetic torques as actuators to control the attitude of the satellite. These torques generate magnetic fields that interact with the Earth's magnetic field and rotate the satellite to the desired orientation relative to its spin axis or maintain the spin. The sensors used include two magnetometers, 10 sun sensors, and four gyroscopes to measure and monitor the satellite's attitude. AOCS also uses a Global Navigation Satellite System (GNSS) receiver to determine the satellite's position.

The **Communication System (COMMS)** consists of an S-band transceiver that is responsible for the transmission of telemetry data, as well as the reception of telecommands with the S-Band antennas. The transceiver sends telemetry to the ground station, which collects and processes it to monitor the satellite status and payload data. At the same time, the transceiver receives telecommands from the ground station to control and command the satellite's functions.

The Eu:CROPIS **Electrical Power System (EPS)** is responsible for supplying and distributing power to the various components of the satellite. The power subsystem ensures that the satellite is supplied with a sufficient amount of electrical energy and that the energy requirements of the various components are met. It consists of four solar panels and lithium-ion batteries storing the generated energy. Each panel can produce up to 250 watts of power. The Power Control and Distribution Unit (PCDU) is responsible for the distribution of power to the satellite's various components and the sensors that are used to monitor the power subsystem include current and voltage sensors.

Other subsystems include the **Thermal Control System (TCS)**, which is responsible for ensuring that the satellite's components can operate within their specified temperature ranges to maintain their functionality, and the **Structure System**, which is responsible for providing the mechanical support that holds all the components in place. These subsystems also provide telemetry through various sensors and interact with the satellite's avionics. The thermal subsystem, for example, is equipped with a set of around 30 temperature sensors. These sensors allow the system to monitor the temperature inside the satellite and take action to keep it within the desired range.

In addition, the satellite has a **payload** that interacts with the satellite's avionics and is the main driver for developing, building, and launching research satellites. The requirements of the payload influence and determine the key parameters of the satellite, including its size, weight, and the overall cost of the mission. The Eu:CROPIS mission carries a total of four payloads that are accessible via two wired data interfaces. The data processing of the payload data takes place in the dedicated payload computers and the pre-processed data is then transferred to the OBC via various interfaces. The main payload is the Eu:CROPIS experiment, a NASA biology experiment, a radiation detector called RAMIS and SCORE, and a DLR payload. As mentioned, the Eu:CROPIS experiment studies a closed-loop life-support system, while the NASA bio-experiment is classified. RAMIS is a radiation detector that measures ionising radiation, and SCORE is a precursor to a fully developed OBC and is used to gain flight experience in the first instance.

3.1.1.2 Avionics in launcher and space station modules

The avionics architecture of a launch vehicle is quite similar. Taking the Ariane 5 rocket as an example, there are key subsystems that can be classified as follows: the flight control and management system (SSCV), the telemetry system (SSTM), the power distribution system (SSPE) and the safety system (SSSA) (see (92, p. 2)):

- Combining CDH and GNC functionality, the SSCV is mission critical to stabilise launch vehicles in flight, control flight phases and ensure accurate payload delivery. Its main component is the on-board computer (OBC). In the upper stage, a ring-shaped structure called the Vehicle Equipment Bay (VEB) houses most of the SSCV components and the devices communicate via a common MIL-STD 1553 bus. Additional status inputs are provided by various temperature, pressure, flow and vibration sensors located throughout the launcher. These mostly analogue or discrete inputs are acquired by data acquisition units in each compartment.
- The SSTM, which combines CDH and COMMS functionality, is not mission critical. It collects various sensor and status data during flight and transmits it to ground. It is used to prove a successful mission to the customer and for offline engineering by providing trajectory, position, vibration and shock data. The main component is the Telemetry Data Conditioning and Acquisition Unit. It listens to a large number of sensors from other systems via additional physical wires that are connected to remote conditioning units.
- The SSPE, analogous to an EPS subsystem, controls power distribution during the various phases of flight.

- The SSSA is very specific to launcher and it provides safety in the event of a catastrophic failure during the early mission phases. In the event of a serious fault, its task is to completely neutralise the rocket to prevent damage.

Similar subsystems are also found in the Columbus module of the International Space Station. The European Columbus module of the ISS contains a number of subsystems that make it to some extent a stand-alone spacecraft, although all of them are interfaced with the ISS systems and exchange telemetry and data with the station. The subsystems include a CDH system, a communication and tracking subsystem, an EPS, a TCS, and an environmental control and life support system (ECLSS), which is very specific to manned space flight. The only functions that are not carried out by Columbus systems are AOCS and GNC (93). Space station specific wireless applications, thus, arise in particular from the interaction with the astronauts.

3.1.2 Application fields

The dominant topology in space avionics is characterised by a central OBC in a star topology. Various components and subsystems communicate with the OBC via point-to-point connections. The result is a large number of cable harnesses and wire interfaces.

Most of the connections are point-to-point, using differential protocols such as MIL-STD-1553, SpaceWire or RS422 as these are more robust and thus more suitable for space applications. Bus protocols such as I^2C or a Controller Area Network (CAN), which are long established in the automotive sector and increasingly used in space systems. Unlike point-to-point connections, they allow a communication bus to be used, thereby enabling each component to communicate with any other subsystem connected to the bus. All of these different types of connection require complex harness that can often take years to design, develop, and accomodate. The structure of the satellite and the positioning of the various units, which in turn are determined by the requirements of the mission, also limit the space in which these harnesses can be accommodated.

In addition, there are two opposing trends in satellite dimensions. Both are critical to harness design and performance:

- Large, powerful satellites such as the Alphasat require long cables with large cross sections, which has an impact on the mass of the satellite. For instance, on a large telecommunications satellite, the cable harness may require more than 50000 connections spread over approximately 1000 connectors and 20 km of cable, and the mass may exceed 100 kg. Not only satellites, but also rockets and space station modules contain many sensors. Ariane 5, for example, has a total of around 1100 sensors. These have to be connected to the avionics over long distances.

- Smaller satellites, on the other hand, do not have much space to accommodate wiring harnesses. This complicates the design process for cable harness accommodation. Eu:CROPIS, which belongs to the small satellites category, has over 600 digital and analogue interfaces.

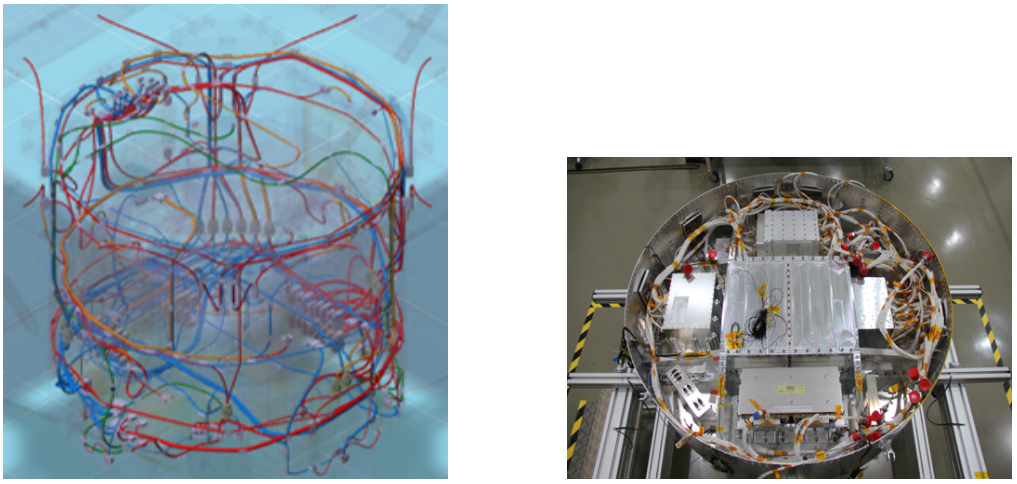

FIGURE 3.2: Left: Harness Model in CAD, Right: FM Harness in Bus Compartment (Source: DLR e.V.)

Figure 3.2 shows part of the cable harness of the Eu:CROPIS satellite and its integration into the primary structure of the satellite. Especially in places where there are multiple connections, wireless networks could increase flexibility and significantly reduce the amount of wiring. Wireless networks thus have the potential to be utilised in different applications in space systems to replace the harness. An example of the potential benefits of wireless networks is shown in a study for Mars Express simulations have shown that replacing 70 per cent of the data harness of a satellite such as Mars Express with wireless networks reduces the integration time of the flight model by about 20 per cent (3, p. 3-8). For Mars Express, this translates into a time saving of 25 days out of a total of 130 days for a team of about 15 people.

However, wireless networks offer capabilities beyond simply replacing wires, extending to new applications indicating a wide range of potential uses. By examining the Eu:CROPIS satellite as an example within the avionics of a typical small satellite system, a clearer categorization of various application fields can be made.

3.1.2.1 Sensing

Table 3.1 shows the different sensors and actuators, which are connected via harness with the avionics on the Eu:CROPIS satellite and their allocation to the different subsystems (94, p. 15f). Voltage and current sensors are excluded from the table, since these type of

sensors are already integrated into the Printed Circuit Board (PCB) and not replaceable for wireless connection.

Table 3.1: Eu:CROPIS sensors and actuators overview

S/S	Device	Type	Number	Sample rate	Critical	Determinism	Latency
AOCS	Sun	Sensor	10	$\leq$ 10 Hz	X	X	X
AOCS	Magnetic	Sensor	2	$\leq$ 5 Hz	X	X	X
AOCS	Gyro	Sensor	4	$\leq$ 5 Hz	X	X	X
AOCS	Torquer	Actuator	4	$\leq$ 5 Hz	X	X	X
TCS	Temperature	Sensor	66	$\leq$ 0.1 Hz	-	-	-

The concept of categorizing sensors as (mission-)critical or non-critical as seen in the Table 3.1 is not new, having been previously introduced in the avionics architecture of the Ariane 5 launcher. Transposing this classification to the domain of spacecraft seems logical.

Critical sensing Critical sensors monitor a variety of spacecraft systems, including the AOCS. They are mission-critical, and the success of the mission depends on their functionality. These sensors are designed to monitor or control specific operations that require rapid availability and/or high reliability. The sensors also have high latency requirements and/or require deterministic communication.

Given that latency is a recurrent challenge for wireless networks, exploring another example becomes important for a comprehensive understanding. The Eu:CROPIS satellite, with its spin stabilisation, is not representative for a conventional AOCS, as the majority of satellites use 3-axis stabilisation. The ESA Sentinel 2A satellite provides an example of such a 3-axis stabilisation AOCS.

The table 3.2 lists typical attitude control instruments of the ESA Sentinel 2A mission and the corresponding sampling rates (see (95, p. 9) and (96, chapter 12)).

The min. latency required is in the range of 10 ms for the Inertial Measurement Unit (IMU).

Furthermore, other critical sensors can also be utilised in human spaceflight to continuously monitor the physiological parameters of crew members, enabling improved medical care and timely response to potential health problems. This could include wearable devices that measure heart rate, blood pressure, and oxygen levels as demonstrated in the BEAT experiment (97). These devices can be vital for the survival of crew members, which is why the same requirements apply in this context as well.

TABLE 3.2: Sentinel 2A AOCS devices

Device	**Type**	**Number**	**Sampling rate**
Magnetometer	Sensor	3	$\leq$ 25 Hz
IMU	Sensor	4	$\leq$ 100 Hz
Sun sensor	Sensor	6	$\leq$ 10 Hz
Star tracker	Sensor	3	$\leq$ 5 Hz
GPS receiver	Sensor	2	$\leq$ 1 Hz
Magnetic torqer	Actuator	3	$\leq$ 5 Hz
Reaction wheel	Actuator	4	$\leq$ 25 Hz
Thruster	Actuator	8	$\leq$ 25 Hz

Non-Critical sensing Non-critical wireless sensing can include isolated sensors used to monitor various subsystems or system states and parameters such as temperature sensors that are collected as historical housekeeping, whereby one or more of these failing does not result in a mission-critical failure (3, Section 3.3.2). Instead of cables, sensors could transmit data in spacecraft or launcher wirelessly to central gateways, reducing weight, increasing flexibility and improving fault tolerance. This would be particularly advantageous for the telemetry system of launchers, where normally long distances up to have to be covered.

In human spaceflight, non-critical sensors are employed to support the continuous monitoring of various environmental parameters within the habitat and space station through the ECLSS. Such wireless sensors measure ambient environmental phenomena to ensure they remain within specified ranges suitable for long-term habitation. This includes monitoring temperature, humidity, and air quality to ensure that the ventilation systems are functioning correctly and providing clean, breathable air to the crew (3, Table 2-3).

3.1.2.2 AIT support

Particular attention should be also paid to the AIT phase of a satellite project which involves the integration of all the satellite's subsystems and components into a functional unit and the testing of that unit to ensure that it meets all the required specifications and performance criteria. An important aspect of the AIT phase is the environmental testing, in which the satellite is exposed to a range of simulated environmental conditions that it is likely to experience in orbit ((91, Chapter 2.6)). These tests are designed to verify the structural integrity of the satellite and its performance and functionality under extreme temperature and vibration conditions:

- The vibration test is usually performed on a shaker table where the satellite is subjected to mechanical vibrations at different frequencies and amplitudes to simulate the dynamic loads it will experience during launch.

- During the thermal vacuum test, the satellite is exposed to different temperatures in a vacuum to simulate the extreme temperature fluctuations in space.

To monitor the test cycle, a variety of sensors are typically used to measure and record various parameters such as temperature, humidity, pressure, acceleration, and structural stresses. These sensors can be attached to the satellite, integrated into the satellite, or placed outside the satellite to monitor the test environment. The data from these sensors is usually collected and analysed using specialised test equipment and software. Many such sensors were used in the Eu:CROPIS campaign as can be seen in Table 3.3, and switching to wireless sensors could significantly reduce the time needed to prepare such a campaign, thus reducing cost and effort.

TABLE 3.3: Sensors used in Eu:CROPIS environmental test campaign

Test	**Device**	**Number**
Vibration	Strain	20
Vibration	Accelaration	25
Thermal Vacuum	Temperature	70

Even during the AIT phase, if equipped with a wireless interface, components can be wirelessly monitored for debugging and functional testing. Additionally, a dedicated wireless EGSE interface could be used to monitor and control various aspects of the spacecraft during testing.

3.1.2.3 Onboard communication

Another important application is the on-board communication between the different subsystems and equipments. An exemplary overview of the different subsystems and components, together with their interfaces, is shown in Figure 3.3.

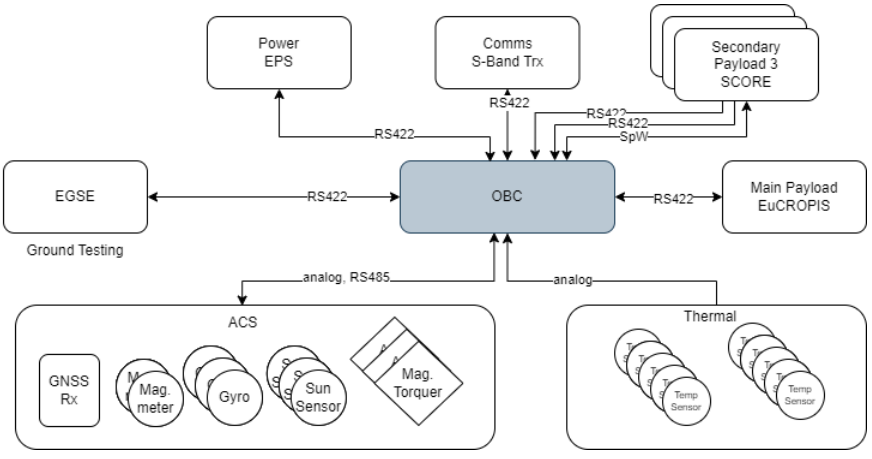

FIGURE 3.3: Eu:CROPIS architecture

The Eu:CROPIS satellite consists of 12 components (including redundant parts) which are interconnected by a variety of interfaces. In larger space systems, the number of equipment would be much higher, e.g. the Ariane 5 launcher contains 44 components and about 1100 sensors and actuators that are interconnected with each other by two MIL-bus systems, a number of proprietary bus systems, and a large number of analogue and discrete I/Os (92, p. 3). The replacement of these interfaces by wireless ones could be advantageous in several ways. For example, components could be tested and integrated more quickly. And it would also allow flexibility to be maintained very late in the integration process for easy removal.

3.1.2.4 High Data-Rate Payloads

Another important application are connections that require extremely high data rates. This requirement is particularly prominent in payload communication. High Data Rate-Payloads thus represent a special category of onboard communication that is characterised by particularly high data rate requirements (3, Section 3.3.9). These can be high-resolution scientific instruments, cameras or other payload components. For example, the Sentinel-2A Multi-Spectral Imager (MSI) payload has a data rate of 450 Mbps (98). This data is usually transmitted via dedicated point-to-point links to ensure efficient and collision-free communication.

3.2 Analysis of a suitable protocol architecture

The main purpose of this Section is to present and implement a Multi-Criteria Decision Analysis approach. The objective of this approach is to determine the suitability of different wireless protocols for specific space applications by systematically investigating which of these protocols can meet the defined minimum requirements of an application. The purpose of this analysis is to ensure that the proposed architecture and the related standards meet the requirements and deliver the desired performance for the applications introduced. A detailed analysis of each application field is essential for gaining an in-depth understanding of the different requirements.

The procedure is performed in several phases:

1. **Definition of criteria**: First, based on the information presented in Sections 2.7 and 3.1.2, a selection of applications and protocols is made. The next step is the definition of the criteria which will be decisive for the evaluation of the suitability of the standards for these specific applications.

2. **Establishment of minimum requirements**: Once the criteria are in place, the next step will be the definition of the minimum requirements for each of the selected applications. This provides a clear indication of what is required of a wireless protocol to be considered suitable.

3. **Evaluation of wireless protocols**: The evaluation of each wireless protocol is then carried out. This provides a systematic and objective analysis of the capabilities of each protocol with respect to the defined criteria.

4. **Suitability matrix**: A separate suitability matrix showing which protocols meet the minimum requirements is created for each application.

5. **Overall assessment**: The detailed analysis is followed by a cumulative assessment. This concludes with a recommendation of a suitable, universally applicable protocol architecture for the progressive steps of this dissertation.

3.2.1 Definition of criteria

The study is based on the evaluations of the protocols already carried out in Chapter 2 and the potential application fields in Section 3.1.2. It is important to make these determinations because they define the framework for the analysis presented here. A further step is to identify relevant criteria that form the basis for further investigation. For this reason, the following criteria have been established for the further analysis and the following evaluation levels have been chosen, where 1 always represents the poorest performance and 3 or 4 the best performance. However, it is important to note that the criteria only refer to the PHY and MAC layers:

- **Latency**: Latency refers to the delay that occurs in transmitting data from one point to another within a network. For some applications, such as attitude control, wireless networks need to have low latency in order to respond in real time. For other applications, however, real-time access is not required, leading to a distinction between real-time and non-real-time capability. In areas such as industrial automation, latencies of less than 10 milliseconds are typically considered real-time (99).
  - 1: no real-time access (above 10 ms)
  - 2: real-time access (below 10 ms)
- **Determinism**: Determinism in a wireless network refers to the ability to provide a predictable and guaranteed data transmission time. It is crucial for applications with strict timing requirements. The evaluation of determinism is based on the

presence of mechanisms in PHY or the MAC layer. For instance, the implementation of TDMA is an indicator of the network's capability to ensure deterministic transmission in a dedicated time slot (100, Section IV.A).

  - 1: no deterministic access (e.g. CMSA-CA in MAC layer)
  - 2: deterministic access (e.g. TDMA in MAC layer)

- **Data rate**: The data rate is a critical metric in communication systems as it defines the amount of information that can be exchanged in a given time frame, thus determining the overall capacity of the system. This evaluation focuses primarily on data transmitted wirelessly from the PHY layer of a transmitting system to the PHY layer of a receiving system. Data rates are categorised according to CCSDS (3, Chapter 1.5).
  - 1: low data rate (below 1 Mbps)
  - 2: medium data rate (between 1 Mbps and 10 Mbps)
  - 3: high data rate (between 10 Mbps and 100 Mbps)
  - 4: very high data rate (above 100 Mbps)
- **Robustness**: Robustness in wireless networks refers to the ability to maintain a stable connection under adverse conditions or in the presence of possible interference. The dissertation focuses specifically on the robustness of the protocol in the PHY and MAC layers. Important factors that influence the robustness in these layers are the interference from other RF systems, as well as the multipath fading. The evaluation performed here, qualitatively analyses various robustness mechanisms to increase the robustness of the protocol. These include channel hopping, which improves robustness against interference (101), and the utilization of IR-UWB transmission, with mainly two techniques, pulses and wideband which is effective against both multipath fading and interference (102, Table 1.7).
  - 1: no established robustness methods in PHY and MAC layer against interference or multipath fading
  - 2: partially established robustness methods in PHY or MAC layer against interference or multipath fading
  - 3: fully established robustness methods in PHY and MAC layer against both interference and multipath fading
- **Scalability**: Scalability in a wireless network is defined by its ability to adjust its size, either by increasing or decreasing, without significantly impacting its performance. This aspect of scalability is often measured in terms of the number of nodes that the network can effectively operate (103).

  - 1: less than 10 nodes
  - 2: between 10 and 100 nodes
  - 3: between 100 and 1000 nodes
  - 4: above 1000 nodes

- **Power Consumption**: The power consumption of a wireless network and its devices is crucial, especially for space applications where energy resources are limited and a huge amount of nodes needs to be covered. Power consumption is categorised according to a common approach for comparing different short-range wireless networks (104).

  - 1: high power consumption (above 500 mW)
  - 2: medium power consumption (between 100 mW and 500 mW)
  - 3: low power consumption (between 10 mW and 100 mW)
  - 4: very low power consumption (below 10 mW)

3.2.2 Establishment of minimum requirements

This Subsection sets out the minimum requirements for each application based on the defined criteria. It is important to recognise that the requirements analyses consider not only the minimum expectations, but also the maximum tolerable limits. This means that while some criteria have clear minimum requirements, such as a latency of less than 10 ms, other criteria may have a maximum tolerable value, such as power consumption between 10 mW - 100mW that is still acceptable for a specific application. The main objective of this analysis is to ensure that the proposed architecture and associated protocols both meet the minimum requirements and operate within the maximum tolerable limits.

A detailed analysis of each application field is essential for gaining an in-depth understanding of the different conditions and to determine what the wireless protocol must do to be considered suitable for the application. A detailed breakdown of how the individual requirements were assessed for the specific applications is provided next:

Non-critical sensing

- **Latency: 1** (no real-time access)
  Justification: Most sensor data is used for offline processing on the ground, hence, some delay in transmitting this data is generally acceptable without significantly impacting the satellite mission. Typically, these sensors do not require real-time communication.

- **Determinism: 1** (No deterministic access)
  Justification: Deterministic communication is not essential as sensor data are often buffered. Inconsistencies usually do not adversely affect satellite functions.

- **Data rate: 1** (below 1 Mbps)
  Justification: Given that the volume of transmitted data is typically low, minimal data rates are sufficient.

- **Robustness: 2** (Partially established)
  Justification: Communication should maintain a degree of robustness, not necessarily in reliability, but at least in withstanding disturbances and space conditions. Since these sensors are not mission-critical, minor interference or degradation in communication can be tolerated.

- **Scalability: 4** (above 1000 nodes)
  Justification: A significant number of sensors might be required. For instance, the Ariane 5 launcher uses up to 1100 sensors. Thus, the network must support a large number of sensing nodes.

- **Power Consumption: 4** (very low)
  Justification: Since sensors are read sporadically, they are particularly suited for battery operation. Additionally, given the large number of sensors, power consumption per node must be kept minimal.

Critical sensing

- **Latency: 2** (real-time access)
  Justification: Mission-critical sensors, such as those involved in the AOCS or thruster system, need quick data availability. This requires low latencies to ensure rapid responses for critical operations.

- **Determinism: 2** (deterministic access)
  Justification: Predictable and consistent communication is important for these sensors. Any delay or inconsistency in communication can lead to system malfunctions or even mission failures.

- **Data rate: 2** (between 1 Mbps and 10 Mbps)
  Justification: Given that these sensors are frequently sampled, a moderate data rate is essential to provide quick data availability. The exact rate may vary based on the sensor type and its sample frequency.

- **Robustness: 3** (Fully established)
  Justification: Sensors critical to the mission must be extremely robust and operate reliably within their specific environment that can be interrupted by interference or multipath fading. Failures or malfunctions in the communication can negatively affect the mission success.

- **Scalability: 3** (between 100 and 1000 nodes)
  Justification: Depending on the system's size and the number of mission-critical sensors, a moderate network size is assumed.

- **Power Consumption: 3** (low)
  Justification: The power consumption must be kept as small as possible since multiple sensors might operate simultaneously. It typically ranges between 1 to 10 mW, making it essential to ensure efficient energy usage to support prolonged mission duration and the concurrent operation of various sensors.

Onboard Communication

- **Latency: 2** (Real-time access)
  Justification: Low latency ensures real-time communication between various onboard subsystems and components. This becomes especially vital when certain threshold values are surpassed, requiring an immediate response from the system.

- **Determinism: 1** (no deterministic access)
  Justification: While strict determinism is not essential, functionalities should be available to prioritise specific communications or give preferential treatment when necessary.

- **Data rate: 2** (between 1 Mbps and 10 Mbps)
  Justification: Moderate data rates are sufficient for onboard communications to facilitate rapid data transfer between subsystems and equipment, since the data usually contains commands and health status / telemetry from the various components.

- **Robustness: 3** (Fully stablished)
  Justification: Onboard communications requires a high degree of robustness given the mission-critical nature of the exchanged data between subsystems and components. This includes robustness against interference and multipath fading.

- **Scalability: 2** (between 10 and 100 nodes)
  Justification: Moderate scalability is adequate in order to connect the various subsystems and components within the avionics architecture.

- **Power Consumption: 3** (low)
  Justification: Given the power consumption of the single components (especially in traditional satellites), the energy used for the communication channel is not a driving factor for operational efficiency.

High Data-Rate Payloads

- **Latency: 1** (no real-time access)
  Justification: For high data-rate payloads, no real-time access is required, since data is mostly post-processed on ground (offline).
- **Determinism: 1** (no deterministic access)
  Justification: Nominally, payloads do not require deterministic communication. However, this depends on the payload application.
- **Data rate: 4** (above 100 Mbps)
  Justification: A very high data rate is particularly essential for scientific instruments, such as imagers.
- **Robustness: 2** (Partially established)
  Justification: Since a temporary disruption in payload communication is not usually considered mission-critical, partial robustness is sufficient against interference.
- **Scalability: 1** (less than 10 nodes)
  Justification: Generally, there are only a few such communication links on satellites, making scalability non-essential in this context.
- **Power consumption: 1** (high)
  Justification: Power consumption is not a primary concern since the focus lies on the processing and handling of high data amounts, which always drives the power and is usually tolerated.

AIT Support

- **Latency: 1** (No real-time access)
  Justification: AIT operations includes test data for monitoring in a relatively short time. However, very low latencies are not required since the AIT support is mainly covering the monitoring activities during test sequences.
- **Determinism: 2** (No deterministic access)
  Justification: No determinism is required for the data transmission during testing on ground.

- **Data rate: 2** (between 1 Mbps and 10 Mbps)
  Justification: AIT ground tests typically involve the transmission of moderate amounts of test data. Additionally, a wireless EGSE interface for functional testing can serve for monitoring purposes and can require a moderately high data rate.

- **Robustness: 1** (No established)
  Justification: Robustness requirements are generally lower during AIT. Identified issues can lead to repeated tests or data communication.

- **Scalability: 3** (between 100 and 1000 nodes)
  Justification: Depending on the spacecraft's size, many devices might be tested simultaneously. Particularly during environmental test campaigns, such as thermal vacuum tests, a large number of sensors might be necessary.

- **Power Consumption: 1** (high)
  Justification: Power consumption is not a primary concern here since it is provided by the testing facility.

The results of the analysis are presented in Table 3.4, showing the identified applications with different requirements for the selected criteria.

TABLE 3.4: Requirements for specific application fields

Application field	**Latency**	**Determinism**	**Data rate**	**Robustness**	**Scalability**	**Power**	**Sum**
Non-critical sensing	1	1	1	2	4	4	13
Critical sensing	2	2	2	3	3	3	15
Onboard communication	2	1	2	3	2	3	12
High Data-Rate Payloads	1	1	4	2	1	1	10
AIT – ground testing	1	1	2	1	3	1	9

Note: For explanations of the scoring criteria (1-4), please refer to Subsection 3.2.1.

This shows that not all applications have the same high requirements. In particular, critical sensing like mission-critical sensing or crew health monitoring applications have the highest requirements. This is because in these applications a robust communication is required and data must be available quickly in order to have a timely response. Any misinterpretation or loss of data can lead to significant system degradation, including total failure, as can happen with the AOCS. In the context of crew health monitoring, the health of the astronaut is involved, so the requirements are also very stringent. On the other hand, the operation of wireless networks in the AIT domain is the application with the lowest level of requirements. This is because the network is operated on the

ground, and any failures or malfunctions are easier to compensate for and typically do not lead to system failure.

3.2.3 Evaluation of wireless protocols

This Subsection provides an evaluation of each wireless protocol. It allows a systematic and objective analysis of the capabilities of each protocol with respect to the defined criteria. The protocol characteristics and parameters already described in Chapter 2 and summarized in Table 2.3 are used for the evaluation and a consolidated overview of the results of the evaluation is given in Table 3.5. A more detailed explanation is presented in Appendix A. Based on this evaluation, the matrix evaluation in the next Subsection is used to determine which standard meets the minimum requirements of the different applications.

TABLE 3.5: Evaluation of protocol standards

Protocol	**Latency**	**Determinism**	**Data rate**	**Robustness**	**Scalability**	**Power**	**Sum**
Wi-Fi	2	1	4	2	2	1	12
Bluetooth	1	1	2	1	1	3	9
ZigBee	1	1	1	1	4	4	12
Industrial 802.15.4-based	1	2	1	2	4	3	14
IR-UWB/LLDN	2	2	3	3	4	2	16

Note: For explanations of the scoring criteria (1-4), please refer to Subsection 3.2.1.

From the sum of the ratings it can be seen that although there are individual protocols that perform better in specific criteria, such as Wi-Fi for data rate or the 802.15.4 based protocols for power consumption, the combination of IR-UWB and LLDN at the MAC layer already provides the best performance for the defined criteria.

3.2.4 Suitability matrix

In this Subsection, a separate evaluation matrix is created for each application. Each submatrix consists of rows for each protocol and columns for each criterion, which is illustrated in Table 3.6 on the next page. Within the matrix, submatrices for the separate applications show whether the standard meets the minimum requirement of the respective criterion of a particular application (”1” for met, ”0” for not met). The values of each row of the matrix are summed to show how well a protocol meets the minimum requirements of an application across all criteria.

The sums show that IR-UWB/LLDN is the best or at least second best for the analysed applications. There are only two applications where the performance of other protocols is better. At the same time, the two weak points of IR-UWB are shown in these two applications. It is therefore important to highlight the limitations of IR-UWB technology. The first is the data rate, especially when it comes to the application of High Data Rate Payloads, which require very high data rates. The maximum achievable data rate is much lower compared to the Wi-Fi protocol. In particular, for communication links requiring very high data rates, the choice of IR-UWB may reach its limits and it may be appropriate to use Wi-Fi instead. For Non-critical Sensors where power consumption is a driving factor, power consumption is another drawback. Other protocols designed for low power applications, such as ZigBee or the industrial protocols based on 802.15.4, have much better performance in terms of power consumption and may be the better choice, especially if a large number of sensor nodes are to be deployed.

TABLE 3.6: Suitability matrix of wireless protocols for space applications

Application	Protocols	Criterion						Sum
		Latency	Determinism	Data rate	Robustness	Scalability	Power Consumption	
Non-critical sensing								
	Wi-Fi	1	1	1	1	0	0	4
	Bluetooth	1	1	1	0	0	0	3
	ZigBee	1	1	1	0	1	1	5
	Industrial	1	1	1	1	1	1	6
	IR-UWB/LLDN	1	1	1	1	1	0	5
Critical sensing								
	Wi-Fi	1	0	1	0	0	0	2
	Bluetooth	0	0	1	0	0	1	2
	ZigBee	0	0	0	0	1	1	2
	Industrial	0	1	0	0	1	1	3
	IR-UWB/LLDN	1	1	1	1	1	0	5
Onboard communication								
	Wi-Fi	1	1	1	0	1	0	4
	Bluetooth	0	1	1	0	0	1	3
	ZigBee	0	1	0	0	1	1	3
	Industrial	0	1	0	0	1	1	3
	IR-UWB/LLDN	1	1	1	1	1	0	5
High Data-Rate payloads								
	Wi-Fi	1	1	1	1	1	1	6
	Bluetooth	1	1	0	0	1	1	4
	ZigBee	1	1	0	0	1	1	4
	Industrial	1	1	0	1	1	1	5
	IR-UWB/LLDN	1	1	0	1	1	1	5
AIT support								
	Wi-Fi	1	1	1	1	0	1	5
	Bluetooth	1	1	1	1	0	1	5
	ZigBee	1	1	0	1	1	1	5
	Industrial	1	1	0	1	1	1	5
	IR-UWB/LLDN	1	1	1	1	1	1	6

3.2.5 Overall assessment

In this Subsection, a cumulative assessment is performed in order to identify the best performing protocol for the analysed application fields. This concludes with a recommendation of a suitable, universally applicable protocol architecture for the progressive steps of this dissertation. To determine which protocol performs best and is therefore most suitable and comprehensive to cover as many applications as possible simultaneously, the results of the respective applications from the suitability matrix are summarised in Table 3.7.

TABLE 3.7: Cumultative suitability assessment for various applications

	Non-critical sensing	**Critical sensing**	**Onboard communication**	**High Data-Rate Payloads**	**AIT – ground testing**	Sum
Wi-Fi	4	2	4	6	5	21
Bluetooth	3	2	3	4	5	17
ZigBee	5	2	3	4	5	19
Industrial	6	3	3	5	5	22
IR-UWB/LLDN	5	5	5	5	6	26

Notably, IR-UWB stands out in performance, underlining its suitability for a wide range of space applications. Therefore, IR-UWB combined with LLDN in the MAC layer is chosen for further dissemination as a highly effective framework because to its robustness, but also because of its low latency, and determinism characteristics, which ultimately lay the groundwork for the wireless network architecture and thus represent its principal component. The IR-UWB physical layer has excellent characteristics that make it very robust, especially in highly reflective environments without interfering with other RF-sensitive components. At the same time, the MAC layer provides features that enable a reliable and deterministic communication to be established. Together they also ensure low latency.

Moreover, the selection of IR-UWB technology offers another significant advantage over traditional wireless technologies. It enables precise positioning, which not only complements the traditionally communication-centric applications assessed earlier but also opens up new possibilities in the area of positioning. This unique feature underscores the versatility of IR-UWB in terms of its use in spacecraft. Possible applications would thus include:

- **Positioning and tracking of astronauts:** In the space station, IR-UWB can be used to precisely locate and track astronauts. This is particularly important for rapid response in the event of an emergency, such as a medical emergency or evacuation. The technology can also help optimise workflows by monitoring the location and movement patterns of crew members.
- **Deployment and monitoring of large structures:** IR-UWB could be used to monitor the correct deployment of structures such as large solar panels, antennas

or other modular elements of the spacecraft. The technology can provide accurate data on the deployment status, helping to detect malfunctions or damage at an early stage.

- **Inventory and equipment tracking:** Tracking equipment and supplies within the space station or habitats is another important potential application. Positioning with IR-UWB can enable items to be located, improving inventory efficiency. This is particularly useful as searching for items in microgravity can be challenging.
- **Automation and robotics:** In space applications, IR-UWB can be used to control robots or automated systems, either outside or inside a station, such as the CIMON and AstroBee free-flying objects on the ISS. These systems can be used for maintenance, repair or scientific experiments. Precise control by IR-UWB is essential to ensure the effectiveness of these systems.
- **Monitoring docking dynamics:** IR-UWB can play an important role in the docking of spacecraft. It can be used as a low-cost technology to accurately determine the relative distance to ensure safe docking. In addition, IR-UWB can be combined with other sensor systems such as lidar, radar or optical systems to provide more comprehensive and accurate monitoring and control of the docking process.

3.3 Summary

Chapter 3 identified and analysed in detail various space applications for on board wireless networks, such as in satellites, launchers and the space station. The specific minimum requirements of these applications were investigated on the basis of defined criteria.

The Multi-Criteria Decision Analysis method was then used to evaluate the suitability of selected wireless protocols for the different applications. The protocols of the second Chapter were evaluated against the same criteria. The result of this process is a matrix showing the most suitable protocol for each application and an overall cumulative assessment of the results. The analysis shows that, despite its limitations, IR-UWB technology offers outstanding advantages. In combination with LLDN at the MAC layer, it is particularly well suited for the applications presented here, which is due to its robustness, low latency and deterministic features. As a result, this duo is chosen as the foundation of the wireless network concept to enhance the state-of-the-art intra-spacecraft communications infrastructure. Furthermore, this selection reveals many new wireless applications in precise positioning that were not possible with the narrowband wireless protocols before, marking a distinct feature in this specific area.

This is particularly interesting for the execution of the Wireless Compose experiment, as it allows for the demonstration not only of wireless network characteristics but also of positioning in orbit.

IR-UWB in combination with LLDN has not yet been explored in the literature and remains to be implemented and demonstrated. This is due to the origin design constraints for the narrow band 802.15.4-based physical layer (at 2.4 GHz). Chapter 4 aims at bridging this gap and deals with the implementation of a wireless network based on the selected architecture that intends to fully exploit its capabilities while addressing the associated challenges in Chapter 5.

Chapter 4

Concept

This Chapter provides a detailed examination of the identified wireless network concept. It specifically focuses on both the implementation and the performance evaluation.

From the analyses in Chapter 3, the synergistic combination of IR-UWB and LLDN emerged as the first choice. IR-UWB provides excellent robustness properties, while the LLDN scheme is characterised by its rigid structure, low latency and deterministic communication. This Chapter provides an in-depth understanding of both layers. It also provides an example of their performance in mission-critical sensing and discusses how the IR-UWB/LLDN can be integrated into the state-of-the-art avionics architectures, highlighting different approaches and their respective advantages and drawbacks.

Furthermore, the details of the implementation of the IR-UWB/LLDN are presented, including the hardware used and the software required. A particular challenge was the adaptation of existing OpenWSN software stack to implement the LLDN MAC layer. Finally, the performance of the wireless network is evaluated, especially in terms of latency, throughput and energy efficiency.

4.1 Proposed Wireless Network Architecture

The architecture of the proposed wireless network is described in more detail in the following. It is based on IR-UWB in the PHY layer and a MAC layer based on the IEEE 802.15.4e LLDN scheme. Explanation of the timing relationships within the different packet formats is important as these have a major impact on performance, particularly latency. Therefore, the packet structure of the physical layer and the specific timing conditions of IR-UWB will be introduced. The LLDN functionality is then explained and the timing relationships continued to show the potential of this combination for time-critical applications as known from the AOCS application.

4.1.1 Physical layer

This Subsection discusses the physical layer as defined in IEEE 802.15.4a in detail. The physical characteristics of the IR-UWB standard were already explained in detail in Subsection 2.5.5.1 and will therefore not be discussed again here. As already described, the focus here is on the presentation of the packet structure and the timing relationships in order to be able to derive the total duration of a frame. As mentioned above, the IR-UWB standard supports data rates in the range of 0.11 to 27.24 Mbps. IR-UWB communication is based on packet-oriented transmission and it uses the packet format shown in Figure 4.2. Each PPDU consists of a Synchronisation Header (SHR), a Physical Header (PHR), and a data field or PSDU.

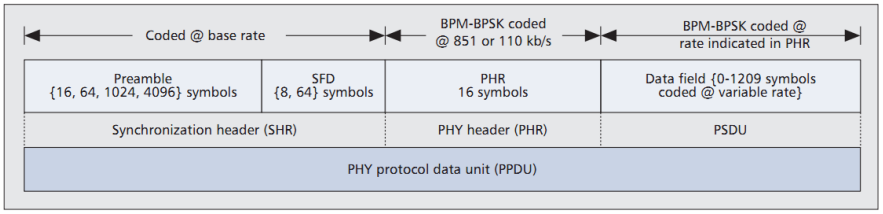

FIGURE 4.1: UWB PHY frame structure (68, Figure 1)

Within the frame structure, different types of modulation are used.

The UWB pulses of the PHR and PSDU are modulated using a combination of BPM and BPSK. The SHR, on the other hand, uses ternary pulse modulation. Each symbol of the SHR contains a preamble code of length N_{bit}, where N_{bit} is 31 or optionally 127, depending on the Pulse Repetition Frequency (PRF) used. The code is a sequence of code symbols from a ternary alphabet −1,0,1 with perfect periodic auto-correlation. The preamble length (PLEN) is defined by how many times (i.e. for how many symbols) the sequence is repeated.

As a result, the transmission rate of each part of the PPDU varies. While the SHR is transmitted at the basic symbol rate (1.01 or 0.99 MS/s), see Table 4.1, the PHR is transmitted at a data rate of 0.11 or 0.85 Mbps. The PSDU can be transmitted at data rates between 0.11 and 27.24 Mbps (105).

TABLE 4.1: Preamble symbol parameters and duration

N_{Bit}	PRF_{mean} (MHz)	PRF_{prb} (MHz)	N_{cps}	t_{PRBSym} (ns)	Symbol rate (MS/s)
31	15.6	31.2	496	993.59	0.99
127	62.4	124.8	508	1017.63	1.01

Forward error correction is also applied and both Convolutional Codes (CC) and Reed-Solomon Codes (RS) are used to protect the payload while a modified Hamming code and an RS code are used to protect the PHR. The PHR also uses six parity bits to further

protect against channel errors, which are corrected by forward error correction codes. Figure 4.2 shows the process chain for generating UWB signals within a transmitter, where the different coding blocks are illustrated.

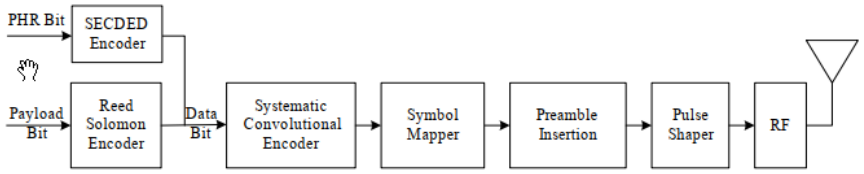

FIGURE 4.2: Processing chain of a UWB transmitter (106, Figure 83)

The SHR contains the preamble followed by the Start of Frame Delimiter (SFD). The SFD marks the end of the preamble and the start of the PHR and is used to support the frame timing definition, which is very important for accurate ranging measurement. Therefore, the UWB physical layer provides a short SFD (8 symbols) at standard and medium data rates and an extra-long SFD (64 symbols) at low data rates of 0.11 Mbps (68, p. 46).

In the preamble, the number of symbols is used according to the requirements of the application. According to the standard, the preamble can contain 16, 64, 1024, and 4096 symbols, resulting in different times depending on the PRF. The longer lengths (1024 and 4096) are usually used with non-coherent receivers to improve the SNR during processing. The preamble symbol duration for the different PRFs is shown in Table 4.1. The preamble is transmitted at a higher pulse repetition frequency PRF_{prb} than the data part at PRF_{mean}.

The following PHR contains information about the data packet size, the data rate, the length of the synchronisation preamble, and parity bits for error detection and correction within the PHR. The header is 19 bits long and is followed by the data field which, by default, can have a maximum size of 127 bytes.

Some important timing parameters for the PHR and the user data are listed in Table 4.2. All Modulation and Coding Schemes (MCS) listed in the table occupy the same bandwidth (499.2 MHz).

At a 0.11 Mbps data rate, the PHR bitrate is also 0.11 Mbps, otherwise the PHR bitrate is 0.85 Mbps at all other data rates, which explains the constant symbol duration t_{PHRsym} in MCS 2 to 4 or 6 to 8.

The duration of the data portion t_D can be determined using Equation (4.1). Note that since a convolutional code (CC) with an encoding rate of 1/2 is used, one byte consists of 16 bits. The factor 1/2 in the formula for t_D and the PHR t_{PHR} is based on the assumption that a symbol can carry 2 bits due to the BPM-BPSK modulation.

Table 4.2: MCS overview (106, Table 99)

MCS	PRF_{mean} (MHz)	Code rate CC	Code rate RS	t_{PHRSym} (ns)	t_{Dsym} (ns)	Data rate (Mbps)
1	15.6	0.5	0.87	8205.13	8205.13	0.11
2	15.6	0.5	0.87	1025.64	1025.64	0.85
3	15.6	0.5	0.87	1025.64	128.21	6.81
4	15.6	1	0.87	1025.64	64.10	27.24
5	62.4	0.5	0.87	8205.13	8205.13	0.11
6	62.4	0.5	0.87	1025.64	1025.64	0.85
7	62.4	0.5	0.87	1025.64	128.21	6.81
8	62.4	0.5	0.87	1025.64	32.05	27.24

$$t_D = \frac{1}{2} \cdot ((N_{DByte} + N_{RSBit}) \cdot 16) \cdot t_{DSym} \tag{4.1}$$

The number of Reed-Solomon bits N_{RSBit} depends on the number of user data bits $N_{DByte} \cdot 16$ and a 48-bit Reed-Solomon block is inserted after each 330-bit data block.

The number of bits of the PHR is the same for all UWB frames with 19 bits, and the duration of the PHR t_{PHR} is calculated by multiplication with the duration of a PHR symbol.

$$t_{PHR} = N_{PHRBit} \cdot t_{PHRSym} \tag{4.2}$$

The total preamble duration t_{PRB} is determined by the Preamble Length Parameter (PLEN) and can be calculated using Equation (4.3).

$$t_{PRB} = PLEN \cdot t_{PRBSym} \tag{4.3}$$

The SFD comes in two versions: a short standard version with eight symbols and an extended version with 64 symbols. At a PRF_{mean} of 15.6 MHz, the constant duration of the short and extended versions is 7.9 μs and 63.3 μs respectively. At a PRF_{mean} of 62.4 MHz, the duration is 8.1 μs for the short and 65.1 μs for the extended version.

To determine the total duration of a frame t_{Frame}, the transmission times of the individual frame components are added (cf. (44, Chapter 2.2.5)).

$$t_{Frame} = t_{PRB} + t_{SFD} + t_{PHR} + t_D \tag{4.4}$$

The total duration of a frame t_{Frame} plays a crucial role and has a significant impact on the timing and latency of a system. Understanding the exact timing relationships and

effects of frame duration is essential in this context. The following Subsection describes the MAC layer in detail and derives the timing aspects further. This will form the basis for a later examination of the actual influence of frame duration on system behaviour using a concrete example from the AOCS, a mission- and time-critical application.

4.1.2 MAC layer

This Subsection focuses on a detailed description of the IEEE 802.15.4e LLDN scheme, which was originally introduced in response to the high demand for low latency in industrial applications such as factory production. LLDN provides several mechanisms to meet these stringent requirements, ensuring latency of less than 10 milliseconds. It also uses other techniques, such as TDMA-based access, to provide deterministic and robust communications (64).

Topology The LLDN network is based on either a star or multi-star topology, with a coordinator responsible for configuring and maintaining the network. There are two primary methods of transmitting messages: uplink and downlink. In uplink messages, devices send their data to the LLDN coordinator; for example, sensors might send their data to the coordinator. In contrast, downlink allows the coordinator to send commands to the devices, which could either telecommand them or actuate. The need for low latency is the main reason why LLDN only supports star or multi-star topologies. By comparison, mesh topologies, such as those found in industry standards like WirelessHART or ISA100.11a, can result in latencies of up to more than one second (67). In addition, mesh topologies add complexity, whereas star topologies are easier to implement, manage and operate.

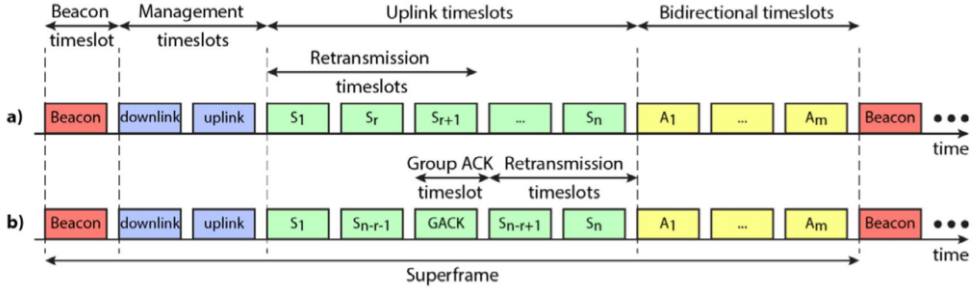

FIGURE 4.3: Slots order in an LLDN superframe with
a) re-transmission TS and
b) separate GACK TS

Superframe All network nodes share a common superframe for communication with the coordinator. The LLDN superframe structure consists of a beacon slot, a management slot (if any) and several uplink and bidirectional time slots of uniform length, as

shown in Figure 4.3. Messages sent to the coordinator are transmitted during the uplink time slots, with each slot containing a message from a single device. The bidirectional time slots allow a bidirectional data exchange between the coordinator and the devices, with the direction of transmission specified in the beacon frame. Typically, uplink time slots are allocated to sensor devices, while bidirectional downlink time slots are allocated to actuator devices. However, it is possible to combine multiple time slots to create a longer slot for a single device, which is beneficial for high data rate communications such as onboard communication. The superframe offers various configuration options and is flexible in its design. It allows packets that haven't been delivered to be re-transmitted within the same frame or at the start of the next superframe, with the number of available re-transmission slots defined during the design phase.

Each superframe begins with a beacon frame, which is critical for synchronising the network devices with the coordinator and exchanging information about superframe creation. This beacon frame is also critical for synchronising devices in low-power or sleep mode. It contains the current transmission configurations and acknowledgements for the data received by the coordinator from the LLDN devices in the previous superframe. However, a separate group acknowledge (GACK) frame may also be included in the superframe. This separate GACK frame, sent by the coordinator, indicates the devices from which data has been successfully received in the same superframe. Devices that have failed to transmit data to the coordinator can identify a re-transmission slot in the same superframe following the GACK slot - a unique LLDN feature, as re-transmissions typically occur at the beginning of the following superframe.

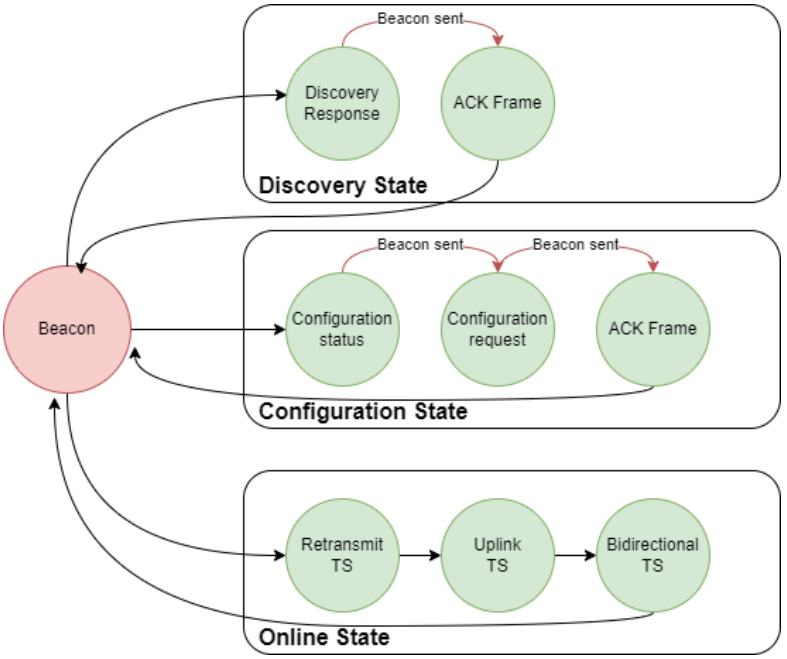

FIGURE 4.4: LLDN state diagram (cf. (107, p. 12831ff))

Network states An overview of the different network states is illustrated in Figure 4.4. Network initialisation typically begins with the Discovery State, where new devices are added to the network. During the Configuration State, all necessary information is exchanged to enable synchronous communication. Following this, the network enters the Online State where data transmission is established. Additionally, security algorithms can be activated during this phase. However, it is important to note that implementing security features may increase the frame size, potentially impacting latency negatively. Typically, the network starts with the Discovery State, especially when the number of participants or their identities are not predetermined. However, in cases where a fixed network configuration and predetermined participants are in place, such as in a spacecraft, the network can begin directly in the Online State.

If security is not enabled, the overhead due to the MAC header (MHR) and MAC footer (MFR) is only 3 bytes, as portrayed in Figure 4.5. Security mechanisms add another 1 to 15 bytes to the frame, whereby this depends on the level of security required. The non-secure MHR consists of a single byte, also called the frame control, which describes the type of frame, the security of the frame, and the requirements for acknowledging the frame. The remaining 2 bytes are the Frame Checksum (FCS) (74, p. 15).

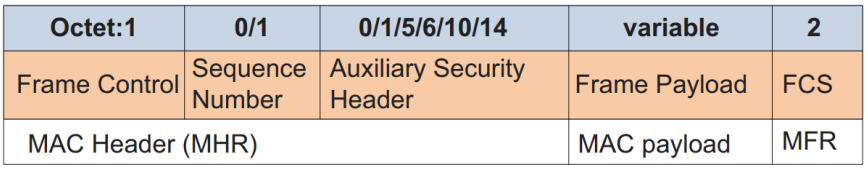

FIGURE 4.5: LLDN frame format (64, Figure 5)

To meet the latency requirements of mission-critical applications such as AOCS, where latencies of less than 10 milliseconds are required, the MAC packet format is optimised and time slots must be designed accordingly. Therefore, it is important to further analyse the timing relationship and its impact on the frame duration, which directly affects the time slot duration.

To calculate the time slot size for the base time slot, Equation (4.4) can be used, taking the bytes for MHR and FCS that are part of the PSDU into account. This results in a modified equation for t_{BTS}:

$$t_{BTS} = t_{PRB} + t_{SFD} + t_{PHR} + t_{MHR} + t_D + t_{IFS} \tag{4.5}$$

whereby

$$t_{MHR} = \frac{1}{2} \cdot (N_{MHRByte} \cdot 16) \cdot t_{DSym} \tag{4.6}$$

and $N_{MHRByte}$ is the number of bytes of MAC overhead (consisting of MHR + FCS).

Since the MAC layer needs time to process the data received from the PHY layer, two consecutive transmitted frames are separated by at least one Interframe Space (IFS) of duration t_{IFS}. The size of the base TS depends on the PSDU. If it is less than or equal to 18 bytes, a Short Interframe Space (SIFS) is used, alternatively a Long Interframe Space (LIFS) is recommended. When LIFS is used, the base TS size increases significantly compared to SIFS as SIFS has a fixed size of 12 preamble symbols while LIFS has a size of 40 preamble symbols.

Latency analysis To demonstrate the latency capabilities, AOCS system will be taken as an example. A typical attitude control system would consist of several ACS sensors sending data to the LLDN coordinator. The LLDN coordinator would act as a controller connected to a processing unit that calculates the control signal values for the actuators based on the received sensor data. The coordinator would then transmit these values as commands to the ACS actuators, as shown in Figure 4.6.

Devices connected to sensors and actuators are typically low-resource, low-power processors. In contrast, the LLDN coordinator may be a more resource-intensive device depending on its tasks (see (64, p. 5569)). As mentioned earlier in the Table 3.2, the highest repetition rate is for the IMU, which is about 100Hz, requiring a latency of less than 10ms. An IMU generally consists of two sensors, the accelerometer and the gyroscope. The data from the VN-100 IMU manual (108) is used as an example to determine the packet size. The calculation is as follows: x, y, z values for the respective axes ($32bit \cdot 6 = 24bytes$), temperature (4 bytes), protocol overhead (4 bytes) and CRC (2 bytes), resulting in a packet of approximately 34 bytes.

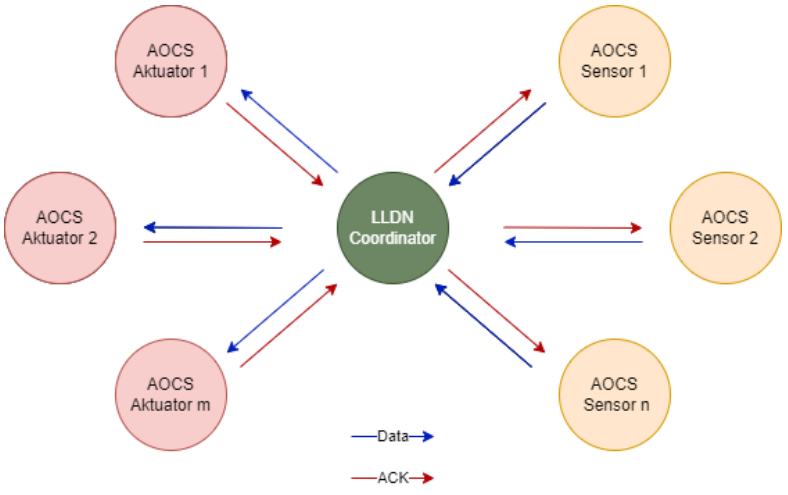

FIGURE 4.6: LLDN topology

As the attitude control system is typically controller-centric, a star topology is most appropriate in this context. A good example of this is the Sentinel 2A satellite, which

consists of about 33 devices (sensors and actuators), as mentioned in the Table 3.2. However, some of these devices are cold redundant and therefore not in operation, so the network size is estimated to be about 25 simultaneously operating devices. The average payload size is 34 bytes per device. Each device is allocated an uplink and downlink time slot within the superframe for bi-directional communication. It is clear that the size of the superframe is a primary driver of the overall latency, which means that the number of devices must not exceed a certain limit, which will be analysed next.

In the initial phase of the analysis, the total duration of a PPDU, the total duration of a PPDU is examined, which corresponds to the basic time slot duration t_{TS}. MCS modes 1 to 4 are used, implying a PRF of 15.6 MHz and data rates ranging from 0.11 Mbps to 27.2 4Mbps.

As previously mentioned, the derived payload size is set to 34 bytes for this example. The minimum MAC overhead is set to 3 bytes, 1 byte for the MAC header and 2 bytes for the FCS, indicating that no security mechanisms are enabled. The shortest possible preamble length of 16 is chosen to provide a lower bound on the resulting latency. The duration of a PPDU and its components can be found in the Table 4.3. These durations are calculated using the equations in Section 4.1.1.

Table 4.3: PPDU duration for a 34 Bytes payload size

MCS	Data rate (Mbps)	t_{PRB} (μs)	t_{SFD} (μs)	t_{PHR} (μs)	t_{MHR} (μs)	t_D (μs)	Sum (ms)
1	0.11	15.9	63.3	155.9	155.9	2625.6	3.06
2	0.85	15.9	7.9	19.5	24.6	328.2	0.39
3	6.81	15.9	7.9	19.5	3.1	41	0.09
4	27.54	15.9	7.9	19.5	0.78	10.3	0.05

At higher MCSs, the proportion of SHR and PHR in the total PPDU duration increases significantly, as these are transmitted at a fixed symbol rate in all MCSs. The proportion of MAC and payload data is therefore less than 25% in MCS 3 & 4.

Figure 4.7 shows the superframe size as a function of the number of devices for a payload size of 34 bytes. To analyse the superframe size as a function of the PSDU size, a fixed number of 25 devices (with two time slots per device) was chosen. Figure 4.8 shows that a payload size of 34 bytes or more can only be transmitted at a data rate of 6.81 Mbps or higher to maintain a latency below 10ms.

The jump in Figure 4.8 is caused by the IFS distance used to process the superframes. This distance increases from 12 to 40 symbols when the size of the PSDU is greater than 18 bytes.

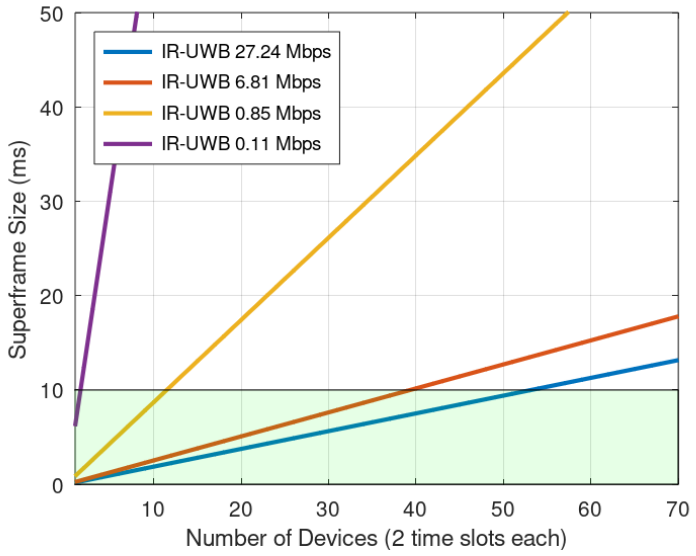

FIGURE 4.7: Superframe size vs the number of devices with a fixed payload data size of 34 bytes

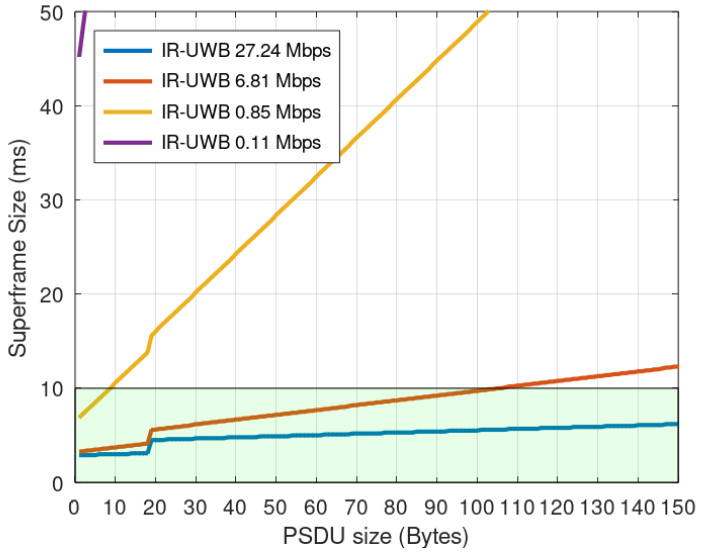

FIGURE 4.8: Superframe size vs payload data size for 25 devices and 2 TS per device

In conclusion, the latency analysis shows that the proposed architecture with IR-UWB in combination with LLDN well meets the latency requirements for mission critical applications such as the AOCS.

4.2 Integration into existing avionics architecture

This Section deals with the integration and utilisation of IR-UWB/LLDN-based wireless network into the traditional avionics architecture of a spacecraft, as shown in Figure 4.10

and discusses the various resulting approaches and how wireless networks can enhance or completely replace the existing state-of-the-art hard-wired interconnections. The flexible application of IR-UWB/LLDN opens up many new possibilities as discussed earlier in Chapter 3. However, as system-specific constraints can vary widely and depend on many factors, including the spacecraft type and its operational focus, the wireless network integration can therefore be realised in different ways which are discussed in the following Subsections.

4.2.1 Traditional Wired Approach

Firstly, the pure wired approach is explained. This approach represents the traditional wired intra-spacecraft communication found on spacecraft or other space systems. At the heart of the system is the on-board computer, which acts as a router and co-ordinates the flow of data across the network. The avionics architecture presented here as an example is based on the avionics of the Sentinel 2A satellite (98, Fig. 4). In part, it contains bus communication for the various subsystem components, and there are also direct links to the OBC where specific interfaces, such as analogue or high data rate, are required. In addition, remote terminal units (RTUs) are used, which in turn form sub-networks and usually implement a star topology, e.g. for the connection of sensors, actuators or other components to the OBC.

The system functionality in Figure 4.9 can be divided into the already introduced application fields:

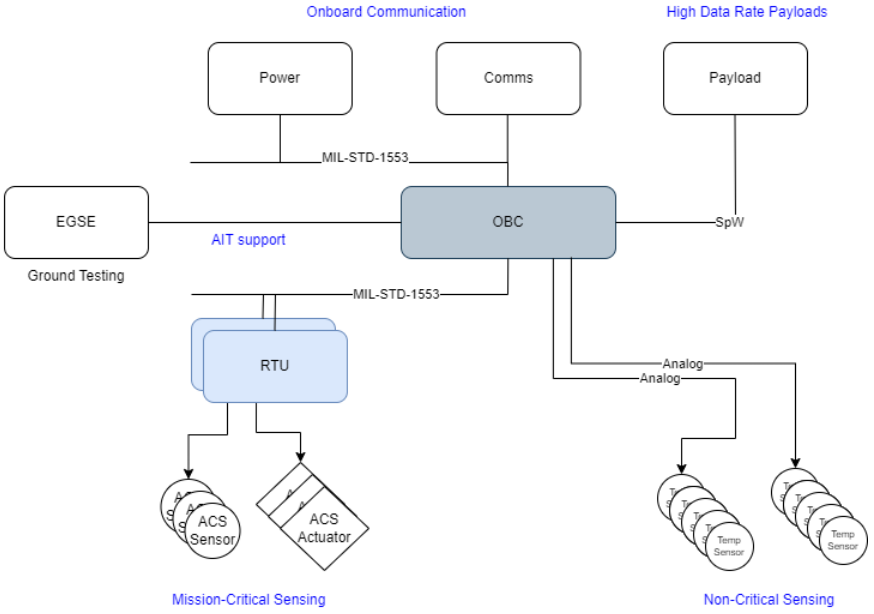

FIGURE 4.9: Avionics Architecture of the Traditional Approach

- Onboard communication: This area contains the main subsystem components. Communication between these units and the OBC is based on the low rate MIL-STD-1553 standard.
- High Data Rate Payloads: This area contains the payloads which are connected to the OBC via high data-rate interfaces such as SpW.
- AIT Support: This area contains the ground test connection with the EGSE.
- Critical Sensing: This area is for mission critical sensors and actuators. For example, the diagram shows ACS sensors and actuators both connected to a RTU.
- Non-critical sensing: This includes analogue sensors that provide non-critical data, such as temperature sensors and which are directly connected with the OBC.

Advantage: The wired approach is highly robust, ensuring a stable and reliable connection even in demanding environments. It offers high data throughput, allowing large amounts of data to be transferred efficiently. Since no radio signals need to be transmitted, the overall power consumption is also low.

Drawback: A disadvantage is the lack of flexibility. Changes or extensions require physical adjustments to the wiring. Especially in large installations, implementation and maintenance costs are high. The complexity of implementation and management is also increased, requiring additional engineering effort.

4.2.2 Enhanced Hybrid Approach

As shown in Figure 4.10, this approach targets the combination of traditional wired architecture with the wireless network based on IR-UWB/LLDN to best balance the strengths of both systems. The wireless network is particularly employed where its benefits like robustness, bidirectional communication, low latency, and deterministic transmission can be maximally utilized.

A key feature of this approach is the ability to wirelessly integrate both critical and non-critical sensors as seen in Figure 4.10. The bidirectional time slots in LLDN protocol also allow actuators or other components to be controlled forming a complete AOCS system.

The LLDN protocol can also be used in a multi-star scenario. This allows multiple independent wireless networks to operate, which is particularly useful when there are different application requirements such as latency and data rate. For example, a dedicated sub-network can be set up for non-critical sensors, with sensor data collected to

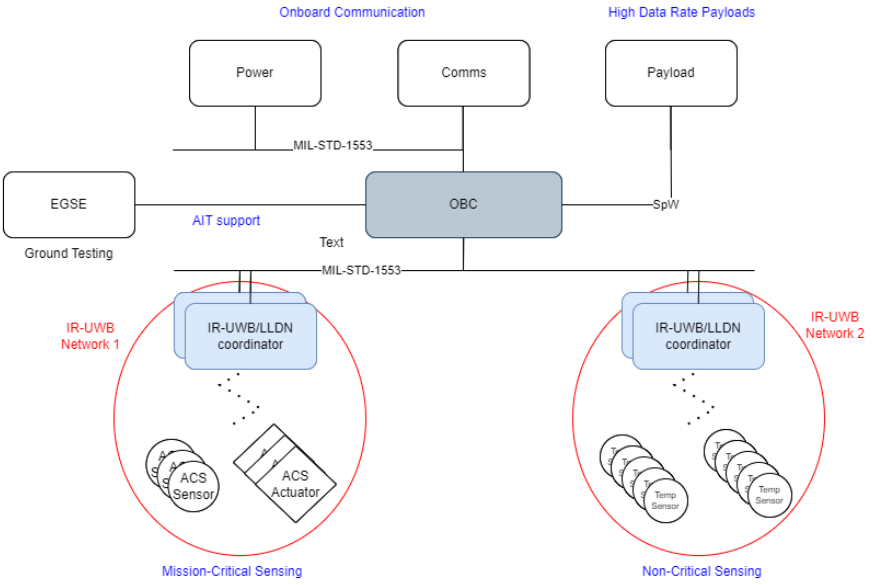

FIGURE 4.10: Avionics Architecture of the Enhanced Hybrid Approach

provide historical telemetry such as from temperature sensors. The dedicated networks could be implemented using different frequency channels to ensure their independent operation.

A critical factor in this approach is system redundancy. While the LLDN coordinator is a potential single point of failure, the implementation of redundant coordinators could significantly increase reliability. Should one coordinator fail, the redundant coordinator could take over immediately.

Due to the flexibility in integrating wireless sensors and actuators, the enhanced hybrid approach offers significant advantages in reducing the harness. In addition, preprocessing of sensor data directly in the coordinator could reduce the load on the onboard computer. Despite these benefits, it is still possible to retain traditional wired connections and interfaces, facilitating the transition to wireless networks without having to completely replace the existing architecture.

Advantage: The enhanced hybrid approach provides a balanced combination of wired stability and wireless adaptability. This allows both robust wired and wireless data transmission and a degree of flexibility in case of changes or extensions through wireless interfaces. IR-UWB/LLDN is only used, where it shows advantages and has its strengths. It allows cost and complexity to be kept in the medium range by reducing some of the wiring harness. In terms of mass reduction, the hybrid approach also offers advantages by using wireless networks to reduce the overall mass, especially when integrating wireless sensors.

Drawback: However, it is not the best option as it still requires some cabling. Power consumption is higher than the wired approach because some of the connections are wireless.

4.2.3 Pure Wireless Approach

As shown in Figure 4.11, this approach represents a complete conversion of the communication architecture to the IR-UWB/LLDN protocol, eliminating all physical cabling. This approach enables the vision of a completely wireless satellite and the creation of specific sub-networks for different communication applications. UWB technology supports up to 12 different subnets with different channels and PRFs that are physically independent and can operate simultaneously.

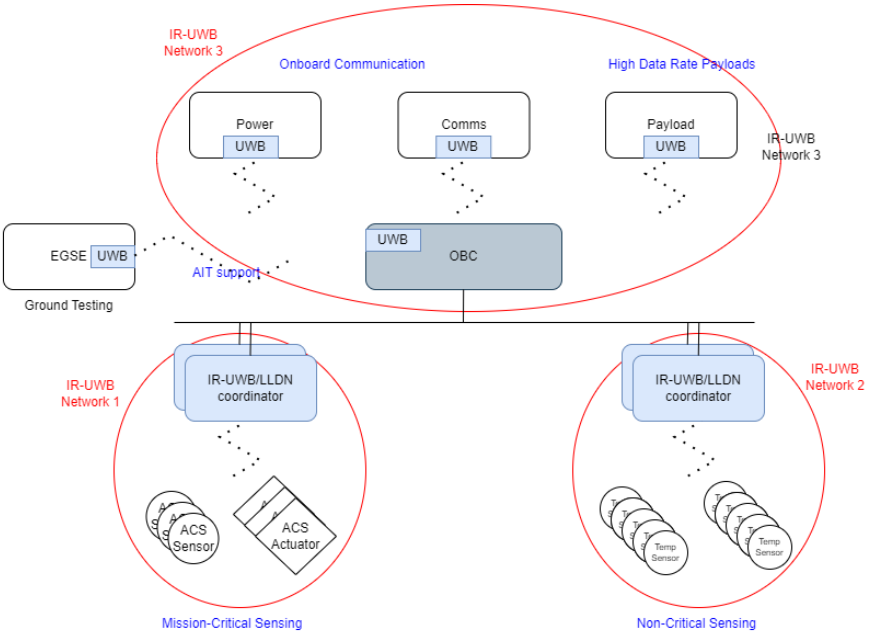

FIGURE 4.11: Avionics Architecture of the Pure Wireless Approach

As shown in Figure 4.11, this approach represents a complete conversion of the wired communication to the IR-UWB based wireless world, eliminating all physical cabling. This approach enables the vision of a completely wireless satellite and the creation of specific sub-networks for different communication applications. IR-UWB technology supports up to 12 different subnets with different channels and PRFs that are physically independent and can operate simultaneously.

Despite the advantages, the purely wireless approach can introduce some complexity in implementation as it attempts to make all connections wireless, which may be sub-optimal for certain applications. One critical aspect is the asynchronous communication between various components. The communication can be time-tagged and/or time-triggered. Components send ACKs for commands and provide housekeeping data at fixed

intervals, e.g. every 30 seconds. The LLDN superframe must be constantly rescheduled and reconfigured. This requires flexible resource allocation, especially in the area of on-board communications. Flexible mechanisms are needed to switch between data acquisition and telecommand, and to reconfigure time slots to handle unforeseen data streams such as firmware updates or error handling.

Another critical aspect of the optimised system operation is network flexibility and, in particular, flexible polling cycles. Changing data transfer and processing requirements may require frequent adjustments to the superframe structure. However, this functionality is available in LLDN so that the superframe structure can be reconfigured at any time. Another prominent feature is the ability to combine time slots for high data rate transmissions, allowing large amounts of data to be transmitted efficiently.

Advantage: The pure wireless approach is particularly advantageous in terms of mass reduction, as no cables or wiring are required. It offers flexibility, as changes or expansions can be easily made without the need for physical adjustments to the cabling. Integratability is also high, as it can be easily integrated into different systems.

Drawback: It has the highest power consumption, as wireless signals need to be constantly transmitted, especially as IR-UWB does not necessarily have the best performance in this area. In terms of robustness, wireless connections are more susceptible to interference, although IR-UWB offers good performance here. Despite its high integratability, it can be complex to implement, especially in environments with many wireless devices and different requirements. In addition, all devices must implement this technology as an interface, which could initially increase costs.

4.2.4 Flexible Multi-Protocol Approach

As shown in Figure 4.12, this approach represents the most efficient integration of wireless networks into the satellite avionics architecture. The aim is to combine the best features of each approach into an integrated solution. This can be achieved by using different wireless protocols or by combining wireless and wired architectures.

The most appropriate protocols are used for each specific application. Coexistence with other networks is a particular strength of IR-UWB. It does not affect or interfere with other wireless standards. This makes it possible to compensate for the disadvantages already mentioned regarding very high data rates and power consumption by using other protocols.

The IR-UWB/LLDN based stack can make a significant contribution to this approach. However, it can be complemented by more suitable protocols that can co-exist with

it without interfering with it. Examples include the use of Wi-Fi for very high data rate payloads or the implementation of industrial 802.15.4-based wireless networks for low power applications. Proprietary protocols such as the Skith wireless bus system developed by the University of Würzburg can also be used in this architecture (109, p. 4).

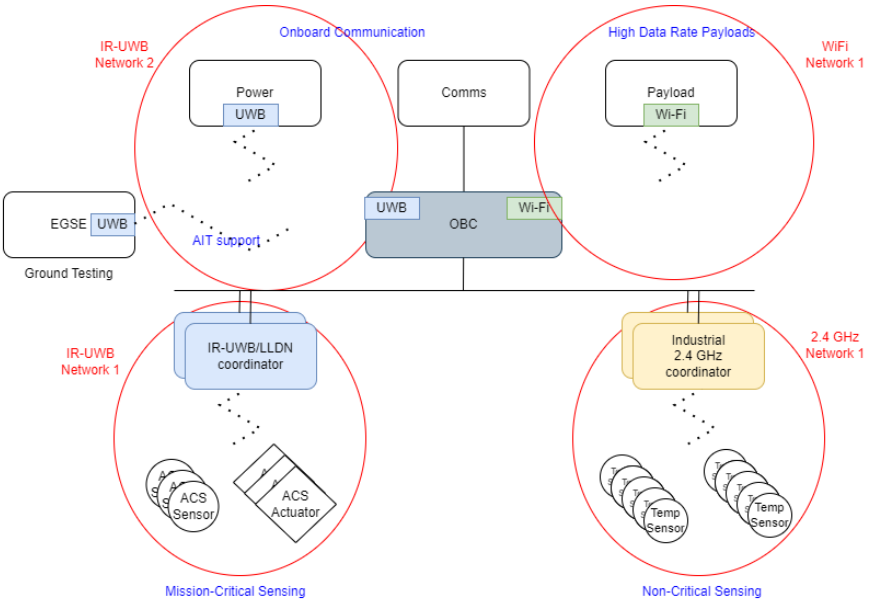

FIGURE 4.12: Avionics Architecture of the Flexible Multi-Protocol Approach

As shown in the figure, a low-power network is used for non-critical sensors, while a Wi-Fi interface is used for high data rate applications to provide the required high data rates. In addition, wired connections can be used where it makes sense and no suitable wireless alternatives are available. However, all the advantages of wireless communication can be exploited.

The flexible multi-protocol approach consequently allows different technologies to co-exist coherently, not only in RF but also for example in optical communications as demonstrated in the LiFi intra-satellite communication experiment SatelLight (110), each bringing its own strengths to bear where they are best suited. It should be noted, however, that dealing with multiple protocols is inherently more complex and can increase the effort required for implementation and testing.

Advantage: The multi-protocol solution offers a high degree of flexibility with the ability to add different wireless technologies as needed. Adaptations and extensions can be easily made without any physical changes, which means that the system remains adaptable. It can support different applications with tailored protocols for low power or high throughput requirements. Moreover, in terms of scalability, the multi-protocol

approach is very powerful. It can easily handle an increasing number of devices or increased traffic volumes.

Drawback: Robustness is problematic, as different protocols may have different requirements and potential vulnerabilities, or may interfere with each other. While implementation is versatile, management complexity can increase as different protocols require specific requirements and settings.

4.2.5 Summary

Various avionics architecture approaches have been introduced for the potential integration of IR-UWB-based wireless networks on board spacecraft. Each approach has its advantages and drawbacks, as previously described. A detailed summary of the characteristics is provided in Table 4.4. The criteria have emerged from the advantages and drawbacks elaborated earlier, that are:

- Robustness: Stability and robustness of the approach
- Flexibility: Adaptability and extensibility of the system
- Cost: Costs associated with implementing and maintaining each approach
- Mass reduction: Extent of potential mass saving
- Power consumption: Efficiency in terms of power consumption
- Data throughput: Data rate the approach can support
- Scalability: System's capability to handle increasing devices or data traffic
- Security: Security level of the data transmission
- Integrability: How the approach can be integrated and support the system integration process
- Complexity: Complexity in implementing and managing the approach

Each approach is examined and qualitatively assessed against this criteria to understand their strengths and weaknesses for deployment in real-world scenarios. In the rating, a score of 1 represents the most unfavourable rating, while a score of 4 denotes the most favorable.

The most important insight is that the traditional wired approach ranks lowest in overall performance, thereby highlighting the superiority of the other three wireless approaches

TABLE 4.4: Comparative summary of different approaches

	Traditional wired	**Enhanced hybrid**	**Pure wireless**	**Flexible multi-protocol**
Robustness	4	4	1	2
Flexibility	1	2	3	4
Cost	1	2	4	3
Mass reduction	1	2	4	3
Power consumption	4	3	1	2
Data throughput	4	3	1	3
Scalability	1	2	3	4
Security	4	3	2	3
Integrability	1	2	4	3
Complexity	1	2	4	2
Sum	22	25	27	29

in this regard. Consequently, the integration of IR-UWB/LLDN as a wireless protocol evidently marks an enhancement of the traditional intra-spacecraft architecture, regardless of which of the three wireless approaches it is employed in.

Even though the multi-protocol approach performs best in Table 4.4 due to its high degree of flexibility and scalability, determining the most suitable approach still requires careful consideration of the specific requirements of each project. For instance, one mission may prioritize robustness, while another may focus on high flexibility or scalability. Consequently, another wireless approach may have advantages based on the weighted criteria. In summary, avioincs architectures with wireless elements offer comprehensive benefits, not limited to mass and cost reduction. Their main strengths lie in flexibility, scalability, and integration capabilities, where they can fully leverage their advantages over the traditional wired approach.

4.3 Implementation

This Section describes the implementation of the LLDN layer in detail. The combination of IR-UWB and LLDN in the MAC layer has not yet been implemented, as mentioned above. From the evaluations that have already been discussed, it is clear that the synergy of the two layers can provide a robust and powerful architecture for a variety of wireless network applications in space systems.

The first part of this Section is a more detailed description of the hardware implementation. The respective hardware modules are described in detail. A prototype is presented, which serves both for later verification and as a basis for demonstration purposes in the Wireless Compose experiment. This is followed by a presentation of the software implementation. The chosen software framework is described, which on the one hand allows

the control of the hardware and on the other hand supports the implementation of the LLDN. Finally, the LLDN implementation itself and aspects still to be resolved are discussed.

4.3.1 Hardware

The implementation requires a special selection of the hardware. In this work, a prototype board is first used, which has almost the same electromagnetic properties as the final flight modules used in a Wireless Compose experiment. The hardware can either be used as a network coordinator or as a wireless node, depending on the software stack. This provides a high degree of flexibility and allows the system to be evaluated.

Microcontroller: At the heart of the data processing and protocol management is a low-power STM32L151 micro-controller (μC) from ST. The choice of this particular μC was motivated by the high requirements for low-power operation in the Wireless Compose mission.

The STM32L151 extends the concept of ultra-low-power technology and represents an acceptable compromise between performance and low-power operation. It uses the Cortex-M3 core and offers a flexible Central Processing Unit (CPU) clock speed from 32 kHz to 32 MHz. In addition to Dynamic Run and Low Power Run modes, the STM32L151 has two additional ultra-low power modes that enable very low power consumption while maintaining a Real-time Clock (RTC), backup register contents, and a low voltage detector (111).

Transceiver module: The implementation of IR-UWB communication is enabled by a transceiver module based on Decawave's DW1000 transceiver Integrated Circuit (IC). The DWM1000 module integrates an on-chip antenna, all RF circuits, power management, and clock circuits into a single module. In addition, the transceiver can be used for ranging measurements.

The DWM1000 is compliant with the IEEE 802.15.4-2011 UWB standard with some modifications and enhancements. It supports four channels in the frequency range from 3.5 GHz to 6.5 GHz and data rates from 110 kbps to 6.81 Mbps. It is important to note that when the implementation commenced, there was no commercially available transceiver on the market that supported the standard's highest data rate of 27.24 Mbps and, due to the rapid progress in the field, this may have changed in the meantime. As an extension to the standard, the DWM1000 offers a maximum packet length of 1023 bytes, which is particularly beneficial for high-throughput applications. It also offers further flexibility in parameterisation, such as additional preamble lengths of 128 or 256, although it should be noted that it does not support preamble lengths of less than 64 (81).

The maximum possible data rate can be determined using Equation 4.4 and is shown in Figure 4.13. Although the preamble length of 16 characters is given for comparison, this is not supported by the DW1000. From the figure, it is evident that the 6.81 Mbps data rate can only be approximated under certain conditions, especially with very large user data packets or short preamble lengths.

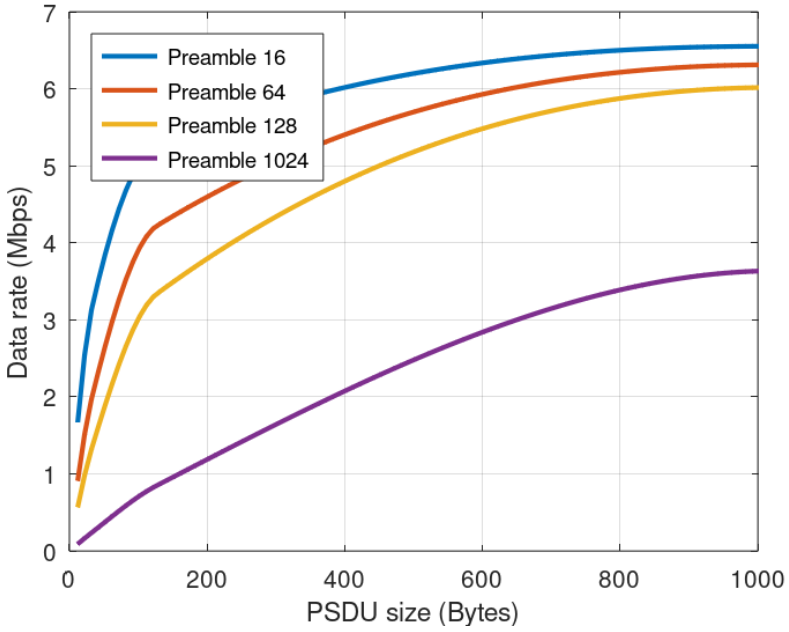

FIGURE 4.13: Maximum possible data rate @ 6.81 Mbps, PRF = 62.4 MHz

It is worth noting the importance of packet size for the throughput, which especially applies when combined with longer preamble lengths. As shown in Figure 4.13, the maximum throughput can be more than doubled by using a larger packet of 1024 bytes. This illustrates that in networks requiring longer preambles (e.g. for ranging or longer distances) or in applications requiring higher data rates, it might be preferable to implement the non-standard packet size of 1024 bytes to maximise performance.

The DWM1000 has a programmable output power for the transmitter and a fully coherent receiver, which is a particular advantage for longer range applications. The DWM1000 communicates with the host μC via a Serial Peripheral Interface (SPI) and offers limited MAC support.

Board and peripherals

A detailed analysis of the grounding and power supply concept is included in the EMC-compliant design of the PCB layout to avoid unwanted circuits, while consideration of critical trace lengths and the termination strategy for unused General Purpose Inputs/Outputs (GPIO) also influence the design. Figure 4.14 shows the PCB schematics and the prototype board.

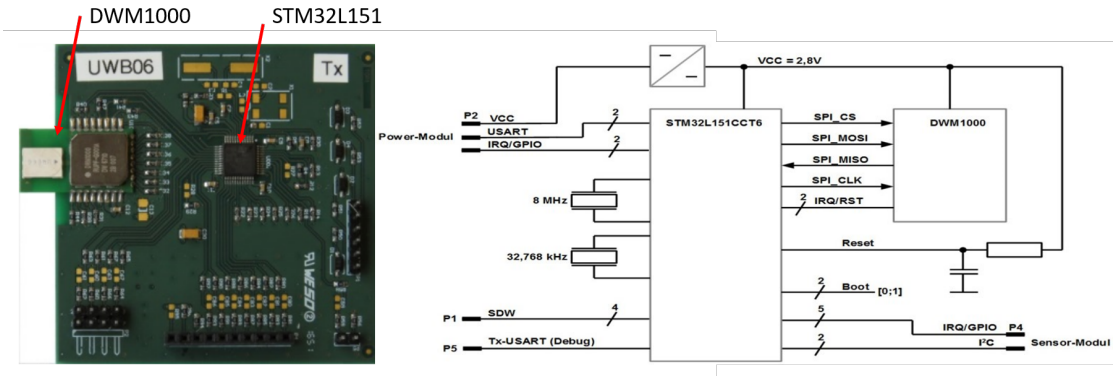

FIGURE 4.14: Prototype board and schematics

In addition, the hardware platform has other interfaces, such as a Universal Asynchronous Receiver-Transmitter (UART) and I^2C, which are used for debugging purposes and for connecting external peripheral sensors. These interfaces allow easy integration and communication with a wide range of sensors and other hardware components.

4.3.2 Software

The software implementation, which is the focus of this Section, is presented here in detail. First of all, the framework will be explained, which is based on the OpenWSN protocol stack. This forms the basis of the software architecture and is implemented on top of the open source real-time operating system FreeRTOS. The OpenWSN protocol stack was originally developed for the 2.4 GHz narrowband used in industrial applications. At the MAC layer, the open source implementation uses the TSCH as the MAC algorithm. The challenge is the porting of this protocol stack to the target system and the replacement of the existing TSCH stack with the LLDN stack. In addition, instead of the previously supported 2.4 GHz IC chips, the IR-UWB RFIC must now be addressed in the physical layer, so the hardware control is different and needs to be adapted.

4.3.2.1 Framework

The OpenWSN Framework, originally developed by the University of California Berkeley and later further developed by Inria and the Open University of Catalonia, forms the basis of the software architecture used to implement the LLDN MAC layer. The goal of OpenWSN is to provide an open, standards-compliant, open source-based and, above all, reliable protocol stack for Internet-enabled IoT applications. It is based on the TSCH extension of 802.15.4e and provides the corresponding higher layers to manage the TSCH process.

OpenWSN is implemented on the FreeRTOS open-source real-time operating system which provides broad support for a variety of hardware platforms, including the ARM architecture. For safety-critical applications, SafeRTOS can be used which is a version of FreeRTOS specifically designed for safety applications and certified to EN 61508 Safety Integrity Level 3 (SIL3) (112).

Although there are similar implementations, such as Contiki and Riot, which are also optimised for use in the IoT, OpenWSN offers some key advantages including its broad support for a wide range of hardware platforms and the ability to rely on SafeRTOS for safety-critical applications. However, all three implementations are designed for the 802.15.4 2.4 PHY and run on platforms such as the Texas Instruments CC2538 System-on-Chip which consists of a 32-bit ARM Cortex-M3 μC and a radio module compliant with the IEEE 802.15.4 standard (113). This requires adaptation to 802.15.4a IR-UWB and the DW1000 platform.

4.3.2.2 Protocol stack

The OpenWSN protocol stack, into which the LLDN MAC layer will be integrated, offers several advantages as it allows access to the existing higher layers and the performance measurements that need to be carried out. Furthermore, the current implementation using TSCH is already a proven component of the stack.

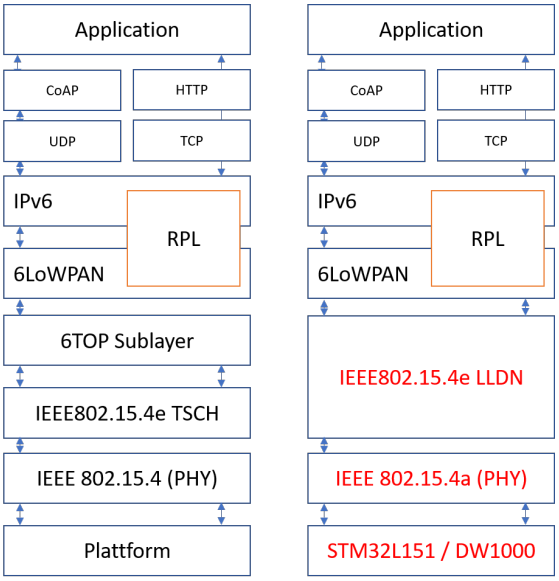

FIGURE 4.15: Original (left) and modified (right) OpenWSN protocol stack

The special feature of the OpenWSN protocol stack is the implementation of special protocols for the IoT and wireless sensor networks. These include 6top as the protocol of the 6LoWPAN IPv6 adaptation layer for the IEEE802.15.4-based network protocol. This layer allows the stack to compress IPv6 headers. The next layer is the Routing

Protocol for Low-Power Lossy Networks (RPL) which is responsible for the stack routing topology. This protocol is specifically designed for low-power lossy networks and was developed by the IETF ROLL working group. RPL uses the Direct Acyclic Graph (DAG) concept.

Finally, the OpenWSN stack implements the Constrained Application Protocol (CoAP). This is a lightweight, Hypertext Transfer Protocol (HTTP)-like application protocol built as a header on top of the User Datagram Protocol (UDP) and the Transmission Control Protocol (TCP). An overview of the protocol stack is shown in Figure 4.15 (left) (see (114)).

The main task is, thus, the integration of the LLDN into the existing network stack. In addition, porting to the intended platform, which includes the ARM L151 μC and the Decawave DW1000 radio module, is another task to be performed within the software implementation. OpenWSN has an abstraction layer consisting of headers for different platforms, which need to be modified for the chosen platform in order for the protocol stack to work with the underlying hardware. For this purpose, OpenWSN provides a board support package that needs to be adapted. On the other hand, the Decawave driver needs to be adapted for the planned micro-controller.

For porting to the STMl151, an adapted peripheral library was required. It was able to adapt such a library to the requirements of the L151, since it already existed for the STMF3. The real-time timer had to be re-implemented together with some changes to the interfaces to be used.

OpenWSN also does not provide support for IR-UWB drivers and it targets the 2.45 GHz PHY radio modules. However, the functionality compared to the DW1000 is similar and, in most cases, the radios are connected using an SPI interface or are integrated into the SoC. An important aspect of the implementation is the various interrupts that are provided. These are used to react quickly to certain events such as transmission or reception. The DW1000 also provides several interrupts that can be used in this way.

However, some of the functions provided by the DW1000 are not compatible with the LLDN and cannot be used, such as the automatic ACK, because special time slots, such as the group ACK, are used for this in the LLDN. Others, such as the checksum calculation, can be used.

The timer is especially important for synchronous transmission, as required by TDMA. The DW1000 provides a highly accurate timer, which is also used to correctly reproduce the ToF in ranging and to wake the transceiver from sleep mode or to support certain MAC-related functions that require accurate timing. The Decawave already provides an Application Programming Interface (API) for the operation of the transceiver, which is used for the implementation.

In addition, there is an abstraction layer “radio” in the operating system which has access to the functions of the DW1000 driver. Another advantage of the DW1000 is the non-standard packet size of 1024 bytes, which was also considered in the implementation.

These adaptations and the integration of the LLDN into the existing network stack are key steps in ensuring the desired versatility and adaptability to different operating modes and technological environments.

4.3.2.3 LLDN MAC

The implementation of the LLDN MAC layer results in the replacement of the previously splitted layer by a unified LLDN MAC layer. This eliminates the need to access 6top as a component of 6TiSCH, since the LLDN procedure does not provide channel hopping management, as shown in Figure 4.15 (right). All nodes are synchronised with the coordinator’s beacon and the decision of whether a node acts as a coordinator or as a simple node in the network must be made at a higher level.

The implementation takes place in two modules, each of which performs an independent task within the MAC layer. The modules comprise the LLDN manager module and the LLDN module. The LLDN manager module is implemented as a state machine in which the state transitions are triggered by the underlying layer and the associated interrupts. No additional timers are required as the timings are mapped over multiples of a time slot. This module has direct access to the higher layer 6LoWPAN and it passes the appropriate MAC parameters and data. Via the SPI interface of the Board Support Package, it communicates with the PHY layer to send or receive packets and controls the Decawave radio module.

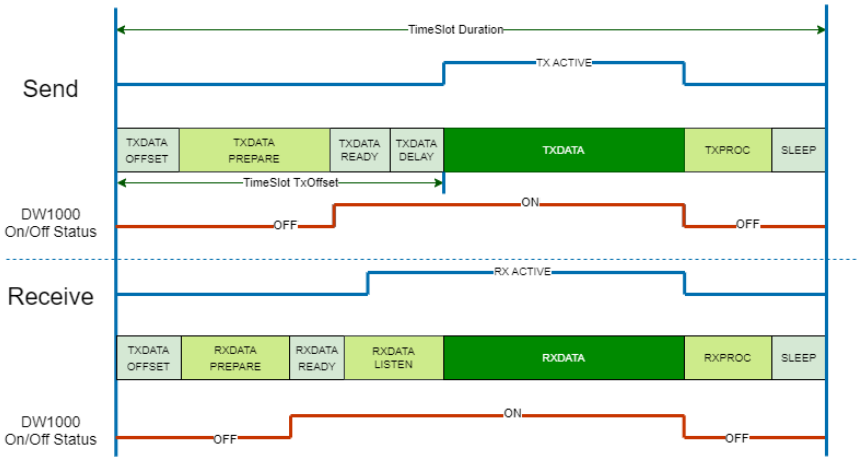

FIGURE 4.16: Chronogram of the TS state machine (cf. (115))

The LLDN module, on the other hand, takes over the responsibility for the operation at the time slot level and regulates the compliance with the assigned time slot duration.

As soon as a transmission or reception is requested within a certain time slot, the LLDN layer is activated, which follows the chronogram shown in Figure 4.16.

This shows the different phases of a time slot, whereby a segmented structure into different operation phases is essential to comply with the strict timing requirements. The phases labelled TXDATA and RXDATA show the actual data transmission and reception of the next layer data products. These can be, for example, the source packets of the CCSDS Space Packet Protocol standard. The "time slot duration" indicates the total duration of a time slot.

In the context of the TX phase, the time taken to transmit an actual packet (time slot TxOffset) is divided into four phases: TXDATA_OFFSET, PREPARE, READY, and DELAY, which are necessary for the handling and preparation of the transmission. The TXPROC phase is used to signal the successful transmission to the higher layer after the transmission has been completed while the sequence of the RX phase is similar to that of the TX phase and the only exception is the RXDATA_LISTEN phase, in which the receiver is requested to wait for incoming data.

In the chronogram in Figure 4.16, the sequence is shown in the synchronous state and if a node is not in a synchronous state, a simplified procedure is used that enters a synchronisation phase and is activated until a synchronisation signal is received.

4.3.2.4 Incomplete aspects

This Subsection discusses aspects of the current implementation that are still incomplete or offer scope for future development. Some of these shortcomings arise from technical challenges or the specific requirements of the intended application environment. For instance, the CSMA-CA scheme cannot be implemented at the hardware level because UWB does not transmit a carrier and Decawave recommends the Aloha mechanism as an alternative. However, this was not considered in the current implementation as the deterministic nature of the LLDN is more important here.

For the specific performance evaluation, other features such as the discovery and configuration phases were not required, whereby these functions offer significant potential for future enhancements to make the network more scalable which will improve the performance and flexibility of the network. Although the state machine already contains the basic states, this does not allow the PAN coordinator to dynamically manage the nodes, instead, the configuration of the network is hard-coded and the LLDN manager calls this configuration to schedule the superframe accordingly while the MAC addresses of each node are used for assignment.

Despite these aspects not being implemented to date, the existing implementation provides a solid foundation as the core components for communication are in place and functional. This allows the network to operate successfully and paves the way for future enhancements and improvements.

In addition, a further implementation of the LLDN was undertaken, but without the inclusion of the FreeRTOS operating system and OpenWSN. This approach was necessary because the integration and validation into the OpenWSN was not yet complete, when the implementation of the Wireless Compose experiment started, which is described in detail in Chapter 6. A timely delivery of the flight model for the Wireless Compose experiment was critical due to the strict time constraints, in order to perform the demonstration as part of the Alexander Gerst Horizon mission. Consequently, due to the time overlaps and the incomplete integration of the LLDN into the OpenWSN stack, a leaner solution was chosen.

Consequently, I implemented a simplified system, integrating the LLDN in a reduced state. This system retained the basic functionality of the LLDN, such as online status monitoring, while omitting more complex mechanisms such as group ACK, retransmissions and security features. For this implementation, a state machine was used directly on the micro-controller, without an operating system, enhancing software flexibility and simplicity. The hardware components, consisting of the ST32L151 micro-controller and the DW1000 RFIC, remained unchanged.

This transition to a simplified implementation enabled the LLDN to operate in conjunction with IR-UWB despite the project-related time constraints.

It is also important to note that the specific operating concept of Wireless Compose requires the software to operate in two distinct phases: Sensing and Tracking. A detailed and mission-specific implementation of the software is further elaborated in Section 6.3.

4.4 Performance evaluation

A comprehensive evaluation was conducted to analyse the performance of the implemented network. Particular attention was paid to the Key Performance Indicators (KPIs) of latency, throughput, and energy efficiency. Some of the results, I have published in (42), which are examined in more detail in this Subsection.

The research was conducted using three hardware nodes, each with a maximum slot length of 10 ms, identical IR-UWB @ 4GHz PHY layer parameters and characteristics, and a 6.81 Mbps data rate. Dummy data was transmitted using a maximum packet length of 127 bytes.

Unlike the analysis in Section 4.1.2, here the whole chain is considered, including the processing time, which thereby allows the measurements to be interpreted as a comprehensive system test.

4.4.1 Minimum achievable latency

Figure 4.17 shows the achievable latency that is given by the synchronisation of the data queue with the uplink slot of each node. The fixed slot structure implemented in the LLDN makes this synchronisation possible, as each node is aware of the uplink slots that are available to it. To obtain the most recent data, sensor data is acquired as late as possible, just before the start of each uplink slot.

In Table 4.3, an analysis of the possible latency times is presented which shows that, depending on the preamble and other parameters, a minimum latency time can be achieved. However, there are some deviations in this analysis as a PSDU of 127 bytes in total and a different preamble was chosen and the Decawave allows a finer selection than is specified in the standard. According to mode 14 in (81, Table 25), a preamble length of 128 characters corresponds to a minimum TS length of 287 μs. In addition, the UWB transceiver has an internal processing time which, in this configuration, is approximately 500 μs and is mainly caused by the SPI communication.

The preparation and processing of the communication during transmission and reception in the micro-controller itself is a critical factor. Due to the utilisation of a low-power 32 MHz controller, a corresponding amount of computing time is required to prepare the packets before transmission and to process them after reception. For the system used, this can be estimated to be approximately 1.6 ms, with about 800 μs for preparation and roughly 800 μs for processing on reception. Ideally, the packets can be received after about 2.38 ms. Since the reception of the test data was timed to 1 ms before the actual slot, giving an ideal latency of 3.38 ms, the slot size was set to 4 ms.

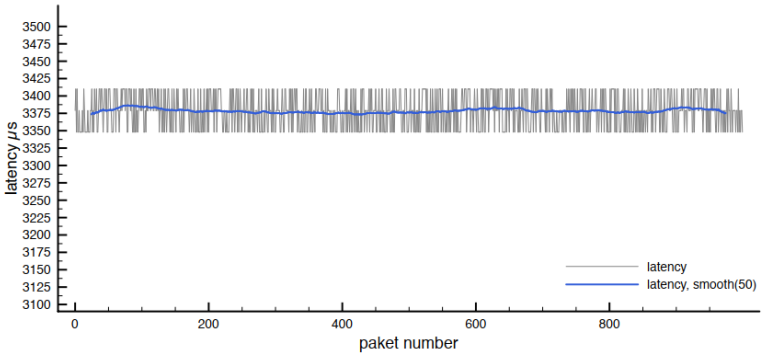

FIGURE 4.17: Minimum achievable latency for LLDN with existing configuration

Figure 4.17 shows that the average latency is approximately 3.378 ms, which aligns with the calculated values. Due to the resolution of the timer, jumps of 31 μs are noticeable.

It is important to note that in real systems, the measured latencies differ significantly from the theoretically achievable latencies as shown in Table 4.3 because the processing time of the hardware must always be taken into account. Although the STM32L151 μC used does not offer the best performance in terms of processing speed, it has advantages in terms of power efficiency and for the Wireless Compose mission for which the target system was designed, this was especially important. However, when used in a positioning system with real-time processing requirements, the priorities may be different and one possible optimisation would be to replace the processor, e.g. with a Cortex M4-based ST32F4XX μC from ST with a clock frequency of 180 MHz (116) instead of 32 MHz to speed up the internal processing. A potential improvement could be to use an even faster processor, at least on the side of the PAN coordinator, which could already lead to a significant improvement in performance.

4.4.2 Throughput

The ratio between the duration of the time slot and the pure transmission time of the packet determines the achievable throughput and thus reducing this ratio will allow the time slot to be used optimally, thereby maximising throughput. The calculations in Figure 4.13 show the theoretical maximum throughput that can be achieved for different system configurations. However, this value can only be achieved if the ratio is 1:1 and the time slot duration t_{BTS} is exactly equal to the active transmit or receive time and thus equal to the frame transmission time t_Frame.

In practice, the actual achievable throughput is lower. As can be seen in the Chronogram in Figure 4.16 , the TS duration must also include the time for the pre- and post-processing of the user data, including the SPI transmission. There is also the fact that the data may have to do some processing by the application itself, and thus this is another condition that must be satisfied.

This results in an additional condition that needs to be considered when determining the size of the time slot to be used:

- The processing of the data up to the transmission into the buffer of the sending module t_{procTX}
- The post-processing and the data up to the transmission from the buffer of the receiving module into the next higher layer t_{procRX}
- For on-line operation, the time t_{App} required by the application to process the message must also be taken into account

These three parameters are directly related to the size of the time slot t_{BTS}, as shown in Equation (4.7):

$$t_{BTS} \geq t_{procTx} + t_{procRX} + t_{App} \tag{4.7}$$

Using the values for $t_{procTx} = 0.8 + 0.5$ ms, $t_{procRx} = 0.8$ ms, and $t_{App} = 1$ ms given in Section 4.4.2, and taking the additional active transmission time of 287 μs into account, this results in a minimum slot size of 3.387 ms.

These conditions reduce the effective throughput for the present configuration with a preamble of 128 symbols, a PRF of 62.4 MHz, and a PSDU of 127 bytes from the theoretically possible maximum of 3.39 Mbps to only 299 kbps, which is equivalent to an efficiency level of 12%.

This phenomenon is a direct consequence of the relatively long processing times and is mainly caused by the choice of a less powerful processor. Hence, choosing a more powerful processor and thus speeding up the processing time could have a significant impact on the throughput, as could the transmission of larger packets as this would allow the time slot to be used more efficiently by reducing the ratio of pure transmission time to processing time.

The factors presented here once again illustrate the significant relationship that exists between throughput and latency. In particular, it becomes clear that optimising to reduce latency will usually also improve throughput and thus these aspects should be considered when optimising the system in the future.

4.4.3 Energy efficiency

The power consumption during a superframe run where a transmission takes place in an uplink slot is shown in Figure 4.18. In addition, the node waits for a transmission from the coordinator in the bidirectional slot. The Figure also shows the cumulative consumption and it is evident that, compared to the basic consumption in sleep mode, the actual transmit and receive phases only have a slight impact on the total energy consumption. It should be noted that after sleep mode, there is still a certain wake-up time until all components are fully activated and efficiency thus refers to the energy that is ultimately used to transmit a given amount of data.

The maximum power consumption for transmitting a single packet is 1.35 mAs (4.12 mJ) for a standard wireless node. The coordinator has a higher power consumption because it is waiting for data to arrive in all the time slots that are available and, for this reason, the maximum power consumption is 2.5 mAs (9.25 mJ) per superframe.

As mentioned above, the overall efficiency is largely determined by the power consumed when idle and it is thus possible to increase the efficiency by transmitting more data.

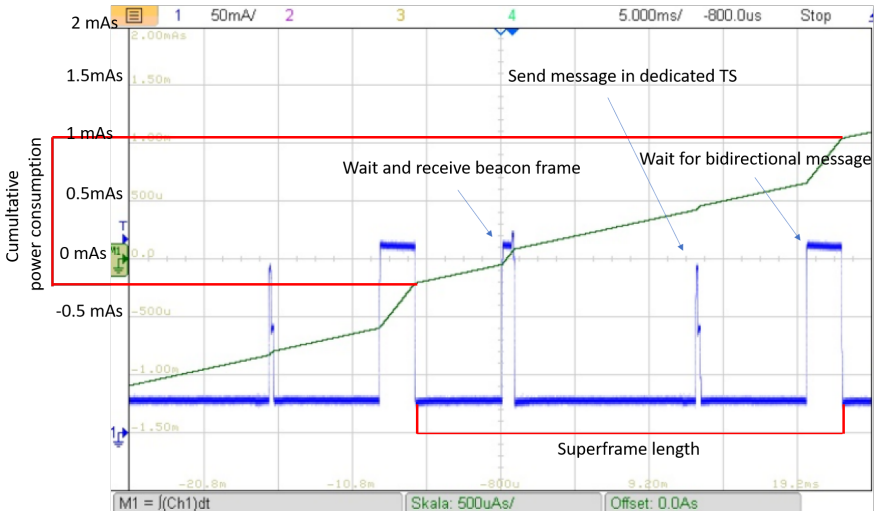

FIGURE 4.18: Power consumption of a node during an entire SF (blue) and integrated (green)

Allowing the DW1000 to transmit data packets of up to 1024 could be one way to increase efficiency that could have a very significant impact on the overall efficiency.

4.5 Summary

This Chapter comprehensively details my concept of the IR-UWB-based wireless network, designed to enhance existing intra-spacecraft communication. It also delves into the network's implementation and performance evaluation.

Initially, this Chapter introduced the concept, building upon the LLDN and IR-UWB technologies as evaluated in Chapter 3. It then examined how IR-UWB/LLDN wireless networks could be integrated into stat-of-the-art avionics architectures to enhance their capabilities. The discussion covered various integration options, emphasising the strengths and weaknesses of each in the context of the integration process.

The analysis presented clearly indicates that the design of avionics architecture is heavily influenced by mission-specific requirements. While there is no one-size-fits-all solution, a flexible, multi-protocol approach where wireless networks play a pivotal role appears essential for adaptation.

Following this conceptual overview, the Chapter detailed the implementation process. This included the presentation of the hardware components, such as the STM32L151 μC and the DWM1000 transceiver module from Decawave, and the necessary software based on the OpenWSN stack, available as open source. However, modifications were required to integrate the LLDN MAC layer onto the IR-UWB physical layer. These adaptations spanned from the board support package and the DW driver to the MAC layer itself.

It is important to note that not all aspects of the LLDN layer were implemented – for instance, only the online phase – as the initial focus was on fulfilling certain functions critical for performance evaluation. Additionally, a simplified implementation without an operating system was adopted due to time constraints for the Wireless Compose mission, which will be elaborated upon in Section 6.3.

The performance evaluation underscored several key aspects of the wireless network, including latency, throughput, and energy efficiency. The findings reveal that the maximum latency and effective throughput are heavily dependent on the system executing the software stack. Thus, a balance between energy efficiency and performance-oriented design, particularly in terms of processor choice, is crucial and should be considered in future optimisations. The current implementation, geared towards a low-power application for the Wireless Compose experiment, demonstrated that the performance of the controller could be influenced by idle and sleep modi – in addition to pure transmission phases. Furthermore, it was discussed that optimisation strategies, such as using larger packets, can enhance energy efficiency. In summary, the current implementation achieved a harmonious balance between efficiency and performance, providing a robust foundation for further development and system optimisation for its in-orbit demonstration through the Wireless Compose experiment.

Chapter 5

Verification

This Chapter provides a comprehensive review of the technological challenges associated with implementing UWB technology in a space system, as mentioned in Section 1.4. A crucial aspect in this context is the technological maturity of this technology, a fundamental prerequisite for its successful application in space. Therefore, issues such as electromagnetic compatibility, radiation exposure, and data robustness, i.e., the system's performance under multipath propagation conditions, are addressed.

In the EMC Section, a comprehensive test is conducted to assess the system's compatibility and immunity under various electromagnetic conditions. In the radiation Section, the results from detailed SEE and TID tests are presented to assess the hardware's durability and performance under radiation exposure. Some of the results I have published in (43) and (45). In the data robustness Section, the outcomes of measurements conducted in the Columbus module mock-up to analyse the system's resilience under multipath propagation conditions are presented. Positioning performance is also examined in this realistic environment.

The conducted verification aims to demonstrate not only the system's technological maturity for use in space but also to verify its operability under the demanding conditions of the Wireless Compose mission described in Chapter 6. Special emphasis is placed on the specific requirements of this mission, ensuring the system's suitability and performance.

5.1 Electromagnetic compatibility

Especially in the context of space applications, ensuring electromagnetic compatibility is a fundamental cornerstone in the design and test phase of electronic devices and systems. Here, the compatibility of systems plays an essential role, as a large number of onboard components have to smoothly work together in a confined space. EMC becomes

even more important when wireless communication is used inside a space system and the challenge of ensuring interference-free operation becomes even more critical when the spacecraft is used to transmit and receive ground communications, and interference could disrupt communications with the ground. EMC testing is therefore an essential component of the qualification process, also for the Wireless Compose mission. The aim is to ensure that the DWM1000 radio modules operate reliably in their intended electromagnetic environment and do not generate unacceptable electromagnetic interference that could affect the operation of other onboard systems.

To verify the EMC requirements, nominally four tests are performed, divided into two main categories, namely radiated and conducted tests. These tests differ in the way they are carried out and, for radio modules in particular, radiated tests represent a technological challenge, either to eliminate interference with other onboard systems or to demonstrate robustness to sources of interference. For this reason, a distinction is made between two types of test:

- **Radiated emissions (RE)** – These tests measure the amount of electromagnetic energy that the device under test emits into its environment in the form of electromagnetic waves. High levels of radiation can cause interference with nearby onboard systems, especially receivers operating at similar frequencies.
- **Radiated susceptibility (RS)** – This aspect, which is also called radiated immunity determines the immunity of a device to incident electromagnetic waves which is especially important in environments with high electromagnetic activity, such as spacecraft.

5.1.1 Test description

The measurements here presented are based on the hardware described in Subsection 4.3.1, whose electromagnetic properties are similar to those of the final Wireless Compose flight units. The board is equipped with a STM32L151 μC and the DWM1000 radio module is used. The chip antenna is integrated into the DWM1000 radio module and covers the frequency range of 3.5–6.5 GHz. Since the electromagnetic compatibility was a key consideration in the development of the PCB layout, a detailed analysis of the grounding and power supply was conducted, whereby the critical cable lengths were considered, as well as termination strategies for unused GPIOs.

Testing was carried out according to the space-related European Cooperation for Space Standardisation (ECSS) and MIL standards (117) and (118). I performed the tests in the EMC chamber of the DLR Institute of Space Systems in Bremen. For the two measurements, two different test setups were used:

In the **radiated emission test**, a test receiver measures the power via a calibrated antenna at a distance of 1 m from the Device Under Test (DUT), as shown in Figure 5.1.

To determine the permissible emission level, it is necessary to convert the measured field strength to the Effective Isotropic Radiated Power (EIRP) of the radio module. This conversion is related to the electric field strength E at the measuring antenna, the radiated power density S, and the free-space impedance Z_0 as follows:

$$S = \frac{EIRP}{4\pi r^2} = \frac{E^2}{Z_0} \tag{5.1}$$

By rearranging this relationship, the EIRP of the radio module can be determined using the measured electric field strength:

$$EIRP = E^2 \cdot r^2 \cdot \frac{4\pi}{Z_0} \tag{5.2}$$

By logarithmizing Equation (5.2), the EIRP can be calculated in decibels:

$$EIRP_{\mathrm{dBm}} = E_{\mathrm{dB}\mu\mathrm{V/m}} + 20\log(\frac{m}{r}) - 105 \tag{5.3}$$

In EMC tests for space applications, the antenna distance r to the measuring antenna is usually 1 m and can be omitted in Equation (5.3). With this simplification and by rearranging Equation 5.3, the UWB transmit mask according to IEEE 802.15.4a can be converted from dBm to dBμV:

$$E_{\mathrm{dB}\mu\mathrm{V/m}} = EIRP_{\mathrm{dBm}} + 105 \tag{5.4}$$

When using this conversion, it is important to ensure that both the level in dBm and dBμV/m refer to the same bandwidth.

For the **radiated susceptibility test**, I used a signal generator to generate interfering signals. These are transmitted to the DUT via the calibrated antenna, as shown in Figure 5.2. A packet of 10 bytes was transmitted from the DUT every 10 ms. The data field of the packet contained a specific pattern that was used to compare the received packets in a receiver module located in a safe distance to the DUT. A subsequent packet error rate analysis allowed the link quality to be determined and any malfunctions to be detected.

The measurement procedure started with pre-scans to identify the most critical scenario. This included testing different data rates, PRFs, and frame lengths and the associated spurious emissions. The most critical test modes and orientations were then measured and the identified test mode was analysed in detail. The same test mode was then used to analyse the susceptibility.

FIGURE 5.1: Setup for the RE test

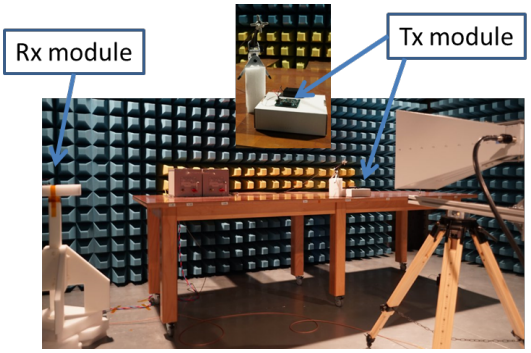

FIGURE 5.2: Setup for the RS test

5.1.2 Measurement results

During the preliminary scans for the initial alignment, one side was identified as having the strongest emissions, as expected. This observation is primarily due to the UWB chip antenna integrated into the UWB radio module, which does not have a uniform radiation pattern in all directions (119). Figure 5.3 shows channel 2 at a centre frequency of 4 GHz from two different angles from which it is evident that not only the desired signal but also the spurious emission is significantly amplified at approximately 8 GHz. This spurious emission results from the first harmonic at twice the centre frequency. Based on these findings, all subsequent measurements were performed using the Z090 side.

In addition, different combinations of PRF, data rate, and frame length were analysed and the measurements show that these parameters have a significant effect on the noise spectrum. Figure 5.4 portrays the noise spectrum for two different PRFs, whereby the distances of 124.5 MHz and 31 MHz respectively represent the distance of the preamble PRFs.

The effect of packet length on the noise spectrum could also be measured. Frames with a PRF of 15.6 MHz produce a noise level 18.9 dB higher than frames with a PRF of 62.4 MHz. However, once the frame duration exceeds 1 ms, the two spectra converge with a difference of between 0.4 and 1.8 dB, as shown in Figure 5.4.

This observation is due to an intelligent power feature on the transmitter. As the standard specifies a limit of -41 dBm/MHz in one millisecond, it allows the power to be increased by 3 dB, for example, if the packet duration is half the time.

Moreover, both the data rate and the preamble lengths influenced the spurious spectrum and it was found that a low data rate with long preamble lengths generally produces a smaller interference spectrum. Based on this observation, it was possible to identify a preferred combination, at least in terms of noise emission, consisting of a long frame length, a long preamble length, a data rate of 110 kbps, and a PRF of 64 MHz.

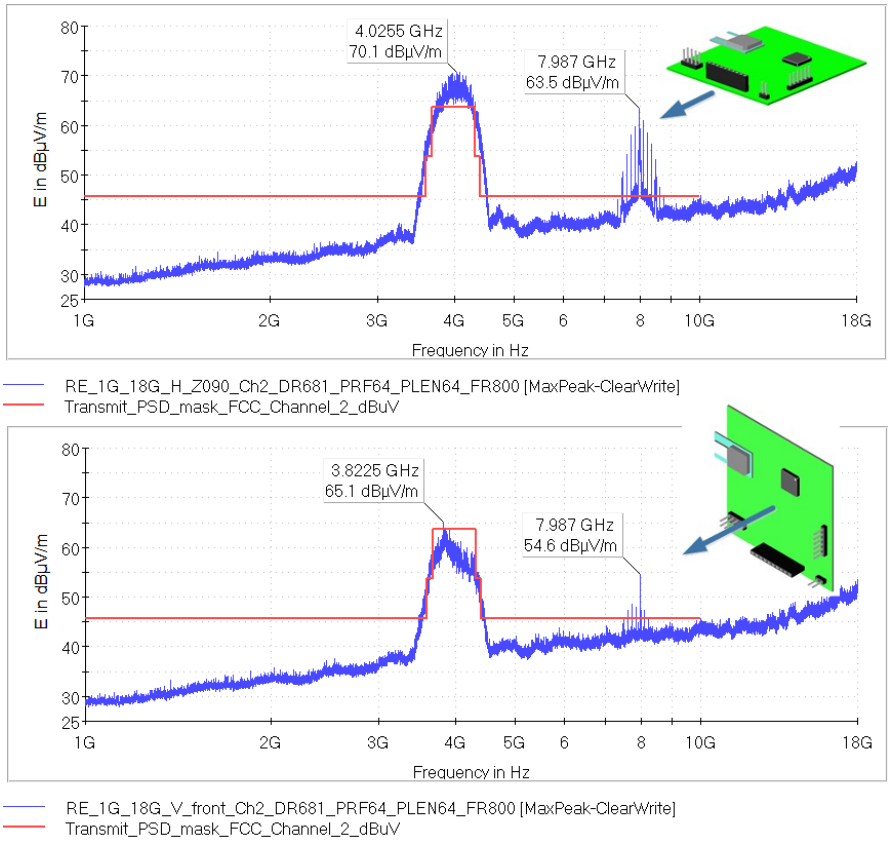

FIGURE 5.3: Emission spectrum with different orientations (top) Z090 and (bottom) front

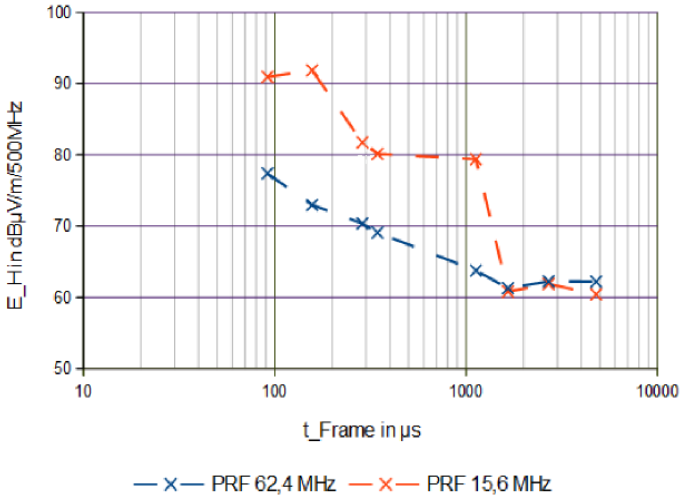

FIGURE 5.4: Noise spectrum depending on the frame size in μs

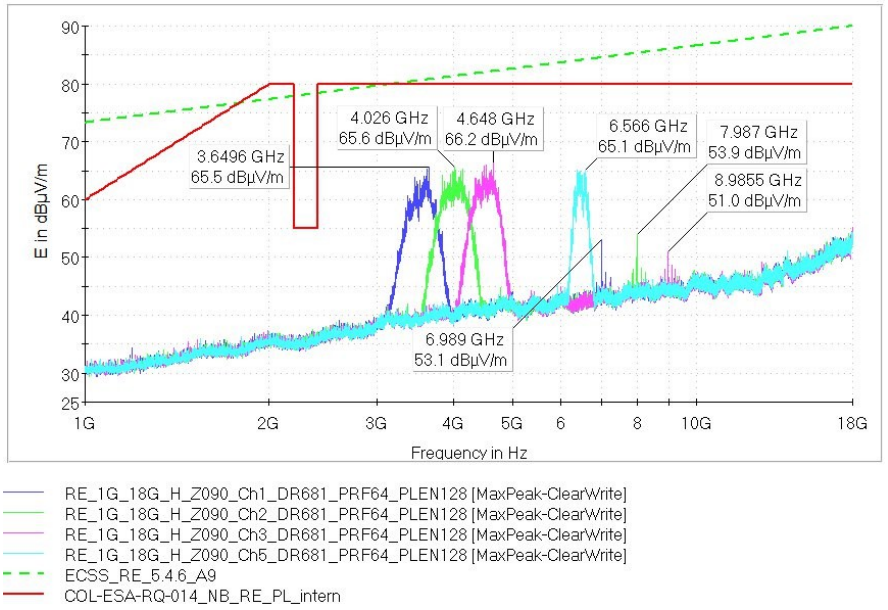

FIGURE 5.5: Emission measurement from 1 GHz to 18 GHz for different IR-UWB channels

An important result is that for all combinations studied, the prescribed limits for maximum emissions inside the spacecraft according to ECSS in (117, A.9), which corresponds to the green line in Figure 5.5, and the Columbus module of the ISS according to (120), which corresponds to the red line in Figure 5.5, are retained for all channels. This shows that the use of IR-UWB does not cause any interference with other onboard systems and even highly sensitive receivers, normally operated in the S- or X-bands, are not affected by IR-UWB, as shown by the notching line at 2.1 GHz in Figure 5.5 for the S-Band receiver. The test results once again underline the advantages of IR-UWB technology over narrowband technologies.

For the susceptibility tests, two interference levels are of interest, inside and outside a space system. Inside a space system, a typical peak can be expected at 1.5 V/m. These levels of 1.5 V/m and higher are achievable only from intentional transmitters (not from accidental emissions from electronics). Outside the station even greater levels of up to 10 V/m can be expected. These high levels nominally are not relevant to the final experiment setup which will be operated inside the Columbus module. However, this level was also tested and it showed an expected performance degradation.

Particularly in the in-band range, i.e. within the active channel bandwidth used by the DWM1000 module, a packet error rate of up to 75% was observed for 1.5 V/m, as shown in Figure 5.6. Higher levels, such as those outside the station with 10 V/m, are therefore even more critical with up to 100% packet loss. The result is not surprising as the receiver is inherently sensitive to interference in the receive band. This sensitivity is usually covered by the DW1000 immunity to interference. However, it is possible for the receiver's Low Noise Amplifier to become saturated and unable to receive data

when the manufacturer's suppression level is exceeded. This situation is illustrated in Figure 5.7 of the DW1000 data sheet, specifically for channel 2 at 4 GHz. If this is a problem, there are several approaches to avoiding in-band interference. For instance, one common approach is to implement a frequency plan and insert notch lines into the spectrum, which is a method usually used for other onboard receivers and hardware must be tested against these limiting levels in the RE test. Alternatively, the flexibility of the DW1000 could allow it to switch to a different channel where there may be less interference.

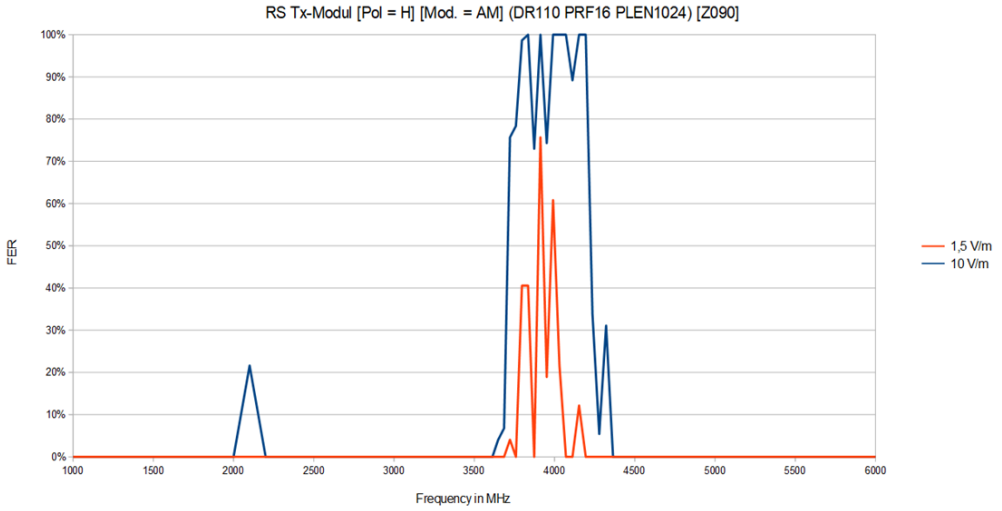

FIGURE 5.6: PER for a frequency range of 800 MHz to 6 GHz with horizontal polarisation at approximately 1.5 V/m and 10 V/m

In addition, MAC-level schemes such as LLDN can be used to retransmit lost packets. Thus, the upper layer will also help increase the robustness of the system to interference.

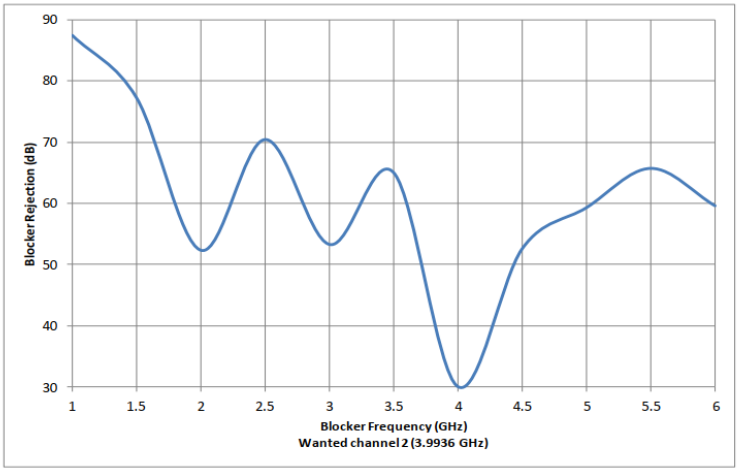

FIGURE 5.7: DW1000 Rx Interferer Immunity on Channel 2 (81, Figure 3)

However, as spacecraft transmitters are typically in the S-band (2 GHz) or X-band (8 GHz) as defined by ECSS in accordance with ITU Radio Regulations, the IR-UWB

channels from 3.5 to 6.5 GHz are outside this range and therefore not critical. This underlines the strength of IR-UWB in terms of adaptability in the complex electromagnetic environment inside a space system.

Overall, the results obtained provide convincing confirmation of the suitability of IR-UWB technology for space applications and underline its superior electromagnetic properties compared to narrowband solutions.

5.2 Data Robustness

The data robustness of a spacecraft's wireless communications network is critical to maintaining communications under challenging conditions. It refers to the ability of the network to maintain its functionality under various adverse conditions, such as interference and multipath propagation through highly reflective structures.

Immunity to possible interference was examined in Section 5.1 and thus this Section focuses on another aspect that is especially critical inside of a space system and can significantly affect the data robustness of the network:

- **Multipath propagation**: This is a phenomenon where the radio signal is reflected from different surfaces and travels along multiple paths to the receiver. These signals can interfere with each other and lead to attenuation of the received signal. In addition, Inter-symbol Interference (ISI) causes problems in decoding the signal. ISI occurs when signals from adjacent symbols overlap and distort the received signal. This can make it difficult for the receiver to interpret the original signal correctly.

To evaluate the robustness of the network in realistic, reflective environments similar to those found in spacecraft or space modules, I performed specific measurements inside a Mock-Up of the Columbus module, also in preparation for the Wireless Compose mission. These tests used advanced prototypes of the Wireless Compose hardware, still based on the STM Cortex M3 micro-controller and a DW1000 RFIC. For preliminary measurements, I used evaluation boards equipped with the same micro-controller and RFIC, along with a sub-miniature version A (SMA) connector. This setup provided a direct coaxial connection between the receiver and transmitter modules, allowing precise adjustment of the signal attenuation. The findings and results of these measurements are presented in the following Subsections.

5.2.1 Pre-measurements

To gain a better understanding of the performance of the IR-UWB under laboratory conditions, preliminary measurements were carried out. Different data rates and preamble lengths were considered to analyse the performance under attenuated signal strength. This is important to know, since the mock-up measurements need to be performed within a range that is still within the receiver's sensitivity limit to exclude packet losses due to a distance-driven attenuation.

The Decawave already carried out some measurements and documented the performance of the DW1000 in the datasheet, whereby the values in the datasheet indicate the following sensitivity for the different data rates for a 10% packet loss:

TABLE 5.1: Packet delivery performance according to (81, Table 6)

PDR (%)	Data Rate	Rx Sensitivity (dBm/500 MHz)
90	110 kbps	-105
90	850 kbps	-94
90	6.81 Mbps	-92

Some important conclusions can already be drawn from this data, one of which is that the PRF has only a marginal effect on the overall sensitivity when attenuation comes into play and the pre-measurements thus concentrated on the different data rates and preamble lengths to verify the system under laboratory conditions.

Firstly, different preamble lengths were tested with the same PRF and data rate. The programmable attenuation level was set to a value of 70 dB which led to a received power of -89.5 dBm. At this level, as expected, the first packet errors were observed for the preamble length of 256 symbols. In the next step, different preamble lengths were applied. However, with the preamble turned down, only 65% of the packets were received with a preamble of 128, and no packets were received with 64, as illustrated in Figure 5.8. This means that it makes sense to use a higher PRF, especially over longer distances and with weak signals and this finding is of particular interest for future configurations in which long distances need to be bridged. As shown in Subsection 4.1.1, the preamble length also has a significant influence on the frame duration, and thus a trade-off should always be made for the specific application to determine the best possible configuration.

Secondly, the packet delivery ratio was measured at different data rates and the receiver sensitivity was confirmed at certain rates, which can also be found in the DW1000 datasheet. The measurement data show a slightly worse performance which is due to the fact that the measurements were taken under laboratory conditions with different equipment and in a varied environment. In order to perform all these measurements, the

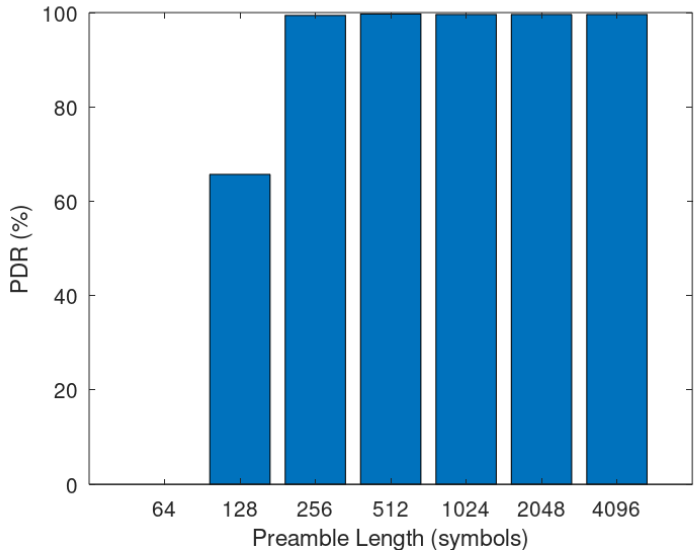

FIGURE 5.8: PDR at different preamble lengths for 6.81 Mbps, PRF = 64 MHz

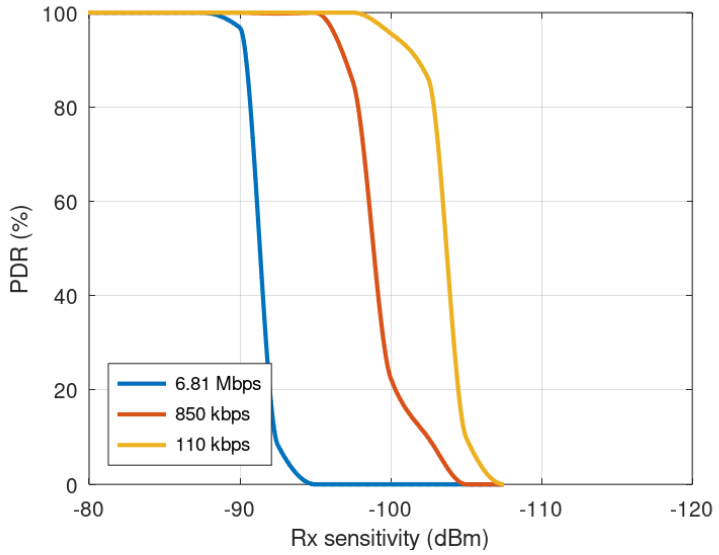

FIGURE 5.9: Rx sensitivity at different data rates for Channel 2

evaluation board was used, which has a separate SMA access, allowing direct measurements to be made without having to consider the Tx and Rx antenna gain separately.

Based on the measurements shown in Figure 5.9, and assuming a transmit power of -41.3 dBm/MHz or, equivalently, -16 dBm/500 MHz, the maximum distances achievable in a free space path loss environment can be calculated using the Friis formula

$$PL_{free}(dB) = 20\log_{10}(d) + 20\log_{10}(f) - 147.55 \tag{5.5}$$

TABLE 5.2: Achievable distance for different data rates in Channel 2 under free space conditions

Data Rate	Free Space Loss PL_{free} (dB)	Rx Power (dBm)	Distance d (m)
6.81 Mbps	72.4	88.4	25
850 kbps	80	96.1	60
110 kbps	83.1	99.1	100

In free space environment, the path loss can be accurately estimated using the free space loss formula. However, in indoor environments additional factors can significantly affect link quality. These include not only the basic transmission loss but also other effects such as fading, which is particularly relevant in environments like inside of satellites or space modules with highly reflective structures (see Figure 5.11).

Fading can be broadly categorized into two types:

- **Large scale fading**: refers to the signal attenuation over long distances caused by the energy distribution over the wireless channel. It takes into account path loss and shadow effects, with the attenuation due to the distance between transmitter and receiver and the variations in average signal strength due to environmental differences.
- **Small Scale fading**: describes rapid fluctuations in received power due to multi-path propagation of electromagnetic waves over short periods of time or distances, where the average signal strength remains constant. It includes variations in time, space and frequency selective fading and can be increased when the receiver moves.

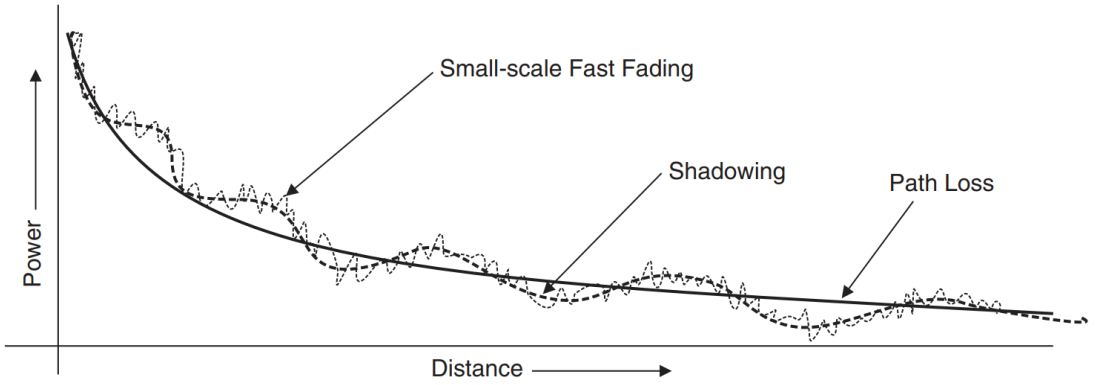

FIGURE 5.10: Propagation loss (84, Figure 3.1)

The main factors that affect the multipath propagation and lead to these small-scale fading phenomena are reflection, diffraction and scattering. **Reflection** occurs when electromagnetic waves hit a surface much larger than their wavelength, causing them

to change direction. **Diffraction** occurs at sharp edges in the path between the transmitter and receiver, altering the path of the wave. **Scattering** occurs when waves hit objects smaller than their wavelength, causing the signal to spread out. Together, these interactions shape the complex behaviour of signal strength over distance and time in wireless networks.

Empirical models have become indispensable for more accurately estimating path losses, especially in environments where these losses are highly dependent on the surroundings. These models offer tailored estimates based on various coefficients.

Examples include the Winner II Model (121, Section 4.3) and the ITU Indoor Propagation Model (122, Table 2), used for predicting path losses in indoor environments considering line-of-sight and non-line-of-sight conditions. However, it is noteworthy that these models are primarily designed for narrowband systems.

For IR-UWB systems according to 802.15.4a, a dedicated path loss model exists, developed from statistical measurements in various environments, including short distances in an industrial environment with dense multipath scattering due to metallic scatterers (123).

Based on this model, the path loss (averaged over small-scale fading) in dB for frequencies between 2 GHz and 10 GHz is calculated as follows (124, p. 4):

$$PL_{UWB}(dB) = G_0 - 10n \log_{10}\left(\frac{d}{d_0}\right) + S \tag{5.6}$$

Where S stands for shadowing and is a Gaussian-distributed random variable with a mean of zero and a standard deviation of σ_S. The coefficients for LoS and NLoS in industrial environments are (124, Section III.E):

- Valid range of d: 2 - 8 m
- Path gain coefficent n: 1.2 (LoS), 2.15 (NLoS)
- σ_S: 6 dB (for both LoS and NLoS)
- G_0: -56.7 dB (for both conditions)

The Figure 5.11 shows the estimated LoS and NLoS avaraged UWB path loss in an industrial environment without taking into account the Shadowing variable.

Furthermore, small-scale fading effects also occur, which can be estimated using the Nakagami model (124, Section II.F). Also, the presence of a person in the room can

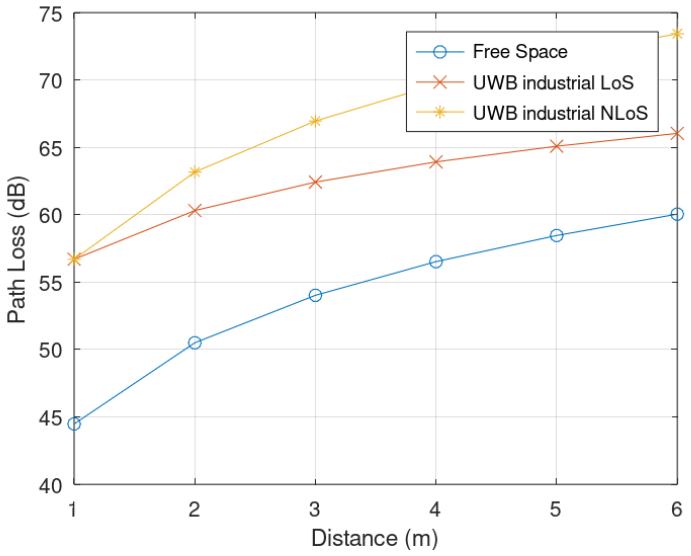

FIGURE 5.11: UWB model Path loss for LoS and NLoS

cause further attenuation of about 1 dB to 10 dB, especially when the network is used as a Body Area Network or parts of the network are worn directly on the body.

In the 2-6 GHz range, analysis of the electromagnetic field near the body using a Finite-Difference-Time-Domain (FDTD) simulator indicated that no energy penetrates through the body. Instead, pulses transmitted from an antenna diffract around the body and can reflect off arms and shoulders, which again increases the multipath effects (124, Section V.A).

To determine an adequate data rate for the Columbus Mock-Up environment, the following worst-case assumptions are made:

- Distance d: max. 4 m (Columbus working area)
- Tx power P_{tx}: -16 dBm (IR-UWB)
- Tx and Rx Antenna Gain G_{ant}: 0 dBi (no antenna alignment)
- Path Loss PL_{UWB}: 63.8 dB (at 4m distance in LoS industrial environment)
- Shadowing σ_S: max. 6 dB
- Human presence / BAN att. A_{human}: max. 10 dB
- Link Margin m: 3 dB

The estimated min. Rx power in (dB) can be calculated as:

$$P_{\text{rx}} = P_{\text{tx}} + G_{\text{ant,tx}} + G_{\text{ant,rx}} - PL_{\text{UWB}} - \sigma_S - S_{\text{human}} - m = 98,8dBm \tag{5.7}$$

As the pre-measurements in Figure 5.9 shown, it is evident that only a data rate of 110 kbps can achieve a Packet Delivery Rate of nearly 100%.

5.2.2 Columbus mock-up measurements

Prior to the Wireless Compose demonstration, I performed the data robustness measurement in the Columbus module Mock-Up at the European Astronaut Centre. During this test, two key aspects of the IR-UWB technology were examined: data robustness and positioning capabilities. The wireless nodes, also referred to as Anchor Motes, were positioned at various locations within the Columbus module. Additionally, a reference receiver, also referred as a Base Station, was utilised to receive the transmitted packets. Furthermore, a wireless node was employed as a mobile Tag Mote to assess the positioning capabilities.

5.2.2.1 Communication

The communication tests were conducted using a data rate of 110 kbps, PRF = 16, and a preamble length of 1024 symbols. This configuration, particularly the combination of a lower data rate with a long preamble, is specifically recommended by Decawave for multi-path environments when performing ranging measurements and the selection of the data rate was the outcome of the analysis presented in 5.2.1. As the Wireless Compose experiment involves collecting ranging data, this data rate was selected to ensure stable link performance. The average Received Signal Strength Indicator (RSSI) was measured to be approximately -79 dBm to -82 dBm at different positions with no human presence during measurements.

This corresponds to a path loss of about 63 dB to 66 dB which well aligns with the UWB path model in 5.11 (considering that human presence and shadowing variable is not covered). An exemplary position of Anchor Mote 4 is depicted in Figure 6.26a.

TABLE 5.3: Mock-up measurement results for 110 kbps at different positions

Position	Channel	Distance (m)	Av. RSSI (dBm)	Messages sent	PDR (%)
1	2	3.25	-82.1	40648	99.95
2	2	2.16	-81.6	34204	99.49
3	2	3.25	-82.2	29413	99.44
4	2	2.02	-79.2	18951	99.13
5	2	2.62	-81.5	18024	99.22

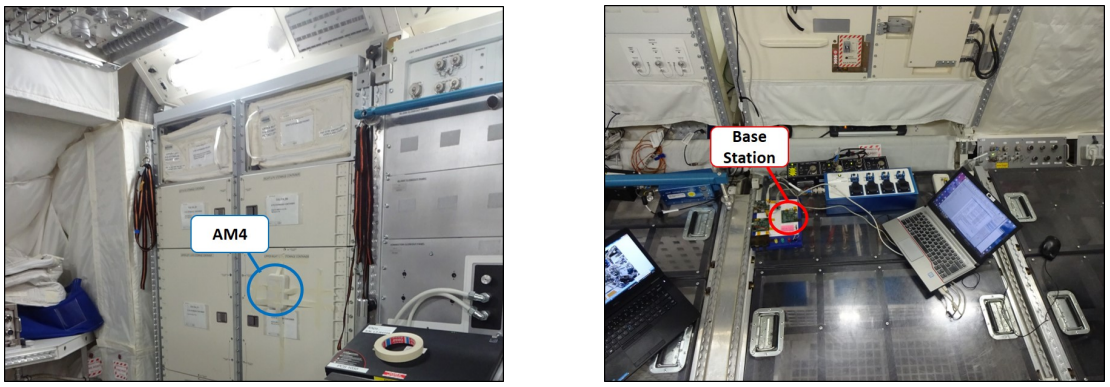

(A) Transmitter/ Anchor Mote 4 (B) Receiver/Base Station Development Model

FIGURE 5.12: Tested positions during the Columbus mock-up test campaign

In this test campaign, the focus was on monitoring the PDR over a longer period of time. The results confirm the robustness of IR-UWB in the tested configuration inside the space station and show that it is able to maintain a stable connection inside the station. These findings emphasise the potential of IR-UWB for reliable communication solutions in complex environments such as a space station.

5.2.2.2 Positioning

Also, I evaluated the positioning within the Columbus module. Firstly, I performed a static test to evaluate the positioning accuracy. A dynamic test was then performed to check the tracking capability. In the static part, the trilateration algorithm described in Subsection 2.6.3 was used to determine the position. A comparison was made between the actual position and the calculated position, and the Root Mean Square Error (RMSE) and standard deviation were determined. As a total of six Anchor Motes were used, both the least squares method and the weighted least squares method were applied and the results were compared. It is important to mention that prior to these tests, several verification and calibration tests were conducted with the Anchor and Tag Motes in a laboratory environment. Particularly, the antenna delay was calibrated as a key calibration value, in accordance with the methodology outlined in (125).

Figure 5.13 shows the positions of the Anchor Motes used to measure the distance to the Tag Mote. The Tag Mote was mounted on a tripod in order to collect data over an extended period of time. The Anchor Motes, Base Station and Tag Mote positions are summarized in Table 5.4.

Figure 5.14 shows the measured distances of the Tag Mote to each anchor and the Base Station over a period of 250 seconds, during which 1000 samples (4 samples per second) were collected.

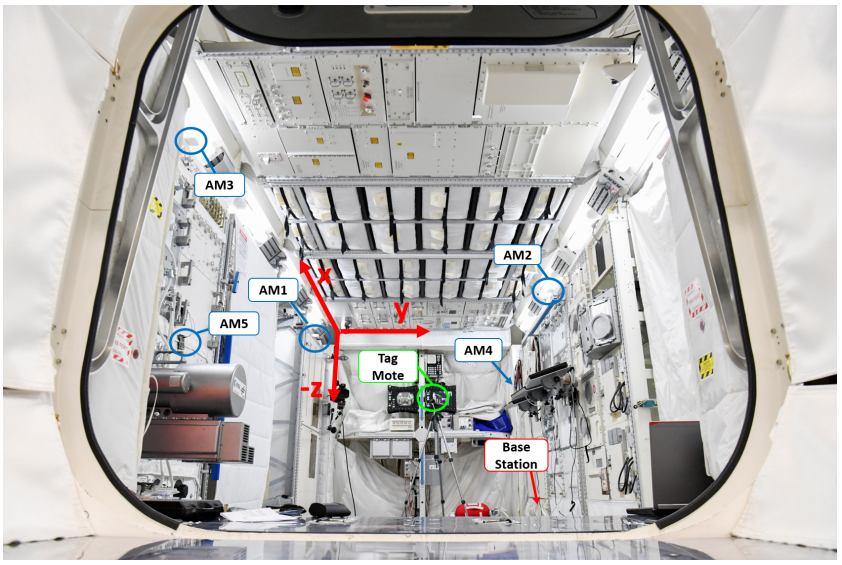

FIGURE 5.13: Positioning measurement setup in Columbus mockup

TABLE 5.4: Actual positions of the Anchor Motes, Base Station and initial Tag Mote position

Device	X (mm)	Y (mm)	Z (mm)
Base Station (BS)	2160	1880	-1970
Anchor Mote 1 (AM1)	500	0	100
Anchor Mote 2 (AM2)	1610	2130	100
Anchor Mote 3 (AM3)	3820	0	100
Anchor Mote 4 (AM4)	660	2130	-640
Anchor Mote 5 (AM5)	3650	0	-910
Tag Mote (initial pos.)	1000	1000	-500

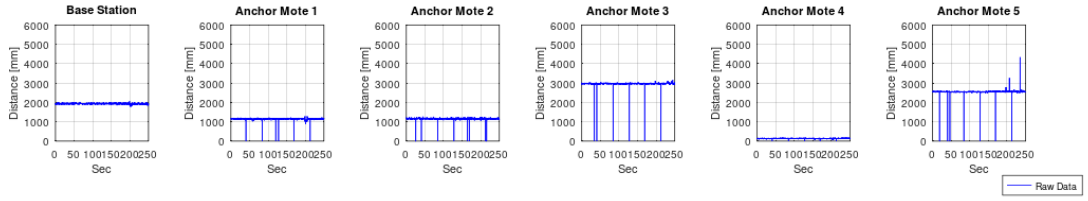

FIGURE 5.14: Static distance measurements between Anchor Motes and Tag Mote

The almost constant distances indicate that the tag did not move. There are some outliers (zero values) in the raw data, due to the loss of a packet, which incorrectly interpreted the distance as zero. However, these measurements were filtered out for the ToA-based trilateration analysis.

The Figure 5.15a shows the deviation of the positions estimated using the Weighted Least Squares algorithm. The transparent green cube represents the possible working area of the astronaut in the Columbus module. The positions of the Anchor Motes and the Base Station are also illustrated in this figure for orientation. It is noticeable that

the estimated positions are very close together, an indication that the Tag Mote was in a fixed position during the measurement with almost LoS conditions. Another Figure 5.15b shows the mean estimated position compared to the actual position, which differ only slightly.

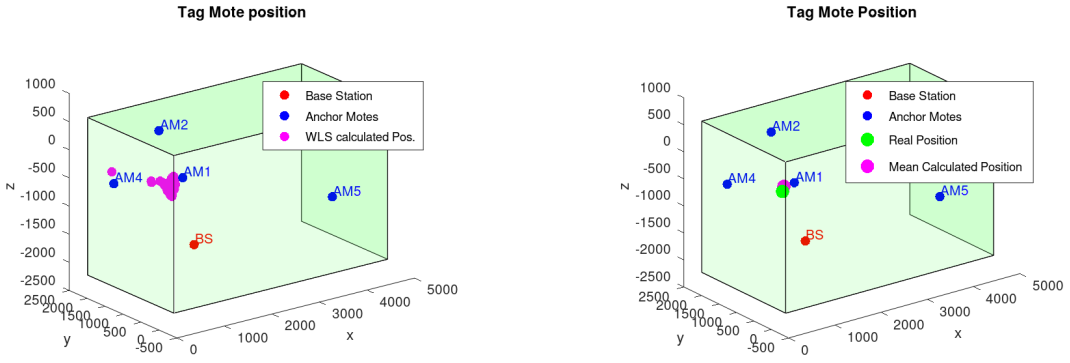

(A) Distribution of WLS calculated tag positions

(B) WLS mean tag position vs. actual tag position

FIGURE 5.15: WLS calculated tag positions

For the further analysis, RMSE and the standard deviation were computed. The RMSE provides a statistical statement about the correctness of the data, whereas the standard deviation assesses the precision or variability of the data. The difference between both values can be shown in Figure 5.16. For the analysis of correctness, the real position, also referred as ground truth is needed, whereas for precision, only the measured values and their standard deviation are examined.

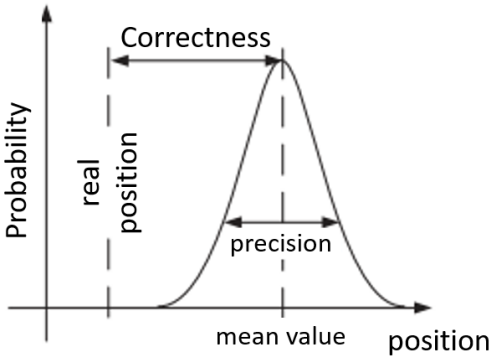

FIGURE 5.16: Correctness and precision of a positioning system according to ISO5725-1

The RMSE measures the average error between the calculated and actual positions. The RMSE was calculated using the following formula

$$RMSE_x = \sqrt{\frac{1}{n}\sum_{i=1}^{n}(x_i - \hat{x}_i)^2}, \tag{5.8}$$

where x_i is the actual value and $\hat{x}_i$ is the value calculated by trilateration.

The overall RMSE, which provides an aggregated error estimate across all three dimensions (x, y, z), was calculated as follows

$$RMSE_{total} = \sqrt{\frac{1}{3}(RMSE_x^2 + RMSE_y^2 + RMSE_z^2)}, \tag{5.9}$$

where $RMSE_x$, $RMSE_y$ and $RMSE_z$ are the RMSE values for each coordinate.

The standard deviation was also calculated to determine the distribution of the estimates around their mean:

$$\sigma_x = \sqrt{\frac{1}{n-1}\sum_{i=1}^{n}(x_i - \bar{x})^2}, \tag{5.10}$$

where $\bar{x}$ is the mean of the calculated values.

The weighting matrix used for WLS algorithm is based on the variances of the individual distance measurements to the Anchor Motes and is defined as follows

$$\begin{aligned} W &= \text{diag}\left[\frac{1}{\sigma^2(d_{BS})}, \frac{1}{\sigma^2(d_{AM1})}, \ldots, \frac{1}{\sigma^2(d_{AM5})}\right] \\ &= \begin{pmatrix} \frac{1}{\sqrt{1016.82}} & 0 & 0 & 0 & 0 & 0 \\ 0 & \frac{1}{\sqrt{943.30}} & 0 & 0 & 0 & 0 \\ 0 & 0 & \frac{1}{\sqrt{963.34}} & 0 & 0 & 0 \\ 0 & 0 & 0 & \frac{1}{\sqrt{789.90}} & 0 & 0 \\ 0 & 0 & 0 & 0 & \frac{1}{\sqrt{280.44}} & 0 \\ 0 & 0 & 0 & 0 & 0 & \frac{1}{\sqrt{4928.52}} \end{pmatrix} \end{aligned} \tag{5.11}$$

When applying the two algorithms - Least Squares and Weighted Least Squares - the results in Table 5.5 show that WLS gives better results in terms of RMSE compared to LS. In addition, the standard deviation is lower for the WLS. The WLS therefore performs better in this static case. For the position analysed here, an RMSE of 106.9 mm can be obtained, which is a sufficient result. However, it is important to note that the error can significantly increase, potentially reaching more than 50 cm per axis in a dynamic environment with NLoS conditions or at least obstructed LoS conditions as can be the case in a real environment on the ISS. Therefore, in motion tracking, a Kalman filter is commonly employed to enhance the accuracy.

Subsequently, the Tag Mote was set in motion. It was moved from its initial position (position 1) to the other end of the Columbus mock-up (position 2) and then to the

TABLE 5.5: Error assessment using LS and WLS for the initial Tag Mote position

	x (mm)	y (mm)	z (mm)	total (mm)
RMSE LS	111.71	178.37	92.79	230.01
RMSE WLS	56.16	47.53	77.56	106.90
σ LS	43.36	78.48	38.57	-
σ WLS	28.21	39.17	37.83	-
Mean position LS	1102.97	889.80	-405.60	-
Mean position WLS	1048.57	1023.05	-422.28	-

center of the Mock-up, alternately moving down (position 3) and up (position 4), as illustrated in Figure 5.17.

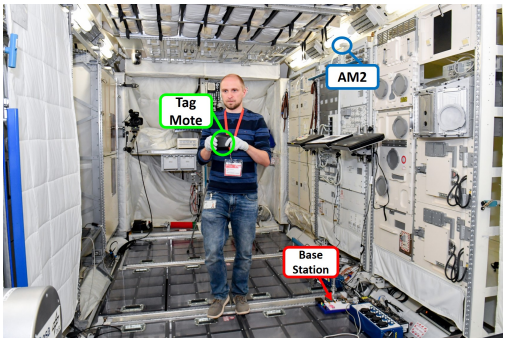

(A) Tag Mote is moved from position 1 to position 2

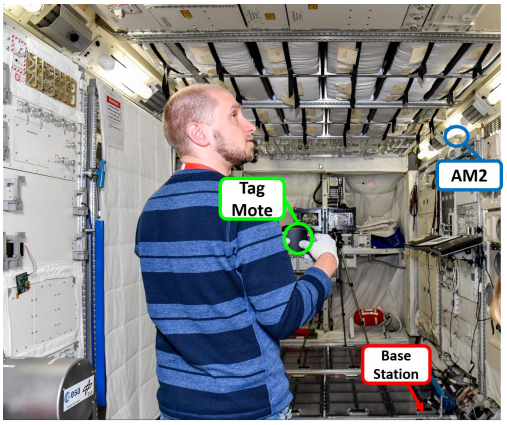

(B) Tag Mote is at position 2

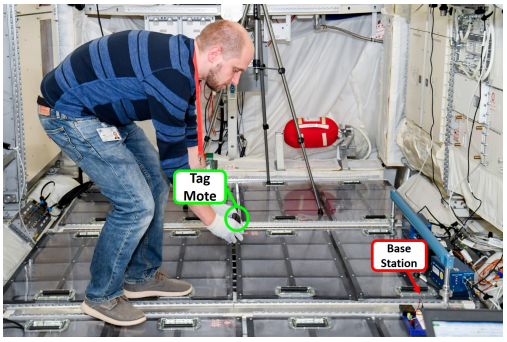

(C) Tag Mote is at position 3

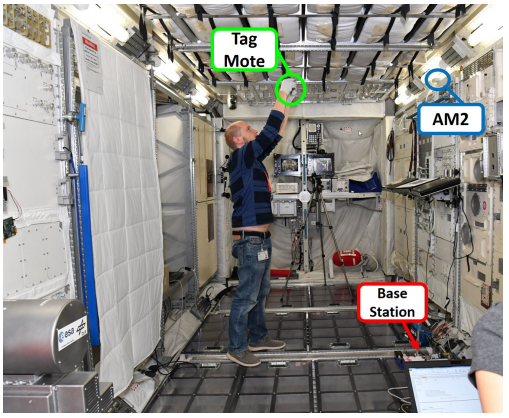

(D) Tag Mote is at position 4

FIGURE 5.17: Tested positions during the Columbus mock-up test campaign

The continuously recorded tracking or distance data indicates significant changes in the distance to each Anchor Mote, as shown in Figure 5.18 from the raw data for all Anchor Motes.

For evaluation, the Extended Kalman Filter, described in Subsection 2.6.5 was used for the analysis.

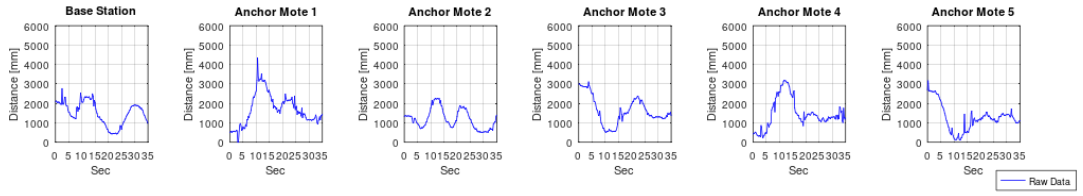

FIGURE 5.18: Motion distance measurements between Anchor Motes and Tag Mote

A linear model with constant acceleration per data point is assumed as the process model, similar to the approach used in various studies on motion tracking as in (126) and (85). This negates the need for linearisation, and thus the matrix A remains unchanged throughout the process.

For this reason, the internal system state x_k includes not only the positions p_x, p_y and p_z but also the respective velocity v and acceleration a:

$$x_k = \begin{pmatrix} p_{x,k} & p_{y,k} & p_{z,k} & v_{x,k} & v_{y,k} & v_{z,k} & a_{x,k} & a_{y,k} & a_{z,k} \end{pmatrix}^{\mathsf{T}} \tag{5.12}$$

In the process model, jerk is perceived as process noise, and it represents the rate at which an object's acceleration changes over time. This leads to the following motion model:

$$\begin{cases} p_{x,k+1} = p_{x,k} + v_{x,k}\Delta t + \frac{1}{2}a_{x,k}\Delta t^2 + \frac{1}{6}j_{x,k}\Delta t^3 \\ p_{y,k+1} = p_{y,k} + v_{y,k}\Delta t + \frac{1}{2}a_{y,k}\Delta t^2 + \frac{1}{6}j_{y,k}\Delta t^3 \\ p_{z,k+1} = p_{z,k} + v_{z,k}\Delta t + \frac{1}{2}a_{z,k}\Delta t^2 + \frac{1}{6}j_{z,k}\Delta t^3 \\ v_{x,k+1} = v_{x,k} + a_{x,k}\Delta t + \frac{1}{2}j_{x,k}\Delta t^2 \\ v_{y,k+1} = v_{y,k} + a_{y,k}\Delta t + \frac{1}{2}j_{y,k}\Delta t^2 \\ v_{z,k+1} = v_{z,k} + a_{z,k}\Delta t + \frac{1}{2}j_{z,k}\Delta t^2 \\ a_{x,k+1} = a_{x,k} + j_{x,k}\Delta t \\ a_{y,k+1} = a_{y,k} + j_{y,k}\Delta t \\ a_{z,k+1} = a_{z,k} + j_{z,k}\Delta t, \end{cases}$$

with j_x, j_y and j_z representing the jerk along their respective axes.

Given the linear nature of the motion model, the function f can be represented using a linear system with the state transition matrix A:

$$x_{k+1} = A \cdot x_k + w_k \tag{5.13}$$

with

$$A = \begin{bmatrix} 1 & 0 & 0 & \Delta t & 0 & 0 & \frac{\Delta t^2}{2} & 0 & 0 \\ 0 & 1 & 0 & 0 & \Delta t & 0 & 0 & \frac{\Delta t^2}{2} & 0 \\ 0 & 0 & 1 & 0 & 0 & \Delta t & 0 & 0 & \frac{\Delta t^2}{2} \\ 0 & 0 & 0 & 1 & 0 & 0 & \Delta t & 0 & 0 \\ 0 & 0 & 0 & 0 & 1 & 0 & 0 & \Delta t & 0 \\ 0 & 0 & 0 & 0 & 0 & 1 & 0 & 0 & \Delta t \\ 0 & 0 & 0 & 0 & 0 & 0 & 1 & 0 & 0 \\ 0 & 0 & 0 & 0 & 0 & 0 & 0 & 1 & 0 \\ 0 & 0 & 0 & 0 & 0 & 0 & 0 & 0 & 1 \end{bmatrix} \tag{5.14}$$

where the sample time period is Δt and the motion model is now defined as follows:

$$\begin{bmatrix} p_{x,k+1} \\ p_{y,k+1} \\ p_{z,k+1} \\ v_{x,k+1} \\ v_{y,k+1} \\ v_{z,k+1} \\ a_{x,k+1} \\ a_{y,k+1} \\ a_{z,k+1} \end{bmatrix} = \begin{bmatrix} 1 & 0 & 0 & \Delta t & 0 & 0 & \frac{1}{2}\Delta t^2 & 0 & 0 \\ 0 & 1 & 0 & 0 & \Delta t & 0 & 0 & \frac{1}{2}\Delta t^2 & 0 \\ 0 & 0 & 1 & 0 & 0 & \Delta t & 0 & 0 & \frac{1}{2}\Delta t^2 \\ 0 & 0 & 0 & 1 & 0 & 0 & \Delta t & 0 & 0 \\ 0 & 0 & 0 & 0 & 1 & 0 & 0 & \Delta t & 0 \\ 0 & 0 & 0 & 0 & 0 & 1 & 0 & 0 & \Delta t \\ 0 & 0 & 0 & 0 & 0 & 0 & 1 & 0 & 0 \\ 0 & 0 & 0 & 0 & 0 & 0 & 0 & 1 & 0 \\ 0 & 0 & 0 & 0 & 0 & 0 & 0 & 0 & 1 \end{bmatrix} \begin{bmatrix} p_{x,k} \\ p_{y,k} \\ p_{z,k} \\ v_{x,k} \\ v_{y,k} \\ v_{z,k} \\ a_{x,k} \\ a_{y,k} \\ a_{z,k} \end{bmatrix} + \begin{bmatrix} \frac{1}{6} j_{x,k} \Delta t^3 \\ \frac{1}{6} j_{y,k} \Delta t^3 \\ \frac{1}{6} j_{z,k} \Delta t^3 \\ \frac{1}{2} j_{x,k} \Delta t^2 \\ \frac{1}{2} j_{y,k} \Delta t^2 \\ \frac{1}{2} j_{z,k} \Delta t^2 \\ j_{x,k} \Delta t \\ j_{y,k} \Delta t \\ j_{z,k} \Delta t \end{bmatrix}$$

Thus, the jerk can be represented as the last term of this equation. Consequently, the noise vector can be expressed using the following equation:

$$\mathbf{w_k} = \begin{bmatrix} \frac{1}{6} j_{x,k} \Delta t^3 \\ \frac{1}{6} j_{y,k} \Delta t^3 \\ \frac{1}{6} j_{z,k} \Delta t^3 \\ \frac{1}{2} j_{x,k} \Delta t^2 \\ \frac{1}{2} j_{y,k} \Delta t^2 \\ \frac{1}{2} j_{z,k} \Delta t^2 \\ j_{x,k} \Delta t \\ j_{y,k} \Delta t \\ j_{z,k} \Delta t \end{bmatrix} = \begin{bmatrix} \frac{\Delta t^3}{6} & 0 & 0 \\ 0 & \frac{\Delta t^3}{6} & 0 \\ 0 & 0 & \frac{\Delta t^3}{6} \\ \frac{\Delta t^2}{2} & 0 & 0 \\ 0 & \frac{\Delta t^2}{2} & 0 \\ 0 & 0 & \frac{\Delta t^2}{2} \\ \Delta t & 0 & 0 \\ 0 & \Delta t & 0 \\ 0 & 0 & \Delta t \end{bmatrix} \begin{bmatrix} j_{x,k} \\ j_{y,k} \\ j_{z,k} \end{bmatrix} = Gj$$

The process covariance matrix Q can therefore be calculated as follows:

$$Q = E[\mathbf{w}\mathbf{w}^T] = E[Gjj^TG^T] = GE[jj^T]G^T = G\begin{bmatrix}\sigma_{j_x}^2 & 0 & 0\\ 0 & \sigma_{j_y}^2 & 0\\ 0 & 0 & \sigma_{j_z}^2\end{bmatrix}G^T$$

To ascertain the starting position $p_0(x_0, y_0, z_0)$, the initial system state x_0 can be a true position or can be calculated using WLS. Subsequent estimation of Tag Mote positions involves approximating the values of the nonlinear function h to the actual Tag Mote positions $p(x_k, y_k, z_k)$.

The static position estimated with WLS in Table 5.5 was used as the EKF starting position for this analysis. The initial state vector in (meters) is, thus, given by:

$$x_k = \begin{pmatrix}1.048 & 1.023 & -0.422 & 0 & 0 & 0 & 0 & 0 & 0\end{pmatrix}^{\mathsf{T}} \tag{5.15}$$

The results illustrated in the Figures 5.19 for

$$E[\mathbf{j}\mathbf{j}^T] = \begin{bmatrix}0.01 & 0 & 0\\ 0 & 0.01 & 0\\ 0 & 0 & 0.01\end{bmatrix} \tag{5.16}$$

as best fit after fine tuning the EKF parameters show a red solid line which is the smoothed position estimate using the Kalman filter that corresponds to the actual movement patterns illustrated in Figure 5.17. In addition, the position estimates from the WLS algorithm are shown in Figure 5.19d. This also reiterates that the variance in a dynamic environment is significantly higher compared to the previously measured static case, indicating that the WLS results alone are not sufficient for precise tracking. On the other hand, it highlights the effective performance of the EKF in the qualitative mapping of motion patterns compared to WLS, where a trajectory is recognisable that visually corresponds to the actual trajectory, even though no measured ground truth exist to statistically analyse the correctness of the data.

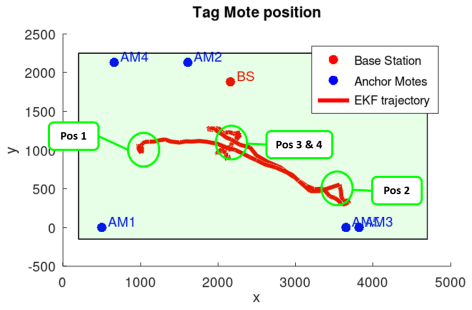

(A) Transmitter/ Anchor Mote 1 at Position 1

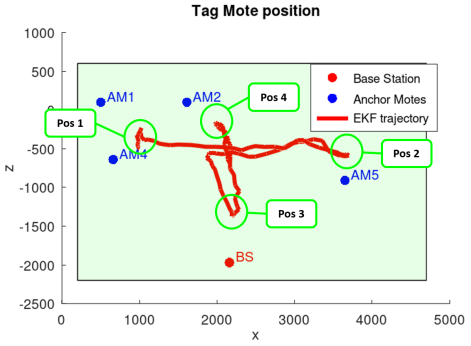

(B) Receiver/Base Station Development Model

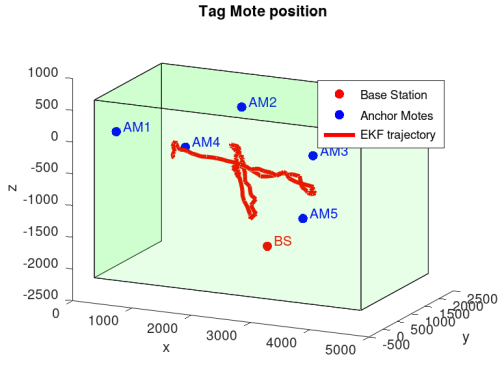

(C) Receiver/Base Station Development Model

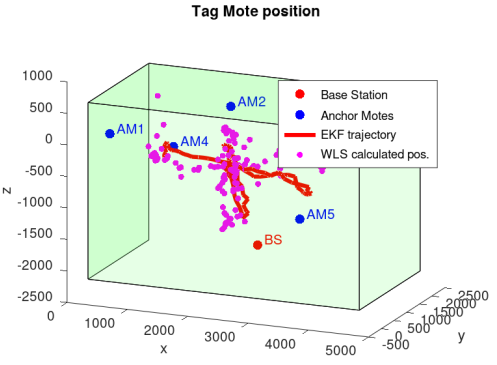

(D) Receiver/Base Station Development Model

FIGURE 5.19: Tested positions during the Columbus mock-up test campaign

5.3 Radiation exposure

The reliable operation of electronic components in the harsh environment of space is essential in spacecraft, which includes considering the effects of ionising radiation on these components. TID and SEE are two important metrics used to assess the resilience of electronic components to such radiation.

- **Total Ionising Dose**: The TID quantifies the total amount of ionising radiation absorbed by a component over time. This radiation can come from a variety of sources, including galactic cosmic rays, solar protons, and the Earth's Van Allen radiation belts. Since ionising radiation can cause cumulative damage to semiconductor materials over time, leading to performance degradation, changes in electrical properties, and eventual component failure it is important to assess the TID resistance of a component to ensure that it will perform reliably over the lifetime of a space mission.
- **Single Event Effect**: As opposed to TID, which focuses on cumulative damage caused by ionising radiation, SEE refers to sudden, discrete events caused by ionising radiation, whereby a single ionising particle can be energetic enough to cause an electronic device to fail. There are several types of SEEs. These include Single Event Upsets (SEU), which change the state of a memory bit, and Single Event Latchups (SEL), which cause a short circuit in a semiconductor device. Although SEEs usually do not cause immediate component failure, they can affect system performance and, in some cases, cause irreparable damage.

In the context of IR-UWB technology, testing the hardware – especially the DWM1000 radio module – for resistance to TID and SEE is thus an important test to assess the technological maturity of such systems. It was also a significant step in the development and qualification of hardware for the Wireless Compose mission.

The use of commercial components presents a significant challenge in this regard, as they can vary widely in their reliability under space radiation conditions, with commercial components often exhibiting problems when exposed to radiation doses exceeding 15 krad(Si), while purpose-built radiation-hardened components can have tolerances of 50 to 300 krad(Si).

Therefore, in order to ensure operational readiness in space, a comprehensive characterisation and evaluation of these aspects is critical.

5.3.1 Space environment

To better understand the requirements, it is helpful to take a closer look at the space environment. In some regions of space, such as in the van Allen belts surrounding the Earth, the radiation environment consists of large fluxes of electrons and protons and, to a much lesser extent, heavy ions. While the electrons can reach energies of up to a few MeV, the protons can reach energies of a few hundred MeV. Electrons cause damage primarily through spacecraft charging and TID. Protons, because they are highly penetrating, relatively massive and present in large numbers, degrade the performance of spacecraft components through TID and SEEs. (127, p. 5)

An early radiation environment model is AP-8, developed by NASA/GSFC in the 1960s, which describes the radiation captured there. However, AP-8 does not consider temporal changes, such as daily variations, and does not provide information on the direction of the fluxes. Its advantage over newer models is its wide energy range, covering protons from 0.1 to 400 MeV and electrons from 0.04 to 6 MeV.

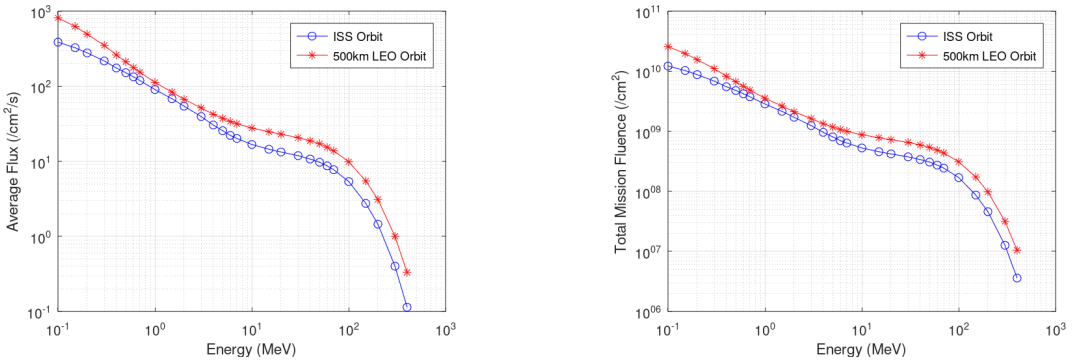

(A) Avarage flux vs. energy (B) Total mission fluence vs. energy

FIGURE 5.20: Integral flux and fluence for reference orbits (ISS and 500km LEO)

Figure 5.20 shows the integral flux and fluence of the AP-8 model for an exemplary ISS and a 500km Low Earth Orbit (LEO) calculated via ESA's Space Environment Information System (SPENVIS) (128). The integral flux represents the particles with energies greater than or equal to a certain value. The total mission fluence, i.e. the total number of particles over the mission period, can be calculated from the flux.

The SPENVIS SHIELDDOSE-2 model allows for the representation of the ionizing dose absorbed over time, analysing the dose absorbed in relation to the thickness of an aluminum (Al) shield. This model projects the expected TID for isotropic shielding, presuming a simple spherical aluminum structure. In Figure 5.21, this relationship is again depicted for an ISS and a 500 km LEO orbit with a mission duration of one year. The data indicates that for this reference mission, an aluminium shielding of 1 mm provides sufficient resilience, with an exposure of 0,52 krad(Si) in 500km LEO orbit and 0,189

krad(Si) in ISS orbit for the mission duration of one year. Notably, increasing the shielding beyond 5 mm does not significantly reduce the total dose, as high-energy protons are not effectively stopped by the shielding. This highlights the importance of the described tests, as the shielding alone cannot fully protect against proton-induced TID or SEE.

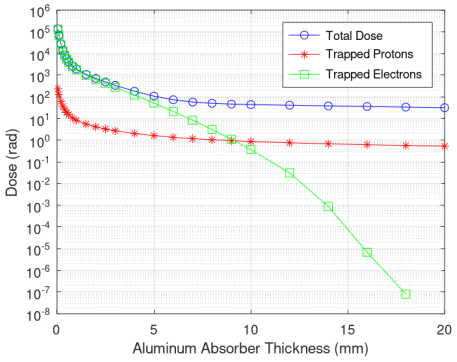

(A) Total mission dose for ISS orbit

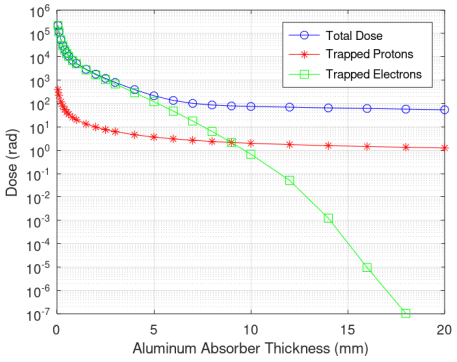

(B) Total mission dose for 500km LEO orbit

FIGURE 5.21: Total mission dose vs. Al Absorber thinkness

5.3.2 Test description

The focus of the tests was on the DWM1000 radio module, as there are no radiation-hard or radiation-tolerant IR-UWB radio modules available to date, although several radiation-hard alternatives are available for micro-controllers that also support the Cortex-M architecture, such as Microship, Gaisler, or Vorago. In total, I conducted two test campaigns: a TID campaign and a SEE campaign. As mentioned, some of the test results I have published in (45).

The TID test campaign I conducted in two runs. The first run aimed at a total dose of more than 20 krad(Si), while the second run aimed at a much higher total dose of 180 krad(Si). Instead of the 10 samples required by the European Space Components Coordination (ESCC) ESCC-22900 standard (129), due to equipment and cost limitations, two DUTs were irradiated and tested in the first run and three in the second run. The test was performed at the Helmholtz-Zentrum Berlin using a cobalt-60 source emitting beta and gamma radiation, with gamma radiation being responsible for the final exposure. The dose rate and fluence depended on the distance from the source and the exposure time. The DUTs were operated individually, powered by an external power supply and monitored by a data acquisition unit. During the test, the DUTs were in idle mode in the first run, while in the second run they actively transmitted dummy packets received by a shielded reference receiver. To minimise the effect of radiation on the μC, the STM32L151 μC were shielded with lead bricks in the second run. However, in the first run, a DUT was also irradiated together with an STM32L151 microcontroller.

In the SEE test campaign, I evaluated the SEEs by irradiating them with protons of different energies, ranging from 70 MeV to 184 MeV, performed at the Kernfysisch Versneller Instituut (KVI) in the Netherlands. The basic mechanisms of proton-induced SEE events differ from those caused by heavy ions. While heavy ions cause SEE events directly by ionisation, protons first enter into a nuclear interaction. The resulting products then cause SEE events by direct ionisation. Because of these nuclear interactions, when testing proton-induced SEE events, the cross section is measured as a function of the proton energy and not as a function of the Linear Energy Transfer (LET) as is usual for heavy ions. Due to beam time constraints, initially three DUTs were investigated for similar reasons. Also the strict beam time did not allow for irradiating with energies below 70 MeV. However the focus was on the higher energies, since here more SEE were expected. Another reason is, that with increased shielding thickness, the low-energy proton fluence is significantly reduced, while the fluence of protons with energies greater than 50 MeV is hardly affected (127, p. 6). The DUTs consisted of an evaluation board comprising a DWM1000 radio module and an STM32L151 μC. Again, reference receivers were placed at a safe distance of 4.75 m from the DUTs to evaluate the received data. All DUTs were guided into the beam by a motorised frame, connected to a programmable power supply and supplied their diagnostic data via serial data links to a notebook with dedicated control software, whereby soft and hard resets were attempted when faults were detected.

The experimental data acquisition generated diagnostic data after each frame transfer and the error diagnostics included an analysis of the register errors, RF power, and packet delivery ratio. If errors were detected, the registers were rewritten while a hard reset was performed if the system failed. Errors were classified as critical, non-critical, and errors in the DW1000 chip's One-time Programmable Memory (OTP). The RF diagnostic data also provided estimates of received power.

The test conditions for both campaigns included an execution at an ambient temperature of 20$\pm$10°C and dedicated control software was used to control and monitor the execution and data collection. A burn-in period was observed prior to the start of the tests to ensure that temperature changes, especially heating of the receivers in listening mode, did not affect the performance of the radio modules during the experiment.

5.3.3 Test results

TID The TID tests of the first run focused on checking the response of the instrument to γ radiation up to a value of more than 20 krad(Si), which would correspond to a lifetime of at least 10 years in a 500km LEO orbit, considering a shielding of 1 mm Al and a radiation exposure of 0,52 krad(Si) per year and a safety factor of 2. The current measurement of Sample 1 showed no anomalies and the test was terminated at

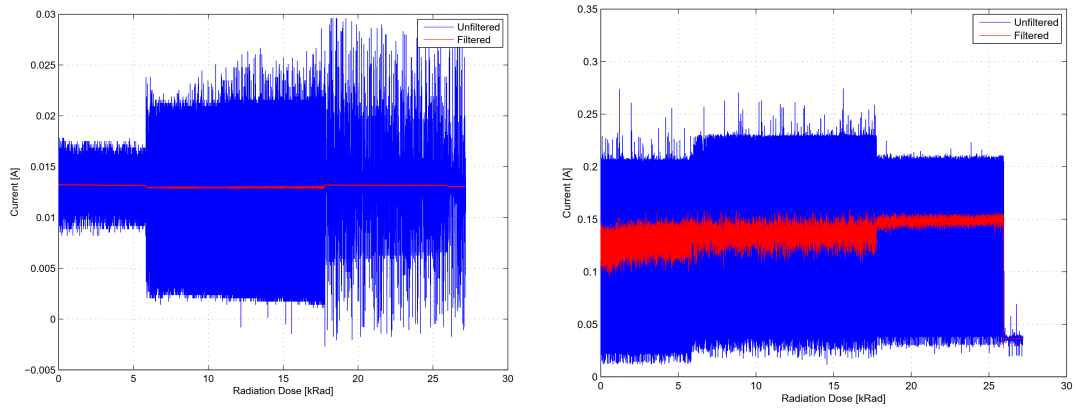

(A) Sample 1 (45, Figure 5) (B) Sample 2 (45, Figure 6)

FIGURE 5.22: Applied current conditions vs TID in the first run

27.5 krad(Si). Sample 2 showed a significant drop in current at around 26.2 krad, with the transceiver still in IDLE mode which led to the conclusion that the micro-controller was damaged, which was confirmed by subsequent functional tests, as shown in Figure 5.23b.

No degradation was detected in any of the radio modules which suggests that the micro-controller is significantly more sensitive to radiation than the UWB modules and a second run was performed to verify this finding. However, in this case, the target dose was significantly higher at 180 krad(Si). As the modules were actively sending messages during this time, all μC were shielded so that there would be no unwanted test interruption due to a failure of a micro-controller. The aim of the test was to determine at what level the radio modules could be damaged and Sample 3 showed clear degradation and damage, with the receiver suddenly reporting 100% packet loss from approximately 88.2 krad(Si) while the power consumption also began to fluctuate. A first peak of about 0.1 was observed at approximately 94 krad(SI) and from roughly 96.4 krad(Si), the current fluctuations increased significantly and dominated the measurements, which was due to a destructive effect.

However, for Samples 1 and 2, no decrease in PDR was observed, which was nearly 100%, and the test was successfully completed at 180 krad(Si).

SEE During the SEE tests, the behaviour of the DWM1000 radio modules at different radiation levels was investigated, and the energy, flux, and fluence levels of the tests are shown in Table 5.6. It is important to note that the flux is set by the test facility according to its capabilities. The fluence then corresponds to the maximum number of protons achieved during the test time frame at a given flux for a specific proton energy. The test is normally terminated when approximately 100 errors have been registered or a fluence of $10^{11} protons/cm^2$ is achieved or after destruction of the DUT.

(A) Test setup with a Cobalt-60 source and the DUTs

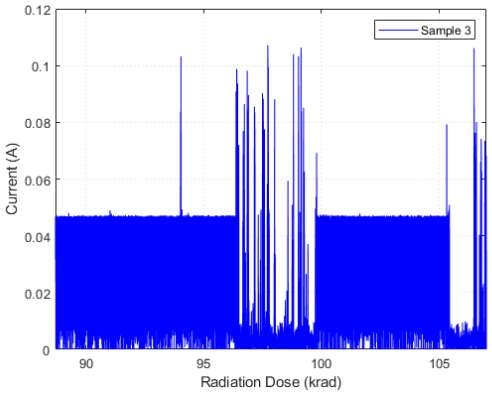

(B) Sample 3 (45, Figure 7)

FIGURE 5.23: Applied current conditions vs. TID in the second run

TABLE 5.6: Test configuration

Test	DUT	Energy (Mev)	Mean Flux ($1/cm^2$)	Total Fluence ($1/cm^2/s$)
#1	#1	184	1.05×10^9	4.07×10^8
#2	#1	150	1.0×10^{10}	3.58×10^6
#3	#1	120	1.0×10^{10}	1×10^7
#4	#2	70	4.8×10^{10}	4.16×10^7
#5	#2	70	1.0×10^{10}	6.38×10^6

The data flows were reviewed, together with the register entries and the evaluation of the transmitted data and the results are summarised in Table 5.8.

It should be noted that the test was carried out together with the μC, which appeared to be much more susceptible than the radio module, as was the case in the TID tests. This resulted in many hard resets due to the controller not responding or sending an incorrect data format, which may have directly affected the interface to the experimental PC. In contrast to the ESCC 25100, correspondingly lower fluences than the recommended $10^{11} protons/cm^2$ had to be set in combination with the maximum possible flux, as otherwise the analysis data could not be read out due to the constant lock-ups in the μC.

As the range between the DUTs and the reference receivers was also reduced at the same time, no degradation of the measurements could be detected. The packet delivery ratio was at 92.3%, which correlated with the observations when either register errors occurred or lock-ups were followed by a hard reset. Finally, it should be noted that only two DUTs could be tested due to the many lock-ups in the μC and the associated test interruptions, as well as the strict time requirements for the beam time.

The following Table 5.8 shows the cross section, which indicate the amount of the events in relation to the total fluence per device.

Table 5.7: DUT register errors

Test	**σ Hard resets** (cm^2/dev)	**σ Errors**		
		OTP	**Critical**	**Non-critical**
1	3.6×10^{-8}	1.6×10^{-8}	1.9×10^{-9}	0
2	5.2×10^{-8}	5.3×10^{-9}	1.0×10^{-9}	1.0×10^{-10}
3	2.6×10^{-8}	1.6×10^{-9}	1.3×10^{-9}	3.0×10^{-10}
4	7.3×10^{-9}	0	3.54×10^{-10}	6.25×10^{-11}
5	4.1×10^{-8}	1.0×10^{-10}	5.0×10^{-10}	6.0×10^{-10}

To calculate the worst-case event rate, the maximum measured cross section is multiplied by the minimum proton flux at which at least one event was observed. This is also referred to as the threshold energy E_{th}. The maximum number of events for the reference missions can therefore be calculated as follows (130, p. 15):

$$E_{th} = flux(E_{th}) \times d_M \times \sigma_{max} \tag{5.17}$$

where

E_{th} is the integral flux of the threshold energy, d_M the mission duration and σ_{max} the max. observed cross section for a specific event.

As the hard resets were caused by the micro-controller, the highest cross section for the second sample was set at 184 MeV with 1.6×10^{-8} measured, there were SEUs, no destructive events like SELs could be observed. As tests were only carried out above 70 MeV and no threshold energy could be identified within the test campaign, the ESCC 25100 test range from 20 to 200 MeV is taken into account, whereby 20 MeV is assumed here as the lowest energy to test. The integral fluence was taken for the reference orbits from Figure 5.20.

For the one-year mission duration, this results in the following event rates:

Table 5.8: SEU rate

Orbit	**σ_{max}**	**Fluence at 20 MeV**	**SEU rate**
	(cm^2/dev)	$(/cm^2)$	/year
ISS Orbit	1.6×10^{-8}	7.2345×10^8	11,57
500km LEO orbit	1.6×10^{-8}	4.1918×10^8	6,71

5.4 Summary

The results of my comprehensive investigation of the technological challenges of implementing UWB technology for space missions were presented in this Chapter. The verification process centered on three critical aspects: electromagnetic compatibility, radiation exposure, and data robustness in multipath fading scenarios.

The electromagnetic compatibility study concluded that the system's emission levels is well below the limit values, which is an indication that no interference with other equipment on board the spacecraft or the ISS is to be expected. However, the interference tests indicate the possibility of packet losses, which could mean a degradation of the network functionality and thus it is necessary to implement mitigation techniques at the software and hardware level. Further analyses should focus on preventing interference and adjusting operating bandwidths to align with the system's frequency plan, particularly when strong interference occurs.

The challenges of multipath propagation were the focus of the data robustness measurements. The measurements show that the system performs well under these conditions in the Columbus module Mock-Up. An almost 100% PDR was achieved despite the highly reflective structure and multipath propagation, also the positioning capabilities under the same conditions were successfully demonstrated.

The radiation tests show that the devices can withstand space conditions for a 10-year LEO mission, although the micro-controller appears to be more susceptible to radiation than the UWB module. Despite this result, it has no impact on the use in a one-year mission as expected for the Wireless Compose experiment. In addition, no destructive effects were found and the errors found during the SEE tests were SEUs and therefore correctable.

In summary, this Chapter provides a detailed verification of the three critical aspects of advancing IR-UWB technology for space. The results are crucial not only for the Wireless Compose experiment, but also for the development of future space missions that rely on this technology. The studies and results presented here are an important step towards achieving the necessary technological maturity for space adaptation.

Chapter 6

Demonstration

This Chapter describes the in-orbit demonstration of the implemented wireless network utilizing IR-UWB/LLDN technology. It forms the basis of the Wireless Compose experiment conducted on board the International Space Station. The experiment in which I was the principal investigator (PI) was carried out as a technology experiment in the Columbus module that involved the operation of a wireless network. This network's design and implementation were previously detailed in Chapter 4, and the technology employed is a key focus of this thesis. Much of this experiment, namely developing and operating the IR-UWB-based network, was carried out as part of my dissertation, and some of the conceptual content presented in this Chapter I already published in (46). This experiment marks a historic first: the operation and demonstration of an IR-UWB-based wireless network in the unique environment of space. The applications I assessed through this experiment include environmental monitoring and positioning, showcasing the network's potential in these critical areas.

Following a brief introduction, the technical details of the implementation at both hardware and software levels are explained, and the Chapter concludes by presenting and discussing the results, highlighting the achievements and lessons learned during the mission.

6.1 Sensor network on the ISS: Wireless Compose

Wireless Compose is a technology demonstration experiment that was part of the Alexander Gerst Horizon mission. It was operated during ISS Increment 56/57 in 2018 and the initiative stemmed from the conceptual groundwork laid out in this dissertation. The primary objective was the verification and demonstration in a real environment in space. The key features included sensing and tracking functionalities, alongside an evaluation of the energy harvesting capability. The focus of the experiment was on future potential

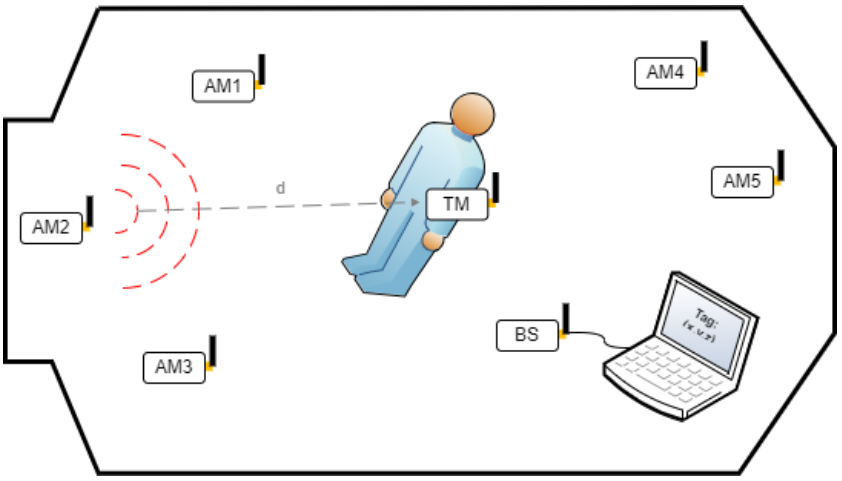

FIGURE 6.1: Wireless Compose deployment in the Columbus module

applications for positioning and environmental monitoring, whereby it is important to note that the energy harvesting aspect, although critical, falls outside the scope of my dissertation and will not be discussed further. The network architecture comprised several nodes and a network-centric gateway, as illustrated in Figure 6.1. The components were based on the modules presented in Subsection 4.3.1 and more detailed descriptions of the different types of components are provided in Section 6.2. Although commercially available components were used, a significant aspect of this experiment was the customisation and ruggedisation of the overall system in order to meet the stringent safety standards required for human-rated space missions.

6.1.1 Installation

The network was designed to perform two distinct tasks, namely positioning and sensing while different diagnostics data was also collected to monitor the network performance and different modules were developed to perform these tasks. In total, there are three different types of modules with different functions: Anchor Mote (AM), Tag Mote (TM), and Base Station (BS):

- The Anchor Mote has two functions: on the one hand, it acts as a sensor node and is therefore used for environmental monitoring. It also acts as a fixed reference point for positioning measurements. Because of these functions, the AMs were fixed at defined positions within the Columbus module and an overview of the final positions is provided in Figures 6.2 and 6.3. The power supply for these sensor nodes is provided either by commercially available (space-qualified) batteries or, as an essential extension for the five AMs, by power generation from the Columbus module's internal light sources. This means that no wiring is required to power the motes.

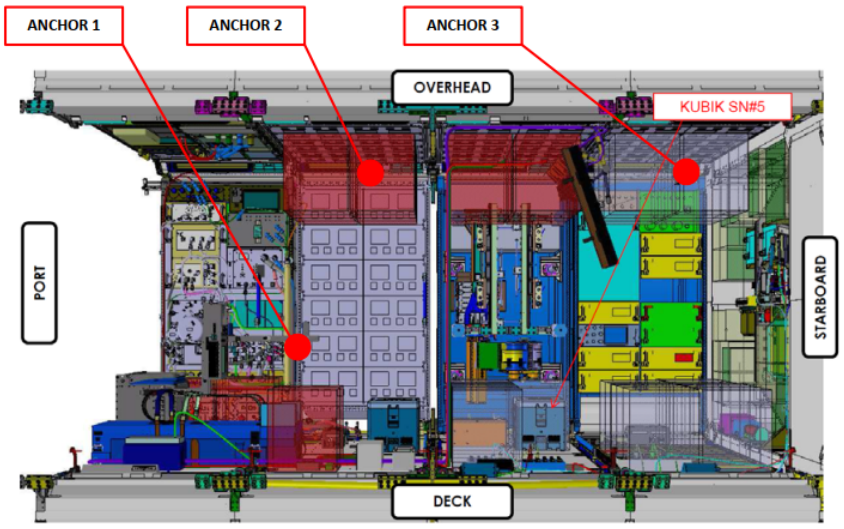

FIGURE 6.2: Positions in the Columbus module from the FWD-side point of view (Source: ESA)

- The Tag Mote is mainly used to track the objects connected to it. During normal activities, these motes are worn by the astronaut and attached to the arm and/or ankle with a strap.
- The Base Station acts as the gateway to the station and is responsible for data storage. The collected data is stored on two Secure Digital (SD) cards: an internal SD card that cannot be accessed, and a removable SD card that can be used to download the data using a laptop. The BS is powered by 5V DC from a Universal Serial Bus (USB) port on the onboard multi-port USB charger.

Each of these components played a critical role in the successful operation of the Wireless Compose experiment and the results presented in this Chapter.

6.1.2 Operational concept

Although the experiment was carried out in three different modes of operation, this Subsection will mainly focus on the results of the battery-powered Sensing and Tracking Mode, as the aim of the Energy Harvesting Mode was to evaluate the energy harvesting capabilities.

- Operational Mode 1, also known as the Sensing Mode, is started automatically when the Anchor Motes are manually switched to this mode. The five AMs record environmental data every 30 seconds, transmit the data to the BS, and enter sleep mode.

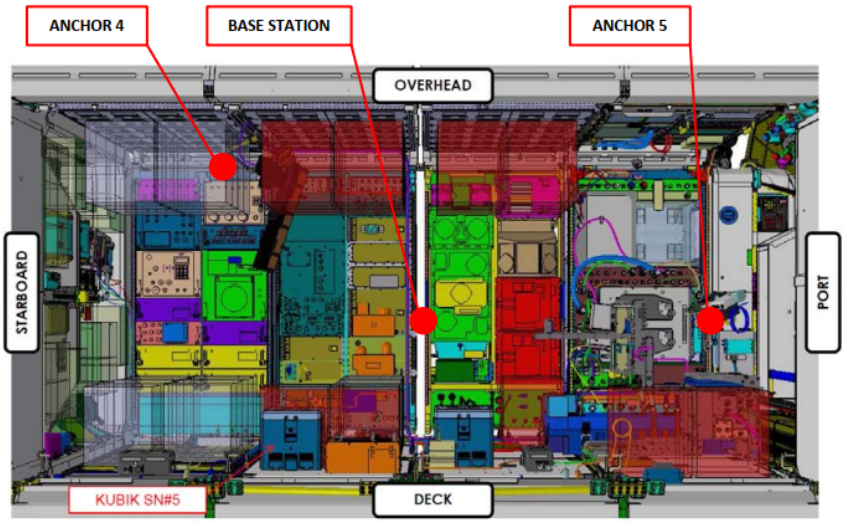

FIGURE 6.3: Positions in the Columbus module from the AFT-side point of view (Source: ESA)

- In Operational Mode 2, also known as the Tracking Mode, experimental sessions lasting 30 minutes were carried out during which the astronaut wore a TM on his or her arm and/or ankle to transmit the ranging data to the various Anchor Motes. This mode is automatically activated and deactivated in the Anchor Motes when the Tag Motes are switched on or off.
- Operational Mode 3, also known as the Energy Harvesting Mode, is specifically related to the energy harvesting experiment and is battery free. It thus has to be switched on and off manually by the astronaut at the different AMs.

The experiment started in Energy Harvesting Mode to save battery power for the later phases and modes. After approximately one month of operating, the three Tracking Sessions were carried out, in intervals of approximately one week. The plan was then to activate the Sensing Mode for approximately two months and then continue with the Energy Harvesting Mode for another four months. During this time, the internal light sources of the Columbus module were used to provide additional power to all Anchor Motes via solar cells mounted on the housing. No more Tracking Sessions were conducted during the remainder of the operational phase.

6.2 Hardware

All the components used in the experiment were designed with a basic configuration required to operate the IR-UWB network which was based on the hardware presented in Subsection 4.3.1, including a low-power STM32L151 micro-controller and the DWM1000 module, ensuring compatibility with the IEEE 802.15.4a standard.

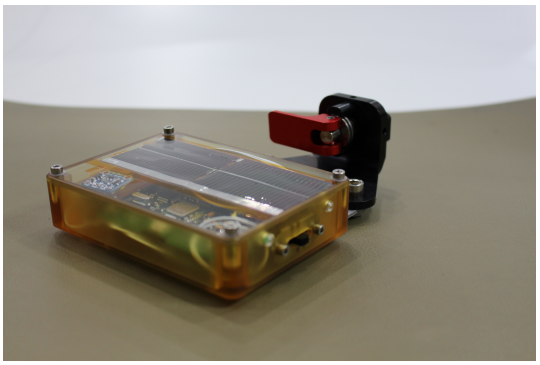

FIGURE 6.4: Anchor Mote Flight Model

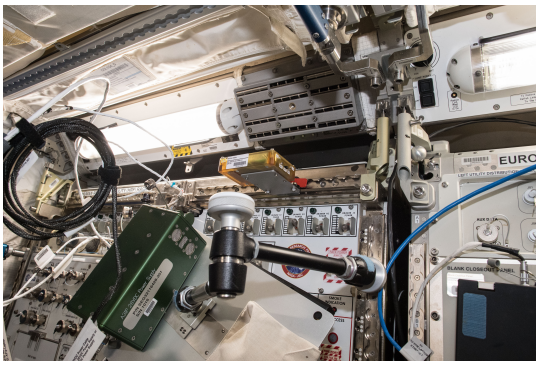

FIGURE 6.5: Anchor Mote installation (Source: ESA)

In addition, the components were each equipped with a battery compartment and a seat track fitting, allowing them to be mounted in pre-defined positions inside the Columbus module. The enclosures used were made of a heat-resistant and high-strength plastic material called ULTEM, which is transparent to RF radiation, and thereby allows the UWB antenna to be integrated into the module.

In addition to these common features, the individual modules had other specific characteristics, which are described in more detail below.

- The Anchor Mote was equipped with additional hardware to fulfil its tasks. For environmental monitoring, it contained a multi-sensor system consisting of different low-cost Micro-Electro-Mechanical System (MEMS) sensors:

  - BOSCH BMP180 sensor capable of measuring temperature, barometric pressure (131)
  - ST L3GD20 sensor for acceleration (132)
  - ST LSM303 sensor for rotation (133)
  - TAOS TSL2561 sensor for ambient light (134)

  The different types of sensors were interfaced with the main controller via SPI or I^2C. Additionally, the Anchor Mote included a secondary PCB—a power board equipped with a special energy harvesting circuit and two solar cells mounted on the top plate of the housing. The setup enabled the generation of power from the interior lighting of the Columbus module.

- The Tag Mote maintained the basic configuration to cover the main functionality for ranging measurements. However, the TMs were also equipped with the accelerometer (L3GD20) and gyroscope (LSM303) low-cost MEMS sensors to complement the motion measurements.

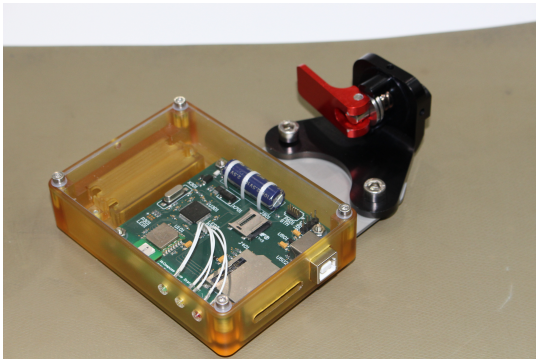

FIGURE 6.6: Base Station Flight Model

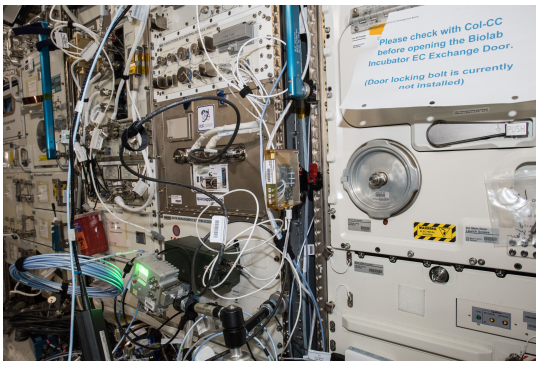

FIGURE 6.7: Base Station installation (Source: ESA)

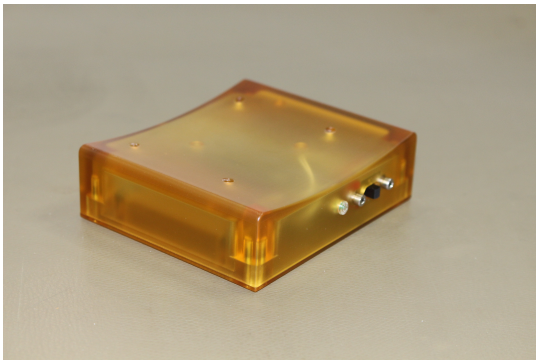

FIGURE 6.8: Tag Mote Flight Model

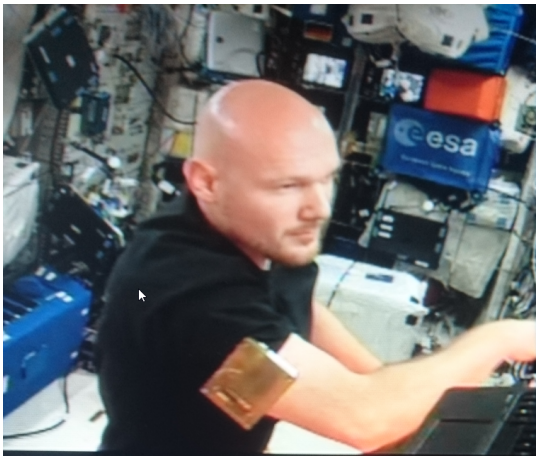

FIGURE 6.9: Tag Mote worn by A. Gerst (Source: ESA)

- The Base Station was similar in design to the other modules but was connected to a 5 V power source via a USB interface that kept it continuously activated. It also featured an external real-time clock and an internal SD card for data archiving. An additional external SD card was included for data storage, which could be removed to transfer data to a Columbus laptop.

6.3 Software

This Section focuses on the practical implementation of the software for the developed operational concept in which the specific requirements are addressed.

As previously mentioned in Section 4.3.2.4, given the stringent time constraints and the critical requirements for the flight model delivery, a bespoke software solution was necessary. The integration of the LLDN into the OpenWSN stack, as originally planned, could not be fully realized due to the overlapping timelines. Consequently, a more streamlined version of the LLDN, operating without an OS, was implemented. The

primary objective of this Subsection is to outline the specific software concept that I have developed for Wireless Compose.

In this software, two operational modes were considered: Sensing and Tracking, each employing distinct approaches to MAC management. In Sensing Mode, the receiver remains continuously active, with nodes transmitting their messages every 30 seconds. This is done without stringent scheduling or management, a condition that may lead to message collisions. Conversely, in Tracking Mode, the LLDN was utilised, which proved to be exceptionally suited for the cyclical demand scheme necessary for ranging, requiring both uplink and downlink slots.

6.3.1 Network states

In the following, the implementation of the state machine and the network roles is presented. These form the backbone of the software for the entire network. The state machine manages the two main operating modes of the network. These modes were found to be particularly suitable in the context of the given framework and Figure 6.10 shows a schematic representation of the network states.

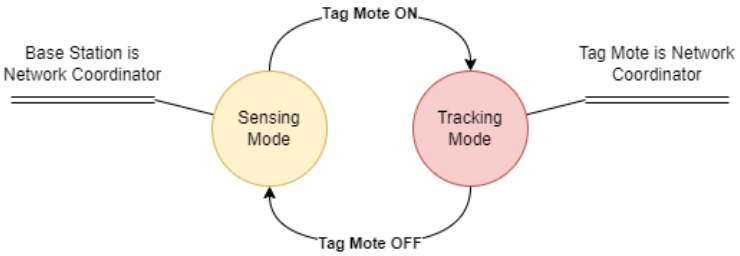

FIGURE 6.10: Operational modes transition

Firstly, the Sensing Mode is described. In this mode, the Base Station is always active and is responsible for receiving, storing, and forwarding the packets sent by the Anchor Motes. The Anchor Motes alternated between a sleep mode and an active phase at regular 30-second intervals, with the Anchor Motes waking up, requesting the mode of operation, collecting the data, and sending it back to the BS as illustrated in Figure 6.11

If the request was not replied to, the Anchor Mote went into sleep mode, and waited for another period to try again as illustrated in Figure 6.12. One of the main reasons for using this method was the ability to always poll the Base Station first, thereby allowing for rapid switching between the Tracking and Sensing Modes. It also prevented the Anchor Mote from unnecessarily recording and sending sensor data when the Base Station

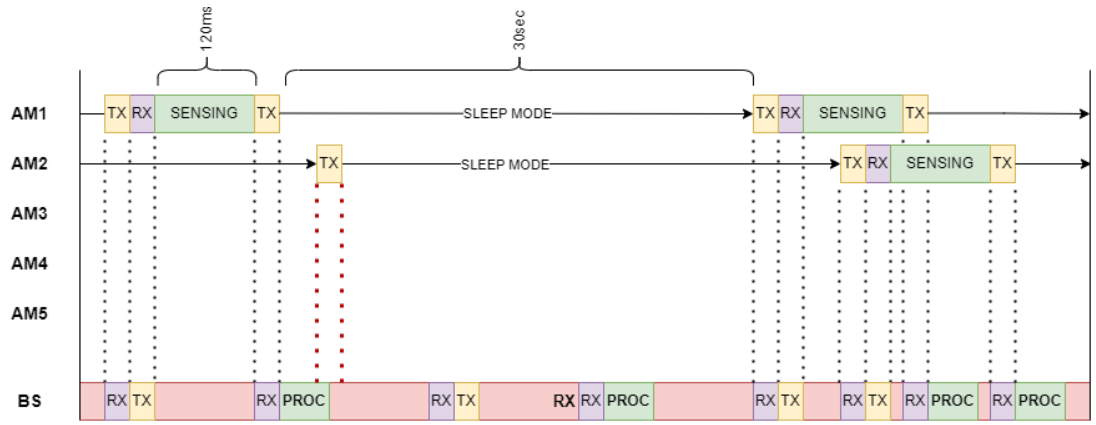

FIGURE 6.11: Sensing Mode chronogram

was busy, in another mode, or switched off. For the light sensor, it took approximately 120 milliseconds just to query the sensor to integrate the light whereas a request, on the other hand, could be sent much faster and it only took a few milliseconds. An ACK after sending the sensor message was intentionally omitted, as the tests showed that a Packet Delivery Rate of almost 100% is achieved with the selected data rate.

This scheme thus took the strict requirements for low power consumption of the battery-powered sensor nodes into account. In addition, to avoid collisions, the network design allowed the five modules to operate sequentially and the transmission time data processing on the Base Station was approximately 10 milliseconds. This kept the risk of collision low and eliminated the need for a special time-controlled procedure. An additional safeguard against the possibility of a collision was that the modules were activated manually by the astronaut, one after the other. Since simultaneous activation was impossible, this resulted in an initial random time spread. The selected scheme thus allowed reliable data transmission and storage in a relatively simple mode.

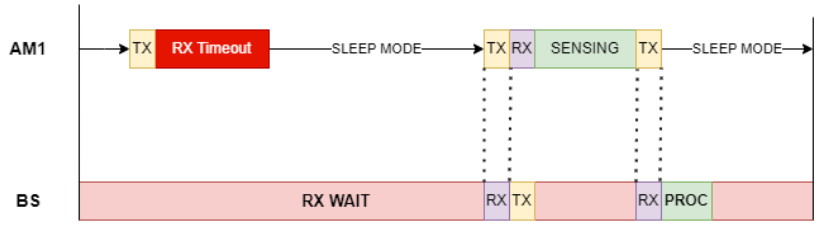

FIGURE 6.12: Tx Request timeout in Sensing Mode

Secondly, the Tracking Mode is presented in which the mobile Tag Mote takes over the role of the network coordinator. This is a significant difference to the Sensing Mode as the astronaut activates or deactivates a Tag Mote to switch to this mode. It initiated requests via beacons, which also contained the time stamp for the ToF measurement. The customised LLDN superframe thus comprises a beacon, six uplink timeslots, and three bidirectional slots combined into one downlink slot as illustrated in Figure 6.13.

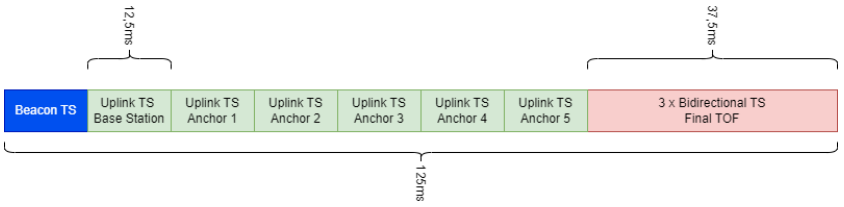

FIGURE 6.13: Superframe structure

The collected data and ToF calculations were then distributed within the network, with the Base Station remaining responsible for storing the data on the SD card. The specific requirements of the ranging process are the reason for this role change as it was necessary for the TM to perform the ToF requests because the focus was on the movement of the mobile TM and the BS could not perform this task efficiently.

It was therefore possible to ensure a meaningful and efficient range measurement by switching the network coordinator and this change demonstrates the flexibility and adaptability of the system developed as it can be adapted to different operating conditions and requirements. It is also a good example of the need for careful planning and configuration of the network roles in wireless communication systems under challenging conditions such as those of the Wireless Compose mission. A detailed flow chart during the mode transition is shown in Figure 6.14.

Due to the different tasks, the state machine also differs for the different modules and more detail on the specific modules and transitions that occur in the two main network operating modes is provided below.

6.3.2 Implementation

The complexity and number of tasks that each module performs within the network varies and is highly dependent on the particular way in which the network operates. To clarify the implementation process and provide a detailed overview, activity diagrams are used to explain how the software works in the different modules. The diagrams illustrate the specific modules and transitions that take place in the two main operating modes of the network, providing a detailed insight into the implementation.

Checking that a received message is destined for a particular Mote or BS is one of the standard MAC operations and is performed by every module on the network. If this is not the case, the message will be discarded. Although this operation is central, it is not explicitly highlighted in the activity diagrams. Additionally, for the implementation of the Ranging measurements, an example implementation of Decawave that is described in more detail in (135) was adapted.

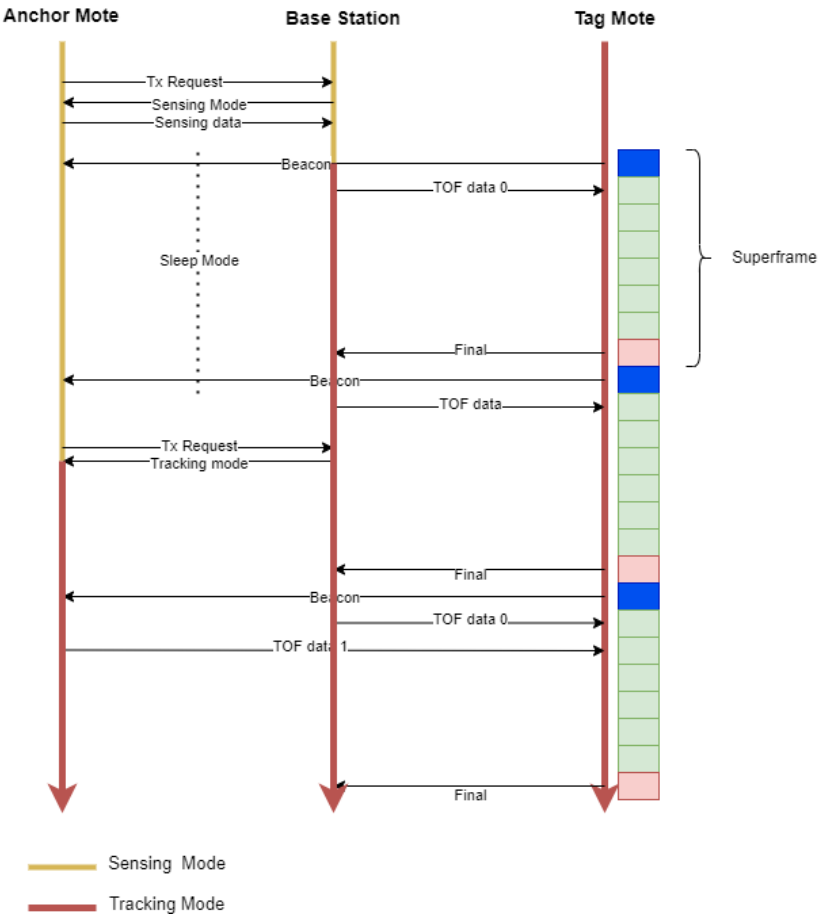

FIGURE 6.14: Mode transition flow chart

6.3.3 Base Station

In the implementation phase, the BS plays a central role. It goes through different states and performs different tasks depending on the network mode. The BS activity diagram in Figure 6.15 is explained below.

At start-up, the BS is in **Sensing Mode**. First, the hardware is initialised and the start time (ON time) is stored on the SD card. Immediately afterwards the "Rx WAIT for incoming data" state is activated in which the BS waits for incoming messages. When a message is received, the type of message is checked first. If it is a Tx request message, then the BS sends a response in order to receive sensing data as the next step. The data is then stored on the SD card and the Base Station returns to the Rx WAIT state.

On the other hand, if the Base Station receives a beacon from the Tag Mote, it switches to the **Tracking Mode** and returns to the Rx WAIT state. The incoming message is checked again to determine whether it us a beacon or a Tx request message. If it is a Tx request message, it is assumed that some Anchor Motes are still in **Sensing Mode** and hence, as a response, a mode change to **Tracking Mode** is requested.

However, if another beacon is received from the Tag Mote, the tracking activity flow will continue. The Base Station sends the ToF in the designated Time Slot and waits for the final message from the Tag Mote with the ToF results and the sensor measurements. When this arrives, the data is stored on the SD card and the Base Station returns to the RX WAIT state.

If no beacon is received from the Tag Mote after a certain waiting time, a timeout is triggered. The Base Station then changes back to **Sensing Mode** and it enters the Rx WAIT state to wait for the next incoming messages.

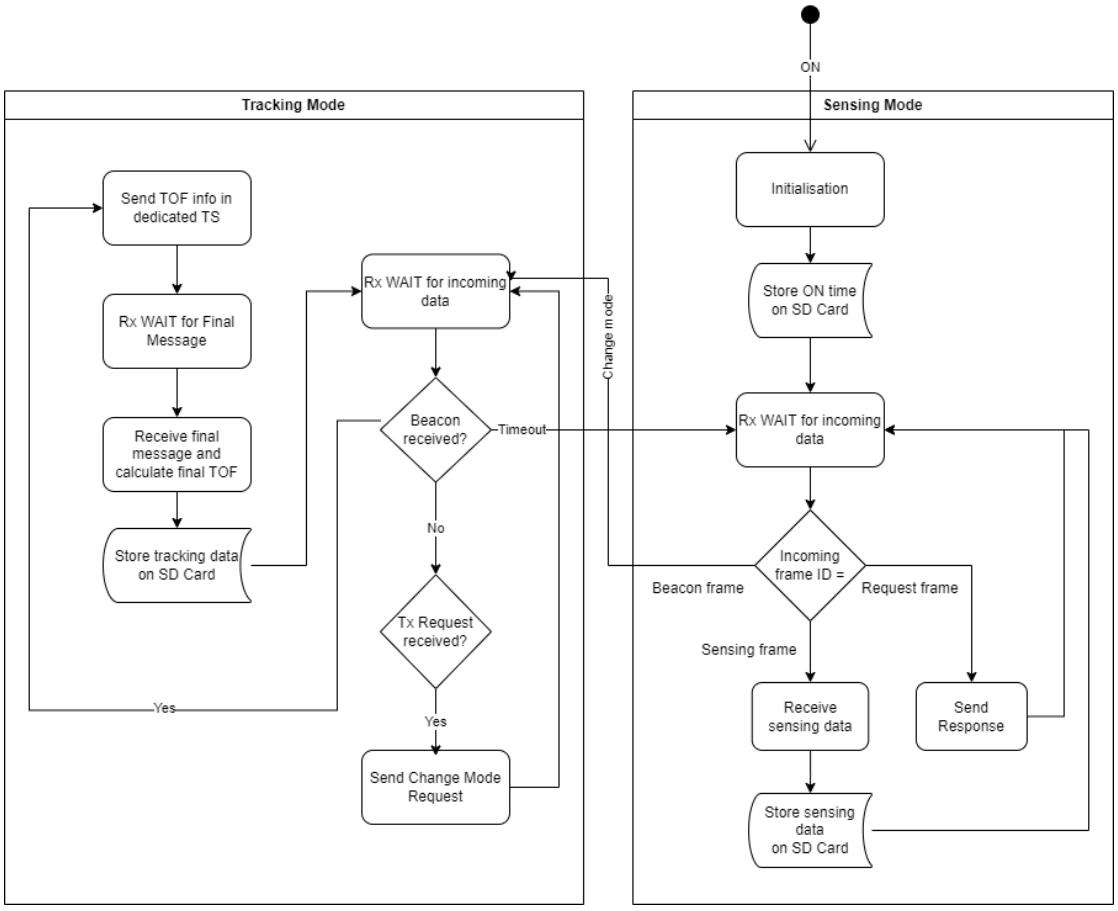

FIGURE 6.15: Activity diagram of the Base Station

6.3.4 Anchor Mote

When the Anchor Mote is activated, it always starts in the **Sensing Mode**, as shown in Figure 6.16. It first initialises its hardware and sends a Tx request to check the availability of the Base Station and the network mode. When it receives a response, it checks the mode. When the Sensing Mode is active, it collects various sensor data. It prepares a sensing message and transmits it to the Base Station. The Anchor Mote then

goes into Sleep Mode for 30 seconds. When the AM wakes up, the cycle starts again with the initialisation of the hardware.

However, if the AM receives a Mode Change Request message from the BS instead, it will switch to the **Tracking Mode**. Here, the Anchor Mote waits for a beacon message. After receiving the beacon message, it sends back the ToF information in the designated TS based on the time information contained in the beacon message.

The Anchor Mote then waits for the final message and, when it is received, calculates the final ToF, which is used as the basis for the next calculation. It then waits for the next beacon to repeat this process cyclically.

If no beacon is received after a defined timeout, the Anchor Mote goes back to **Sleep Mode**. After 30 seconds, the AM wakes up in **Sensing Mode** and the activity flow repeats.

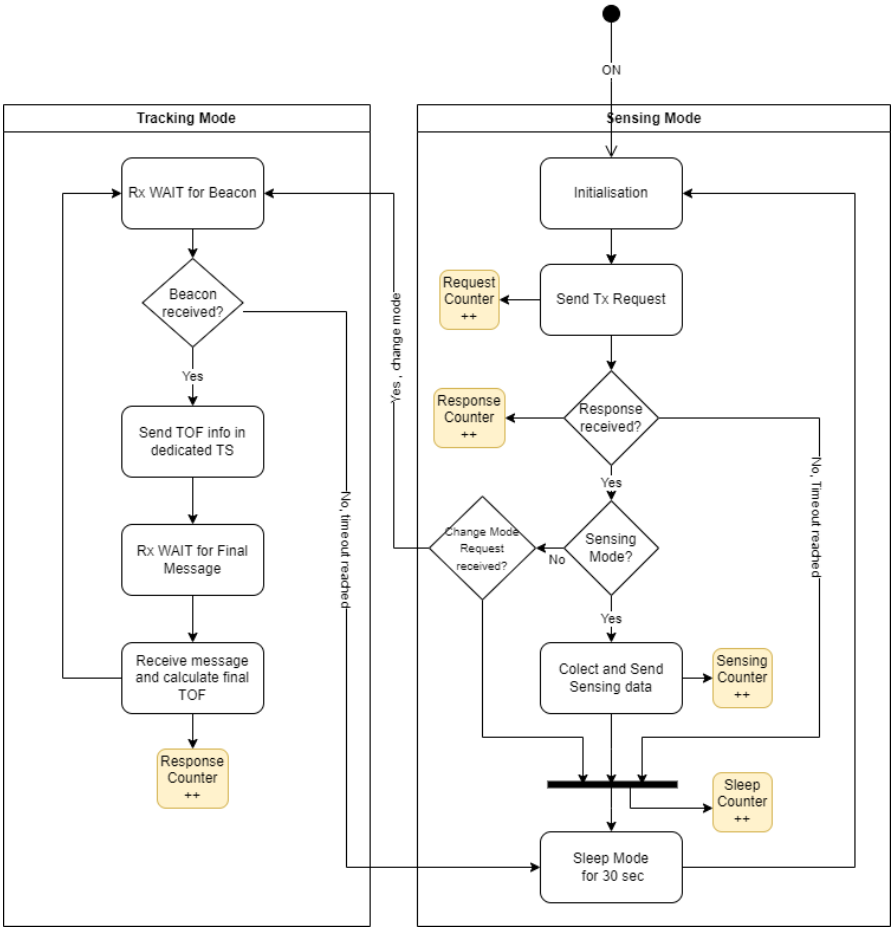

FIGURE 6.16: Activity diagram of the Anchor Mote

6.3.5 Tag Mote

The Tag Mote is relatively easy to configure compared to the other modules. When powered on, it goes straight into **Tracking Mode**. First the hardware is initialised, and then a beacon message is sent, as shown in Figure 6.17.

After sending the beacon, the Tag Mote switches to Rx WAIT and waits for messages from the Anchor Motes and the Base Station, which should arrive in the corresponding Time Slot. In addition to the ranging information it receives, the Tag Mote itself collects sensor data. This data includes readouts from the accelerometer and gyroscope. The sensor data, together with the ranging information, is sent as a final broadcast message to all network participants.

When these activities have been completed, the Tag Mote transmits another beacon and repeats this cycle continuously. This mode of operation is maintained until the TM is manually switched off.

When the Tag Mote is switched off, the absence of the beacon triggers a timeout at the Base Station and the Anchor Motes. This event causes these devices to enter **Sensing Mode** until a next Tracking Session is initiated. This underlines the flexibility of the implemented network to respond to different operational scenarios.

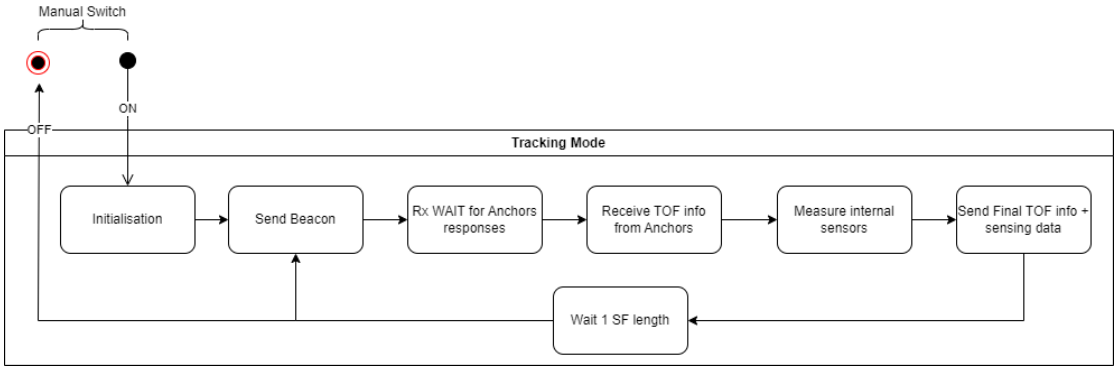

FIGURE 6.17: Activity diagram of the Tag Mote

The different modes of operation can directly be controlled by the astronaut, which has the advantage that the use of the network is not strictly tied to a schedule. This flexibility proved particularly useful in practice, as Tracking Sessions often had to be postponed or rescheduled due to external factors such as delays in the execution of other experiments.

6.4 Tracking

A key objective of the Wireless Compose experiment was to demonstrate and evaluate the ranging function of IR-UWB within the Columbus module and to track the astronaut. By studying and analysing the astronaut's movement patterns, it would be able to optimise the workflow in future missions.

During the mission, special Tracking Sessions were designed and carried out with the astronaut wearing a Tag Mote. This allowed active ranging measurements to be made between the anchor and Tag Motes. The propagation times (T_{prop}) obtained were converted into distance data and transmitted to the BS. These data allowed subsequent positioning by trilateration processing, a method described in detail in Section 2.6.3.

Several measurement methods were considered to perform the ToF measurements. Considering the structured and rigid superframe architecture of the LLDN MAC layer, the DS-TWR method, specifically with three messages and asynchronous communication, proved to be the most effective solution, as shown in more detail in Subsection 2.5.5.2. This method represents a balanced compromise between measurement accuracy and resource efficiency as the asynchronous communication allows various participants to act with different response times in predefined time slots. A total of six measurement requests were made, namely five to the Anchor Motes and one to the Base Station. This process is illustrated using the example of AM 2 in Figure 6.18 in which the other Anchor Motes send their replies in the time slots reserved for them.

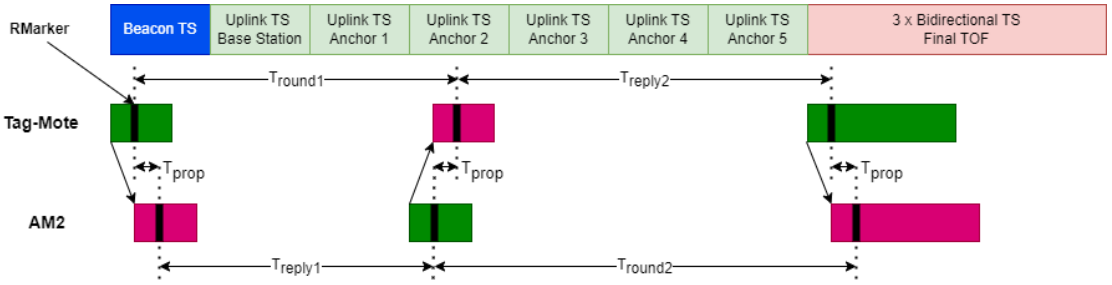

FIGURE 6.18: DS-TWR in the LLDN superframe structure

Another challenge was the consideration of multiple Tag Motes in the operational scenario. To solve this problem, an initialisation phase was added. In this phase, each Tag Mote first listens to check if beacons are already being transmitted by another Mote as illustrated in Figure 6.19. If this is the case, it will line up in time to send the beacon in the next superframe. On the other hand, the superframes are always transmitted so that each Tag Mote uses every second superframe to poll. As there was a fixed utilisation of two Tag Motes in the configuration in the operational scenario, it was easy to implement this solution.

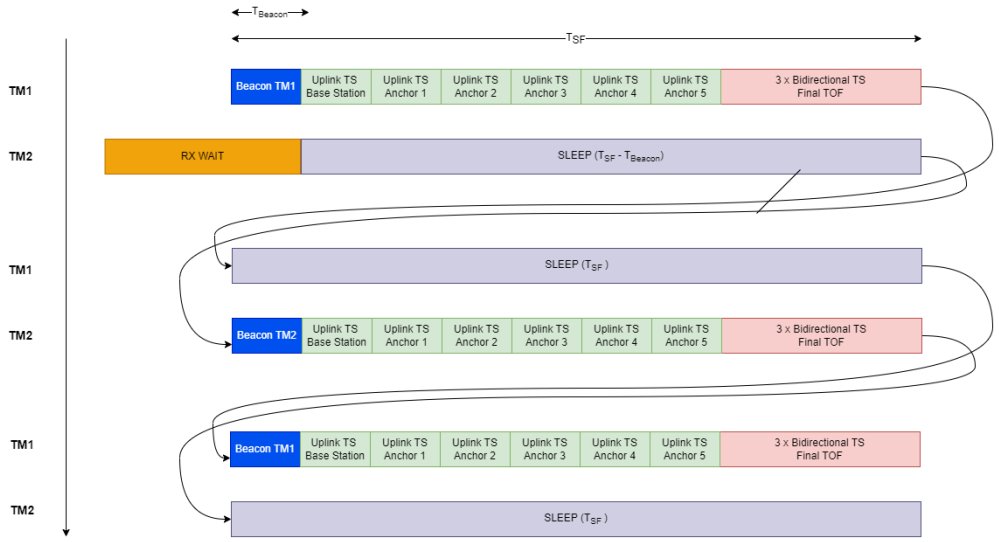

FIGURE 6.19: Multiple TMs scheme

As already introduced in Subsection 5.2.2.2, the ToA method was used to calculate the trilateration. In Wireless Compose, a total of six Anchor Motes were used which allows two redundant nodes to be used to optimise the trilateration solution and compensate for errors, since the estimation of the position in 3D is still solvable with only four Anchor Motes.

Using these equations in Subsection 2.6.3, it was able to calculate the position of the Tag Mote relative to the coordinates of the Anchor Motes and track the astronauts movements over the recorded duration of a Tracking Session.

6.5 Results

This Section presents the experimental results obtained. First, the performance of the Wireless Compose network is examined in detail after which the data collected by the sensors in Sensing Mode is presented. Finally, the results of the Tracking Sessions are discussed, with a particular focus on the first session, as a high quality video of this session is available for visual verification of the calculated TM positions.

6.5.1 Network

The battery-powered part of the network was operated for a total of approximately 90 days starting on 7/06/2018 at 15:27:39 Universal Time Coordinated (UTC), and the on/off states and mode transitions are shown in Figure 6.20.

Only the battery powered modes are relevant to this thesis and are discussed further in detail. During the first month, the energy harvesting experiment was performed and the

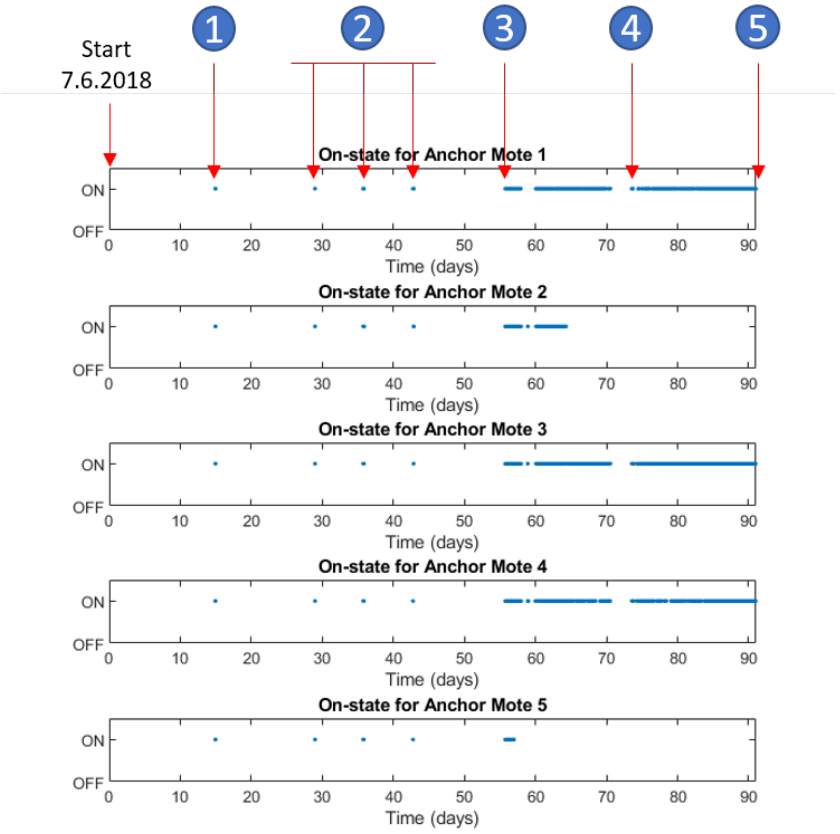

FIGURE 6.20: On/off states of the network

network was switched to the battery-powered Sensing Mode for a very short period only to verify its operability in orbit, as shown in 1 in Figure 6.20. This was followed by three battery-powered Tracking Sessions, as shown in 2 in Figure 6.20. In the next phase, the anomalies that were observed in the energy harvesting mode were investigated. From day 55, the network was switched to continuous Sensing Mode, as shown in 3 in Figure 6.20. Apart from minor interruptions, e.g. for downloading SD cards and changing batteries, the network was operated continuously in Sensing Mode for 35 days before it was deactivated. The Energy Harvesting Mode was then reactivated, as shown in 5 in Figure 6.20.

The three individual Tracking Sessions were carried out with an interval of approximately one week between them. During the three Tracking Sessions, a total of 84913 tracking messages were received. More information on the duration of the sessions and the number of packets collected per session is provided in Table 6.1.

The sessions were scheduled to last approximately 30 minutes, after which the tags were to be manually switched off by the astronaut, thereby allowing the network to automatically switch to a low-power mode to save the battery power for later operation. As shown in the table 6.21, this did not always work in practice as only Tracking Session

TABLE 6.1: Statistics of the Tracking Sessions

	Session 1		Session 2		Session 3	
Start date	5.07.2018		13.07.2018		20.07.2018	
Start time (UTC)	14:07:01		08:43:55		09:43:43	
Duration	33 min 49 sec		45 min 18 sec		100 min 21 sec	
Tag	TM1	TM2	TM1	TM2	TM1	TM2
Tracking messages	8088	8102	10707	10763	23192	23341
PDR (%)	99.91	99.78	99.26	96.66	97.00	96.97

1 had a duration of approximately 30 minutes. While the second Tracking Session ended after 43 minutes, this did not cause an issue as there was a certain amount of margin in the batteries allowed for this. During the third Tracking Session, the astronaut forgot to manually deactivate the Tag Motes and thus, even after the TMs were put back into the Cargo Transfer Bags, tracking was still active. Some Anchor Motes, especially AMs 2, 3, and 5, still had sufficient signal to keep the Tracking Mode active. The packet reception monitored in Tracking Session 3 for Tag Mote 1 is shown in Figure 6.21.

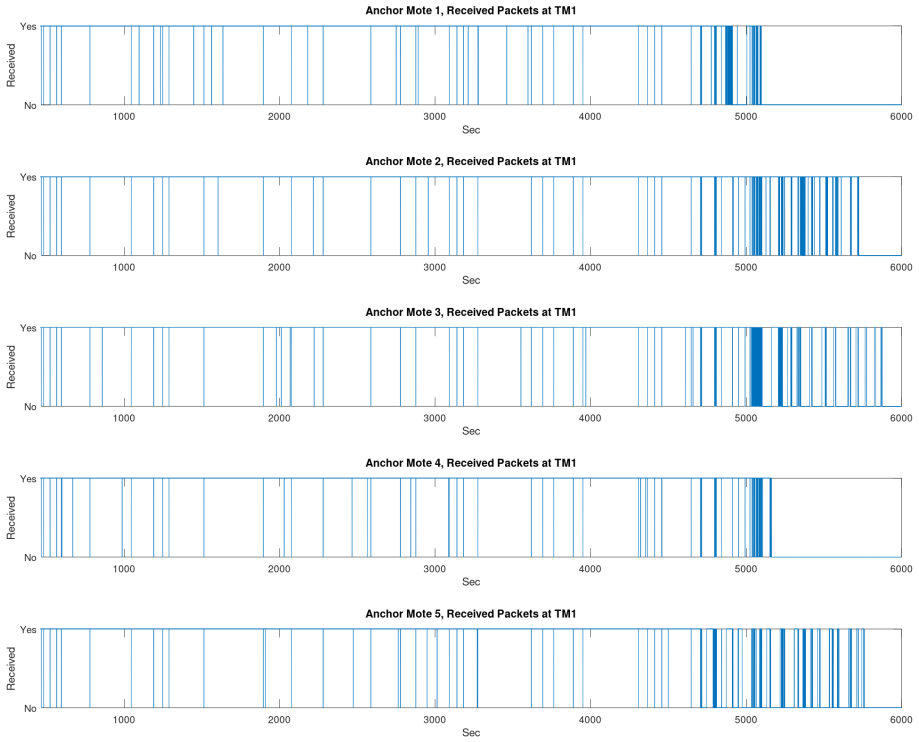

FIGURE 6.21: Tracking Session 3 packet reception at TM 1

It can be seen that towards the end of the session the communication link to the Tag Mote degraded significantly and there were frequent interruptions to the Anchor Motes. As a result of this malfunction, the network was active in Tracking Mode for over 100 minutes, which was well beyond the design margin of the batteries. This had a negative

effect on the continuous sensor mode, which then started to operate from day 55 onwards. The operation of AM 2 and 5 was terminated after a few days due to battery discharge. Although it was possible to replace the batteries on day 73, see 4 in Figure 6.20, the exchange was unsuccessful for AMs 2 and 5, and thus only the remaining Anchors 1, 3, and 4 were active in Sensing Mode until deactivated.

In Sensing Mode, a total of 208962 sensing messages were received from the various Anchor Motes. More information about the distribution is provided in Table 6.2.

Table 6.2: Statistics of the Sensing Mode

	AM11	AM2	AM3	AM4	AM5
Sensing messages	56670	11889	73712	63766	2925
PDR (%)	99.56	98.73	99.38	99.65	99.619
LOS (%)	45.317	14.282	76.509	47.712	59.863
NLOS (%)	46.497	85.087	7.3258	49.073	38.632
Average RSSI (dBm)	-81.05	-81.27	-80.77	-81.34	-81.35

The PDR was close to 100% for all Motes, which is in line with the RSSI measurements for the specific data rate. LoS and NLoS conditions were also examined and by measuring various diagnostics parameters in the UWB module, it was possible to analytically determine whether there was a LoS to the BS or not.

In (80, p. 45), Decawave states that if the difference between the received power and the first path power is less than 6 dB, the channel is probably LoS, while if the difference is more than 10 dB, the channel is probably NLoS. It is important to note that values between 6 dB and 10 dB were not considered here, as this range is not meaningful. Both power values were measured during the Sensing Mode and the LoS condition could be calculated. Figure 6.22 shows that some Motes have more preferred positions in terms of LoS than others.

As also observed in the mock-up measurements, the RSSI values typically range between -80 dBm and -85 dBm. However, as can be seen in the Figure 6.22, there are occasional drops to almost -98 dBm, as can be seen in Table 6.3 for Anchor 4. This closely aligns with the worst-case analysis in the link estimation in Subsection 5.2.1, where a min. Rx power of -98.8 dBm was estimated considering the different influencing aspects.

Table 6.3: RSSI values for Anchor 4

Anchor 4	**Min**	**Max**	**Mean**	**Std**
RSSI (dBm)	-97.670649	-79.750164	-81.353569	0.487917

Unfortunately, due to performance reasons it was decided not to measure the LoS/NLoS indicators for tracking. However, it was discovered at a later stage that doing so would

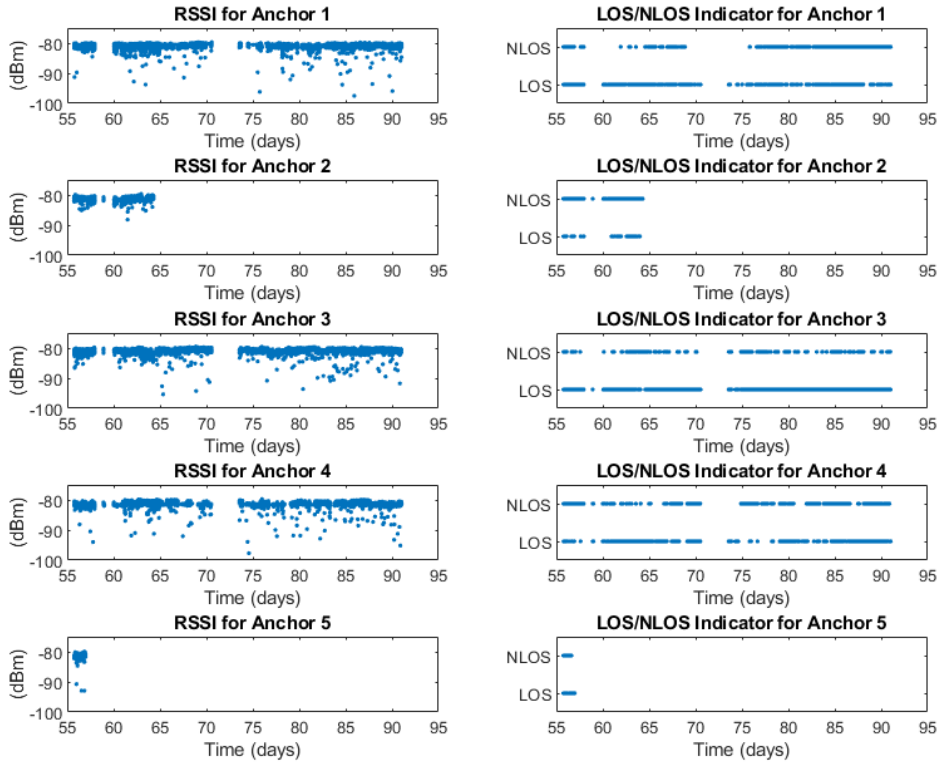

FIGURE 6.22: AM LoS and RSSI during continuous Sensing Mode

have been beneficial, especially for smarter weighting the favourable LoS Anchor Motes for the trilateration algorithm.

6.5.2 Sensing

The data collected in the Sensing Mode is presented below. As the continuous Sensing Mode was not started until after Day 55, the data shown here is from that period. Unfortunately, as explained above, data from Mote 2 and Mote 5 is only available for a short period.

The first data shown is the light intensity data, which was measured with the PSL2561 light sensors that were pre-calibrated in a laboratory environment on ground. The objective was to analyse the switch frequency and the light intensity on different locations in order to draw conclusions for possible energy harvesting.

Figure 6.23 shows that the lamps are switched on/off in a daily repeating cycle which is an indication that the lamps are only utilised during working hours. However, there are also phases in which the lamps are switched on for a longer period and the results are especially interesting for energy harvesting analysis, as the sensor data can be used

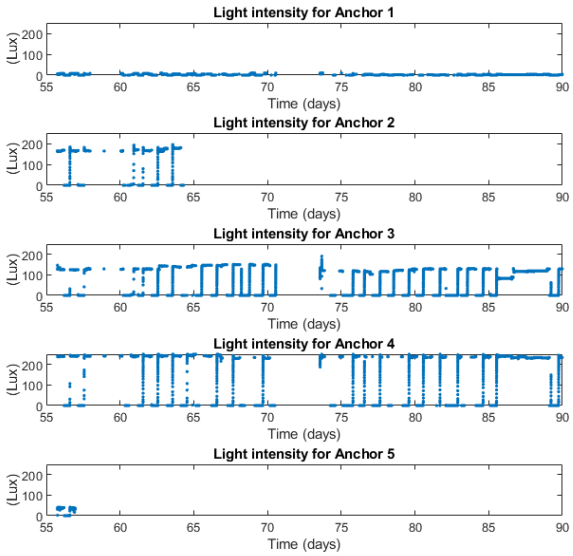

FIGURE 6.23: Light illuminance measured during Sensing Mode

to validate how much light energy is available for the harvesting. It is also possible to see the different intensities for each of the positions. In particular, the AMs that were very close to the light source perceived an illuminance a max. of 304 lux which corresponds to an artificial illuminance in a working environment on the ground, see Appendix B for more details. This means that these positions are well-suited for indoor harvesting. However, it was also found that more distant positions, where the solar cells are not aligned with the light source, are unfavourable for energy harvesting and they can thus only be used to a limited extent (or not at all) for energy harvesting. Another important environmental value is the temperature. Figure 6.24 shows that it

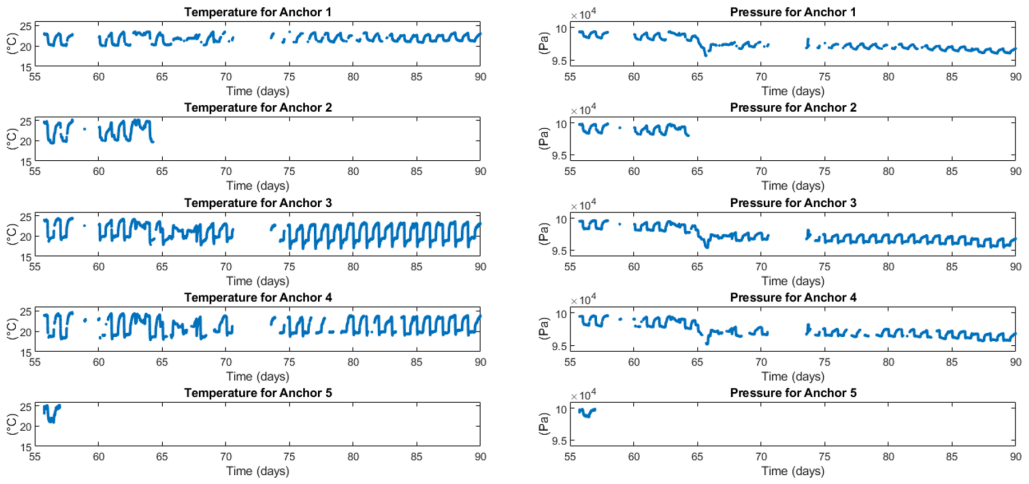

FIGURE 6.24: Temperature and pressure measured during Sensing Mode

behaves almost the same for all the Motes, although some positions do tend to vary in a higher range more than others. This can be explained by the different locations and the experiments running near them, as they dissipate heat which can have a local effect on the overall temperature fluctuations. During the day working hours, a temperature of 24 °C was measured, whereby it is interesting to note that the temperature drops to 17 °C during the night. This also correlates with the recorded pressure data, which fluctuates depending on the temperature. Furthermore, a long-term drift in pressure can be observed in the collected data. This trend is evident from the continuous data collection over the period under investigation. The detailed results are presented in Table 6.5.

TABLE 6.4: Min, Max, and Mean values for Temperature, Pressure, and Light Intensity

	Temperature (°C)	Pressure (Pa)	Light Intensity (Lux)
Anchor Mote 1			
Min	20.0	95630	0.0
Max	23.4	99390	10.0
Mean	21.8	97237	2.2
Anchor Mote 2			
Min	19.4	97978	0.0
Max	25.2	99882	195.0
Mean	22.6	99065	102.5
Anchor Mote 3			
Min	16.9	95361	0.0
Max	24.5	99672	191.0
Mean	20.9	96990	72.1
Anchor Mote 4			
Min	17.9	95151	0.0
Max	24.6	99612	304.0
Mean	21.2	97126	138.2
Anchor Mote 5			
Min	20.9	98615	0.0
Max	25.2	99863	41.0
Mean	23.3	99347	27.2

Data was also collected from the accelerometer and gyroscope. Calibration of the sensors on ground in a laboratory environment has shown that all sensors are biased. This bias is minimal for the accelerometers but more pronounced for the gyroscopes. As mentioned in the data sheet, a temperature sensitivity was observed, especially for the gyroscopes. Long-term drift of the gyroscope values was not observed. This is due to the operational concept in this test, similar to the ISS operation, where the Anchor Motes are switched off after a short data acquisition phase and reactivated after 30 seconds for the next measurement.

Figure 6.25 shows the calibration measurements of Anchor Mote 3, demonstrating the temperature sensitivity and the different offsets of the zero-level. The z-axis, also known

as the yaw axis, is the most sensitive.

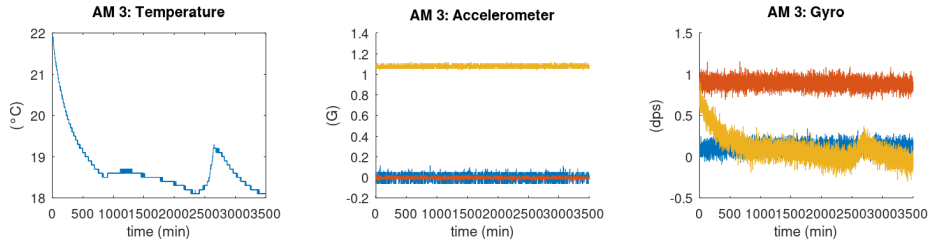

FIGURE 6.25: Calibration measurement for Anchor Mote 3 on ground

The detailed results of the calibration campaign are documented in Appendix B. By correcting the offsets on the ISS, it was found, as expected, that the acceleration data for all Anchor Motes were close to zero, as shown in the Table 6.5.

TABLE 6.5: Mean and standard deviation σ for Gyroscope and Accelerometer

	Gyroscope (G)			Accelerometer (dps)		
	X-axis	Y-axis	Z-axis	X-axis	Y-axis	Z-axis
Anchor Mote 1						
Mean	0.04	-0.34	-0.07	0.00	-0.01	0.00
σ	0.19	0.24	0.07	0.01	0.01	0.01
Anchor Mote 2						
Mean	1.54	-0.93	-0.96	-0.01	0.00	0.02
σ	0.47	0.39	0.26	0.01	0.01	0.01
Anchor Mote 3						
Mean	-0.18	-0.22	-0.27	-0.01	0.00	-0.01
σ	0.09	0.13	0.34	0.04	0.01	0.01
Anchor Mote 4						
Mean	-1.22	-1.96	-0.88	-0.00	0.01	-0.02
σ	0.39	0.36	0.25	0.01	0.01	0.01
Anchor Mote 5						
Mean	-0.95	-0.10	-0.50	-0.00	-0.00	-0.01
σ	0.20	0.77	0.20	0.03	0.01	0.02

This indicates that the motes maintained their position and therefore only micro-gravity was measured in all axes. Analysis of the gyroscope data shows that the data is still biased in all three axes. This is because the gyroscope was calibrated to a maximum temperature of 22 °C, whereas the temperature on the ISS can reach 25 °C, causing a slight offset from zero. Although the data show a bias, there is no constant drift over time. This is again due to the fact that the ON phase lasts a maximum of 100 ms before the gyro is turned off for 30 seconds. However, a slight cyclic variation was observed from Anchor Mote 3 as can be seen in Figure 6.26, where the data is low-pass filtered to eliminate noise and aliasing effects. This correlates with the daily working cycle, as was also observed in the temperature data. As the gyroscope data is temperature sensitive, this variation can be explained by the fact that AM3 was exposed to the

greatest variation in temperature (up to 7 °C) compared to Anchor Mote 1 with lowest. This correlates well with the observed results as shown in the Figure 6.26.

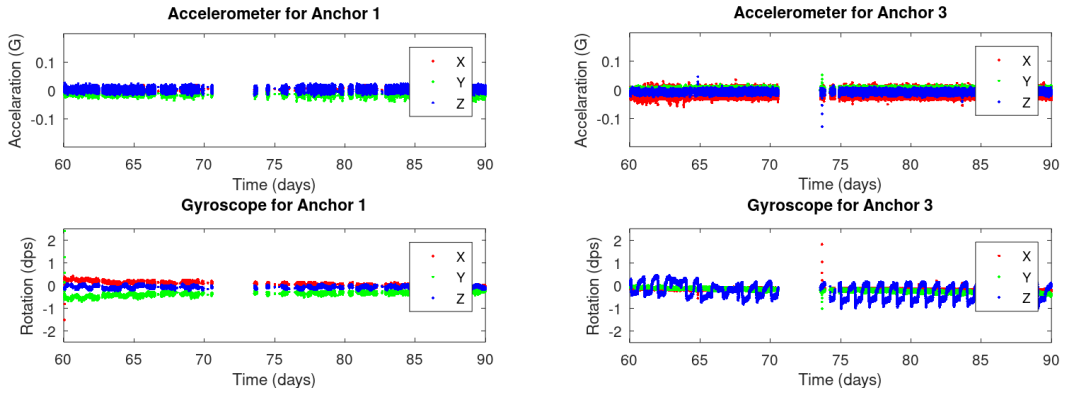

(A) Anchor Mote 1 (B) Anchor Mote 3

FIGURE 6.26: Low-pass filtered results for gyroscope and accelaration

As conclusion, the analysis of the presented data demonstrates the feasibility of environmental monitoring with low-cost MEMS sensors and an IR-UWB based wireless network on the International Space Station. Depending on their application field and the performance requirements, the sensors might need further calibration, or more precise (high-quality) sensors might have to be employed.

6.5.3 Tracking

The results presented here were obtained during Tracking Sessions that were conducted in collaboration with astronaut Alexander Gerst. During the sessions, he wore two Tracking Motes, one on his right arm and one on his left ankle, to monitor his movements. These Tracking Sessions provided an environment to evaluate the positioning capabilities under the specific conditions. For the further analysis, data from Tracking Session 1 were used, as in Tracking Session 2 the astronaut was only partially in the Field of View of the camera and in Tracking Session 3 the camera was not activated.

6.5.3.1 Static positioning

In Tracking Session 1, the astronaut mostly remained in a static position, interacting on his working station, which allowed a visual verification of the almost static position (see Figure 6.27).

Both TMs were also equipped with an accelerometer and a gyroscope in order to collect additional parameters for the later analysis. The raw data from Tracking Session 1 for these two sensors are shown in Figure 6.28.

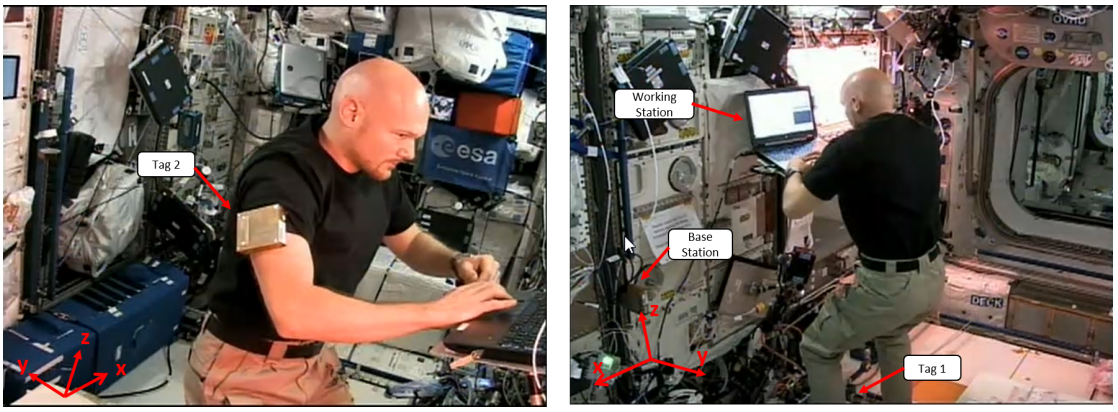

FIGURE 6.27: Almost static position 1 during Tracking Session 1 (Source: ESA)

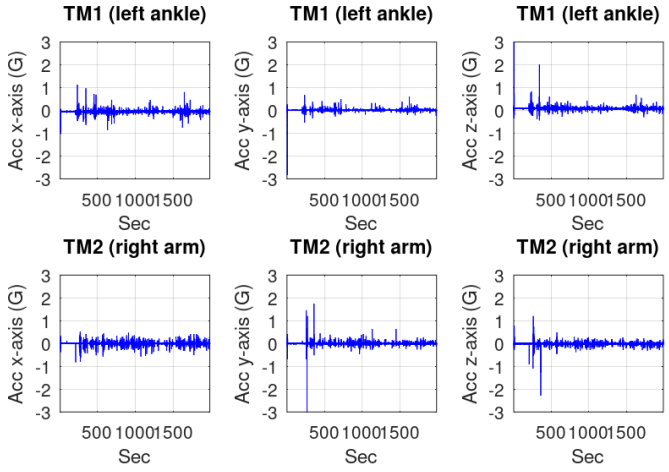

(A) Acceleration during Tracking Session 1

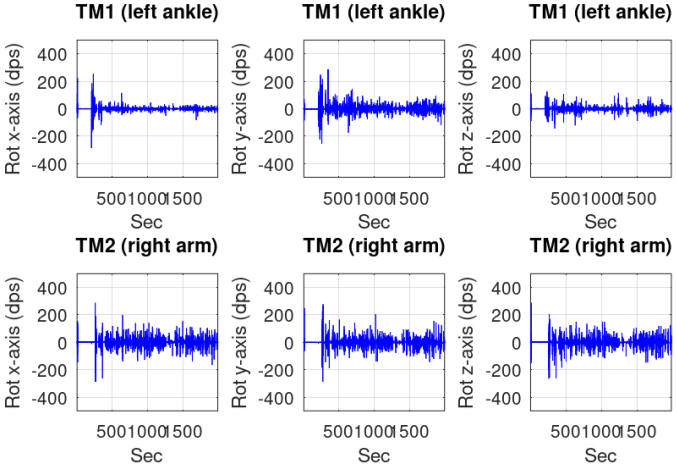

(B) Rotation during Tracking Session 1

FIGURE 6.28: Acceleration and Rotation raw values in Tracking Session 1

At the start of the session, both Tag Motes were initially placed on a box, resulting in a very calm phase in the recording. This phase, which lasted a few minutes, was used to perform an in-orbit calibration to determine the variance and the zero-level offset as

measured in Table 6.6.

TABLE 6.6: Mean and standard deviation of accelerometer and gyro data

	Gyroscope (G)			Accelerometer (dps)		
	X-axis	Y-axis	Z-axis	X-axis	Y-axis	Z-axis
Tag Mote 1						
Mean	-0.2765	-1.0248	-0.2918	-0.0507	0.005	0.0937
σ	0.0293	0.0282	0.0397	0.00016	0.00008	0.00017
Tag Mote 2						
Mean	1.0269	0.6212	-1.0556	0.0051	-0.0040	-0.0073
σ	0.0149	0.0251	0.0228	0.00010	0.00008	0.00015

Afterwards, the data were first low-pass filtered to eliminate noise and aliasing effects, and the gyro data were processed with a high-pass filter to remove the long-term drifts observed in the gyros, see Appendix B. The correction also included the elimination of the zero-level offset. An example of the drift and the corrected data for Tag Mote 2 Z-axis is shown in Figure 6.29.

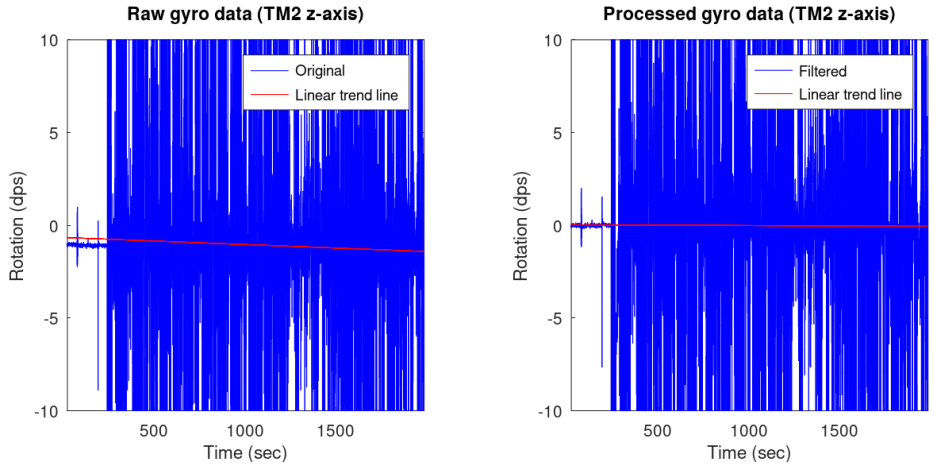

FIGURE 6.29: TM2 z-Axis gyro data uncorrected and corrected

Over the course of the session, significant differences in the motion activity of the arm and leg became apparent, with the arm showing significantly more movement, as indicated by the accelerometer and gyroscope data in Figure 6.28.

This pattern of movement was due to the astronaut's working activities, mainly with his hands at his working station (notebook) and performing location-focused experiments with his arms during the session that could be confirmed by the video footage recorded during the session. This consistency allowed for a reliable verification of the static position 1 and was particularly evident in the distance data to all five AMs and the BS over a period of 30 minutes as illustrated in Figure 6.30. For completeness, distance measurements of Tracking Session two and three can be found in Appendix B.

Specifically indicating that the astronaut maintained a relatively constant position, the ranging measurements to the Anchor Motes and the Base Station showed little change

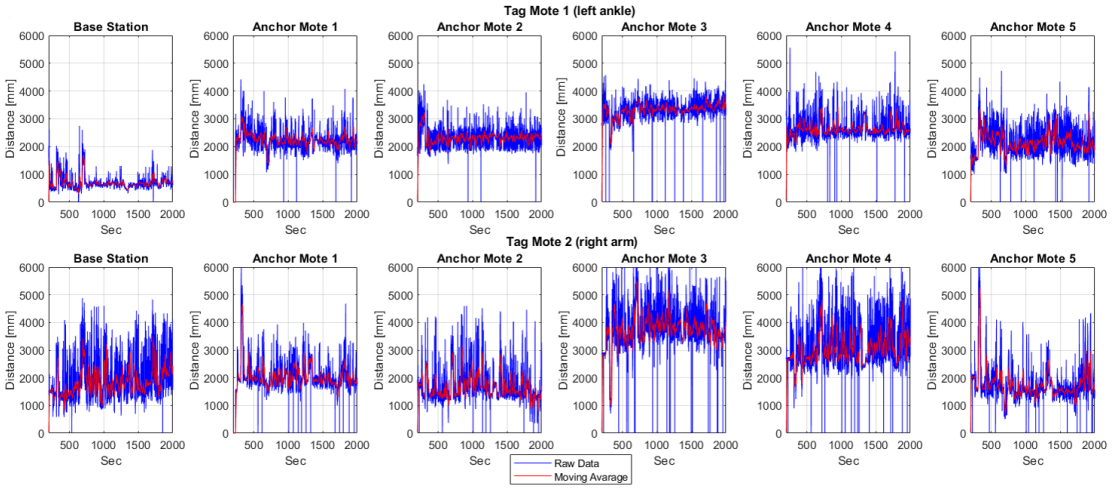

FIGURE 6.30: Ranging data from all Motes to TMs 1 and 2 during Tracking Session 1

throughout the session. A notable observation was the occurrence of a few outliers in the data, where zero values are an indication of data loss. These packets were lost, since no re-transmission scheme was implemented.

It can be noted that these dropouts and the increased noise in the distance measurements primarily occurred with the TM 2 on the right arm, especially in conjunction with AMs 3 and 4 and a plausible explanation for this observation is the TM's position relative to the AMs. As AMs 3 and 4 were positioned on the astronaut's left side, shadowing by the astronaut's body with non line of sight with these AMs, which led to a poorer signal quality.

However, this could be addressed by operating two additional Anchor Motes (Anchor Mote 5 and Base Station) in order to achieve an over-determined system and to compensate for the inaccuracies caused by the Motes in hard NLoS or obstructed LoS conditions with the WLS method. It emphasises the significance and advantages of implementing redundant AMs in environments like the ISS, where LoS conditions cannot always be assured, to enhance overall accuracy.

Further analysis focused on specific positioning periods in which the astronaut made no to minimal movements and a position was held for 20 sec or longer. As a result, four different positions were identified in Tracking Session 1. In total, 80 single trilateration values were obtained during a period of 20 sec. Subsequently, the resulting position data was visually compared with the video. As the next Figures show, they were in good agreement with the positions of the astronaut's Tag Motes in the video footage.

Position 1 as shown in Figure 6.27 was firstly analysed in which the astronaut stayed for a longer duration because he was performing tasks at his working station. When calculating the trilateration, a deviation of the data points is visible which is higher on the astronaut's ankle than on his arm, as shown in Figure 6.31.

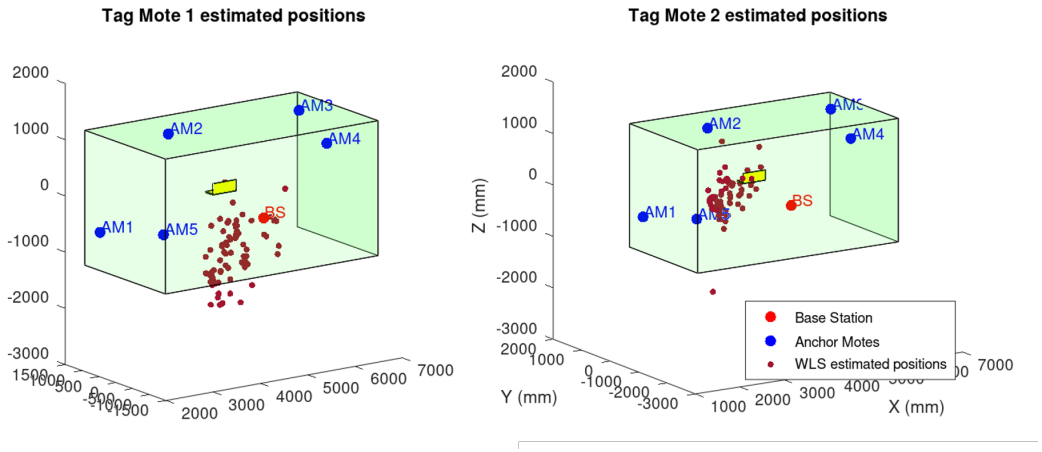

FIGURE 6.31: Trilateration results for TM1 and TM2 for position 1

However, by averaging 80 values over 20 sec, it was possible to determine a mean position during the analysed period. The calculated mean positions for Tag Motes 1 and 2 in Figure 6.32 correspond to the positions in the image in Figure 6.31 and the Tag Motes in Figure 6.32 are also connected by a red line to illustrate the distance between them.

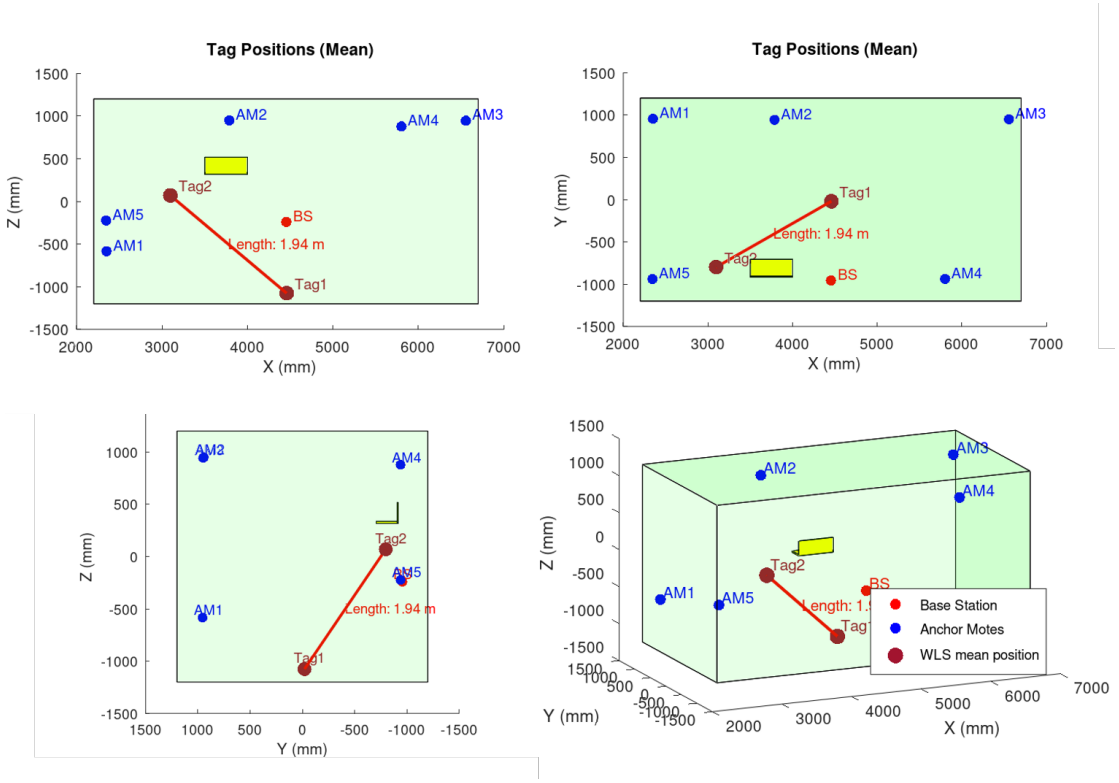

FIGURE 6.32: Trilateration results for the mean position 1

Although the astronaut remained in rather one place in front of his working station during his session, three other positions that he took for more than 20 sec were analysed. The results of these analyses are shown in the Figures 6.33 to 6.35 which visually align

with the actual positions in the video footage. More detailed Figures for these positions including the WLS position estimates are outlined in Appendix B.

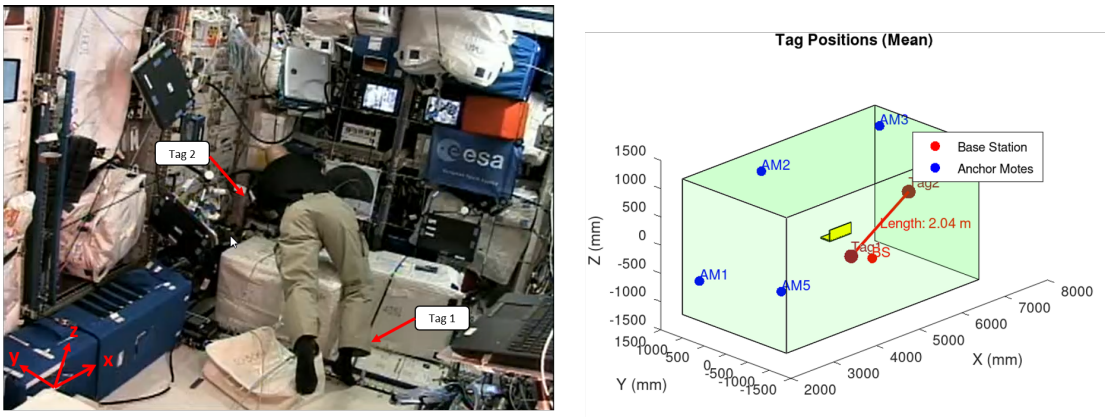

FIGURE 6.33: Trilateration results for the mean position 2
(Left image source: ESA)

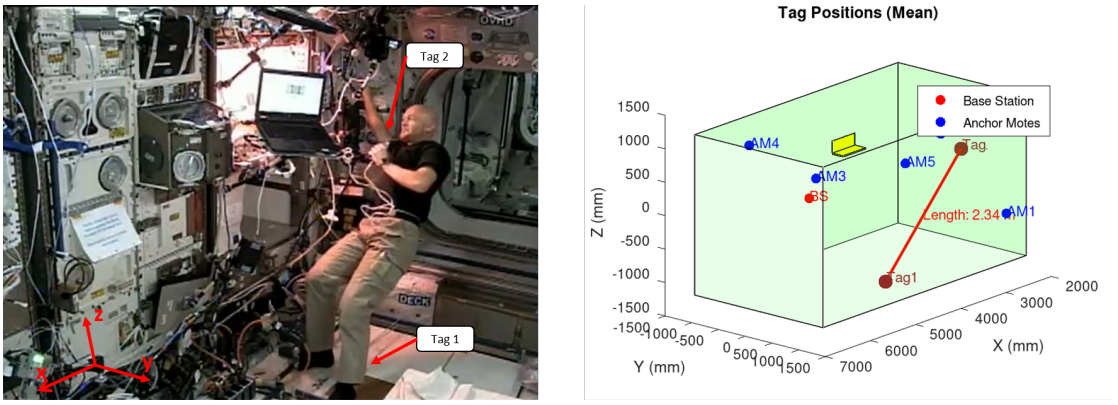

FIGURE 6.34: Trilateration results for the mean position 3
(Left image source: ESA)

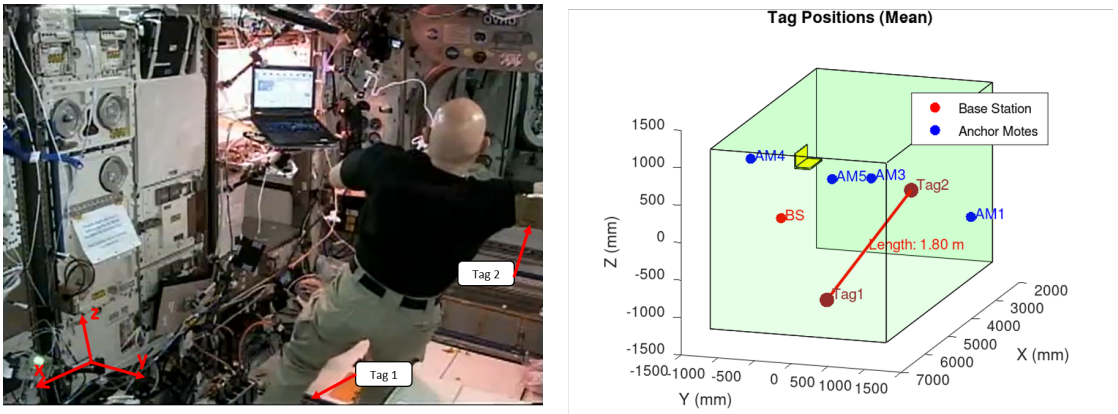

FIGURE 6.35: Trilateration results for the mean position 4
(Left image source: ESA)

It can be concluded that suitable results are obtained for positions that remain almost unchanged for 20 sec or longer whereas for shorter periods, the mean position becomes

less accurate, as can be seen in Figure 6.36 in which the mean position 4 is shown for all axes for an increasing number of samples. It can be seen that a meaningful result can only be expected from a number of approximately 60 values, which corresponds to approximately 15 sec. This especially applies if the distance measurements are noisy (which is to be expected with obstructed LoS conditions, when the body of the astronaut shadows the Tag Mote). However, increasing the sampling rate is one option how to mitigate it in future.

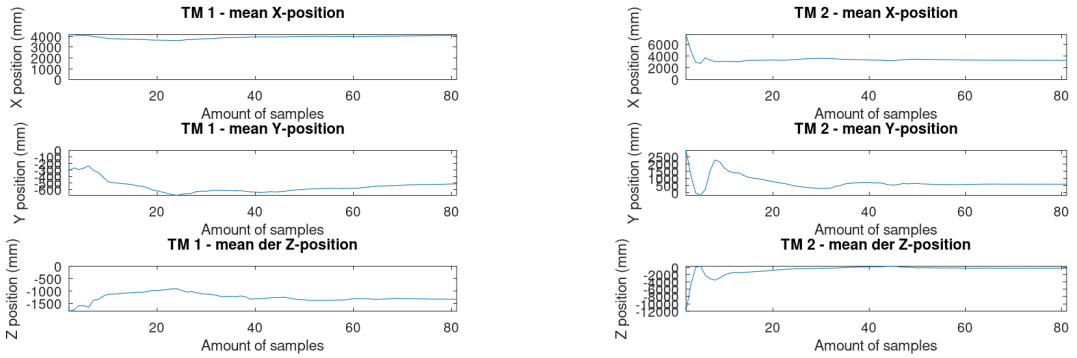

(A) Acceleration during Tracking Session 1

(B) Rotation during Tracking Session 1

FIGURE 6.36: Acceleration and Rotation raw values in Tracking Session 1

Table 6.7 summarises the results and the exact positions of the TMs.

TABLE 6.7: WLS algorithm results for the mean estimated positions for 20 sec

	Start Time (UTC)	TM1 mean posistion			TM2 mean position			Distance TM1 - TM2
		x (mm)	y (mm)	z (mm)	x (mm)	y (mm)	z (mm)	(m)
Pos1	14:12:18	4458	-19	-1076	3096	-797	69	1.94
Pos2	14:13:00	5347	410	-860	7249	956	-391	2.03
Pos3	14:18:49	3829	-35	-1488	2019	-54	-64	2.30
Pos4	14:38:10	4122	-435	-1440	3402	544	-220	1.72

Since the actual position, also known as the ground truth, is not precisely known and can only be estimated from the visible video footage, it was not possible to determine the RMSE statistically. However, even though the data's correctness could only be validated qualitatively, the precision of the different position estimations is summarized in 6.8. It can be demonstrated that positioning is feasible, however, the results show a significantly greater deviation compared to the mock-up measurements outlined in Table 5.5. This discrepancy can be attributed to several factors. Firstly, the mock-up measurements were conducted under almost line-of-sight conditions, with the object fixed on a tripod and no human presence in the Mock-Up during measurements. Such conditions are not replicable in the working environment of the Columbus module in orbit. In this setting, a clear line-of-sight is not always possible for all motes. In a dynamic environment

with astronauts, LoS conditions are frequently compromised by factors such as body occlusions and physical obstacles, including storage boxes and extended experiments.

TABLE 6.8: Standard and maximum deviation for positions 1 - 4 and TM 1 & 2

	Tag Mote 1			Tag Mote 2		
	X-axis (mm)	Y-axis (mm)	Z-axis (mm)	X-axis (mm)	Y-axis (mm)	Z-axis (mm)
Position 1						
σ	246.23	326.39	540.47	599.44	712.81	476.19
max σ	531.04	1187.6	1367.6	1476.4	2079.1	2281.2
Position 2						
Std	298.97	196.96	433.95	479.35	562.91	957.92
max σ	1209.8	431.07	1519.3	1453.9	2751.1	2356.6
Position 3						
Std	337.54	405.64	674.59	917.24	845.68	1916.9
max σ	1071.4	1159.9	1559.8	2063.8	2338.7	4756.5
Position 4						
Std	358.40	312.96	632.69	902.25	619.84	1666.3
max σ.	816.15	1053.2	1616.1	1854.5	2272.7	5192.0

Another critical factor contributing to the increased deviation is the constant movement of the body. Although an astronaut may remain almost static over a 20 sec period, there is continuous arm movement due to tasks such as working on a laptop or performing other actions. The data shows a greater deviation in the arm compared to the leg, which tends to move less, as the astronaut primarily uses arms for tasks. However, a constant relative movement is also present in the leg, due to the astronaut being in zero-gravity conditions. This is further supported by accelerometer and gyroscope data, as illustrated in Figure 6.28.

Consequently, a larger set of measurement points is required for accurate positioning. Despite these challenges, the system's ability to determine a static position has been successfully verified.

6.5.3.2 Motion tracking

In this subsection, the motion tracking with the Extended Kalman Filter, which was used for the trajectory calculation in Section 5.2.2.2, is analysed. It also examines how the tag's IMU data can be used to extend the Kalman filter through sensor fusion in order to obtain more accurate trajectory resolution. As the astronaut maintains a relatively static position throughout the session, only one video sequence was identified for this analysis. Two static positions presented in Figure 6.27 and Figure 6.33 within this motion sequence have already been analysed. The entire flight sequence is shown in Figure 6.37.

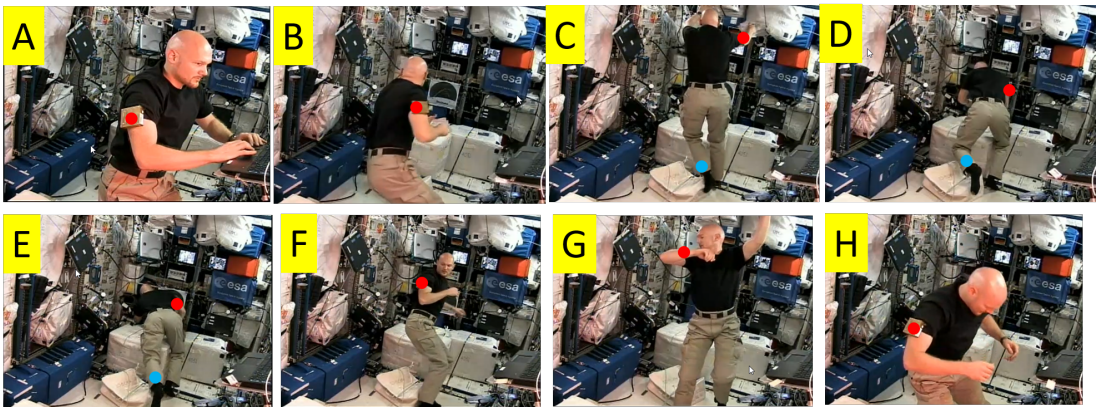

FIGURE 6.37: Entire flight sequence considered for motion tracking with TM1 (blue) and TM2 (red) (Source: ESA)

The first step is to apply the EKF with UWB data only. For this purpose, the process noise covariance matrix **Q** was estimated using the approach outlined in Equation 5.16, which has been determined to be the best fit. The measurement noise covariance matrix **R** was calculated from the error variance of the UWB range measurements. Figure 6.37 provides the trajectory as a red solid line with the smoothed position estimates using EKF, illustrating the data from both Tag Mote 1 and Tag Mote 2. It also demonstrates the benefits of the Kalman filter by showing brown dots as position estimates from the WLS algorithm.

The flight paths of the two tags are in good agreement with the visual observations from the video. However, it is not possible to directly compare the calculated trajectory or calculate an RMSE without a ground truth path. Nevertheless, by superimposing it on the visual data, it can be confirmed that the direction of the trajectory is well captured and that the distinct snapshots A to F of Figure 6.37 are well represented. This allows an approximate localisation of the astronaut's arm or leg positions, which helps in the identification of the body orientation relative to the station and the determination of the work zone.

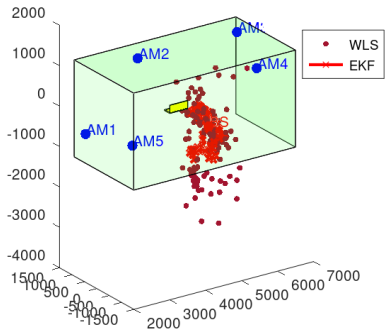

(A) Transmitter/ Anchor Mote 1 at Position 1

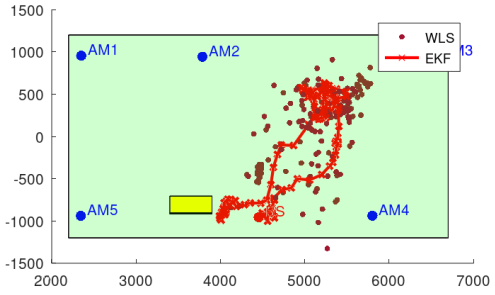

(B) Receiver/Base Station Development Model

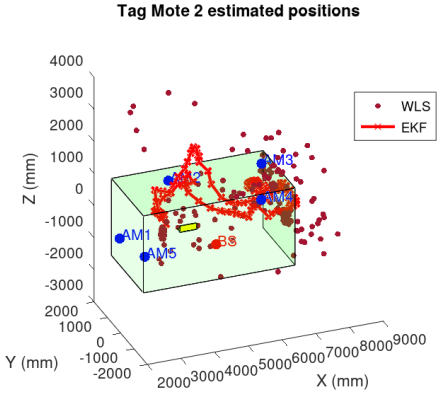

(C) Receiver/Base Station Development Model

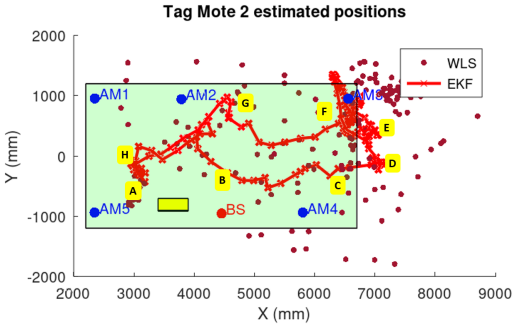

(D) Receiver/Base Station Development Model

FIGURE 6.38: Tested positions during the Columbus mock-up test campaign

This information can be used to create rough activity profiles to verify which quadrants of the module the astronaut was in at any given time and which experiments were being performed. However, some discrepancies with the actual trajectory are evident. For example, in snapshot F, the astronaut leaves the green working area with the Tag Mote 2.

The next step is to improve the model through sensor fusion using the IMU data of Tag Mote 1 and 2, which include acceleration and gyroscope values. Before sensor fusion can be performed, the IMU data from the astronaut's Tag Motes must be transformed into the Columbus module's coordinate system. Due to the zero-gravity environment and the associated lack of reference in the acceleration data, the use of a complementary filter to process the IMU data is precluded. Instead, gyroscope data is integrated separately to transform the acceleration data into the appropriate coordinate system.

A high pass filter is applied after data integration and the bias offset is subtracted to correct for the inherent long term drift of the gyroscope. The acceleration data are transformed from the IMU inertial frame to the Columbus module global frame, that is used for positioning. See Figure 6.39 for the different frames to be considered in this transformation process.

FIGURE 6.39: Tag Mote inertial frame (red) and Columbus global frame (yellow)

A rotation matrix $C(t)$ is used to represent the orientation to each other. The acceleration in the global frame is represented by the vector $\mathbf{a}_g(t) = (a_{g,x}(t), a_{g,y}(t), a_{g,z}(t))^T$ and in the IMU's inertial frame by $\mathbf{a}_{imu}(t) = (a_{imu,x}(t), a_{imu,y}(t), a_{imu,z}(t))^T$. The transformation can be thus be calculated using the next equation

$$\mathbf{a}_g(t) = C(t)\mathbf{a}_{imu}(t)$$

The initial rotation matrix C_{init} was set for Position 1, where a snapshot of the video sequence was chosen that approximately matches these angles.

$$C_{init} = \begin{bmatrix} 0 & 0 & 1 \\ -1 & 0 & 0 \\ 0 & -1 & 0 \end{bmatrix}$$

The next step involves processing the data, including converting the gyroscope data into Euler angles γ (Roll), θ (Pitch) und ψ (Yaw). These are then integrated over the time interval. The angles can be calculated with the following expressions:

$$\begin{aligned} \gamma &= \text{atan2}(C_{32}, C_{33}) \\ \theta &= \text{atan2}(-C_{31}, \sqrt{C_{32}^2 + C_{33}^2}) \\ \psi &= \text{atan2}(C_{21}, C_{11}) \end{aligned}$$

where C_{ij} are the elements of the rotation matrix. These angles describe the rotations around the axes of the inertial frame, enabling the construction of a rotation matrix that is constantly adjusted via integration:

$$C = \begin{bmatrix} \cos\psi\cos\theta & \cos\psi\sin\theta\sin\gamma - \sin\psi\cos\gamma & \cos\psi\sin\theta\cos\gamma + \sin\psi\sin\gamma \\ \sin\psi\cos\theta & \sin\psi\sin\theta\sin\gamma + \cos\psi\cos\gamma & \sin\psi\sin\theta\cos\gamma - \cos\psi\sin\gamma \\ -\sin\theta & \cos\theta\sin\gamma & \cos\theta\cos\gamma \end{bmatrix}$$

The acceleration data is transformed to the Columbus module coordinate system using this rotation matrix. Both the raw and transformed data for the x, y and z axes are shown in Figure 6.40.

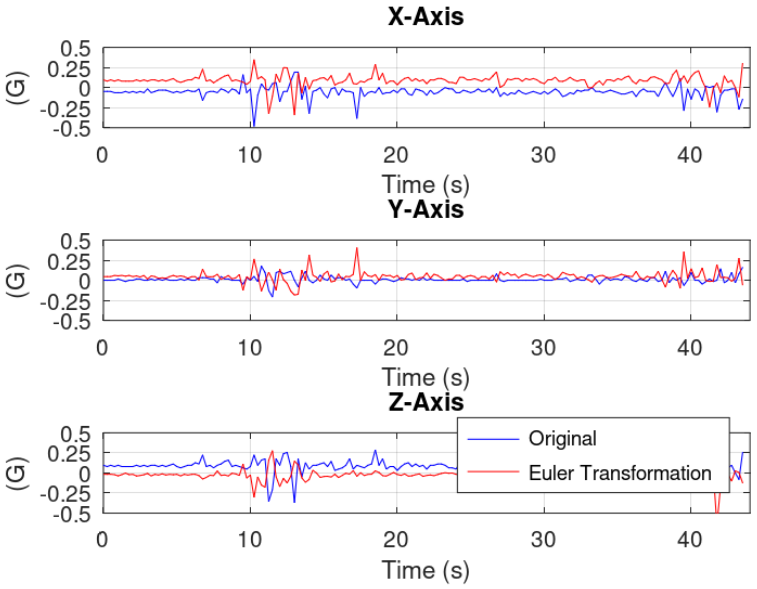

FIGURE 6.40: Tag Mote inertial frame (red) and Columbus global frame (yellow)

The transformed acceleration data is then fused with the UWB position data according to (136, pp. 8). This means that the measurement vector z_k is expanded to include the acceleration values for the X, Y, and Z axes. Similarly, the H matrix at time k, which is derived from the Jacobian matrix, is also expanded to incorporate the accelerometer dynamics. The measurement noise now encompasses not only the noise from the UWB measurements but also from the accelerometer measurements on the X, Y, and Z axes with

$$R = \begin{bmatrix} \sigma_{px}^2 & 0 & 0 & 0 & 0 & 0 \\ 0 & \sigma_{py}^2 & 0 & 0 & 0 & 0 \\ 0 & 0 & \sigma_{pz}^2 & 0 & 0 & 0 \\ 0 & 0 & 0 & \sigma_{ax}^2 & 0 & 0 \\ 0 & 0 & 0 & 0 & \sigma_{ay}^2 & 0 \\ 0 & 0 & 0 & 0 & 0 & \sigma_{az}^2 \end{bmatrix}$$

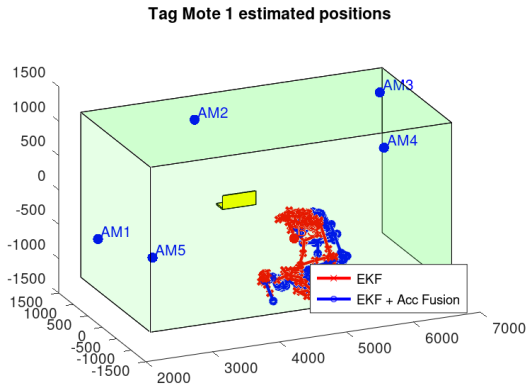

(A) Transmitter/ Anchor Mote 1 at Position 1

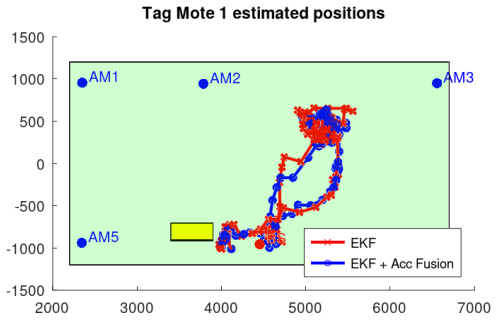

(B) Receiver/Base Station Development Model

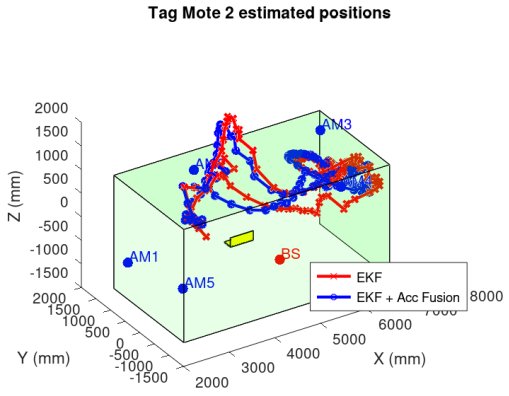

(C) Receiver/Base Station Development Model

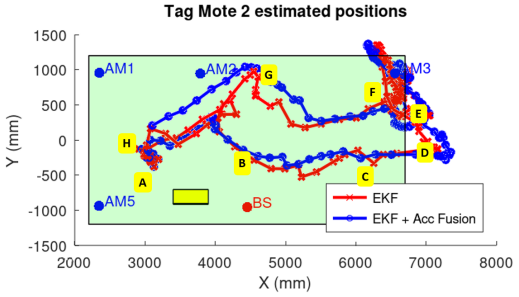

(D) Receiver/Base Station Development Model

FIGURE 6.41: Tested positions during the Columbus mock-up test campaign

This approach allows for a more accurate estimation of the position and orientation of the Tag Mote as demonstrated in Figure 6.41. This figure shows both trajectories: one red solid line as smoothed position estimates from EKF using only position data and one blue solid line from EKF with sensor fusion. The blue trajectory appears smoother, which corresponds more closely to the flight path of the astronaut. Additionally, the height (Z axis resolution) is better captured, both to the snapshot in Figure 6.37 D and from then to the snapshot in Figure 6.37 F. Thus, the integration of the accelerometer once again offers an improvement in motion tracking compared to the UWB only EKF. Also here, unfortunately, no final RMSE can be calculated here either, as the ground truth is only captured visually and can therefore only be assessed qualitatively. However, also here the visual data is sufficient for a qualitative assessment of the results.

In summary, despite these limitations, the IR-UWB-based system used can provide valuable information about the activity, position, and motion patterns of an astronaut. It was also shown to be able to determine positions and motion tracks within the Columbus module which offers a promising way to improve the efficiency and safety of astronauts activities in dedicated working zones on the ISS and it could also help to further optimise workflows and activity patterns.

6.6 Summary

This Chapter provided an overview of the Wireless Compose experiment, which was conducted as a technology demonstration on the ISS in the Columbus module. The experiment focus included the design and implementation of an IR-UWB based wireless network, that was covered in this thesis. Also, the technical details of the hard- and software implemented, as well as the collected results, were discussed.

The Wireless Compose experiment was part of the Alexander Gerst Horizon mission and was conducted during the ISS increment 56/57 in 2018. Based on the technological concept presented in Chapter 4, the experiment demonstrated the exploitation of an in-orbit operated wireless network with the aim of evaluating future positioning and environmental monitoring applications using the proposed IR-UWB-based wireless network architecture. A reduced form of the LLDN approach could be implemented despite the time constraints and strict mission requirements. The simplified system implementation, which integrates the essential functions of the LLDN approach, proved to be feasible and could serve as a model for future technology experiments. Two operational modes, Sensing and Tracking, were integrated into the software and each mode used different approaches to MAC management. The operational modes allowed for a detailed study of the behaviour of the network under different operational conditions while the data collected facilitated the analysis of network performance and provided insight into the system's positioning and environmental monitoring capabilities.

The experimental results showed high performance of the Wireless Compose network. A total of 293875 messages were received during the different modes and the Packet Delivery Rate was close to 100% for all Motes, which is consistent with the RSSI measurements for the specific data rates. Analysis of the data verified that environmental monitoring is feasible with the IR-UWB-based sensor network and it demonstrates the robustness of the protocol architecture used under the harsh conditions in space.

Investigating LoS conditions and their impact on measurement accuracy showed that positioning accuracy is strongly dependent on the environmental conditions. In spite of the limitations, the IR-UWB-based system was able to provide valuable information on the activity, position, and motion patterns of the astronaut and it was shown to be able to determine accurate positions and trajectories inside the Columbus module. Thus, it is a promising way to potentially improve the efficiency and further optimise future manned in-orbit workflows.

Overall, the feasibility and potential of an IR-UWB-based network for positioning and environmental monitoring applications was successfully demonstrated by the Wireless Compose experiment. It not only demonstrated the technical feasibility of the concepts

developed in this thesis but also provided valuable data for the future development of in-orbit localisation and sensing systems.

Chapter 7

Discussion and outlook

The final Chapter of this dissertation provides an in-depth evaluation of the research results. After a detailed consideration of the various aspects of wireless networks in space systems, a structured summary and discussion of the results is provided, together with an outlook concerning possible future research directions and application areas.

The main focus initially is on summarising the main findings of the research. This includes a review of the wireless network developed and implemented during the thesis, highlighting its successful verification and demonstration in a space environment.

Following this, there is an in-depth analysis of the results. This Section delves into the potential advantages and limitations of the wireless network architecture that was investigated. It explores how this architecture could be applied practically in future space missions.

The Chapter concludes with a forward-looking perspective, outlining potential future developments and demonstrations in this field. Based on the insights gained from this research, it identifies promising areas for further study and potential applications. The goal is to provide a pathway for future research, leading to the final establishment of this innovative architecture into space systems.

7.1 Summary

Looking back, it is clear that combining IR-UWB with the 802.15.4e LLDN MAC protocol has a huge potential for enhancing traditional wired communication systems on board spacecraft with a robust wireless alternative. The capability of IR-UWB to handle multipath propagation in the reflective environment of a satellite, alongside the deterministic, low-latency features of the 802.15.4e MAC, proved essential.

The developed architecture, including the LLDN protocol, demonstrated data robustness and positioning efficiency. It provided dependable communication across various conditions and fulfilled the demanding latency and throughput requirements common in space applications. While there were initial concerns about energy efficiency, these are addressable in future refinements, e.g. by using larger packet sizes.

The dissertation also addressed the technological challenges associated with IR-UWB in spacecraft, in particular electromagnetic compatibility, radiation exposure and robustness in multipath conditions. The results confirmed that our IR-UWB-based architecture can withstand these typical space challenges, making it a viable option for the harsh environment of space.

The Wireless Compose experiment and its results demonstrated that the wireless network implemented here was capable of providing robust communication in the real space environment. The network effectively performed positioning and environmental monitoring tasks on the ISS, demonstrating the dual utility of IR-UWB for both communication and positioning.

In conclusion, this research represents a significant step towards the establishment of a unified on board wireless network architecture. It provides valuable insights into the practicality and effectiveness of IR-UWB and the 802.15.4e LLDN protocol in space. While some challenges and issues remain for future research, the results provide a strong foundation for continued development in this area.

7.2 Discussion

The performance of IR-UWB-based network in space proved to be robust and powerful. Therefore, despite some limitations, the choice of an architecture based on IR-UWB technology and the IEEE 802.15.4e standard was a good one as both of them offer a good balance between performance and robustness, and are well-suited to meet the specific requirements of intra-spacecraft communications. Key findings from the Wireless Compose mission include the network's ability to deliver almost 100% of data packets correctly in the space system's reflective, multipath environment. Radiation tests confirmed the survivability of the equipment for a typical 10-year mission in Low Earth Orbit. However, the radiation susceptibility of the micro-controller, more so than the radio module, is a concern for the radiation reliability of the network, as radiation-induced failures can be expected.

A consideration of the benefits and limitations of the chosen technology in terms of electromagnetic compatibility was another critical point in the discussion, whereby the verification showed that the system's emissions are well below the limits and 100%

packet delivery was achieved. However, there are still some limitations that should not be ignored. For example, the interference tests indicated potential packet losses, particularly due to in-band interference, which could lead to degradation of network functionality. This highlights the need for further research into interference mitigation strategies, such as automatic channel switching.

Another significant limitation identified was the impact of environmental factors on the accuracy of positioning results. Conducting a calibration with known position data in-orbit would have been beneficial for fine-tuning the system. As it stands, validation was only possible qualitatively, using video evidence. A future system should also incorporate RF diagnostics to gather information on line-of-sight conditions. This would enable selective prioritisation and processing of Anchor Motes with more favorable conditions, potentially enhancing overall accuracy. Moreover, for more effective tracking, a higher sampling rate would be advantageous. This would allow for the movements to be captured with better resolution, thereby improving the overall accuracy of the system.

Scaling the system is another open issue. Although the wireless network was successfully demonstrated in the Wireless Compose experiment, larger networks or more complex scenarios may require adaptations such as more efficient protocols, changes in network topology, or hardware and software optimisation. Addressing high latency requirements will require system-wide adaptations, including micro-controller improvements. The balance between advanced processing capabilities and power efficiency remains critical. In addition, while the current system is suitable for the different space applications within the data rate limits of IR-UWB, high data rate applications may require alternative technologies such as Wi-Fi, if IR-UWB does not evolve towards higher data rates.

In addition, the absence of certain features, such as the discovery and configuration states of the LLDN MAC layer, also limits scalability. Furthermore, the analysis about the integration into various avionics architectures showed that onboard communication between various components is not well covered by LLDN in its original version, which instead works perfectly well with wireless sensor networks. Therefore, modifications need to be implemented regarding a more flexible way to communicate between components and subsystems. A flexible multi-protocol approach, combining different wireless technologies with the implemented wireless architecture and hardwired links, emerged as a holistic solution for different mission-specific requirements.

In conclusion, the current implementation, while promising, requires further enhancement and testing for scaling to larger networks and complex applications. Future work could focus on increasing system robustness, improving scalability and improving positioning accuracy in different environments.

7.3 Outlook

The research and experiments conducted have demonstrated that the implemented wireless network effectively enhances intra-spacecraft communication also by enabling new applications. However, there are still opportunities for optimization and further investigation to improve the system's performance and operational capabilities.

In terms of optimising the architecture and implementation, future studies could focus on improving energy efficiency and latency, with particular attention to optimising processor performance. Developing algorithms for dynamic adaptation of processor operation to network requirements could be a research focus. Another area is the development and deployment of advanced IR-UWB transceivers, especially those supporting 27 Mbps, to enhance performance and enable platform-independent architectures, facilitating industry-wide adoption.

Another important area for future research is the investigation of radiation resistance. Although this thesis demonstrated positive outcomes, a more comprehensive understanding of radiation impact is needed. This is in line with a current project initiated by this work, namely the development of a radiation-hardened IR-UWB transceiver, funded by ESA and currently in the implementation phase. Once completed, it will contribute significantly to adapting IR-UWB in space applications.

A further key aspect is the time synchronisation in wireless networks. This is of particular importance for many space applications. The challenge is to achieve time synchronisation between all systems, both wireless and wired. This can be particularly challenging in the context of multiple-protocol architectures because the interaction and coordination of different network topologies can make it a complex task. Designing robust and efficient time synchronisation mechanisms is essential for improving performance and reliability in space applications.

As part of this work, other applications were also defined that are yet to be demonstrated and which could provide further insights and optimisation possibilities. For example, it is planned to fly a wireless network based on this research with a full implementation of the LLDN on the PLUTO satellite, a nano satellite mission currently developed at the DLR Avionics Systems Department (137). Another EU-funded project called reuSable strAtegic space Launcher Technologies & Operations (SALTO) is currently investigating how the here developed IR-UWB based network can be used specifically in the field of reusable launch vehicles to read out critical sensor data or cameras (138). The same IR-UWB network will also be investigated and demonstrated for Moon and Mars habitat utilisation. The wireless network is planned to be used in the EDEN-LUNA experiment, a joint DLR-ESA ground demonstrator for future lunar habitats (139).

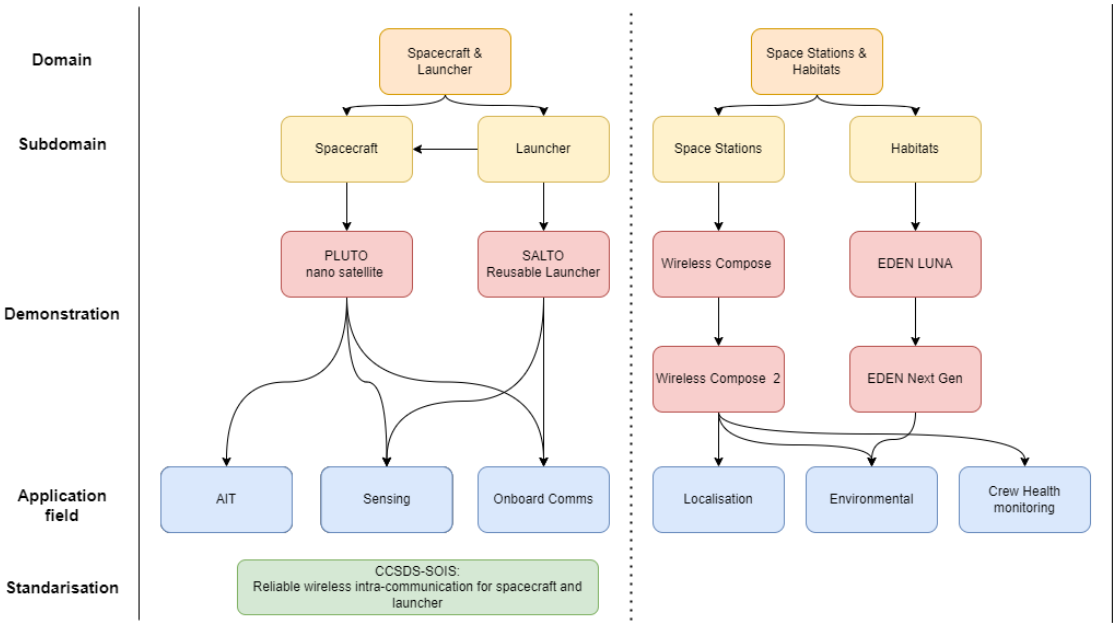

FIGURE 7.1: Overview of ongoing and future research activities

In addition, the knowledge gained from monitoring astronauts' motion patterns could help to improve operational efficiency and safety, and be linked to crew health monitoring, as was impressively demonstrated by the Wireless Compose-2 (WICO2) experiment, which is an more advanced version of the wireless network implemented in this dissertation (140). The follow-on WICO2 mission was implemented and operated as part of German astronaut Matthias Maurer's Cosmis Kiss mission. It included using more powerful processors and an advanced LLDN implementation, with a focus on crew health monitoring using the IR-UWB network. However, the evaluation of the results is still ongoing and future experiments should focus on practical implementation aspects and performance evaluation under diverse operating conditions. An overview of the different demonstration missions and the connection between the areas on the one hand, and the applications on the other hand, are illustrated in Figure 7.1. The outcome of this dissertation was the starting point for all the ongoing and planned research activities presented in this figure.

Another important step towards the establishment of the wireless network architecture will be the standardisation which will not only ensure a widespread adaption and visibility but also enhance the compatibility and interoperability with other systems. The knowledge and experience from this work are driving standardisation efforts within the CCSDS Wireless Working Group, where I am actively involved in standardising reliable wireless intra-communication for spacecraft and launchers based on IR-UWB (141).

The recommendations presented here will guide future research and development in this crucial field and there is no doubt that the continued improvement and development of a uniform wireless network architecture are vital for the success of future space missions.

Bibliography

[1] B. D. Yost, S. Weston, J. Hines, and C. Burkhard, *An Overview of the Current State of the Art on Small Spacecraft Avionics Systems.*

[2] R. Trautner, P. Armbruster, P. Fabry, A. Fernandez-Leon, J. Ilstad, D. Jameux, M. Suess, and R. Weigand, "Avionics Architectures and Components for Planetary Entry Probe Payloads and Systems," in *6th Int. Planetary Probe Workshop (IPPW6)*, 2008.

[3] Consultative Committee for Space Data Systems, *Wireless Network Communications Overview for Space Mission Operations, Report Concerning Space Data System Standards*, vol. CCSDS 880.0-G-3 of *Green Book*. Consultative Committee for Space Data Systems, issue 3 ed., May 2017.

[4] C. Zhang, X. He, D. Zhou, P. Zhan, Z. Qi, and Y. Xu, "Research on Wireless Networks for Intra-Spacecraft," in *Wireless and Satellite Systems* (M. Jia, Q. Guo, and W. Meng, eds.), (Cham), pp. 365–370, Springer International Publishing, 2019.

[5] T. Vladimirova, C. Bridges, G. Prassinos, X. Wu, K. Sidibeh, D. Barnhart, A.-H. Jallad, J. Paul, V. Lappas, A. Baker, K. Maynard, and R. Magness, "Characterising Wireless Sensor Motes for Space Applications," in *Second NASA/ESA Conference on Adaptive Hardware and Systems*, 08 2007.

[6] C. Plummer and P. Plancke, "Spacecraft Harness Reduction," in *Data Systems in Aerospace* (R. A. Harris, ed.), vol. 509 of *ESA Special Publication*, p. 57.1, July 2002.

[7] D. Turnes, "Reduction of the Harness - The One Interface Illusion - reloaded -," in *11th ESA Workshop on Avionics, Data, Control and Software Systems (ADCSS)*, ESA, October 2017. Accessed: 2020-06-04.

[8] D. Lacombe and L. Farhat, "Harness Reduction: Future Trends and Prospects," in *11th ESA Workshop on Avionics, Data, Control and Software Systems (ADCSS)*, ESA, October 2017. Accessed: 2020-06-04.

[9] C. Plummer and P. Plancke, "The Spacecraft Sensor Bus as a Means of Harness Reduction," in *DASIA 2003 - Data Systems In Aerospace*, vol. 532 of *ESA Special Publication*, p. 47.1, Jan. 2003.

[10] K. Spak, *Modeling Cable Harness Effects on Space Structures*. PhD thesis, Virginia Tech, 2014.

[11] G. F. Studor, "Fly-by-Wireless: A Revolution in Aerospace Vehicle Architecture for Instrumentation and Control," in *CANEUS "Fly-by-Wireless" Workshop*, 2007.

[12] Dayashankara, Hariharan, Rao, Rajan, and Bokil, "EMC Considerations in Spacecraft Harness Design," in *1997 Proceedings of International Symposium on Electromagnetic Compatibility*, pp. 239–242, 1997.

[13] S. Esposito and M. Violante, "Commercial Off-the-Shelf Components in Space Applications," in *Semiconductor Devices in Harsh Conditions*, pp. 25–42, CRC Press, 2016.

[14] R. Magness, *Wireless onboard spacecraft and in space exploration*. TEC-E wireless technology dossier, ESA-ESTEC, 2006.

[15] R. Amini, E. Gill, and G. Gaydadjiev, "The challenges of intra-spacecraft wireless data interfacing," in *International Astronautical Federation - 58th International Astronautical Congress 2007*, International Astronautical Federation, pp. 4020–4025, 12 2007.

[16] W. C. Wilson and G. Atkinson, "Wireless Sensors for Space Applications," *Sensors and Transducers*, vol. 13, pp. 1–9, 12 2011.

[17] W. H. Zheng and J. T. Armstrong, "Wireless intra-spacecraft communication: The benefits and the challenges," in *2010 NASA/ESA Conference on Adaptive Hardware and Systems*, pp. 75–78, 2010.

[18] S.-H. Yang, *Wireless Sensor Networks: Principles, Design and Applications*. Springer Publishing Company, Incorporated, 2013.

[19] R. Zurawski, *Industrial Communication Technology Handbook*. Industrial Information Technology, CRC Press, 2017.

[20] S. Zeadally, M. A. Javed, and E. B. Hamida, "Vehicular Communications for ITS: Standardization and Challenges," *IEEE Communications Standards Magazine*, vol. 4, no. 1, pp. 11–17, 2020.

[21] *Resolution 424 (WRC-15): Use of Wireless Avionics Intra-Communications in the frequency band 4 200-4 400 MHz*. Radio Regulations Resolutions and Recommendations Edition of 2016, ITU, 2016.

[22] National Research Council, "NASA Space Technology Roadmaps and Priorities: Restoring NASA039;s Technological Edge and Paving the Way for a New Era in Space," tech. rep., Washington, DC, 2012.

[23] S. Kottmeier, C. Fiona-Hobbie, F. Orlowski-Feldhusen, F. Nohka, T. Delovski, G. Morfill, L. Grillmayer, C. Philpot, and H. Mueller, "The Eu:Cropis Assembly, Integration and Verification Campaigns: Building the first DLR Compact Satellite," in *International Astronautical Congress (IAC2018)*, 09 2018.

[24] M. Malagoli and L. Cosquéric, *Space Harness Design Optimization Opportunities on ECSS derating rules.* ESA Space Passive Component Days Conference, 2013.

[25] C. Schiefelbein, *Entwurf einer drahtlosen Schnittstelle für die Onboard-Kommunikation am Beispiel des Kompaktsatelliten Eu:CROPIS.* Masterarbeit, Universität Bremen, Juli 2016.

[26] M. Drobczyk and H. Martens, "Deployment of a Wireless Sensor Network in Assembly, Integration and Test Activities," in *2016 IEEE International Conference on Wireless for Space and Extreme Environments (WiSEE)*, pp. 129–134, 2016.

[27] E. Puschita, O. Ratiu, M. Drobczyk, N. Panagiotopoulos, B. S. Kirei, S. Vos, V. Ratiu, T. Gärtner, A. Pastrav, and T. Palade, "A UWB Solution for Wireless Intra-Spacecraft Transmissions of Sensor and SpaceWire Data," *International Journal of Satellite Communications and Networking*, vol. 38, no. 1, pp. 41–61, 2020.

[28] A. Wedler, M. Hellerer, B. Rebele, H. Gmeiner, B. Vodermayer, T. Bellmann, S. Barthelmes, R. Rosta, C. Lange, L. Witte, N. Schmitz, M. Knapmeyer, A. Czeluschke, L. Thomsen, C. Waldmann, S. Flögel, M. Wilde, and Y. Takei, "ROBEX - Components and methods for the plantary exploration demonstration mission," in *13th Symposium on Advanced Space Technologies in Robotics and Automation (ASTRA)*, ASTRA, ESAWebsite, 2015.

[29] C. Philpot, M. Drobczyk, C. Strowik, and C. F. Düvel, "Wireless Compose - Communication and Positioning Network in ISS and Antarctic Greenhouse," in *2019 IEEE Wireless Communications and Networking Conference (WCNC)*, Oktober 2019.

[30] B. Grzesik, T. Baumann, T. Walter, F. Flederer, F. Sittner, E. Dilger, S. Gläsner, J.-L. Kirchler, M. Tedsen, S. Montenegro, and E. Stoll, "InnoCube—A Wireless Satellite Platform to Demonstrate Innovative Technologies," *Aerospace*, vol. 8, no. 5, 2021.

[31] L. für Informatik VIII, "SKITH - Skip The Harness." `http://s.dlr.de/uy0p5`, 2018. Accessed: 2023-07-02.

[32] N. Toth, F. Dannemann, S. Montenegro, T. Walter, and M. Faisal, "Wireless Avionics for a Solar Sailer (GOSSAMER-I)," in *DASIA 2012 - DAta Systems In Aerospace*, vol. 701 of *ESA Special Publication*, p. 36, Aug. 2012.

[33] R. Alena, S. R. Ellis, J. Hieronymus, and D. Maclise, "Wireless Avionics and Human Interfaces for Inflatable Spacecraft," in *2008 IEEE Aerospace Conference*, pp. 1–16, 2008.

[34] L. Chi, F. Sun, Z. Liu, and C. Lin, "Overview of Fractionated Spacecraft Technology," in *2020 International Conference on Computer Engineering and Application (ICCEA)*, pp. 689–692, 2020.

[35] L. Zhang, L. Wang, H. Yu, Y. Zong, Y. Zhang, X. Ming, and Z. Zhang, "Research on Wireless Power Transfer in Modular Spacecraft," in *2019 IEEE Wireless Power Transfer Conference (WPTC)*, pp. 470–474, 2019.

[36] S. U. Hwu, Y. Loh, and C. C. Sham, "Space Station Wireless Local Area Network Signal Characteristics Modeling and Measurements," in *2006 ieee/aiaa 25TH Digital Avionics Systems Conference*, pp. 1–8, 2006.

[37] J. H. C. Van Den Heuvel, J. Romme, J. F. Dufour, G. Dolmans, N. F. Kiyani, K. Philips, and H. De Groot, "UWB Radio Channel Characterization and Design for Intra Spacecraft Communication," in *IEEE International Conference on Communications*, 2013.

[38] P. Dallemagne, D. Piguet, J.-D. Decotignie, and D. Brunet, Y. Barras, "Ultra-wide Band based Real-time Communication System for Spacecrafts, Scientific and Technical Report," tech. rep., Centre Suisse d'Electronique et Microtechnique, 2014.

[39] P. Moravek and V. Stencel, "UWB Network Demonstrator for Space Applications," in *2014 IEEE International Conference on Wireless for Space and Extreme Environments (WiSEE)*, pp. 1–2, Oct 2014.

[40] M. Drobczyk and H. Martens, "A Study on Low-Latency Wireless Sensing in Time-Critical Satellite Applications," in *2016 IEEE Sensors*, pp. 1–3, 2016.

[41] A. Lübken, *MAC-Schicht Optimierung zur Nutzung eines auf UWB basierenden drahtlosen Kommunikationsnetzwerks innerhalb von Satelliten.* Masterarbeit, Universität Bremen, Juni 2018.

[42] M. Drobczyk and A. Lübken, "Novel Wireless Protocol Architecture for Intra-Spacecraft Wireless Sensor Networks (inspaWSN)," in *2018 6th IEEE International Conference on Wireless for Space and Extreme Environments (WiSEE)*, pp. 89–94, 2018.

[43] M. Drobczyk, M. Lehmann, and C. Strowik, "EMC Characterization of the UWB-based Wireless Positioning and Communication Experiment (Wireless Compose) for the ISS," in *2017 IEEE International Conference on Wireless for Space and Extreme Environments (WiSEE)*, pp. 57–62, 2017.

[44] M. Lehmann, *Entwicklung und EMV-Charakterisierung eines Funkmodul-Prototypen für Raumfahrtanwendungen.* Masterarbeit, Hochschule für Technik und Wirtschaft Dresden, April 2017.

[45] A. Lübken, M. Drobczyk, and J. Budroweit, "Characterization of an IR-UWB Transceiver Under Radiation Conditions," in *2020 IEEE International Conference on Wireless for Space and Extreme Environments (WiSEE)*, 2020.

[46] M. Drobczyk, S. C, and C. Philpot, "A Wireless Communication and Positioning Experiment for the ISS Based on IR-UWB," in *2017 IEEE Wireless Communications and Networking Conference (WCNC)*, pp. 1–6, 2017.

[47] M. Schwartz and AbramsonN., "The Alohanet - Surfing for Wireless Data [History of Communications]," *IEEE Communications Magazine*, vol. 47, no. 12, pp. 21–25, 2009.

[48] D. A. Gratton, *The Handbook of Personal Area Networking Technologies and Protocols.* Cambridge University Press, 2013.

[49] S. Farahani, *ZigBee Wireless Networks and Transceivers.* Elsevier Science, 2011.

[50] H. Zimmermann, "OSI Reference Model - The ISO Model of Architecture for Open Systems Interconnection," *IEEE Transactions on Communications*, vol. 28, no. 4, pp. 425–432, 1980.

[51] E. Perahia and R. Stacey, *Next Generation Wireless LANs: 802.11n and 802.11ac.* Cambridge University Press, 2 ed., 2013.

[52] M. S. Gast, *802.11 Wireless Networks - the Definitive Guide: Creating and Administering Wireless Networks: covers 802.11a, g, n and i (2nd ed.).* O'Reilly, 2005.

[53] W. Stallings, *Wireless Communications & Networks.* Pearson Education, 2009.

[54] B. Lee and S. Choi, *Broadband Wireless Access and Local Networks: Mobile WiMax and WiFi.* Artech House mobile communications series, Artech House, 2008.

[55] G. V., "Untangling IRDA and Bluetooth," *EDN Magazine*, pp. 57–62, 2001.

[56] R. Morrow, *Bluetooth: Operation and Use.* McGraw-Hill telecom professional, McGraw-Hill Education, 2002.

[57] SIG, *Bluetooth Specification Version 4.0 [Vol 2]*, 2009.

[58] A. S. Tanenbaum, *Computer Networks*. No. S. 3 in Computer Networks, Prentice Hall PTR, 2003.

[59] A. G. Ramonet and T. Noguchi, "IEEE 802.15.4 Historical Evolution and Trends," in *2019 21st International Conference on Advanced Communication Technology (ICACT)*, pp. 351–359, 2019.

[60] O. G. A., "A Survey of ZigBee Wireless Sensor Network Technology: Topology, Applications and Challenges," *International Journal of Computer Applications*, vol. 130, pp. 47–55, 2015.

[61] S. C. E., "ZigBee/IEEE 802.15.4 Summary," 2004.

[62] IEEE Computer Society, *IEEE Standard for Low-Rate Wireless Networks*, 2020. IEEE Std 802.15.4-2020.

[63] G. Anastasi, M. Conti, and M. Di Francesco, "A Comprehensive Analysis of the MAC Unreliability Problem in IEEE 802.15.4 Wireless Sensor Networks," *IEEE Transactions on Industrial Informatics*, vol. 7, no. 1, pp. 52–65, 2011.

[64] M. Anwar and Y. Xia, "IEEE 802.15.4e LLDN: Superframe Configuration for Networked Control Systems," in *Proceedings of the 33rd Chinese Control Conference*, pp. 5568–5573, 2014.

[65] N. Marcelo, M. D. Ivanovitch, and A. G. Luiz, "Routing and Scheduling Algorithms for WirelessHART Networks: A Survey," *Sensors*, vol. 15, pp. 9703 – 9740, 2015.

[66] I. Domuta, T. Palade, E. Puschita, O. Ratiu, and R. Arsinte, "ISA100.11a Capabilities for Intra-Spacecraft Communication," *Acta Technica Napocensis - Electronics andTelecommunications*, vol. 56, pp. 14–19, 06 2015.

[67] T. D. Chung, R. Ibrahim, V. S. Asirvadam, N. Saad, and S. M. Hassan, "Latency Analysis of WirelessHART Control Message with Variable Payload," in *2016 2nd IEEE International Symposium on Robotics and Manufacturing Automation (ROMA)*, pp. 1–5, 2016.

[68] E. Karapistoli, F.-N. Pavlidou, I. Gragopoulos, and I. Tsetsinas, "An overview of the IEEE 802.15.4a Standard," *IEEE Communications Magazine*, vol. 48, no. 1, pp. 47–53, 2010.

[69] J. Fernandes and D. Wentzloff, "Recent Advances in IR-UWB Transceivers: An Overview," pp. 3284–3287, 05 2010.

[70] V. Niemelä, J. Haapola, M. Hämäläinen, and J. Iinatti, "An Ultra Wideband Survey: Global Regulations and Impulse Radio Research Based on Standards," *IEEE Communications Surveys Tutorials*, vol. 19, no. 2, pp. 874–890, 2017.

[71] Z. Sahinoglu, S. Gezici, and I. Gvenc, *Ultra-wideband Positioning Systems: Theoretical Limits, Ranging Algorithms, and Protocols*. Cambridge University Press Assessment, 2008.

[72] D. d. Guglielmo, G. Anastasi, and A. Seghetti, "From IEEE 802.15.4 to IEEE 802.15.4e: A Step Towards the Internet of Things," in *Advances onto the Internet of Things* (S. Gaglio and G. L. Re, eds.), vol. 260 of *Advances in Intelligent Systems and Computing*, pp. 135–152, Springer, 2014.

[73] D. d. Guglielmo, S. Brienza, and G. Anastasi, "IEEE 802.15.4e: A survey," *Computer Communications*, vol. 88, pp. 1–24, 2016.

[74] L. Salomonsson, *Low Latency Wireless Sensor and Actuator Networks: Analysis of LLDN and RT-WiFi*. Bachelor thesis, 2018.

[75] G. Patti, G. Alderisi, and L. Lo Bello, "Introducing Multi-Level Communication in the IEEE 802.15. 4e Protocol: The MultiChannel-LLDN," 09 2014.

[76] B. Gladysz and K. Santarek, "An Approach to RTLS Selection," *DEStech Transactions on Engineering and Technology Research*, 2018.

[77] M. Strohmeier, T. Walter, J. Rothe, and S. Montenegro, "Ultra-Wideband Based Pose Estimation for Small Unmanned Aerial Vehicles," *IEEE Access*, vol. 6, pp. 57526–57535, 2018.

[78] H. Zhang, Z. Zhang, N. Gao, Y. Xiao, Z. Meng, and Z. Li, "Cost-Effective Wearable Indoor Localization and Motion Analysis via the Integration of UWB and IMU," *Sensors*, vol. 20, no. 2, 2020.

[79] Q. Zeng, *Wireless Communications, Networking and Applications: Proceedings of WCNA 2014*. Lecture Notes in Electrical Engineering, Springer India, 2015.

[80] Decawave Ltd., *DW1000 User Manual*. Decawave Ltd., 2015.

[81] Decawave Ltd., *DW1000 Datasheet*. Decawave Ltd., 2016.

[82] M. Pelka, "Position Calculation with Least Squares based on Distance Measurements," *Lübeck University of Applied Sciences, Technical Report*, 2015.

[83] Z. Li, *Fine-Grained Indoor Positioning and Tracking Systems*. Inauguraldissertation, Universität Bern, Bern, Switzerland, 2023. Licensed under Creative Commons Attribution-Non-Commercial-No Derivative Works 2.5 Switzerland.

[84] S. Frattasi and F. Della Rosa, *Mobile Positioning and Tracking: From Conventional to Cooperative Techniques*. John Wiley Sons Ltd, 2017.

[85] Feng, D. and Wang, C. and He, C. and Zhuang, Y. and Xia, X.-G., "Kalman-Filter-Based Integration of IMU and UWB for High-Accuracy Indoor Positioning and Navigation," *IEEE Internet of Things Journal*, vol. 7, no. 4, pp. 3133–3146, 2020.

[86] R. G. Yudanto and F. Petré, "Sensor Fusion for Indoor Navigation and Tracking of Automated Guided Vehicles," in *2015 International Conference on Indoor Positioning and Indoor Navigation (IPIN)*, pp. 1–8, 2015.

[87] Y. Leehter, A. W. Yeong-Wei, Y. Lei, and L. Zhenkun, "An Integrated IMU and UWB Sensor based Indoor Positioning System," *2017 International Conference on Indoor Positioning and Indoor Navigation (IPIN)*, pp. 1–8, 2017.

[88] J. Li, Y. Bi, K. Li, K. Wang, F. Lin, and B. M. Chen, "Accurate 3D Localization for MAV Swarms by UWB and IMU Fusion," in *2018 IEEE 14th International Conference on Control and Automation (ICCA)*, pp. 100–105, 2018.

[89] B. Yang, E. Yang, L. Yu, and C. Niu, "Adaptive Extended Kalman Filter-Based Fusion Approach for High-Precision UAV Positioning in Extremely Confined Environments," *IEEE/ASME Transactions on Mechatronics*, vol. 28, no. 1, pp. 543–554, 2023.

[90] A. Abedi and D. Wilkerson, "Wireless Technology Use Case Requirement Analysis for Future Space Applications," tech. rep., NASA, 2016. Final Report.

[91] S. Kottmeier, C. F. Hobbie, F. Orlowski-Feldhusen, F. Nohka, T. Delovski, G. Morfill, L. Grillmayer, C. Philpot, and H. Müller, "The Eu:Cropis Assembly, Integration and Verification Campaigns: Building the first DLR Compact Satellite," in *69th International Astronautical Congress 2018*, September 2018.

[92] B. Annighöfer, C. Nil, J. Sebald, and F. Thielecke, "ARIANE-5-based Studies on Optimal Integrated Modular Avionics Architectures for Future Launchers," in *6th European Conference for Aeronautics and Space Sciences (EUCASS)*, 07 2015.

[93] A. E. M. Casini, R. Sabatini, N. Viola, and M. Carrano, "Overview of the ISS Columbus Module Avionics," in *16th Australian Space Research Conference (ASRC)*, (Melbourne, Australia), National Space Society of Australia (NSSA), 09 2016.

[94] M. Martens, *Implementierung eines drahtlosen Sensornetzwerks zur unterstützenden Sensorauslese am Beispiel des Kompaktsatelliten Eu:CROPIS*. Masterarbeit, Hochschule Magdeburg-Stendal, Juli 2016.

[95] G. Wiedermann, W. Gockel, S. Winkler, J.-M. Rieberm, B. Kraft, and D. Reggio, "The SENTINEL-2 Satellite Attitude Control System – Challenges and Solutions," in *9th International ESA Conference on Guidance, Navigation & Control Systems*, (Porto, Portugal), June 2014.

[96] M. Macdonald and V. Badescu, "Guidance, Navigation and Control," in *The International Handbook of Space Technology*, Chichester, UK: Springer, 2014.

[97] U.-V. Albrecht *et al.*, *Beat to BEAT – Non-Invasive Investigation of Cardiac Function on the International Space Station*, vol. 295 of *Studies in Health Technology and Informatics*. Amsterdam: IOS Press, 2022.

[98] European Space Agency (ESA), "Copernicus Sentinel-2 Satellite Missions." `http://s.dlr.de/5Jdge`, 2012. Created June 14, 2012; Accessed February 10, 2023.

[99] F. Chen, T. Talanis, R. German, and F. Dressler, "Real-Time Enabled IEEE 802.15.4 Sensor Networks in Industrial Automation," in *2009 IEEE International Symposium on Industrial Embedded Systems*, pp. 136–139, 2009.

[100] Y. Li, Y. Dong, P. Fan, and K. B. Letaief, "How Far Are Wireless Networks from Being Truly Deterministic?," *IEEE Internet of Things Magazine*, vol. 5, no. 4, pp. 64–71, 2022.

[101] M. Feldman, G. Cainelli, G. Kunzel, I. Muller, and C. Pereira, "Adaptive Channel Map for Time Slotted Channel Hopping Industrial Wireless Networks," *IFAC-PapersOnLine*, vol. 53, no. 2, pp. 8237–8242, 2020. 21st IFAC World Congress.

[102] H. M. A. Fahmy, *Wireless Sensor Networks - Concepts, Applications, Experimentation and Analysis*. Signals and Communication Technology, Springer Nature Switzerland, 2016.

[103] S. V. Dhage, A. N. Thakare, and S. W. Mohod, "An improved method for scalability issue in wireless sensor networks," in *2015 International Conference on Innovations in Information, Embedded and Communication Systems (ICIIECS)*, pp. 1–6, 2015.

[104] R. Mubashar, M. A. B. Siddique, A. U. Rehman, A. Asad, and A. Rasool, "Comparative Performance Analysis of Short-Range Wireless Protocols for Wireless Personal Area Network," *Iran Journal of Computer Science*, vol. 4, no. 3, pp. 201–210, 2021.

[105] R. Reinhold and R. Kays, "Improvement of IEEE 802.15.4a IR-UWB for Time-Critical Industrial Wireless Sensor Networks," in *2013 IFIP Wireless Days (WD)*, pp. 1–4, 2013.

[106] IEEE Computer Society, *IEEE Standard for Local and Metropolitan Area Networks–Part 15.4: Low-Rate Wireless Personal Area Networks (LR-WPANs)*, 2011. IEEE Std 802.15.4-2011 (Revision of IEEE Std 802.15.4-2006).

[107] G. Pereira, S. Laurindo, G. Budke, C. Montez, and R. Moraes, "Experimental Assessment of IEEE 802.15.4e LLDN Mode Using COTS Wireless Sensor Network Nodes," *IEEE Access*, vol. 10, pp. 12829–12837, 2022.

[108] Vectornav, *VN-100 IMU User Manual - UM001*, 2009. User Manual.

[109] S. Montenegro, T. Baumann, *et al.*, "InnoCubE Der erste Drahtloser Satellit," Deutsche Gesellschaft für Luft- und Raumfahrt - Lilienthal-Oberth e.V., 2022.

[110] M. Jahnke, S. Grau, and U. Kulau, "Demo Abstract: SatelLight – Using LiFi for Intra-Satellite Communication," in *the 21th ACM Conference on Embedded Networked Sensor Systems*, SenSys 2023, (Istanbul, Turkey), November 2023. Accepted for Publication.

[111] STMicroelectronics, *STM32L151xD Datasheet*. STMicroelectronics, 2015.

[112] STMicroelectronics, "Wittenstein SAFERTOS: Safety Critical RTOS." `http://s.dlr.de/0WZ6f`, 2023. Accessed: 2023-05-27.

[113] Vilajosana, X. and Tuset-Peiro, P. and Watteyne, T. and Pister, K., "Openmote: Open-source prototyping platform for the industrial iot," in *International Conference on Ad Hoc Networks*, 09 2015.

[114] T. Chang, P. Tuset-Peiro, X. Vilajosana, and T. Watteyne, "OpenWSN OpenMote: Demo'ing a Complete Ecosystem for the Industrial Internet of Things," in *2016 13th Annual IEEE International Conference on Sensing, Communication, and Networking (SECON)*, pp. 1–3, 2016.

[115] OpenWSN Team, "State Machine." `http://s.dlr.de/YQryT`, 2014. Accessed: 2023-05-27.

[116] STMicroelectronics, "STM32F4 Series - High-performance Digital Signal Controllers." `http://s.dlr.de/RnyqG`, May 2023. Accessed: 2023-05-27.

[117] European Cooperation for Space Standardization, *ECSS-E-ST-20-07C - Electromagnetic Compatibility*, 2008. Accessed: 2021-02-01.

[118] U.S. Department of Defense, *MIL-STD-461F - Requirements for the Control of Electromagnetic Interference Characteristics of Subsystems and Equipment*, 2007. Accessed: 2021-02-05.

[119] Decawave Ltd., *DWM1000 Datasheet*. Decawave Ltd., 2016.

[120] European Space Agency, "Columbus EMC & Power Quality Requirements Document," tech. rep., 2001. COL-ESA-RQ-014.

[121] P. Kyösti, J. Meinilä, L. Hentila, X. Zhao, T. Jämsä, C. Schneider, M. Narandzic, M. Milojević, A. Hong, J. Ylitalo, V.-M. Holappa, M. Alatossava, R. Bultitude, Y. Jong, and T. Rautiainen, "WINNER II Channel Models," *IST-4-027756 WINNER II D1.1.2 V1.2*, 02 2008.

[122] International Telecommunication Union, "Propagation Data and Prediction Methods for the Planning of Indoor Radiocommunication Systems and Radio Local Area Networks," Recommendation ITU-R P.1238-12, International Telecommunication Union, Radiocommunication Sector, 8 2023. Accessed: 2023-12-21.

[123] J. Karedal, S. Wyne, P. Almers, F. Tufvesson, and A. Molisch, "Statistical Analysis of the UWB Channel in an Industrial Environment," in *IEEE 60th Vehicular Technology Conference, 2004. VTC2004-Fall. 2004*, vol. 1, pp. 81–85 Vol. 1, 2004.

[124] A. Molisch, K. Balakrishnan, D. Cassioli, C.-C. Chong, S. Emami, A. Fort, J. Karedal, J. Kunisch, H. Schantz, U. Schuster, and K. Siwiak, "IEEE 802.15.4a Channel Model - Final Report," vol. 15, 01 2004.

[125] Decawave Ltd., *APS014 - Application note - Antenna Delay Calibration of DW1000-based Products and Systems*. Decawave Ltd., 2018.

[126] B. V. Krishnaveni, K. S. Reddy, and P. R. Reddy, "Indoor Tracking by Adding IMU and UWB Using Unscented Kalman Filter," *Wireless Personal Communications*, vol. 4, 2022.

[127] S. Buchner, P. Marshall, S. Kniffin, and K. LaBe, "Proton Test Guideline Development – Lessons Learned." NASA Electronic Parts and Packaging (NEPP) Program, Electronics Radiation Characterization (ERC) Project, 8 2002.

[128] Royal Belgian Institute for Space Aeronomy, "SPENVIS - The Space Environment Information System." `http://s.dlr.de/SEArZ`, 2023. Accessed: 2023-08-03.

[129] European Space Agency, *Single Event Effects Test Method and Guidelines*, 2016. Issue: 5.

[130] J. Budroweit, M. P. Jaksch, and M. Sznajder, "Proton Induced Single Event Effect Characterization on a Highly Integrated RF-Transceiver," *Electronics*, vol. 8, p. 519, May 2019.

[131] Bosch, *BMP180 Data Sheet: Digital Pressure Sensor*, April 2013.

[132] STMicroelectronics, *L3GD20 MEMS Motion Sensor: Three-Axis Digital Output Gyroscope*, February 2013.

[133] STMicroelectronics, *LSM303DLHC Ultra-Compact High-Performance eCompass Module: 3D Accelerometer and 3D Magnetometer*, November 2013.

[134] Texas Advanced Optoelectronic Solutions Inc (TAOS), *TSL2560, TSL2561 Light-to-Digital Converter*, 2009.

[135] Decawave Ltd., *DecaRangeRTLS ARM Source Code - Understanding and Using the DecaRangeRTLS ARM Source Code*. Decawave Ltd., 2015.

[136] C. Liu, T. Kadja, and V. P. Chodavarapu, "Experimental Evaluation of Sensor Fusion of Low-Cost UWB and IMU for Localization under Indoor Dynamic Testing Conditions," *Sensors*, vol. 22, no. 21, 2022.

[137] DLR - Institute of Space Systems, "PLUTO - Payload Under Test Orbiter." `http://s.dlr.de/2tinf`, 2023. Accessed: 2023-07-02.

[138] SALTO Consortium, "SALTO ReuSable StrAtegic Space Launcher Technologies Operations." `http://s.dlr.de/4YVMo`, 2023. Accessed: 2023-07-02.

[139] A. E. M. Casini, P. Mittler, J. Schlutz, T. Uhlig, F. Rometsch, L. Ferra, A. Cowley, and B. Fischer, "Lunar Missions' Simulations in Analogue Facilities: the Operational Concept and the First Commissioning of the ESA-DLR LUNA Facility," in *Proceedings of the International Astronautical Congress, IAC*, September 2022.

[140] M. Drobczyk, A. Lübken, C. Strowik, U.-V. Albrecht, J. Rust, J. Beringer, and U. Kulau, "A Wireless Communication Network with a Ballistocardiography Experiment on the ISS: Scenario, Componensts and Pre-Flight Demonstration," *IEEE Journal of Radio Frequency Identification*, pp. 258–268, April 2022.

[141] Consultative Committee for Space Data Systems, *Spacecraft Onboard Interface Services - Reliable Wireless Intra-Communication for Spacecraft and Launcher - PHY*, 2019. Accessed: 2023-07-02.

[142] A. Cilfone, L. Davoli, L. Belli, and G. Ferrari, "Wireless Mesh Networking: An IoT-Oriented Perspective Survey on Relevant Technologies," *Future Internet*, vol. 11, no. 4, 2019.

[143] M. H. Sabo, I. Rosdiazli, B. Kishore, D. C. Tran, and S. Nordin, "Application of Wireless Technology for Control: A WirelessHART Perspective," *Procedia Computer Science*, vol. 105, pp. 240–247, 2017. 2016 IEEE International Symposium on Robotics and Intelligent Sensors, IRIS 2016, 17-20 December 2016, Tokyo, Japan.

[144] A. Ovechkin, T. Claeys, D. Vanoost, J. F. Dawson, G. A. E. Vandenbosch, and D. Pissoort, "Characterizing the Robustness of Wi-Fi and Bluetooth against Continuous Wave EM Disturbances inside a Reverberation Chamber," in *2021 IEEE*

International Joint EMC/SI/PI and EMC Europe Symposium, pp. 1031–1036, 2021.

[145] D. Christin, P. S. Mogre, and M. Hollick, "Survey on Wireless Sensor Network Technologies for Industrial Automation: The Security and Quality of Service Perspectives," *Future Internet*, vol. 2, no. 2, pp. 96–125, 2010.

[146] F. P. Rezha and S. Y. Shin, "Performance evaluation of ISA100.11A industrial wireless network," in *IET International Conference on Information and Communications Technologies (IETICT 2013)*, pp. 587–592, 2013.

[147] Kurunathan, H. and Severino, R. and Koubaa, A. and Tovar, E., "Ieee 802.15.4e in a nutshell: Survey and performance evaluation," *IEEE Communications Surveys Tutorials*, vol. 20, no. 3, pp. 1989–2010, 2018.

Appendix A

Protocol evaluation

IEEE 802.11n:

- **Latency: 2 (142, Tab. 17)**
  But cannot be guaranteed due to CSMA/CA, and depending on network load often above 10ms, however below 10ms can be achieved
- **Determinism: 1**
  CSMA/CA method is used
- **Data rate: 4 (102, p. 40)**
  Theoretical up to 600 Mbps, average approx. 100+ Mbps
- **Robustness: 2 (102, p. 40)**
  Poor performance against multipath propagation, causes interference with other participants and has limited immunity to interference
- **Scalability: 2 (143, Tab. 1)**
  Conditionally scalable in terms of network size

Bluetooth:

- **Latency: 1 (142, Tab. 17)**
  Typically between 10ms and 50ms
- **Determinism: 1**
  Not designed for deterministic applications
- **Data rate: 2 (143, Tab. 1)**
  Up to 2 Mbps

- **Robustness: 1 (144)**
  Susceptible to multipath propagation, not immune to interference, especially problems when interfering with broadband signals

ZigBee:

- **Latency: 1 (102, Tab. 1.3)**
  Varies greatly by CSMA-CA, and depends on the number of participants.
- **Determinism: 1 (145, Tab. 3)**
  Limited deterministic capabilities due to CSMA-CA
- **Data rate: 1 (102, p. 40)**
  Up to 250 kbps
- **Robustness: 1 (102, p. 40)**
  Susceptible to interference and multipath propagation
- **Scalability: 4 (143, Tab. 1)**
  Scales moderately

Industrial 802.15.4-based:

- **Latency: 1 (146)**
  Latency is usually less than 100ms, but can be significantly higher (depending on number of hops and network topology)
- **Determinism: 2 (145, Tab. 3)**
  High degree of determinism due to time control / TDMA
- **Data rate: 1 (143, Tab. 1)**
  Up to 250 kbps
- **Robustness: 2 (145, Tab. 4)**
  Moderate robustness due to mesh network topology and channel hopping, susceptible to multipath propagation
- **Scalability: 4 (143, Tab. 1)**
  Well scalable for larger networks

IR-UWB/LLDN:

- **Latency: 2 (147; 40)**
  Especially by choosing a suitable method (e.g. LLDN) in combination with a faster PHY layer, latencies below 10ms can be achieved

- **Determinism: 2 (145, Tab. 3)**
  High degree of determinism due to timing control / TDMA
- **Data rate: 3 (102, p. 40)**
  Up to 27 Mbps (as per standard)
- **Robustness: 3 (102, p. 40), (145, Tab. 4)**
  IR-UWB PHY provides high robustness against interference and multipath propagation, while 802.15.4e provides additional features to improve reliability
- **Scalability: 4 (147, Tab.1)**
  Well scalable, also depending on the choice of MAC scheme

Appendix B

Measurement results

B.1 Distance measurements

More pronounced movements of the astronaut were recorded on video during the second session, which was also analysed. The variety of these movements, shown in Figure B.1, is an indication of frequent changes in the astronaut's position. This could be confirmed by the associated video, which is an indication of a correlation between the measurements and the video footage. For completeness, the first 30 minutes of Session 3 are also shown in Figure B.2. Although there is no video footage of this session, it can be seen that unlike in Session 1, the astronaut takes different positions over a longer period.

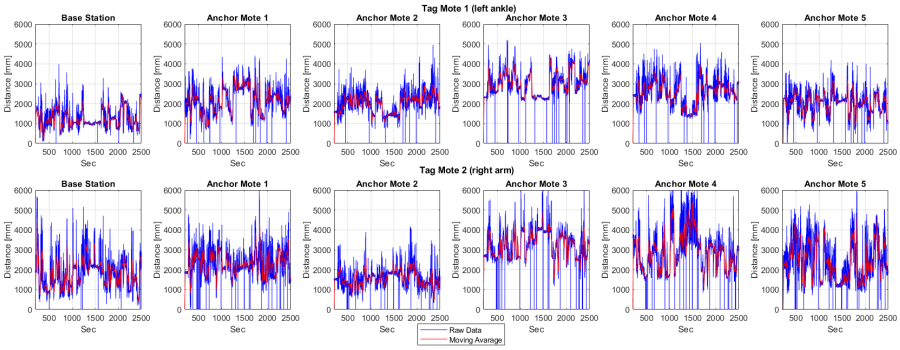

FIGURE B.1: Ranging data from all Motes to TMs 1 and 2 during tracking Session 2

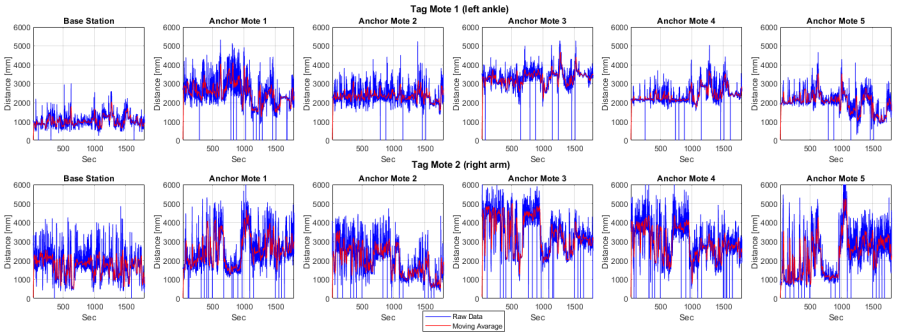

FIGURE B.2: Ranging data from all Motes to TMs 1 and 2 during tracking Session 3

B.2 Calibration Campaign

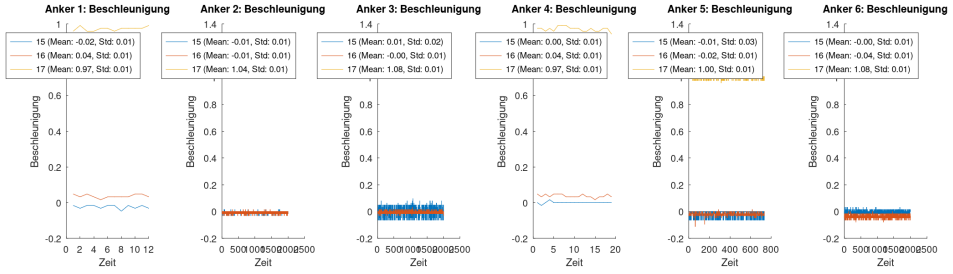

FIGURE B.3: Ground Calibration with Anchor Motes Accelerometer

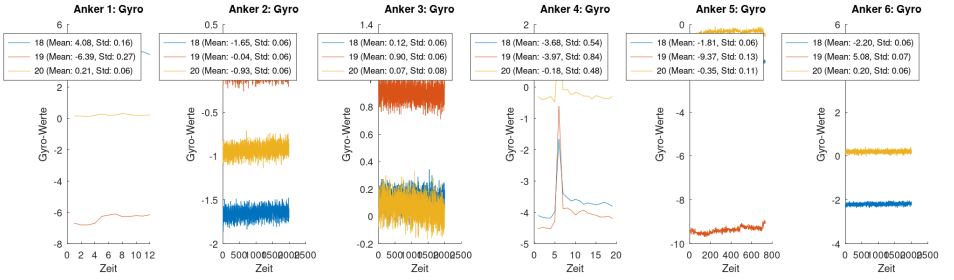

FIGURE B.4: Ground Calibration with Anchor Motes Gyroscope

B.3 Gyroscope raw data

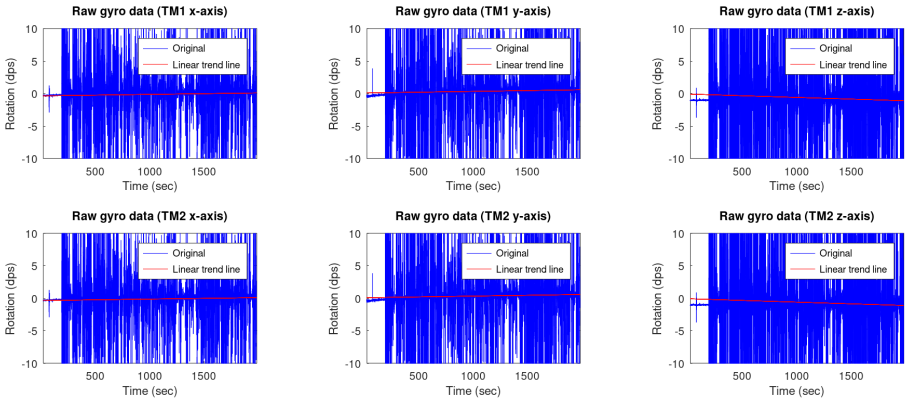

FIGURE B.5: Gyroscope raw data for TM1 and TM2

B.4 Detailed Position estimates

B.4.1 Position 2

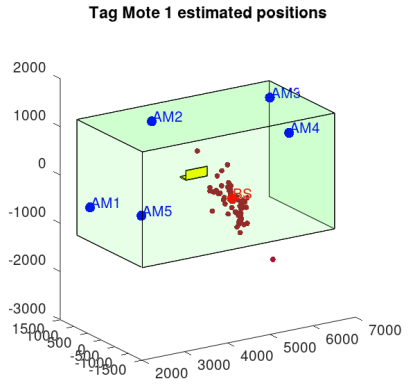

(A) Tag Mote 1 position estimations

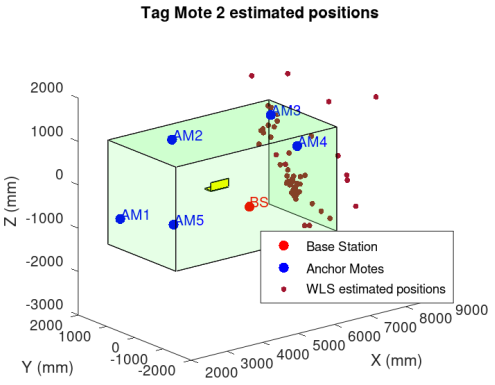

(B) Tag Mote 2 position estimations

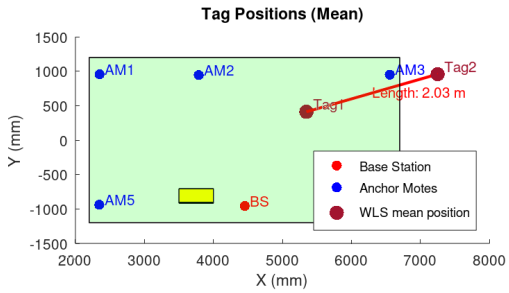

(C) Mean position for TM1 and TM2 in x-y Axis

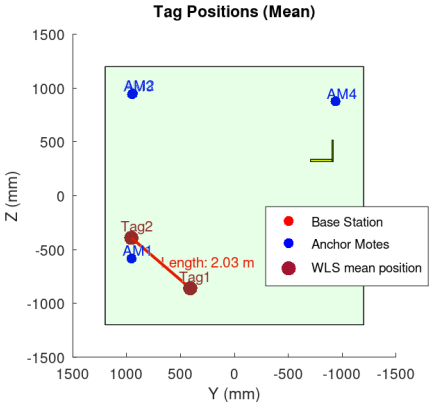

(D) Mean position for TM1 and TM2 in y-z Axis

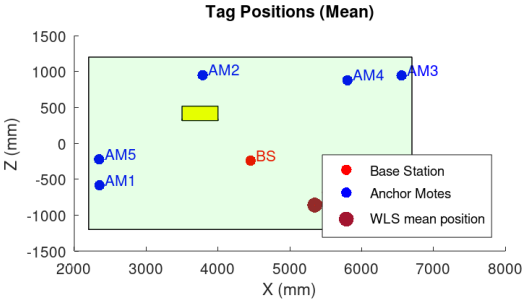

(E) Mean position for TM1 and TM2 in x-z Axis

FIGURE B.6: Trilateration results for position 2

B.4.2 Position 3

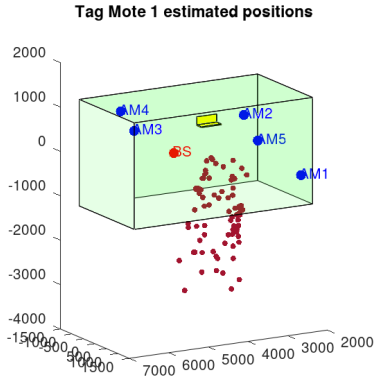

(A) Tag Mote 1 position estimations

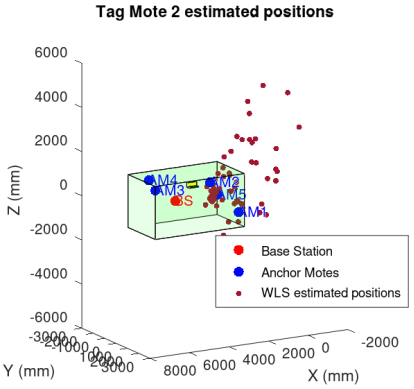

(B) Tag Mote 2 position estimations

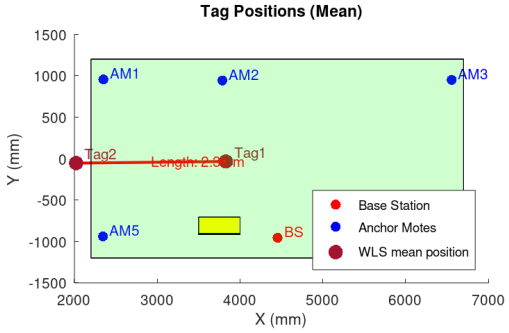

(C) Mean position for TM1 and TM2 in x-y Axis

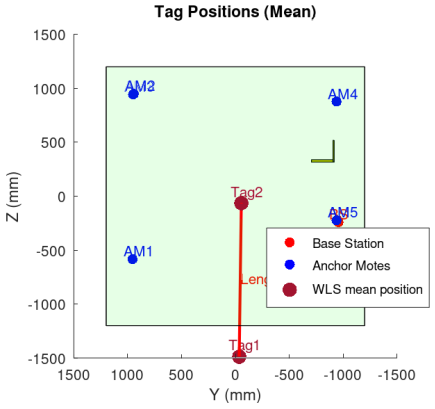

(D) Mean position for TM1 and TM2 in y-z Axis

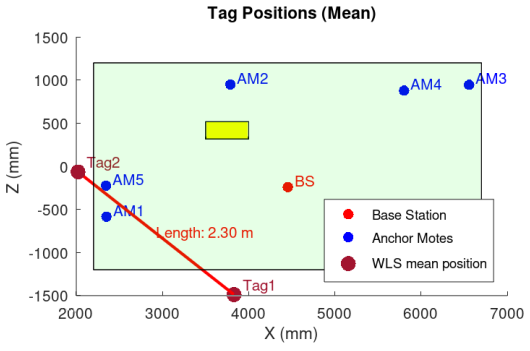

(E) Mean position for TM1 and TM2 in x-z Axis

FIGURE B.7: Trilateration results for position 3

B.4.3 Position 4

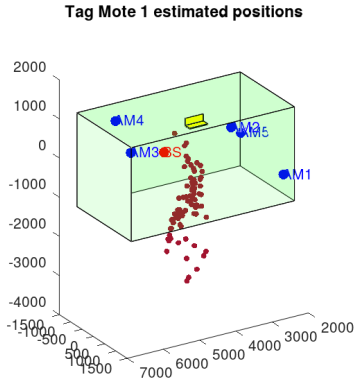

(A) Tag Mote 1 position estimations

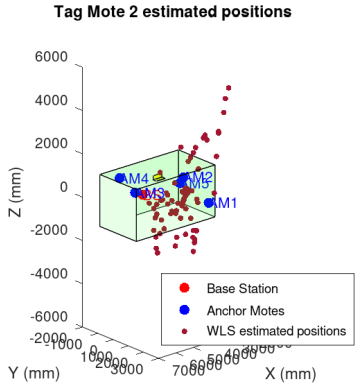

(B) Tag Mote 2 position estimations

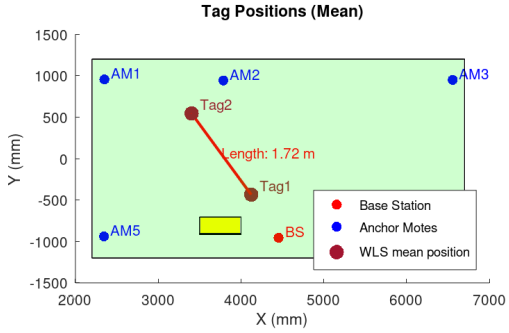

(C) Mean position for TM1 and TM2 in x-y Axis

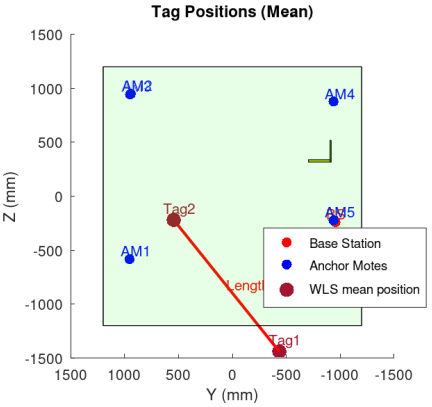

(D) Mean position for TM1 and TM2 in y-z Axis

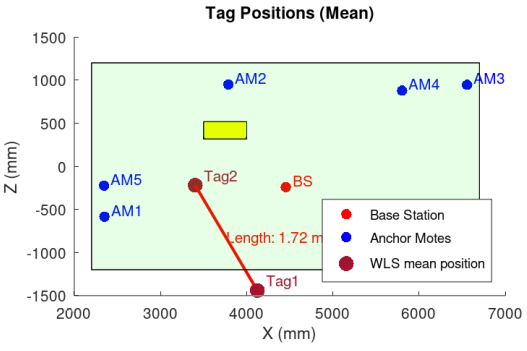

(E) Mean position for TM1 and TM2 in x-z Axis

FIGURE B.8: Trilateration results for position 4

Appendix C

Motes position

	Location	Coordinates of ref point (mm)		
		X COL	Y COL	Z COL
Base Station	COL1-A2	4448,461	-1097,32	-241,854
Anchor Mote 1	COL-F1	2357,094	1096,632	-584,075
Anchor Mote 2	COL-O2	3787,573	949,675	1090,524
Anchor Mote 3	COL1-F4	6556,249	1091,344	950,552
Anchor Mote 4	COL1-A4	5802,695	-1079,45	884,325
Anchor Mote 5	COL1-A1	2351,676	-1080,75	-224,943

TABLE C.1: Coordinates of the reference point in Columbus coordinate system

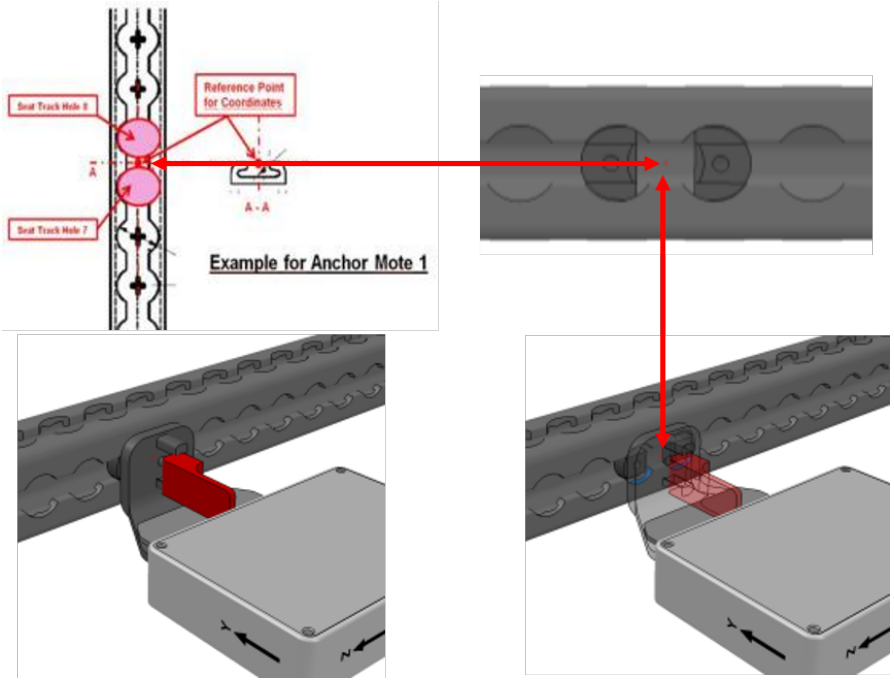

FIGURE C.1: Reference point position

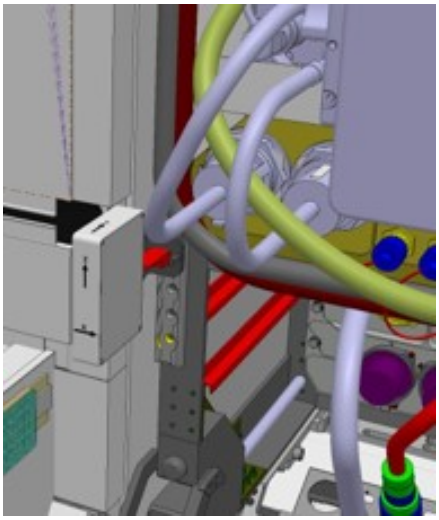

(A) Anchor Mote 1

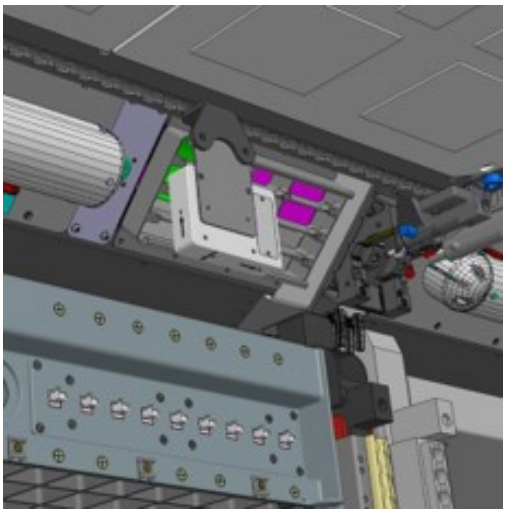

(B) Anchor Mote 2

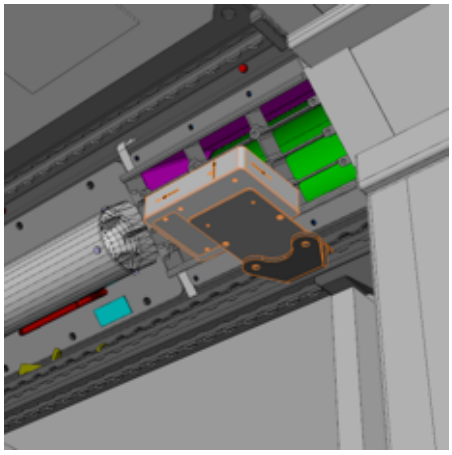

(C) Anchor Mote 3

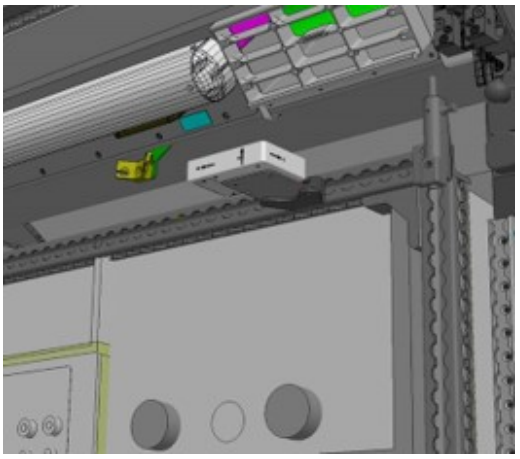

(D) Anchor Mote 4

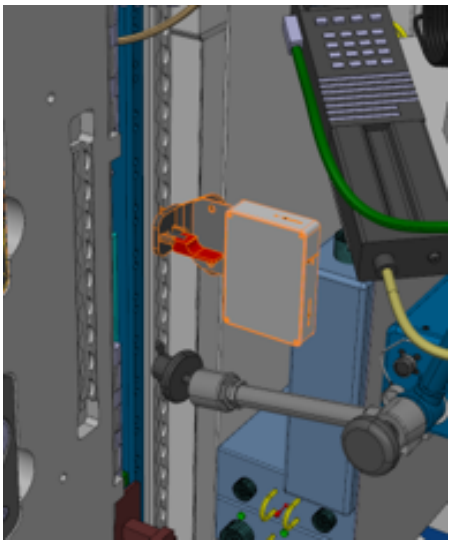

(E) Anchor Mote 5

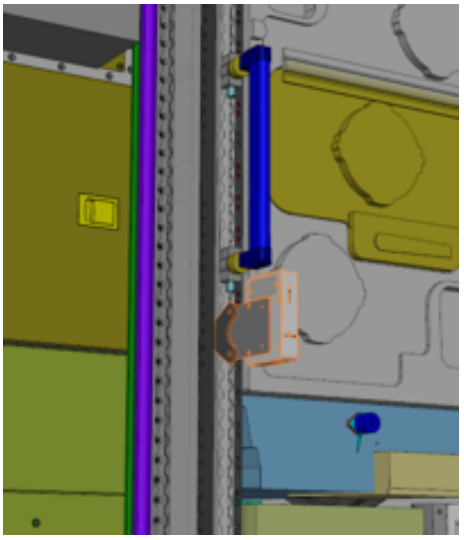

(F) Base Station

FIGURE C.2: Positions and orientation of the Wireless Compose Motes in COL module

Erklärung zur Dissertation

I hereby declare that I have prepared the submitted doctoral thesis independently, i.e. in particular independently and without the help of a commercial doctoral advisor, and that I have not used any sources and aids other than those indicated by me.

Hiermit erkläre ich, dass ich die eingereichte Doktorarbeit eigenständig, d.h. insbesondere selbständig und ohne Hilfe einer kommerziellen Promotionsberatung angefertigt und keine anderen als die von mir angegebenen Quellen und Hilfsmittel benutzt habe.

Bremen, April 22, 2024:

(Martin Drobczyk)